A STUDY OF THE ROLE OF FRICTION IN SUPERPLASTIC BLOW FORMING OF ALLOY SHEET

Yanyun Chen BSc MSc

Engineering Design & Simulation Group
School of Engineering and Built Environment
University of Wolverhampton

A thesis submitted in partial fulfilment of the requirements of the University of Wolverhampton for the degree of Doctor of Philosophy

This research programme was carried out in collaboration with Rolls-Royce

June 2005

THESIS CONTAINS CD/DVD

Declaration

This work or any part of thereof has not previously been present in any form to the University or to any body whether for the purpose of assessment, publication or for any other purpose (unless previously indicated). Save for any express acknowledgements, references and/or bibliographies cited in the work, I confirm that the intellectual content of the work is the result of my own efforts and of no other person.

The right of Yanyun Chen to be identified as author of this work is asserted in accordance with ss.77 and 78 of the Copyright, Designs and Patents Act 1988. At this date copyright is owned by the author.

Signature:

yanyun chen 陈艳云

Date 12/06/2005

Abstract

Superplastic forming (SPF) is a manufacturing process whereby certain materials, under specific temperatures and strain rates, exhibit high ductility resulting in large deformations. Superplastic forming has found a wide application in industry, especially in the aerospace sector for the fabrication of complicated structures, because of its superior advantages of significant cost savings and weight reduction over conventional forming processes. However, failures of SPF components are present in the manufacture of aircraft parts with complex shapes. In particular, severe component thinning or even cracking during a superplastic blow forming process contributes to a major problem for Rolls Royce Plc, which is strongly associated with the poor level of current understanding of friction behaviour in the SPF process. It is thus the aim of this research to investigate the superplastic blow forming process and the role of friction, to minimize uneven component thinning to meet design criteria. The objective was tackled by way of finite element modelling together with experimental validation.

The superplastic blow forming of a Pb-Sn alloy sheet into a complex component as well as a cylindrical cup was simulated to investigate the deformation process, pressure versus time curve and thickness distribution. To study the effect on thickness distributions, the role of friction was modelled by specifying a friction coefficient associated with the contact between the dies and the component. The finite element model has been validated using experimental data from literature. It was found that a lower friction coefficient results in a better uniform thickness distribution. The simulations also verified that reverse blow forming resulted in less thinning in the formed component.

A set of laboratory test apparatus for performing superplastic blow forming experiments under controllable temperature and pressure was designed and built in order to investigate the friction behaviour and component thinning mechanism. A set of equations were derived theoretically for the calculation of the friction coefficients at different contact regions. The experimental deformation in a superplastic blow

forming has been recorded through a transparent die, and the friction coefficients at different contact regions were calculated according to the derived friction equations. The friction coefficients and the experimental parameters were then entered into the validated finite element model. The predicted deformation process is in good agreement with the experimental observation. In addition, the maximum discrepancy between the predicted and experimental thickness distributions is less than 40%. The implementation of the methodology from this study will improve the understanding of the friction mechanism in blow forming process and thus help achieve less component thinning in the industry.

Acknowledgements

I would like to thank my supervisors Dr Kevin Kibble and Professor Richard Hall for their guidance and help throughout the duration of the research. Without their valuable advice, continual encouragement and support, it would have been impossible to complete this study.

I would like to thank Mr Julian Spence of Rolls-Royce Plc for his advice throughout the project as well as co-ordinating meetings. Special thanks go to Mr Colin Durnall for all the technical support, without whom the test rig would not have been possible. My thanks also go to the rest of technician team at the University of Wolverhampton, including Mr John Harris, Mr John Pitt, Mr Kevin Worrall, Mr James Stamps, Mr Matthew Lindop, for their help on the experimental device and thickness measurement. I would like to express my gratitude to Dr Stefan Scholze for his kind help with the tensile test data logging.

To my parents, my sister and brother, I offer heartily thanks for their love and support throughout the years. To my husband, xiaoguang, for his fully support and precious advice on my PhD research all these years. To my baby son, danwei, thank you for your patience and cooperation during the pregnancy while it was the period of my final experiment.

Finally I would like to dedicate the thesis to my father, who passed away during my PhD studies and I have no chance to take a last look. I owe an eternally gratitude and sorrow to him.

谨以此文献给关爱我一生的父亲

Contents

List of Figure

List of Tables

Chapter 1

Introduction

1.1 General

Superplastic forming (SPF) is a manufacturing process whereby certain materials, under specific temperature and strain rate conditions, exhibit high ductility resulting in large strain deformations (Hamilton and Paton, 1989; Pilling and Ridley, 1989; Pearce, 1991). It is characterised by low flow stress, low strain rate, large deformation and nonlinear material behaviour. This property has allowed the development of forming operations which permit thin sheet to be blown into die cavities to produce complex structures. Nowadays metals, ceramics and intermetallics have been found to exhibit superplastic behaviour by judicious control of their microstructure and deformation conditions.

Superplastic forming is becoming an important manufacturing technique, especially in the aerospace industry where weight saving is of critical importance, because it has some advantages over conventional forming processes, such as greater design flexibility, lower die cost, the ability to form complex lightweight parts with very thin regions and integrated structures that are often stronger than the assemblies. Interest in this phenomenon and its commercial potential has significantly increased in recent years, and the application of SPF has expanded very quickly to the automotive, rail, architectural, sports, dental and entertainment industries (Hamilton, 1985; Ghosh, 1985). Significant savings of between 20% and 50% in manufacturing cost and weight reductions of the order of 10% to 40% are typically achieved when structural components are redesigned and manufactured by superplastic forming (Ghosh and Hamilton, 1982). It is reported that military airplanes, such as the Boeing F-15E and Euro-Fighter 2000, have achieved tremendous design gains by the application of

superplastic formed structures (Sanders, 1999). Components made from superplastic forming are now flying on every model of aircraft that is currently produced by Boeing.

There are a wide variety of SPF processes, e.g., blow forming, thermo-forming, superplastic forming/diffusion bonding (SPF/DB) etc. Blow forming methods are utilized by Rolls Royce Plc, who provided support for this work, and therefore this is the primary method studied in this research.

1.2 Research Problem

Almost all metal forming processes involve deformation of a workpiece between dies. During a superplastic blow forming operation, gas pressure is applied on one side of a metal sheet to make it flow plastically into a die of the desired shape and complexity. The sheet experiences a large plastic deformation by the driving gas pressure, and thinning takes place because of frictional restraint due to contact between the sheet and the dies. As the shape of the die becomes more complicated, thinning will become more severe. This is undesirable because high stresses exist in those localised thinning areas and may lead to manufacturing failure.

Friction is one of the most important factors, in a superplastic blow forming process, influencing material flow, strain distribution, and the necessary forming force (Wang, 1982). Although the strain distribution in a deformed component is mainly controlled by the tooling geometry and material properties, friction can alter the straining pattern within the workpeice, e.g., the magnitude and location of the maximum strain, and thus determine the failure type (e.g. tearing, wrinkling, and surface distortion) and the area where failure occurs. Excessive friction tends to restrain the flow of the material and thus results in locally excessive thinning or even cracking in a component. Therefore a good understanding of friction behaviour is crucial for improving the quality and reliability of SPF products. This thesis was initiated and guided by the need to widen the knowledge of how friction behaves in a SPF process.

Given the importance of friction in superplastic blow forming, it is surprising that little is known about its effect in this process. This is mainly because friction force is a complex function of interacting variables that are constantly changing during an SPF process. These variables include not only operational parameters such as the thermal boundary, contact pressure, strain rates and the possible presence of lubricant, but also material properties and contact surface characteristics such as surface roughness and hardness differences.

In recent years numerical modelling techniques have been intensively applied to investigate the SPF process to help designers improve the efficiency and cost effectiveness of their designs. However, comparisons between finite element simulations and experimental results showed that lack of accurate information on frictional changes under realistic forming conditions is a serious deficiency in current state of the art (Bochmann E and Doege, 1992). The limitation of current modelling is that the value specified for friction is assumed to be constant throughout the entire process. For example, using a Coulomb friction model, the model seems to work well for some simulations, however, some applications present difficulties, where simulations have to be carried out with friction values which are not in correspondence with practice (Wang, 1982). From a tribological point of view, this is not satisfactory because the coefficient of friction depends on the local contact conditions, such as pressure, the combined surface roughness of the sheet and dies, lubricant viscosity etc (Schipper, 1988). This means that during a SPF process the contact conditions and thus the coefficient of friction might differ for each sheet/die contact region. Therefore the question arises, is it possible to solve the problem and to increase the accuracy of simulations by using varied friction coefficients which depend on the local contact conditions?

In order to study the friction behaviour, experiments need to be carried out under conditions close to the practical production process. Although a great deal of effort has been spent on investigating friction behaviour in metal forming, there is no generally accepted test method for the wide range of forming conditions encountered during metal forming processes. In particular, there is a lack of information on friction tests for the SPF process. Finite element analysis offers an efficient method to visualize and model the thinning process in an intuitive way in the analysis of

complicated SPF components. It provides valuable information on how the parameters in an SPF process can be modified to meet design requirements. In this thesis based on the preliminary finite element (FE) modelling, an experimental setup to study the role of friction was designed and built. Friction coefficients obtained from experimental tests were fed back to the FE model to gain a clear understanding of the role of friction in the component thinning mechanism. The finite element modelling in collaboration with the experimental investigation will fulfil the research.

1.3 Research Objective

The primary objective of this research work is to investigate the role of friction in the thinning mechanism during SPF, by establishing a methodology applicable to improve thinning control in the industrial SPF under inhospitable temperature and pressure.

1.4 Research Methodology

To fulfil the research objective, four stages of analysis were carried out in this project.

(i) The preliminary work was concerned with finite element simulations using ABAQUS in order to understand the SPF process. The effects of the friction coefficient were investigated in the blow forming of a cylindrical cup as well as a complex reverse forming component.

(ii) The second stage was to investigate the friction coefficient at different contact regions using theoretical derivation.

(iii) The third stage of the work was concerned with laboratory-scale tests of Pb-Sn alloy sheets to evaluate the frictional behaviour under superplastic blow forming.

(iv) The last stage was to simulate the experiments and comparisons were made to validate the friction coefficient obtained from the experiments.

1.5 Structure of the Thesis

The thesis is divided into nine chapters. In Chapter 1, a general introduction to the research is given, including the research problem, objective and research methodology.

In Chapter 2, a review of superplasticity is given, this includes the application of superplasticity, and production aspects such as blow forming and thinning. In addition, a comprehensive review of previous work on blow forming, including analytical models and finite element investigations, is presented.

In Chapter 3, basic friction theories, including friction mechanisms and friction models, relevant to metal forming are reviewed. Attention is next directed to the existing literature on friction testing methods in metal forming process. A brief introduction to friction studies in superplastic blow forming is presented.

In Chapter 4, a brief introduction to ABAQUS, the finite element analysis package used in this research, is described. In addition, several key features of the finite element modelling within ABAQUS, including contact interactions, friction algorithms, loading and strain rate control, are generally described.

In Chapter 5, a preliminary finite element simulation of an alloy sheet into a cylindrical cup is presented and validated by experimental data to obtain a better understanding of the blow forming process. The effects of major factors such as the friction coefficient and the strain rate sensitivity index have been investigated. Furthermore, simulation of a complex reverse formed component has been carried out. A comparison between the reverse forming and non-reverse forming has been made to demonstrate the better thickness control in the reverse forming process.

In Chapter 6, the theoretical calculations of friction coefficients at four typical contact regions under the superplastic blow forming process, i.e., die-entry region, bottom region, side-wall region and bottom corner region, are derived.

In Chapter 7, the design and manufacture of a test rig, with controllable temperature and forming pressure, for the study of friction behaviour in a blow forming operation is described. Using the test rig, blow forming experiments of Pb-Sn alloy sheets into cylindrical cups and reverse formed components were carried out. The experimental results, including deformation processes, thickness distributions and friction coefficient calculations are presented. In addition, sheets with profiled thickness distribution were used in the reverse forming in order to obtain successfully formed components.

In Chapter 8, simulations are carried out to model the experiments. The material properties and the friction coefficients calculated from experiments (Chapter 7) have been input in the simulation in order to evaluate the experimental methodology. The comparisons between simulations and experiments, in terms of deformation process and thickness distribution, are presented, which demonstrates that the experimental methodology is capable of obtaining the friction coefficient indirectly.

In Chapter 9, the conclusions from this research are summarized and recommendations for further work are presented.

The main contributions of the work reported in this thesis are:

1. Provision of a comprehensive finite element model, incorporating the die geometry, material properties, contact and friction behaviour, to evaluate the superplastic blow forming process and the role of friction (Chapters 5 and 8).
2. Provision of a set of equations for the calculation of friction coefficients at different contact regions of die and metal sheet (Chapter 6).
3. Development of experimental test rigs to investigate the superplastic blow forming and reverse blow forming processes (Chapter 7).
4. Provision of an experimental methodology to obtain friction coefficients at different contact regions of the die and the metal sheet (Chapters 6, 7 and 8).

Chapter 2

Review of Superplastic Blow Forming

2.1 Introduction

As the phenomenon of superplasticity draws attention from laboratory research into the industrial applications, particularly in the aerospace industry, the need for quality and process control during superplastic forming (SPF) becomes increasingly important. This requires a basic understanding of laboratory characterisation of superplastic materials which can reflect their behaviour in actual forming applications. Such requirements are not limited to determining tensile elongations under optimum superplastic conditions, but include detailed characterisation of the material constitutive relationship for superplastic flow.

The need for accurate process control confines SPF to a rather narrow range of temperatures and strain rates over a given fine grain size superplastic material. In addition, reasonably precise control of the forming pressure cycle is necessary. A general knowledge of the manufacturing process provides a good basis for an accurate modelling of the SPF process. This topic is therefore briefly reviewed.

After a brief overview of superplastic behaviour in several commonly used superplastic materials, such as titanium and aluminium alloys, attention is next turned to superplastic forming. The advantages and industrial applications of such a manufacturing method as well as the thinning problem are highlighted. Finally a literature review of the superplastic blow forming process, including experimental investigations, analytical models and finite element simulations, is presented at the end of this chapter.

2.2 Superplasticity

Superplasticity is the capability of particular polycrystalline materials to undergo large uniform strains in certain temperature and strain rate ranges prior to failure (Hamilton and Paton, 1989; Pilling and Ridley, 1989; Pearce, 1991). An elongation in excess of 200% is usually indicative of superplasticity during uniaxial tensile deformation, whereas for conventional materials, equivalent values are usually less than 100%. Several materials can attain extensions greater than 1000%. For example, the highest elongation in Pb-Sn eutectic alloy is up to 7750%, and in aluminium bronze alloy it is greater than 8000% (Pilling and Ridley, 1989).

Superplastic behaviour was first discovered and reported in the UK by Bengough (1912). Further development was shown by Pearson (1934) with a spectacular demonstration of a tensile elongation of 1950% without failure for Bi-Sn alloys in constant stress tensile tests, see Figure 2.1. Laboratory studies were carried out in the USSR and the term "superplasticity" was coined by Bochvar to literally mean "ultrahigh plasticity" (Bochvar, 1946). Considerable interest in superplastic research arose again after a review paper of Soviet research on this topic was compiled and published by Underwood (1962). The development of superplasticity research proceeded and Backofen et al (1964) first introduced the concept of a strain rate sensitivity index "m" after a systematic superplastic investigation on Zn-Al alloy. The important finding from the early researchers was that it was possible to stretch metal alloys with superplasticity far beyond the limitations of conventional alloys and

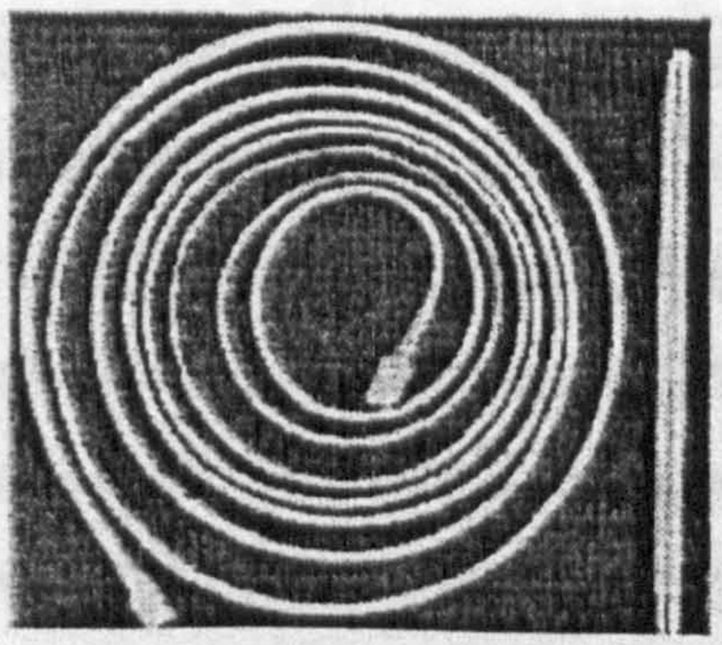

Figure 2.1 A Bi-Sn alloy with 1950% elongation (Pearson, 1934)

forming methods. Although their findings were obscure at that time, they opened the door to a very broad segment of material science research and development. Since the early 1970's, SPF has been fulfilling its initial promise to create complex sheet metal parts for a wide range of end users. Research on superplasticity has centred on developing new alloys and materials, process optimisation, computer simulation of deformation, and microstructural studies to understand the fundamental mechanisms of this process. Universities and laboratories in the United States, Japan, Russia, United Kingdom, France and other nations have focussed on developing new materials and attaining suitable microstructures (Vetrano, 2001). Industrial laboratories have concentrated on developing suitable methods for forming parts. By using computers to simulate the forming process, the laboratories hope to accelerate the ability to design and form a component utilizing superplasticity.

There are two well-established types of superplasticity in terms of the micro-structural mechanism and deformation conditions, i.e., micrograin (or microstructural) superplasticity and transformation (or environmental) superplasticity. In this chapter concentration will be mainly paid to the former since micrograin superplasticity is of considerable significance from a commercial viewpoint. For micrograin superplasticity, high ductility can be observed under three basic requirements (Pilling and Ridley, 1989):

1) fine and equiaxed grain size that is stable during deformation;

2) controlled strain rate ranging from 10^{-5} to 10^{-1} per second;

3) temperature greater than $0.5T_m$, where T_m is the melting point in degrees Kelvin.

A fine grain size, which should be less than $10\,\mu m$, is a typical microstructural requirement, although a limited amount of superplasticity can still be observed at a grain size up to 20 μm. Several methods are available for grain refinement, including inhomogeneous deformation of duplex alloys, phase separation of duplex alloys, phase transformation, and recrystallization. The fine grained structure should remain stable under the relatively high temperature at which the superplastic behaviour occurs. Optimum superplasticity of most superplastic alloys generally occurs at an intermediate strain rate ($10^{-5} \sim 10^{-2}$ per second). There is a decrease in the elongation to failure at both faster and slower strain rates. At relatively high strain rates (above

10^{-2} per second) superplasticity has been observed in many alloy systems, including metal matrix composites, mechanically alloyed materials and alloys fabricated using powder metallurgy procedures, that have very fine grain structures (Valiev et al, 1993; Ghosh and Bieler, 1998). Relatively high strain rate superplasticity has become more and more attractive because it promises that complex engineering products can be formed more rapidly than by conventional superplastic forming. It has also been demonstrated that the temperature at which superplasticity occurs can be reduced by reducing the grain size to sub-micron. Several techniques have been developed to produce ultrafine grain structures, primarily using severe-plastic-deformation methods, such as equal channel angular pressing (ECAP), 3D forging, high pressure torsion (HPT) and accumulative roll bonding (ARB) (Sakuma, 1999).

2.2.1 Stress-Strain Rate and Flow Behaviour

Characterisation of stress-strain rate behaviour is usually made by a step strain rate test, in which a tensile specimen is successively deformed to a fixed amount of strain (usually 3~5%) at different strain rates and the flow stress at the fixed strain is strongly linked to the inelastic strain rate $\dot{\varepsilon}$ and more lightly to the strain ε and the grain size d. In order to evaluate the flow stress dependence on the strain rate the following empirical power law model is used (Arieli and Mukherjee, 1982; Ghosh and Hamilton, 1982; Pilling and Ridley, 1989; Rebelo et al, 1990; Kim et al, 1996; Cheng, 1996; Hwang et al, 1998; Carrino and Giuliano, 2001),

$$\sigma = K\dot{\varepsilon}^m \tag{2.1}$$

Where σ is the flow stress, $\dot{\varepsilon}$ the strain rate, K is a material constant and m the strain rate sensitivity index. K and m are functions of the strain, the strain rate, the grain size and the forming temperature. In Ashby and Verall model (Ashby and Verall, 1973),

$$K = Ad^p \exp(\frac{Q}{RT}) \tag{2.2}$$

Where A is a constant, d the grain size, p the grain size dependence coefficient ($0 \le p \le 3$), Q the activation energy for flow, R Boltzmann's constant and T the absolute temperature. In this model, superplastic materials are assumed to be ideally

rate sensitive (i.e., little strain hardening occurs during deformation) and have stable grain size, so that K remains relatively constant at the specific superplastic temperature. Equation (2.1) represents a linear relationship between the stress and strain rate in logarithmic space, this being a popular choice in many of the analysis programs owing to its simplicity (Rebelo et al, 1990; Kim et al, 1996; Cheng, 1996; Hwang et al, 1998; Carrino and Giuliano, 2001).

The strain rate sensitivity index m is commonly used as a measure of superplasticity, which is given by,

$$m = \frac{\partial \ln \sigma}{\partial \ln \dot{\varepsilon}} \tag{2.3}$$

If $m = 1$, the flow stress is uniquely related to the strain rate and the material behaves as a Newtonian viscous fluid like hot glass. For superplastic material behaviour, m is equal to or greater than 0.3 with the majority between 0.4 to 0.8. From the mechanical point of view, a higher value of m confers an excellent resistance to strain localization and leads to large overall elongation. In the range of strain rate where superplasiticity occurs, there exists an optimum value of strain rate and a corresponding optimum value of strain-rate sensitivity index. Superplastic

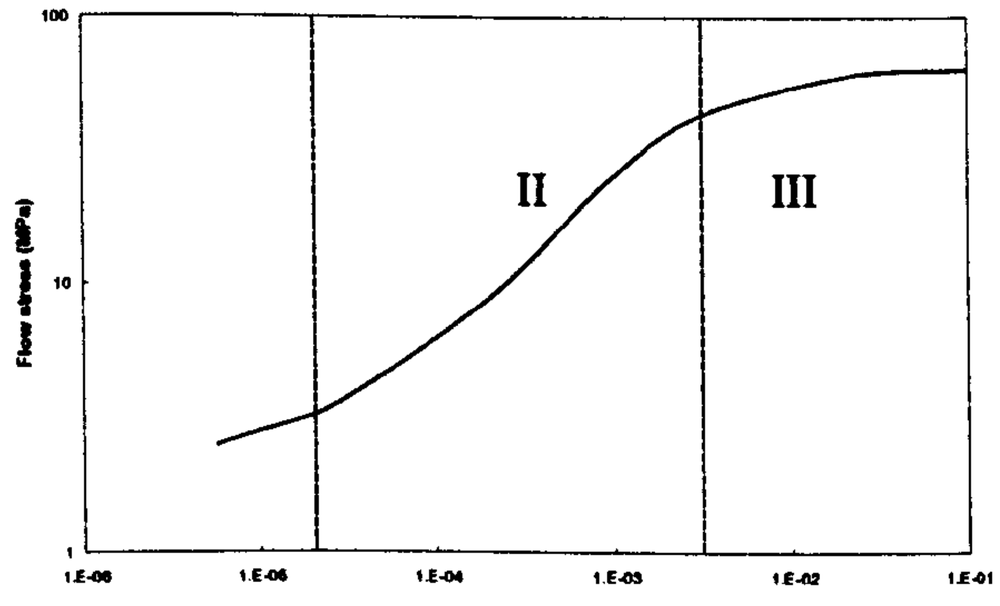

(a)

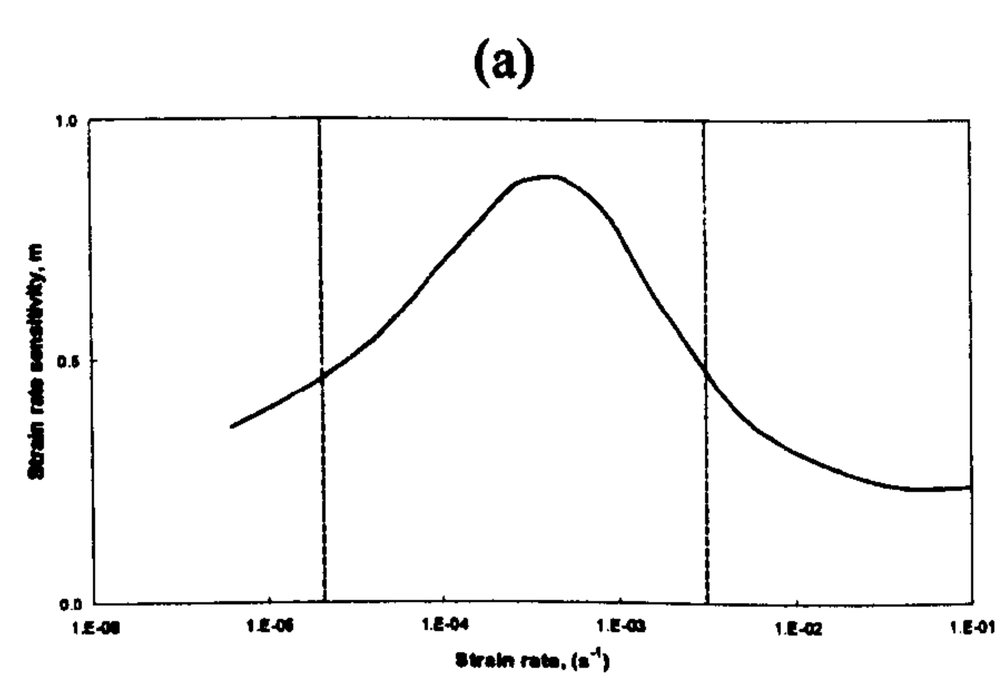

(b)

Figure 2.2 (a) Variation of the flow stress with strain rate (Pilling and Ridley, 1989);

(b) Variation of the strain rate sensitivity index m with strain rate (Pilling and Ridley, 1989)

deformation is characterised by low flow stress and high sensitivity of the flow stress to strain rate.

Several plausible hypotheses for the superplastic deformation mechanism in fine grain materials have been proposed such as grain boundary sliding and migration, grain rotation and rearrangement, and dislocation activity, yet none has been found capable of accurately describing both the mechanical and microstructural features of superplastic deformation. Grain boundary sliding (GBS) is currently believed to be the dominant strain producing mechanism during superplastic deformation. A typical relationship between the flow stress and strain rate is shown in Figure 2.2a, with the corresponding variation of strain-rate sensitivity versus strain rate shown in Figure 2.2b. As shown in Figure 2.2a, the sigmoidal shape of the flow stress versus strain rate can be divided into three regions, where different microstructural mechanisms dominate the deformation behaviour (Pilling and Ridley, 1989). Superplasticity occurs only in region II, where the strain rate sensitivity index m has a high value at moderate strain rates accompanied by a very large elongation. The deformation process in region II is not very well understood and no mechanism can fully describe the deformation in this region. However, it is believed that grain boundary sliding accompanied by diffusion or dislocation glide and climb is the dominant mechanism. Grain boundary sliding has been demonstrated experimentally by the offset of scratch lines on a sample surface (Beilei et al, 1998). The occurrence of grain boundary sliding is essential since it reduces the stress concentration developed at obstructions along the grain boundaries. Therefore, void nucleation and early failure can be prevented. In order to advance grain boundary sliding, special thermodynamic processes are normally undertaken in material processing to create and to distribute evenly the second phase, which inhibits grain growth. In this region, the crystallographic texture becomes less intense due to limited dislocation activities within the grain. In region III, the deformation mechanism is dominated by conventional recovery controlled dislocation creep, however, the deformation mechanism in region I is the subject of controversy.

2.3 Superplastic Materials

Since the discovery of the phenomenon of superplasticity, a large number of superplastic alloys have been made and this number will certainly increase with time. Eutectic and eutectoid alloys were amongst the first studied. For example, some eutectic alloys of Pb-Sn are superplastic at room temperature and are thus highly suitable for laboratory use. Eutectoid zinc-aluminium which is superplastic at about 250°C has also received considerable attention. In addition to eutectic and eutectoid alloys, other materials such as aluminium alloys, titanium alloys, zirconium alloys, nickel alloys, chrome steels and copper alloys have shown superplasticity (Hamilton and Paton, 1989; Weisert, 1984). In the last twenty years, the development of grain refinement has brought more material classes to the superplastic material group, such as ceramics, intermetallics and metal matrix composites. The diversity of superplastic materials has enabled researchers to exploit this property in a wide range of applications. A detailed review of all superplastic materials is not necessary. Therefore, the following review is limited to commonly used materials, such as titanium and aluminium alloys.

2.3.1 Titanium Alloys

Superplasticity in titanium alloys has been known for more than 30 years (Lee and Backofen, 1967). Titanium alloys exhibit good superplasticity, but they are expensive and difficult to fabricate into structural shapes by traditional forming and machining methods. Superplastic forming of titanium alloys can offer significant cost and weight savings in the fabrication of structural parts in aerospace applications because of their superior combination of strength, light weight, corrosion resistance and other metallurgical properties (Ezugwu and Wang, 1997).

Superplasticity has been observed in a range of titanium-based alloys, including Ti-6Al-4V, Ti-3Al-2.5V, Ti-6Al-4V-2Ni, Ti-6Al-2Sn-4Zr-2Mo, Ti-6Al-4V-2Co, Ti-8Al-1Mo-1V, Ti-13V-11Cr-3Al, γ titanium aluminide alloys etc (Semiatin et al,

1998). Among them, Ti-6Al-4V is the most commonly used titanium alloy, which accounts for over 45% of the total titanium production. Superplasticity in Ti-6Al-4V alloy was extensively studied (Ghosh and Hamilton, 1979, Paton and Hamilton, 1979, Agarwal et al, 1980, Boyer and Magnuson, 1979, Picksley, Hall and Pillinger,1994).

The superplastic behaviour of Ti-6Al-4V sheet under certain strain rate and temperature conditions was investigated by Lee and Backofen (1967), in which the most favourable conditions for superplastic forming of Ti-6Al-4V were found to be T=925°C and $\dot{\bar{\varepsilon}} = 10^{-4} s^{-1}$. Paton and Hamilton (1979) investigated the microstructural features of superplastic Ti-6Al-4V alloys, such as grain size, grain size distribution, grain aspect ratio, and crystallographic texture. It was reported that flow stress with a smaller distribution of grain size, is significantly lower than the alloy with a larger grain size distribution. Sastry et al (1983) also verified the effect of α grain size on the flow stress and m value dependence on strain rate in α/β Ti-6Al-4V alloy. It was found that a difference in α grain size of a factor of 2.5 led to differences in flow stress of about a factor of 2 and a difference in m values of about a factor of 0.5.

Another advanced material is the Ti-Al intermetallic compound, which is one of the most promising lightweight heat resistant materials. Several superplastic Ti-Al alloys with a wide range of aluminium contents, microstructures and degrees of microstructural refinement, have been tested over a wide range of temperatures and strain rates (Imayev et al, 1992; Cheng et al, 1992; Nobuki et al, 1994). For most of the materials, testing at the optimal strain rate resulted in a value of m between 0.4 and 0.8.

2.3.2 Aluminium Alloys

A number of aluminium alloys have demonstrated superplastic behaviour (Ghosh and Hamilton, 1982; Holt and Backofen, 1966; Matsuki et al, 1979). For example, Al-33% Cu eutectic alloy, one of the earliest alloys studied, can elongate up to 2000% at a temperature of about 500°C. Investigations of the superplastic properties of the

aluminium-copper eutectic alloy were made by Holt and Backofen (1966) and later by Johnson (1970). For this type of alloy, a very fine-grained micro-structure is stabilised by a fine and uniform distribution of Cu-Al_2 particles which results from the eutectic solidification followed by hot working process. However, the Al-33%Cu eutectic alloy is not attractive for commercial sheet forming application because of its poor mechanical properties at ambient temperature. Studies on aluminium alloys were performed on eutectic structures like Al-Cu, Al-Ca, Al-Si and Al-Pd, as well as on non-eutectic structures, such as Al-Cu-Mg, Al-Zn-Mg, Al-Mg-Si and Al-Mg-Zr (Nieh et al, 1997).

Ground breaking work was carried out by Grimes et al (1976) who developed Al-6%Cu-0.4%Zr (Supral 100) and Al-6%Cu-0.4%Zr-0.2%Mg-0.1%Ge (Supral 220) superplastic alloys. It is known that Zirconium can act as a grain refiner during the casting of aluminium, and it can also have a marked effect in inhibiting the recrystallization of aluminium alloys. The Supral alloys are of considerable significance and have resulted in a great deal of interest in superplastic forming of aluminium alloys. Typically an elongation of 1000% can be consistently obtained in these alloys. The exponent of strain rate sensitivity in these alloys is about 0.4~0.6, the flow stress is about 9 MPa at 480°C with a strain rate of $3\times10^{-3}s^{-1}$.

Progress in grain refinement techniques has enabled another high strength aluminium alloy of the Al7000 series Al-Zn-Mg-Cu to exhibit superplasticity. Wert et al (1981) reported that grain refinement in these alloys is possible through thermo-mechanical treatments. The fine grain size 7475Al alloy exhibits 1200% elongation at 516°C and a strain rate of $2\times10^{-4}s^{-1}$. It is worthy to note that Al-based metal-matrix composites and mechanically alloyed materials exhibit superplasticity at unusually high strain rates up to 0.1~1.0 per second (Nieh et al, 1997).

The potential for superplasticity in Al-Li alloys has received a great amount of attention from the aerospace industry because Li is one of only two elements (the other is Be) that simultaneously and significantly increase the elastic modulus and decrease the density of Al. For aerospace, improvements in specific modulus and specific strength can lead to weight saving. The optimum superplastic property found

in Al-Li based alloys, at a strain rate of $5\times10^{-3}s^{-1}$, is more attractive than those in the Al7475 alloy in which the optimum rate is only $2\times10^{-4}s^{-1}$. The high strain rate of superplasticity in the Al-Li alloys is clearly advantageous for commercial superplastic forming operations.

2.4 Superplastic Forming

Superplastic forming (SPF) refers to the manufacturing process that takes advantages of superplasticity to form complex parts. With SPF, sheet metals can be stretched to large elongations much greater than the limit that was previously possible (Sanders, 2001). Compared to traditional forming methods, superplastic forming technology offers the potential to reduce the weight and cost of structural components for applications. The main advantages of SPF are as follows (Ghosh and Hamilton, 1982):

1) Single step forming. Complex components are usually formed as final shapes in one step operation.
2) High material elongations.
3) Elimination of machining and assembly operations.
4) Weight savings in the order of 10%~40% because of the use of superior strength material.
5) Cost savings between 20% and 50% because of low die cost and reduction in the number of parts and processes.

Because of these advantages, SPF is becoming an important manufacturing technique in industries where weight saving is of critical importance, especially in the field of aerospace. For example, the European fighter aircraft makes use of many SPF parts, including sine-wave spars, auxiliary power unit shear walls, tank shear walls, doors, boxes, fire walls, and outlets. This has led to considerable commercial interest in the use of this technique to build complex, lightweight and integral airframe structures which eliminate detailed parts and assembly fasteners within the Boeing company (Sanders, 2001). A typical example of superplastic forming was reported by the Aircraft Division of the Northrop Corporation. The forward avionics lower deck assembly for the F-5E Tiger, conventionally requires 134 tools, 48 separate parts and

nearly 45 man hours of labour to assemble. With superplastic forming, only 8 tools and 5 parts can fulfil the same assembly in approximately 12 man hours (Sanders, 2001). Whilst SPF techniques have a widespread utilisation in the aerospace industry, they are scarcely applied in large scale production, such as in the automotive and transportation industries, due to a relatively low production rate and relatively high processing temperature required (Barnes, 2001).

Several superplastic forming techniques, including vacuum forming, blow forming, thermo-forming and superplastic forming/diffusion bonding (SPF/DB), have been employed in various industries, among which the blow forming process is the main subject in this research and is described in more detail in Section 2.4.1.

2.4.1 Superplastic Blow Forming Process

The superplastic blow forming process is one of the most commonly applied SPF processes to produce very complex, but light and strong, thin-walled components. Nowadays this technique has received more and more attention. Characterised by a multi-axial stress state, a gas pressure is usually applied to drive deformation.

A typical blow forming process is schematically demonstrated in Figure 2.3, in which the die and the sheet are normally maintained at the forming temperature during the whole process. A sheet is sealed around its periphery and a gas pressure is applied, at a controlled rate forcing the material to take the shape of the die pattern. The gas in the lower die chamber is vented to atmosphere. If necessary, a back pressure can be applied in order to suppress cavitations. During the process, the equilibrium of the sheet is dependent on the applied pressure, the material's mechanical properties and the boundary conditions imposed by the dies (Jovane, 1968).

In order to obtain high quality blow forming components, it is necessary to control process parameters precisely. Processing information normally includes: (a) forming pressure curve; (b) thickness distribution and thinning of the component after forming; (c) limit of uniform strain that can be attained before local failure occurs;

and (d) back pressure required to prevent cavitation damage. In industrial applications, a uniform strain rate is usually maintained within an optimum superplastic range by varying the applied gas pressure. The forming pressure curve can be determined either by trial and error or by analytical modelling methods. An optimum relationship between forming pressure, forming time and uniform strain rate will result in a strain rate sensitivity value of m close to the maximum. The higher the value of m, the better the formability.

The advantage with a blow forming technique is that neither moving die components nor mating die components are necessary. Large and complex parts can be readily formed using the blow forming process. Multiple parts can be formed in a single process cycle, thus production rate of some parts may be increased, though superplastic forming is recognised as a fairly slow process compared with conventional forming techniques (Barnes, 2001).

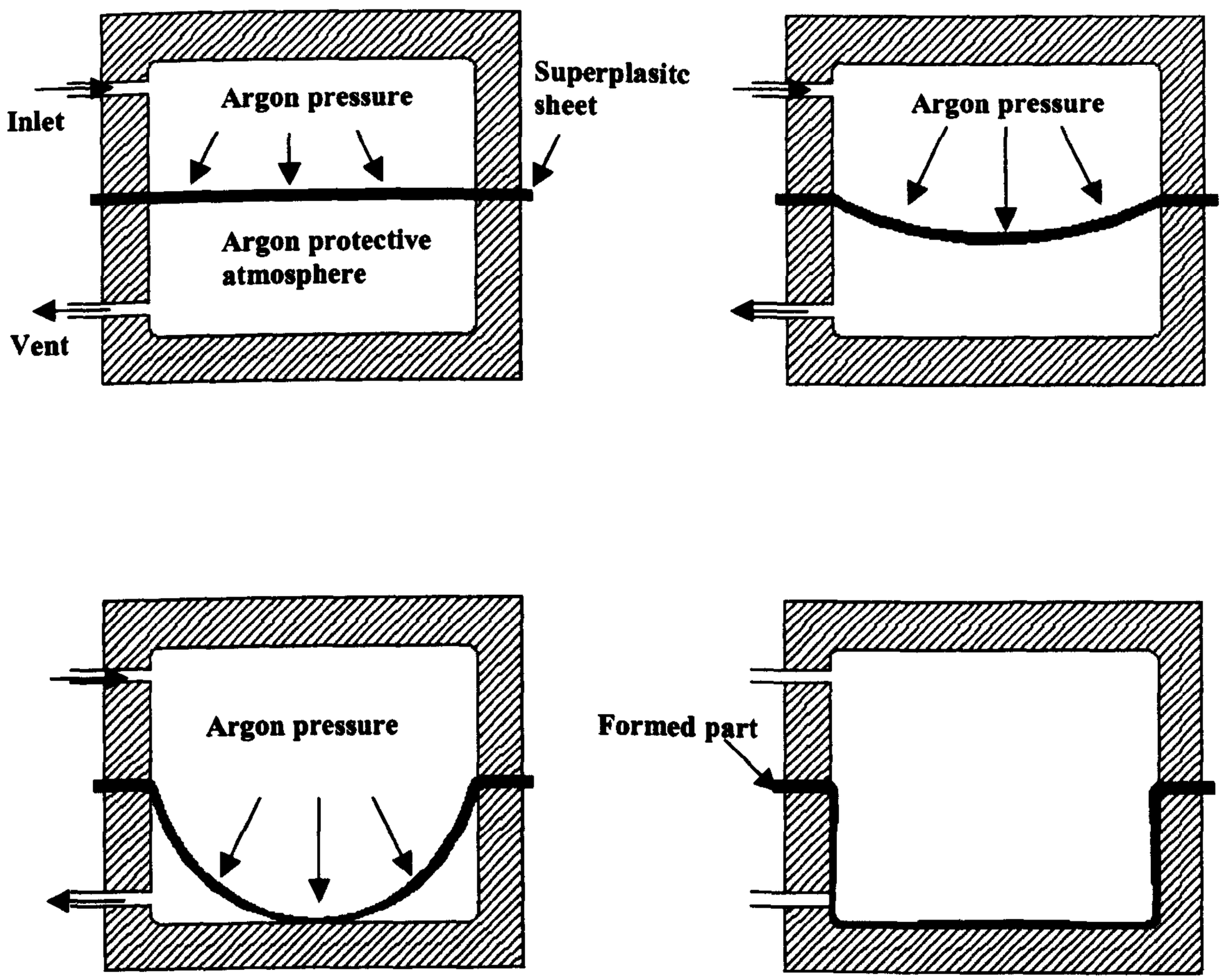

Figure 2.3 Schematic diagram of superplastic blow forming (Carrino and Giuliano, 1997)

2.4.2 Thinning

Superplastically formed parts typically experience a great amount of elongation during the process. As shown in Figure 2.3 in a bulge forming process, with the periphery of the sheet clamped, the material that lies in the die cavity is stretched to flow into the die geometry. The component is formed entirely at the expense of the sheet thickness. Therefore, thinning of the component takes place against frictional restraint from the surface contact between the sheet and the die. As the geometry of the product becomes more complicated, thinning becomes more severe. A non-uniform thickness distribution of SPF formed components is a common technical problem for the industry. It is undesirable because extensive local thinning affects forming limit, service performance and possibly leads to early failure of the components during the forming process (Phaipu, 1998). Therefore it is necessary to investigate the forming process to improve the uniformity of the thickness distribution.

When a sheet is formed into a die, different straining mechanisms take place in the two stages of the operation. During the initial stage where the material is formed under free bulging, the differential straining can be minimised if the material exhibits a high strain rate sensitivity of flow stress, and a high value of m is maintained throughout this stage (Ghosh and Hamilton, 1982). In the subsequent stage, as the material encounters the die, the thickness straining is locally restricted, but the remaining part of the sheet continues further thinning. The last part that comes in contact with the dies inherits the thinnest cross-section. Accordingly, the tendency to develop a dangerous thinning gradient increases as sheet thinning increases. Figure 2.4 shows the numerical thinning gradient for a cylindrical 8090Al-Li component cross-section with an initial 1.65 mm thickness blank (Hwang et al, 1997). It is clearly demonstrated that thicknesses at the edge of the die entry and at the centre of the die bottom are relatively greater than those elsewhere. The minimum thickness is observed at the bottom corner of the die. It is reported that the final thickness distribution of an experimentally formed rectangular part with an initial thickness of

1.68 mm, varied from 1.68 mm (flange) to 1.02 mm over the die radius and 0.64 mm in the corners where a maximum thinning of 62% was found (Pearce, 1991).

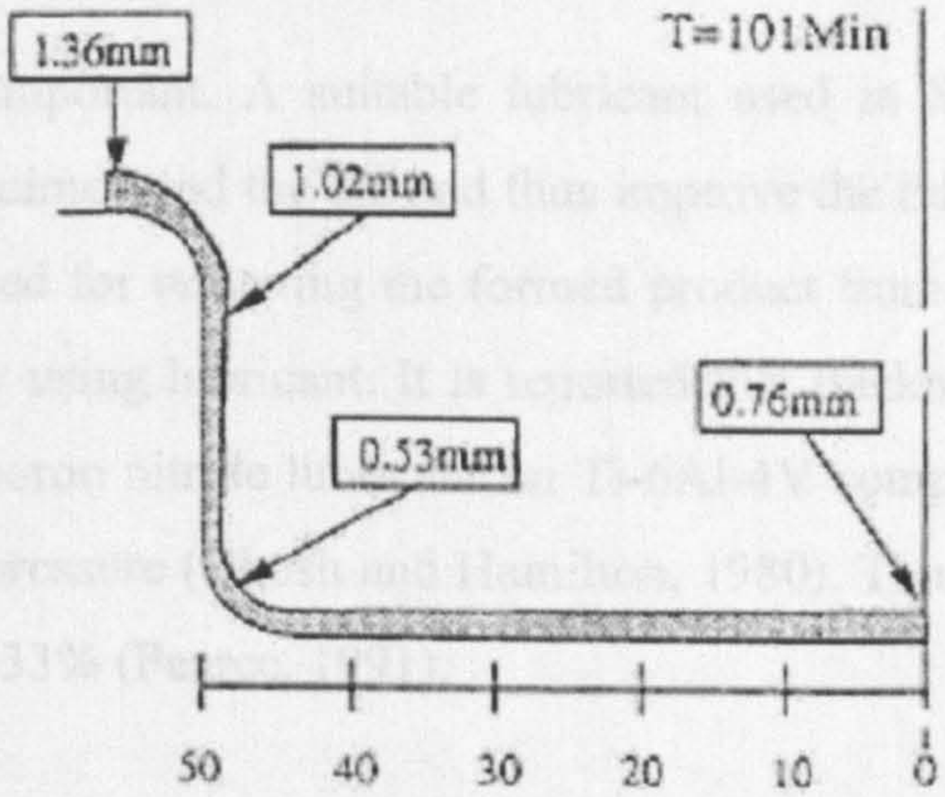

Figure 2.4 Thickness distribution of blow formed part (Hwang et al, 1997)

The thinning characteristic is strongly influenced by the forming method employed, associated die interactions and the material properties, especially the strain rate sensitivity of flow stress. To control the thinning of the formed component the following methods are often used in SPF fabrication:

- The characteristics of the material used;
- Optimal forming parameters such as pressure loading curve, forming strain rate, forming temperature to achieve a high value of m;
- Surface lubricant;
- Application of thermo-forming methods to control the localised deformation;
- Optimisation of blank thickness profile;
- Optimisation of process design.

The thermo-forming method has been shown to be an effective technique that can control the thinning gradients that occur in relatively deep and complex shaped components (Johnson et al, 1972). In addition, it is preferable to use a movable tool rather than only simple female forming. The movable tool is used to contact the forming sheet before the finished shape is produced, local friction minimises deformation in some locations, while the free-forming section continues to deform. Lee and Huh (2001) utilized such a technique, based on a male tool movement in

blow forming, and concluded that the moving die forming process can improve the thickness distribution.

Surface lubrication is important. A suitable lubricant used in SPF can reduce the friction between the specimen and the die and thus improve the thickness distribution. The ejection force needed for removing the formed product from the die can also be reduced significantly by using lubricant. It is reported that thickness distribution can be improved by using boron nitride lubricant on Ti-6Al-4V components with careful adjustment of forming pressure (Ghosh and Hamilton, 1980). Thinning in such a case was reported to be only 33% (Pearce, 1991).

The application of preformed or pre-machined sheets can be a solution to obtaining a uniform thickness distribution or sometimes thicker regions in the final product (Al-Naib et al, 1970; Johnson et al, 1972; Laylock, 1982; Takahashi et al, 1990). In this method the initial thickness variations in the plates can be used to offset the subsequent variations that result from the stress state and component geometry. The areas where excessive thinning occurs, can be compensated by more material so that a more uniform thickness profile in the final part can be obtained. Therefore, the major issue is how to design an optimal blank shape for near-net shape manufacturing, so as to predict the thickness distribution of the initial blank for superplastic blow forming or to predict the initial blank shape for minimizing trimming operations. Cheng (1994) proposed a procedure to design the sheet thickness profile of a hemispherical dome by combining finite element analysis and an analytical method. However, large errors were found due to the simplified assumptions made in the analytical solution. Huang et al (2000) investigated the optimized blank shape by combining numerical simulation and optimisation techniques. Two optimisation methods, i.e., gradient search and proportional control, were applied in the analysis. Similar optimisation work was carried out by Kim et al (2001), in which a weight parameter was introduced in order to simplify the multi-variable optimisation problem to a single-variable problem.

Pre-forming design in a multi-stage operation and shape optimisation of the die profile are process optimisation methods that avoid the need for machining the blank sheet. The methods involve the design of an intermediate geometry close to the final

shape, that result in a final product without defects and excessive loss of material. Akkus et al (1999) studied the influence of preforming design on the final thickness distribution of superplastically formed domes. A titanium alloy sheet was initially preformed to a "torus type" shape and then subjected to final hemispherical bulge forming. The experimental results confirmed that the final thickness distribution of the dome can be modified by preforming blanks. The geometrical parameters of the preforming play an important role on the final thickness distribution. Suzuki et al (2001) investigated a bulged hemispherical dome with uniformity of thickness by the application of a two-stage forming method. A truncated cone was superplastically formed at the first stage, and its bottom was re-formed to a hemisphere during the second stage. The shape of the preforming die was designed in order to obtain the uniform thickness distribution in the second stage.

2.5 Review of Superplastic Blow Forming Analysis

There have been a number of experimental, theoretical and numerical analyses published in the area of superplastic blow forming. In this section a detailed review of blow forming will be presented to draw attention to some important features of the blow forming of superplastic sheets.

Development of the blow forming technique and establishment of the theoretical background goes back to 1960s. Jovane (1968) was the first to study the blow forming process using a thin circular Pb-Sn sheet at room temperature. A uniform deformation theorem was adopted to analyze the relationship between the optimized pressurisation profile and the strain-rate sensitivity. This enabled analytical expressions, for the stress and strain state on the basis of membrane theory and elementary geometrical conditions to be obtained. However, the assumption that the sheet thickness was constant during deformation proved to be invalid from experimental results. Jovane himself observed substantial variations in the dome thickness from his study.

Cornfield and Johnson (1970) carried out a theoretical and experimental study of a thin circular diaphragm subjected to one-sided hydrostatic pressure. They considered

a non-uniform thickness distribution by introducing a thinning factor, $s/\bar{s}$, where s was the actual thickness and $\bar{s}$ the average thickness. It was assumed that the meridian stress was constant throughout the bulge while the hoop stress varied in a way which maintained a spherical bulge surface throughout its deformation. Their analysis resulted, however, in abrupt changes in the meridional stresses, which was not the case in reality.

Holt (1970) developed a simple mathematical model, relating the geometry of the formed sheet to certain material parameters. The thickness distribution and the bulged profile were predicted as a function of the forming pressure, forming time, geometry, material constant K and strain rate sensitivity m. However, Holt's analysis was based on an assumption that the circumferential and tangential stress and strain state were "balanced biaxial" which was only true at the pole of the bulging sheet.

An analytical equation was presented by Tang and Robbins (1974), which was used to describe the relationship between deformation and time for tin-lead alloys. The bulge was assumed to remain spherical and its thickness distribution varied according to a linear thickness relationship. However, it was reported by Bandon (1979) that the profile is not part of a sphere when the strain-rate sensitivity of the material is less than 0.5. Ragab (1983) also stated, on the basis of experimental results, that the assumption of the profile being part of a sphere was not valid during the early stage of bulging.

Starting from the 1980s, researchers re-examined the Holt model (1970), revising the assumption of a balanced biaxial stress state throughout the dome profile to a balanced biaxial stress state at the dome apex and a plane strain state at the periphery. Most of the interest has concentrated on the investigations of thickness distribution, the bulged profile, forming pressure, forming time, and the effect of variation in the strain rate sensitivity m on bulged shapes. Based on the new assumption, Ghosh and Hamilton (1980) explored the effects of the thickness of the sheets and the shape of the die on the optimized pressurisation profile during blow forming with a long rectangular box die. Ragab (1983) investigated the thickness distribution under a cylindrical or conic die with a sticking model proposed for the contact between the

sheet and the die. However, the thickness distribution predicted from Ragab's model was only dependent on the dimensions of the dome but not on the m value, which does not agree with experiments.

A model (Guo et al, 1988, Guo and Ridley, 1989) was proposed for the blow forming of a dome under constant pressure or constant apex strain rate, which incorporated dome thickness variation with m value, grain growth and dome height. Experimental work was carried out to compare with the analytical results. Later Chandra and Kannan (1992) developed a closed-form equation for the pressure-time loading and thickness distribution in blow forming of a generalized cup. Yang and Mukherjee (1992) assumed an elliptical bulge profile, a relationship for the aspect ratio and a constant polar strain rate in order to achieve a reasonably general axisymmetric analysis for the calculation of an optimum pressure cycle.

Dutta and Mukherjee (1992) extended the uniaxial model to multi-axial loading using the effective stress and strain. A constant effective strain rate was formulated in the new analytical model validated by experiments (Dutta and Mukherjee, 1992). Lee et al (1998) presented another modified model incorporating the grain growth rate during the biaxial bulge forming. Bulge forming experiments of fine grain Ti-6Al-4V alloy sheets at different strain rates were conducted to verify the thickness distribution predicted from the modified model.

All of the above analytical models for superplastic blow forming are based on various assumptions regarding the behaviour of the forming sheet. These algorithms are generally restricted to balanced biaxial stress and plane strain state. The deformation is calculated based on the uniform, non-uniform or logarithmic rate of thinning. Moreover, all these simplified analyses are only valid for simple geometries and the important effect of friction contact between the sheet and the die is seldom taken into consideration. Numerical analysis has emerged as the most potent technique for modelling the superplastic forming process, especially for components with complicated shapes. In particular the finite element method (FEM) has shown a great ability to simulate the superplastic deformation process. This can provide direct

information and guidance in reducing the number of tests, or even in eliminating the need for expensive trial-and-error testing.

A general overview of the numerical simulation of superplastic forming can be found in many references (Chandra, 1988; Bonet et al, 1990; Bonet, Bhargava and Wood, 1994; Wood, 1996). Some recent developments in the field of numerical simulation of superplastic blow forming are described as follows.

Zhou et al (1988) modelled the non-uniform bulging deformation to failure using a viscoplastic finite element method, in which the evolution of cavitation, the influence of both strain rate sensitivity and cavity growth rate were investigated. Chandra and Chandy (1991) further developed a computational model using a membrane element for the superplastic forming of a plane strain box. A Lagrangian finite-element formulation combined with the directional reduced integration scheme was presented by Huh et al (1995). The formulation was associated with a contact algorithm and a pressure control algorithm to predict the optimum pressure cycle and the corresponding deformed shapes in the superplastic blow forming.

Kim et al (1996) simulated the blow forming of thin sheets into various geometries using an incremental rigid-viscoplastic finite element analysis. Two-node membrane elements for both axisymmetric and plane strain cases were employed with a Newton-Raphson non-linear solution scheme. A modified Coulomb friction law was used to model the interfacial friction between the sheet and tool. Li et al. (1996) studied a peripherally clamped circular sheet inflated into a cylindrical die using a rigid-viscoplastic finite element method, in which the interface-friction effect was introduced in the form of a friction function. The effect of loading control of variable strain rate in blow forming was conducted by Ding (1997). An adaptive algorithm to control the bulging pressure, proposed by Xing and Wang (1997), was used to investigate the effects of cavity growth and distribution.

Chen et al (1999) found that the discrepancy in experimental and previously predicted thickness profiles of a bulged workpiece might be due to the simple treatment of the friction coefficient value between the sheet and the die. Different friction coefficients

at different contact regions were therefore simulated, and the predicted thickness distributions were compared with the experimental results. It was found that experimental thickness profile fit best with the prediction obtained using a friction coefficient of $\mu = \infty$ (i.e., nearly complete sticking) at the die entry and $\mu = 0.01$ (i.e., nearly complete sliding) at the bottom region. Although an infinite (i.e., $\mu = \infty$) or zero friction coefficient is physically impossible, the conclusion was explained as follows. In a practical SPF operation, it was usually found that lubricant powders would slide down along with the deformed sheet, from the die entry down to the bottom centre. Gradually, almost no lubrication was present at the die entry (hence $\mu \to \infty$) and nearly complete lubrication and free sliding at the central bottom region (hence $\mu \to 0$).

In summary, most of the SPF simulations employ a viscoplastic or rigid-viscoplastic flow formulation to model the superplastic material as isothermal, incompressible and non-Newtonian viscous (Zhou et al, 1988; Chandra and Chandy, 1991; Huh et al, 1995; Kim et al, 1996; Li et al, 1996). Using such a flow formulation, the elastic effect of the material is neglected and the integration of velocities is involved in conjunction with a non-linear solution scheme, in order to calculate the changing shape of the component as forming progresses (Zienkiewicz et al, 1978; Zhang et al, 1986; Chandra, 1988; Bonet et al, 1990; Kim et al, 1996). Various control algorithms of the pressure versus time cycle have been developed to achieve optimal superplastic forming (Chandrasekaran et al, 1985; Bate et al, 1993; Bonet et al, 1994; Huh, 1995, Ding, 1997; Xing and Wang, 1997). A common strategy for estimating an optimised pressure history is to adjust the pressure load applied to the finite element model to maintain the maximum strain rate at a target value throughout the forming cycle (Bonet et al, 1990).

Three types of element, i.e., membrane, shell and continuum, have been employed in the finite element analyses of the superplastic blow forming (Bonet and Wood, 1987; Chandra, 1988; Bonet et al, 1990; Rebelo et al, 1990; Chandra and Chandy, 1991; Chenot and Bellet, 1992; Kim et al, 1996; Li et al, 1996; Xing and Wang, 1997; Lee and Huh, 2001). However, the question of which element is the most suitable for the

simulation of superplatic blow forming remains unanswered. This topic will be addressed in an element study in Chapter 5.

The friction interaction between the die and the workpiece in superplastic blow forming is usually modelled by a standard Coulomb friction model (Chanderasekaran, 1985, Hartley, Pillinger, Hall and Sturgess, 1992). Although different contact regions have different friction coefficients in practice, a uniform friction coefficient is generally specified in most of the simulations (Kim et al, 1996; Li et al, 1996; Xing and Wang, 1997; Lee and Huh, 2001). A simple treatment of friction coefficient resulted in the discrepancy between experimental results and numerical predictions (Chen et al 1999). The fundamental problem is attributed to the fact that there is no methodology readily available to measure the friction coefficients at different contact regions in a superplastic blow forming process. Previous researchers had to determine the friction coefficient by iteratively changing the value of friction coefficient in the finite element program until the best fit of the experimental result was obtained (Kim et al, 1996; Hwang et al 1996, 1997, 1998). It is impractical to determine the friction coefficients at different contact regions using the same iterative method. Therefore, it is necessary to develop a methodology to study the friction behaviour at different contact regions because friction is a very important factor affecting thinning or even rupture in SPF products.

The ability to control the superplastic blow forming so that a maximum strain rate is generally maintained is a primary goal for the numerical analysts. Of crucial importance is the prediction of the final thickness distribution, the pressure cycle, contact and friction necessary to achieve successful forming of complex components. These issues have been addressed in the following chapters.

2.6 Summary

As a commonly used superplastic forming method, the blow forming technique has undergone rapid development and application in recent years. Although a number of analytical models and finite element analyses of blow forming were published, almost

all the work carried out to date has been limited with regard to the optimisation of process control and the formability behaviour of superplastic materials. The investigation and control of thinning characteristics due to the high elongation occurring in superplastic deformation can provide very useful information for product quality in manufacturing industry. In addition, there are still some major concerns on the practical application of the blow forming technique which need to be addressed, for example, the friction behaviour during the forming process is a very important factor affecting thinning or even rupture in SPF products. This topic needs addressing and is thus poorly understood. Therefore, one of the main objectives of this research is to study the frictional mechanism in the blow forming process. A detailed review of friction studies is presented in the following chapter.

Chapter 3

Review of Friction in Superplastic Forming

3.1 Introduction

A good understanding of frictional behaviour will provide vital information for process design and product quality, as friction plays an important role in determining and controlling material deformation. Due to the unique characteristics of superplastic blow forming, conditions under which friction takes place are quite different from other metal forming processes. To clarify the scope of the work undertaken in this project, it is necessary to review the previous work completed on friction. In the following sections, a detailed description of friction theories including friction mechanisms and friction models is presented. Attention is then directed toward a broad review of all kinds of friction tests in metal forming processes to explore a systematic view of the often isolated experimental methods. A brief review on frictional measurements in a superplastic blow forming process is finally presented.

3.2 Friction Theories

Friction is technically defined as the resisting force tangential to the common boundary between two bodies when, under the action of an external force, one body moves or tends to move relative to the surface of the other. Tabor (1981) in his plenary lecture titled "Friction: The Present State of Our Understanding" at the 1980 ASME-ASLE International Lubrication Conference, emphasized that the three major elements of the friction process are: the true area of contact, the nature and strength of

the interfacial bonds and the way in which the contacting materials are sheared and ruptured.

In this section, basic friction theories relating to the friction mechanisms and friction models are generally described. It is aimed to discuss the general principles applicable to a theory of friction and allow a more systematic view of the often isolated observations. Although most of the basic information has always been generated in non-metal forming fields, much of it is essential for understanding the phenomena that govern the various metal forming processes.

3.2.1 Friction Mechanisms

Many researchers have produced theories to explain the physical mechanisms of friction. Some of the more prominent frictional mechanisms that have been proposed to explain the nature of dry friction are summarized in this section. More comprehensive reviews on this subject can be found in references (Schey, 1970; Tabor, 1987; Williams, 1994).

The pioneering work of friction can be traced back to Amonton (1699) and Coulomb (1785) who stated that the basic laws of dry friction are such that, 1) the friction force is proportional to the normal load between the surfaces; 2) the friction force is independent of the apparent contact area. A number of friction mechanisms, such as adhesion, mechanical interaction of surface asperities, ploughing of one surface by asperities on the other, deformation and fracture of surface layers etc., have been recognised (ASM Metal Handbook, 1992). These mechanisms will act simultaneously but they may occur in different circumstances.

The first friction mechanism, i.e., interlocking theory, was developed by Coulomb (1785), in which it was assumed that minute surface asperities were interlocked, and the work required to raise the load over their summits, caused the frictional resistance. Later the theory was further developed by Hardy (1936), stating that the frictional forces were due to short range molecular attraction acting across the area of contact.

The best known theory of dry sliding friction, "welding, shearing and ploughing theory", was proposed by Bowden and Tabor (1942). It is based on the fact that even the best surface finish is not flat and smooth on a molecular scale. This theory proposes that extremely high pressure is developed over minute areas of contact, which are sufficient to cause localised plastic flow and adhesion of the surfaces. The frictional force can be identified with the force required to break the welds formed at the points of contact "Welded junctions". In this case plastic flow and adhesion are the primary phenomena leading to subsequent shearing resistance to the relative motion.

The welding theory originally was recognized to be oversimplified. A great deal of attention has been directed toward amplification of details of the process and toward the development of more exact theories. Feng (1952) proposed a modified welding theory. Suggestions were made that the primary phenomena are plastic flow and mechanical interlocking due to matching of the surfaces following plastic deformation, as shown in Figure 3.1, where W is the pressure to cause the contact and F the friction force. This is followed, when relative motion takes place, by shearing and adhesion. Mechanical interlocking and the accompanying strain hardening cause breakage a certain distance away, and the resulting fragment is welded to the other surface. Thus, welding of a fragment is considered a consequence of friction, whereas the original welding theory considers welding as the source of friction.

Mcfarlane and Tabor (1950) proposed that the adhesion mechanism was incomplete and pointed out the great importance of tangential movement. It is assumed that when two surfaces are placed in contact, an infinitely small tangential force is required to initiate movement between them, since the junctions are already plastic under the applied load. As relative motion proceeds, the region of contact grows with a corresponding increase in the tangential force and the adhesive force. A state is finally reached where the tangential force increases more rapidly than the rate of growth of the region of contact and sliding on a macroscopic scale then occurs.

Green (1955) and Edwards and Halling (1968) developed a theory which was based on asperity interaction and deformation. This mechanism was concerned with the

force necessary to overcome friction between the two surfaces, which was the value required to plastically deform the asperities, so they could pass over each other.

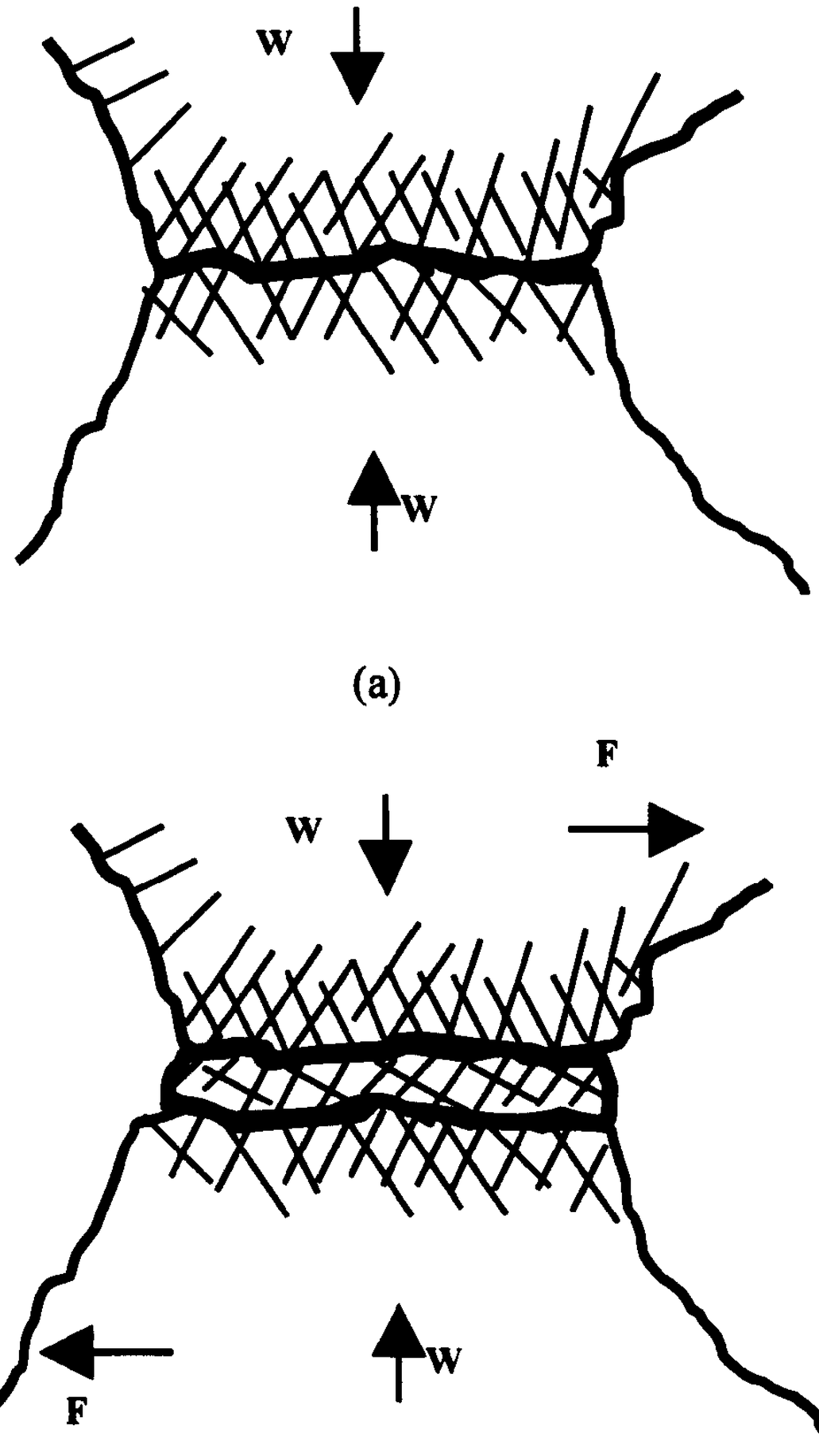

Figure 3.1 (a) The roughened interface because of plastic deformation,
(b) The roughened interface because of the mechanical interlocking (Feng, 1952)

The previously described principles apply primarily to contact in which the normal pressure applied to the surface is low. This means that the bulk of the material is still elastic. However, it is not the case in metal forming, in which the normal pressure may be very high, sometimes reaching four times the current yield stress of the material (Schey, 1983). Hence, the principles which have been previously described do not fully describe the frictional phenomena at high pressure, because the asperities at the surface are considered to deform in isolation. This does not hold for high pressure as the asperities are subjected to a large amount of flattening and the

deformations of neighbouring asperities interact with each other as well as with the underlying bulk material. However, the previous theories for friction mechanisms should not be disregarded as the principles may still be applicable to some degree at higher levels of pressure.

3.2.2 Friction Models

Although extensive research has gone into explaining the mechanisms of friction, it is of no use to engineers without an appropriate analytical friction model which can be used for calculations or for numerical analysis. The accuracy of a calculation or a simulation is often dependent upon the choice of a relevant and accurate friction model. A friction model is always dependant upon its contact algorithm and can be defined as a model giving the friction shear stress as a function of relevant parameters.

It is of course desirable to devise a model which contains all the parameters but this in itself is very difficult. In fact it can be said that current research is a long way from achieving a friction model which is effectively constitutive in that it covers many parameters, i.e., similar to the equations in existence for material models.

The first model for explaining friction in a simplistic manner was proposed by Amonton (1699) and Coulomb (1785), i.e., $\tau = \mu q$. The model states that the frictional shear stress τ is proportional to the normal pressure q applied and the coefficient of friction μ does not depend on relative slip velocity.

However, in practice the use of the constant coefficient of friction is confined to low normal pressure ($q/\sigma_0 < 1.5$), where the deformation of each asperity is considered in isolation. Amonton's law (1699) is applicable under this condition. However, in metal forming processes the pressure at the contact interface between the tool and the workpiece is frequently large in magnitude, and the assumption of isolated plastic deformation does not apply. The asperities are subjected to large amounts of flattening and the deformations of the neighbouring asperities interact with each other as well as with the underlying bulk of the material.

Orowan (1943) was among the first to point out the inconsistency in applying the Amonton model at high pressure, and subsequently proposed his friction model. In Orowan model, the friction stress is equivalent to the Amonton model at low normal pressure which is proportional to interface pressure until a critical value of interface pressure is reached; above the critical pressure, the sticking friction stress is constant at high normal pressure. The Orowan model showed that the product of the coefficient of friction μ and the normal pressure cannot become greater than the shear stress of the material. Therefore it is expressed by

$$\tau = \mu \tau_y \tag{3.1}$$

where μ is the frictional shear factor which has a value $\mu = 0$ for a frictionless interface and $\mu = 1$ for sticking friction, and τ_y is the yield shear stress. Shaw et al (1960, 1963) gave a more precise explanation, stating that the real area of contact between the surfaces increases with increasing normal pressure, approaching the apparent contact areas asymptotically since very high pressure will be needed in the last phase.

The work of Wanheim and Bay (Wanheim, 1973; Wanheim et al, 1974; Wanheim and Bay, 1978) has shown that neither of the two models is valid as a complete friction model and some research work has been carried out focusing on combining the two

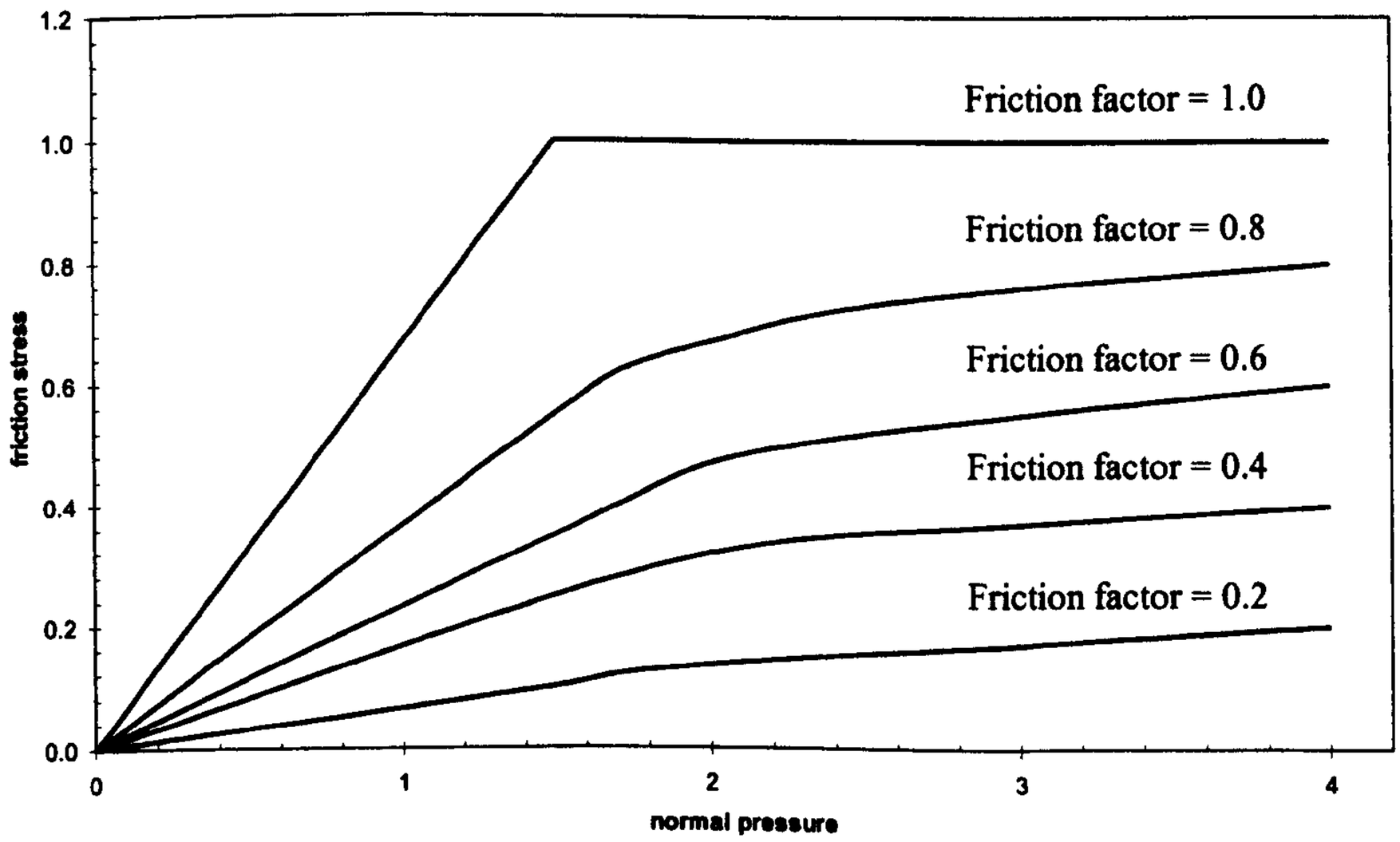

Figure 3.2 Friction model by Wanheim and Bay (1978)

models. Among them, the model proposed by Wanheim and Bay (1978) is often used as shown in Figure 3.2. This model indicates a smooth transition from the Coulomb friction model to a friction factor model with an added transitional range. Friction is assumed to be proportional to the normal stress at low normal pressure level (normal pressure <1.5), but it is towards a constant value at high normal pressure level (normal pressure >3). The Coulomb friction and the friction factor models are linked by the fractional real contact area in the form of

$$\tau = f\alpha\tau_y \tag{3.2}$$

Where f is the friction factor and α the ratio between the real and apparent area of contact. Figure 3.3 shows schematically the interface between a specimen and die. The real area (microscopic) A is the summation of all the localised contact areas ($\sum dA_i$), while the apparent area (shown in Figure 3.3 as apparent) is the macroscopic area, which can be seen by the human eyes.

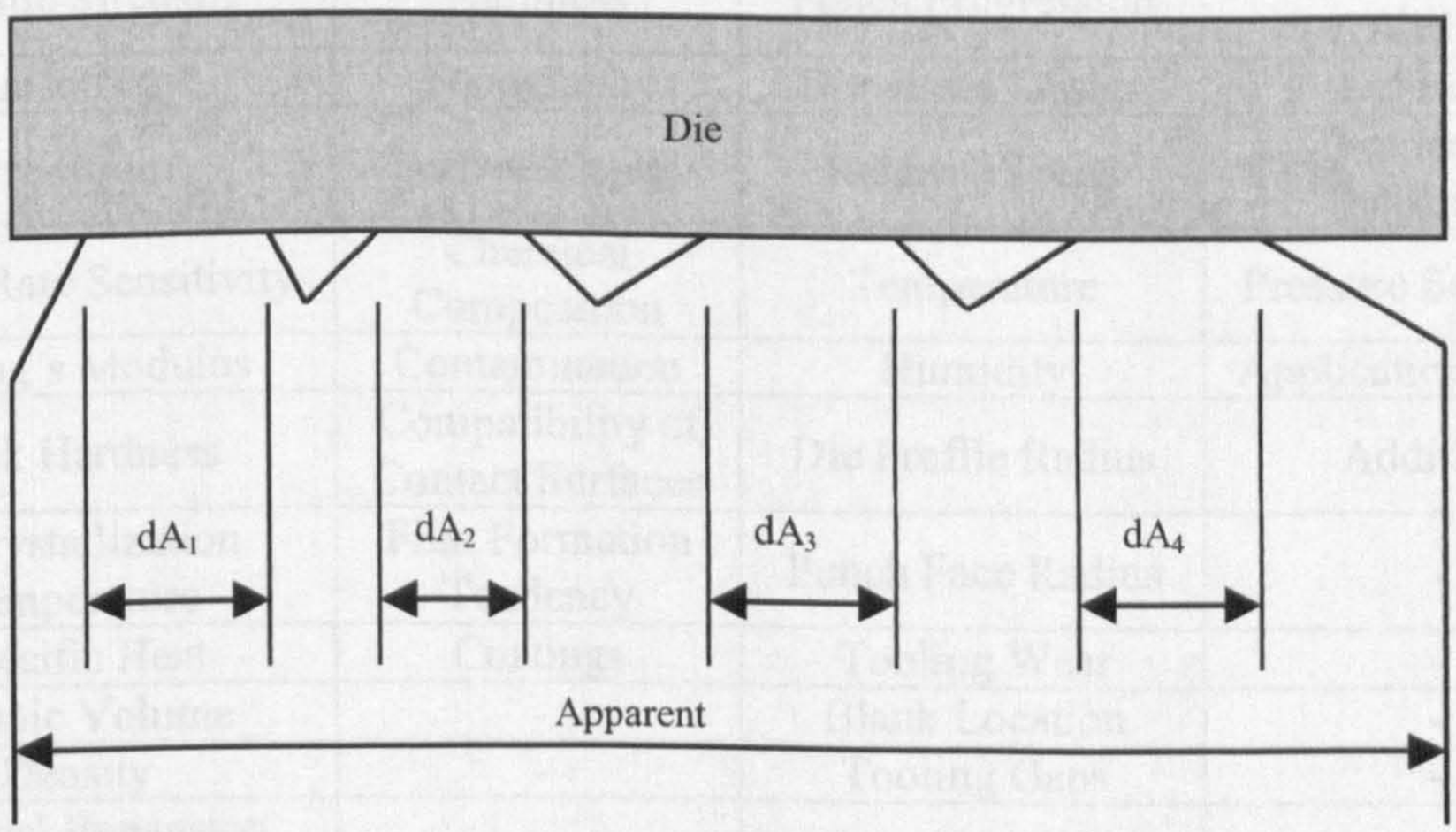

Figure 3.3 Definition of the ratio between real area ($\sum$dAi) and apparent area (Wanheim and Bay, 1978)

3.3 Friction in Metal Forming Processes

Friction is an important or even dominating parameter at the tool-workpiece contact interface in a metal forming process. Friction exerts a vital influence on workpiece

flow, form filling, strain distribution and total load as well as local tool stress. The workpiece usually experiences large plastic deformation and entirely new surfaces are created in metal forming operations. The frictional mechanism in the metal forming process, as described by Schey (1983), is a very complex subject because it is a complicated function of material properties and process parameters. A detailed list of parameters that can affect the frictional behaviour is shown in Table 3.1 (Lenard, 1991). These variables interact with each other constantly during forming processes so that friction is affected by the process in a complex way. The complexity of frictional phenomena occurring in the metal forming process is in contrast with the simplicity of friction models available in the literature. Until now, it has been impossible to construct a suitable friction model that includes all these parameters.

Table 3.1 Properties that affect friction during forming processes (Lenard, 1991)

Tooling and Workpiece Properties	**Surface Properties**	**Process Properties**	**Lubrication Properties**
Yield Strength	Roughness	Die Face Design	Viscosity
Tensile Strength	Hardness	Punch Progression	Bond-Forming Ability
Anisotropy	Topography	Drawbead Design	Lubricant
Pre-Strain	Surface Energy	Relative Speed	Temperature Sensitivity
Strain Rate Sensitivity	Chemical Composition	Temperature	Pressure Sensitivity
Young's Modulus	Contamination	Humidity	Application Method
Bulk Hardness	Compatibility of Contact Surfaces	Die Profile Radius	Additives
Recrystallization Temperature	Film Formation Tendency	Punch Face Radius	-
Specific Heat	Coatings	Tooling Wear	-
Atomic Volume	-	Blank Location	-
Density	-	Tooling Gaps	-
Thermal Expansion Coefficient	-	'Dirt' Pick-ups	-
Melting Temperature	-	-	-

3.4 Friction Tests

In order to study the behaviour of friction within a specific process it is necessary to devise a test which can successfully evaluate the friction phenomena. Due to the

different characteristics of each forming process, a great variety of measurements have been developed to undertake frictional investigations in metal forming. In order to utilize the experimental results in the simulation and production process, several criteria must be satisfied in the design of the friction test. First of all, conditions under which the experiment is carried out should stay as close as possible to those in production. These conditions include forming temperature, contact pressure, strain, strain rate, tool geometry, lubrication, sliding velocities etc. Secondly, a correct friction law should be chosen to quantitatively calculate frictional effects from the experimental data. Finally, the friction coefficient should be obtained independently and directly from the experimental data. Not only the mean values, but also the variation of the friction coefficient during the forming process should be measured and evaluated. Some other factors should also be taken into account in the design of a friction test. For example, the device should be cost efficient and easy to operate in both laboratories and workshops.

Direct measurement of friction forces by embedding pin or strain gauge technique (Van Rooyen and Backofen, 1960; Pearsall and Backofen, 1963; Al-Salehi et al., 1973; Lim and Lenard, 1984, Fletcher et al, 1998) seems very convenient from an engineering point of view since detailed information on the distribution of interfacial frictional shear stresses can be obtained by these methods. However, any direct interference with the contact area affects the tribological system and consequently the measured variable (Doege and Bederna, 1994). Moreover, for hot metal forming processes, the forming temperature may be in excess of 1200°C, which makes the direct measurement task even more daunting (Petty, 1994). Complicated test rigs were developed to directly determine the friction coefficients under high temperature at National Physical Laboratory (NPL) (Brooks and Loveday, 2000).

Indirect measuring methods make use of a derived process variable such as forming force or specimen deformation or other indirect indices to determine friction conditions. Most of the current indirect friction tests are designed to embody specific tribological aspects. They can be broadly classified into two categories, namely: 1) simulative test; 2) engineering test. In particular, simulative tests are not practical deformation processes but are designed to embody specific tribological aspects. They

only simulate the tribological conditions under controlled circumstance in which the main parameters are well defined as shown in Table 3.2.

Table 3.2: Simulative friction tests

Simulative Friction Tests	Reference
Pin-on-Disk	Schey, 1983, Brooks and Loveday, 2000
Twist Compression	Schey, 1983, Flether et al, 1998
Ridge Ploughing	Bay and Hansen, 1985
Compression with Simultaneous Sliding	Schey, 1983, Tan, 2001
Special Forging	Schey, 1983, Wolff, 2001

Engineering tests on the contrary can be described as tests which are representative or analogous to an actual process, as demonstrated in Table 3.3.

Table 3.3: Engineering friction tests

Process	Engineering Friction Tests	Reference
Extrusion	Double Cup Extrusion	Sanchez et al, 1985, Barcellona, 1995
Rolling	Forward Slip Measurement	Capu & Cockcroft,1964, Beynon, 2000
Drawing	Drawing with back Tension	Lunt & Maclellan, 1946, Siegert, 2000

3.4.1. Simulative Tests

The pin-on-disk test using a flat pin or hemispherical pin end has been investigated by several researchers. The level of friction was evaluated in these tests by measuring the normal force P and lateral force F. A flat-ended pin riding on a flat surface as shown in Figure 3.4 (a) provides an ostensibly constant apparent area of contact, but the

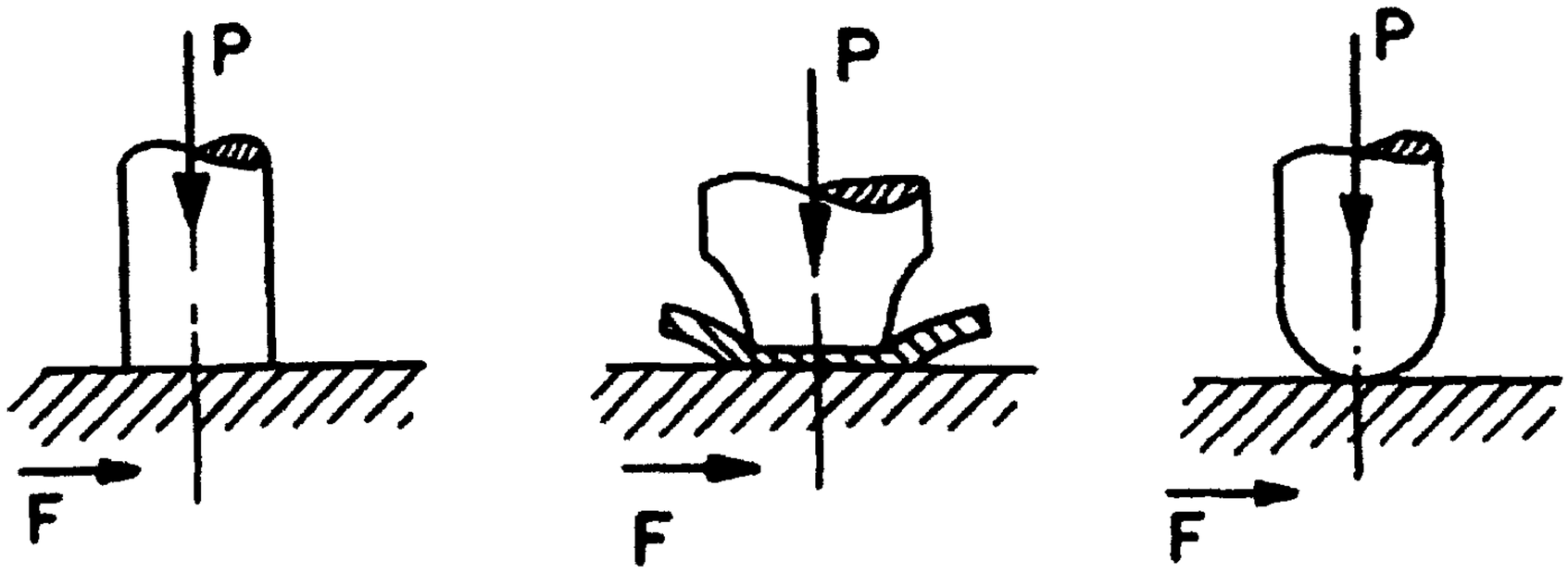

(a) (b) (c)

Figure 3.4 Pin-on-disk test (Schey, 1983)

slightest cocking of the pin – resulting from elastic deflection in the supporting members – is bound to cause localized contact and plowing. Peterson and Ling (1966) used a variant of the test by compressing a thin sheet of the specimen material between a flat anvil and a punch as shown in Figure 3.4 (b). Much more practical is a pin with a hemispherical end as shown in Figure 3.4 (c). The pin may be allowed to penetrate deeply into the specimen surface without basically altering the contact condition. A novel pin-on-disc high temperature friction apparatus, developed at National Physical Laboratory, heats strip samples up to 1000°C in a few seconds using a DC electrical current. The sample may then be rapidly brought into contact with a rotating disc of tool steel using a motorised drive mechanism, with transducers measuring the resultant normal and lateral forces (Brooks and Loveday, 2000). The pin-on-disk can be characterised as a low pressure test, with its usefulness associated with simulating conditions when the tool material meets the new workpiece. However, if there is adhesion or cohesion, it will need to be load controlled rather than displacement, i.e., the need to know when there is sufficient load to initiate movement.

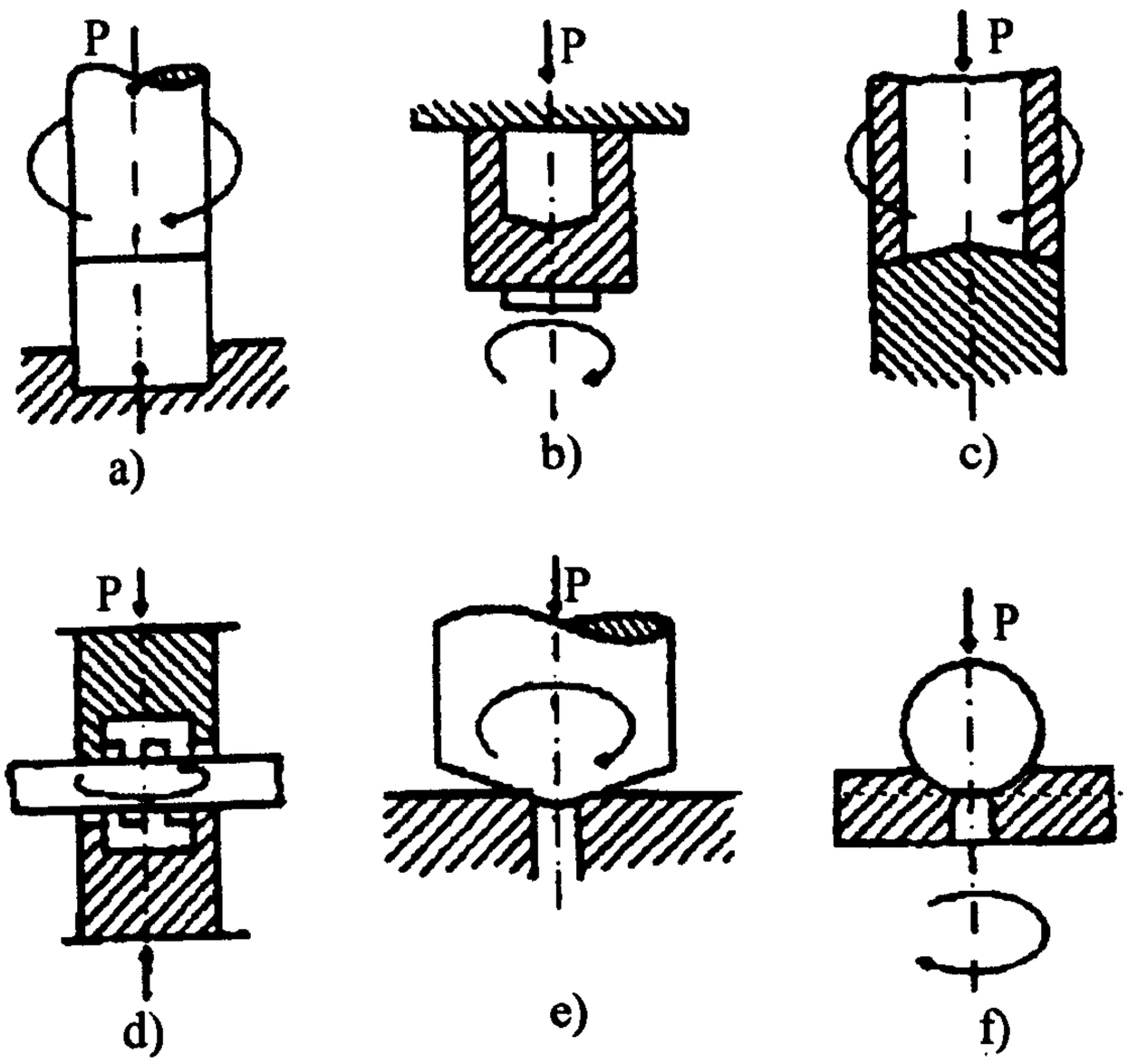

Figure 3.5 Twist compression test methods (Schey, 1983)

The twist compression test involves a ring or a stud of specimen material, pressed and rotated over the same tool surface. There are several different versions of the test which have been used by various researchers (Schey, 1983), as demonstrated in

Figure 3.5. All the tests require the resultant torque and normal force measured in order to evaluate the coefficient of friction, which is calculated by the expression of $\mu = T/rP$, where T is the torque, r the radius of the ring or stud and P the normal force.

In the ridge plough test, shown in Figures 3.6 (a) and 3.6 (b) (Schey, 1983), local plastic deformation of the smooth specimen surface is obtained by a wedge-shape tool. The tool geometry is designed so that ploughing is obtained. This type of test will produce normal pressure about twice the flow stress but the surface deformation is small, hence limiting the application for metal forming.

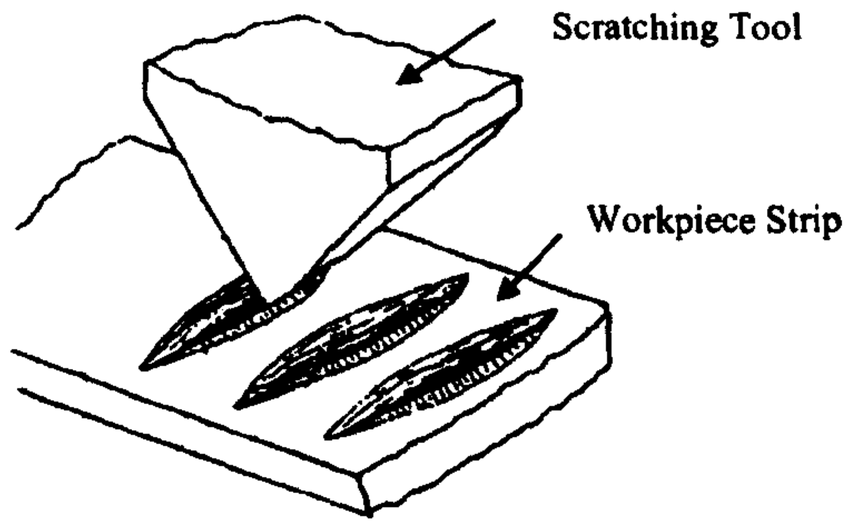

Figure 3.6 Variants of the ridge ploughing test (Schey, 1983)

All the tests mentioned above have one common weakness in their application to metal forming processes, i.e., the amount of plastic deformation is small. A group of tests which account for larger plastic deformation combined with superimposed sliding in the tool/workpiece interface are the "compression with simultaneous sliding tests", described by Schey (1983), shown in Figure 3.7. The average frictional coefficient is obtained by measuring the values of the normal force P and the lateral force F. These tests, however, sometimes have a problem in that the pressure distribution at the interface is not uniform and friction measurement can only be taken as a qualitative indication (Hansen and Bay, 1986).

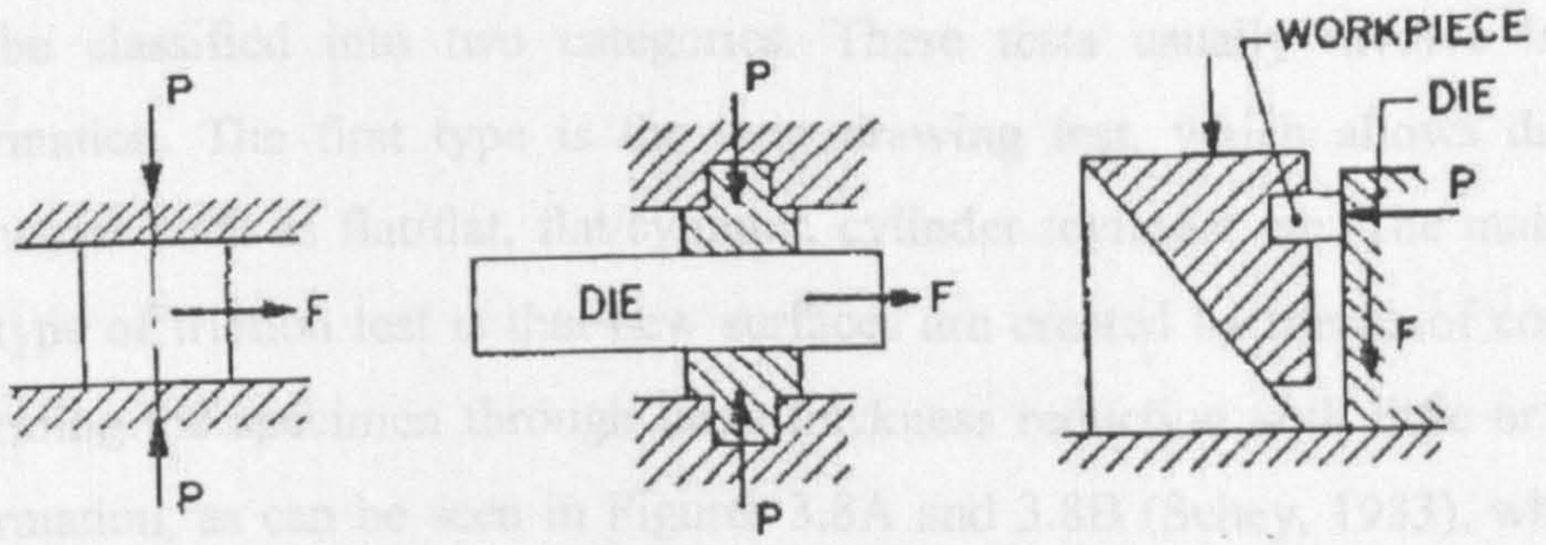

(a) (b) (c)

Figure 3.7 Compression with simultaneous sliding (Schey, 1983)

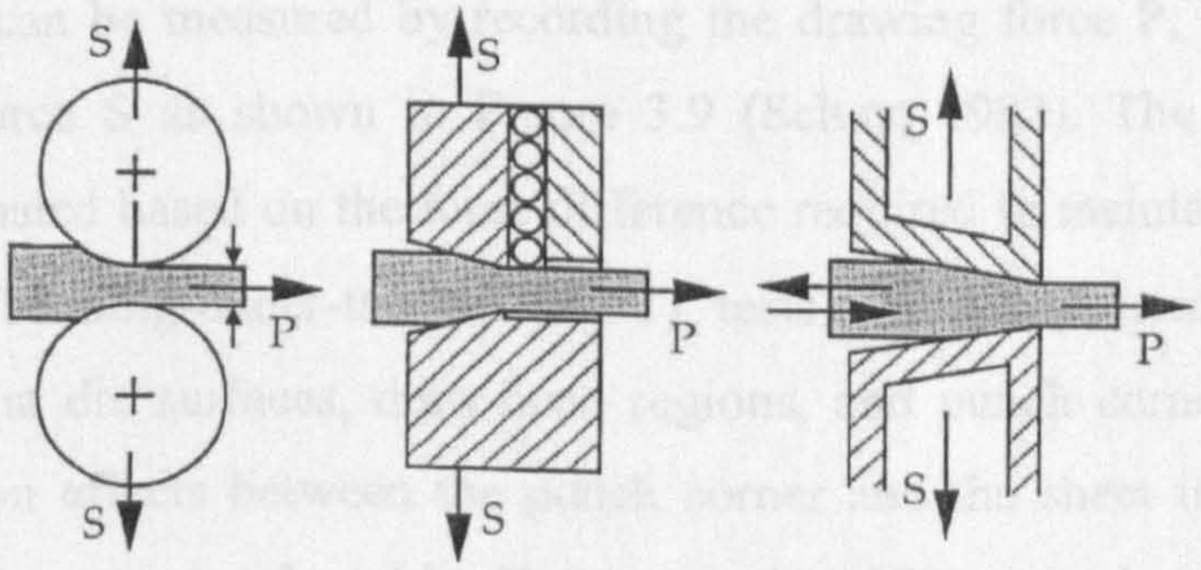

(a) (b) (c)

Figure 3.8A Typical plane-strain drawing tests.
(a) between two rollers,
(b) between a die set and a low friction die support
(c) with deflecting die frame for push-pull operations (Schey, 1983)

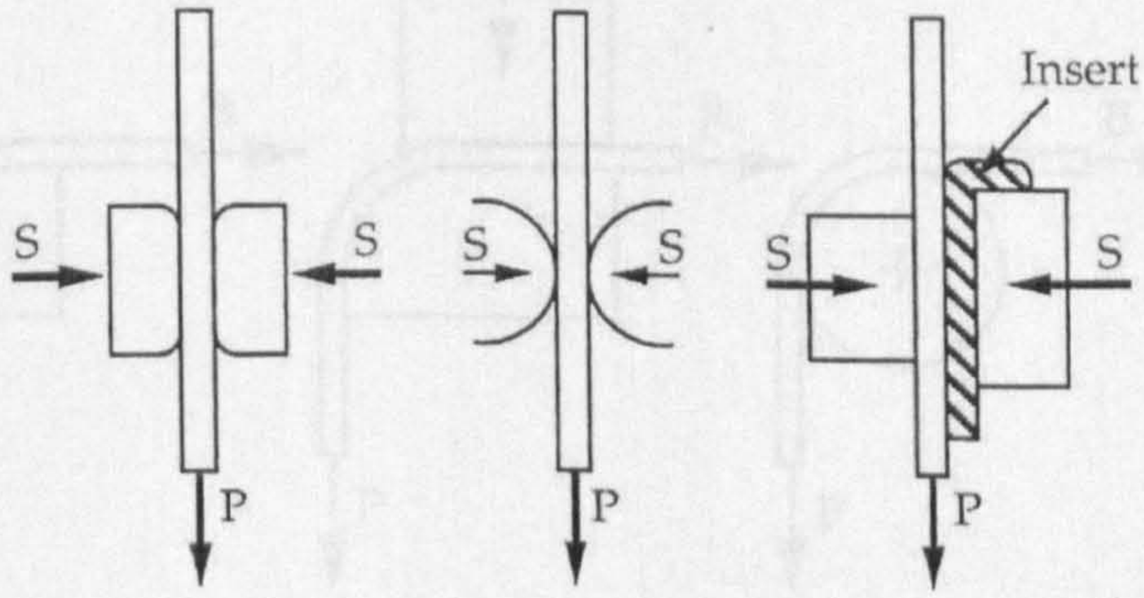

(a) (b) (c)

Figure 3.8B Typical strip sliding tests with limited thinning.
(a) flat dies,
(b) cylindrical dies,
(c) flat dies with exchangeable inserts (Schey, 1983)

A number of friction testing techniques for sheet forming have been developed and can be classified into two categories. These tests usually involve large plastic deformation. The first type is the strip drawing test, which allows different tool geometries such as flat/flat, flat/cylinder, cylinder /cylinder etc. The main feature of this type of friction test is that new surfaces are created by means of compressively deforming the specimen through large thickness reduction with little or no bending deformation, as can be seen in Figures 3.8A and 3.8B (Schey, 1983), where P is the drawing force and S the clamping force. They are mainly used to simulate plane-strain drawing, ironing processes and deep drawing processes. In the second category of friction tests, the workpiece is stretched and bent during the experiment so that the frictional effect can be measured by recording the drawing force P, back tension B and clamping force S as shown in Figure 3.9 (Schey, 1983). The friction at the interface is evaluated based on the force difference required to maintain the drawing. This group of bending-under-tension (BUT) tests is usually used to study the frictional effect at die surfaces, draw-bead regions, and punch corners. In order to assess the friction effects between the punch corner and the sheet in the stretching operation, a device was developed by Duncan et al. (1978) to evaluate friction at the punch corner, as shown in Figure 3.10 (a). The device used a standard tensile machine

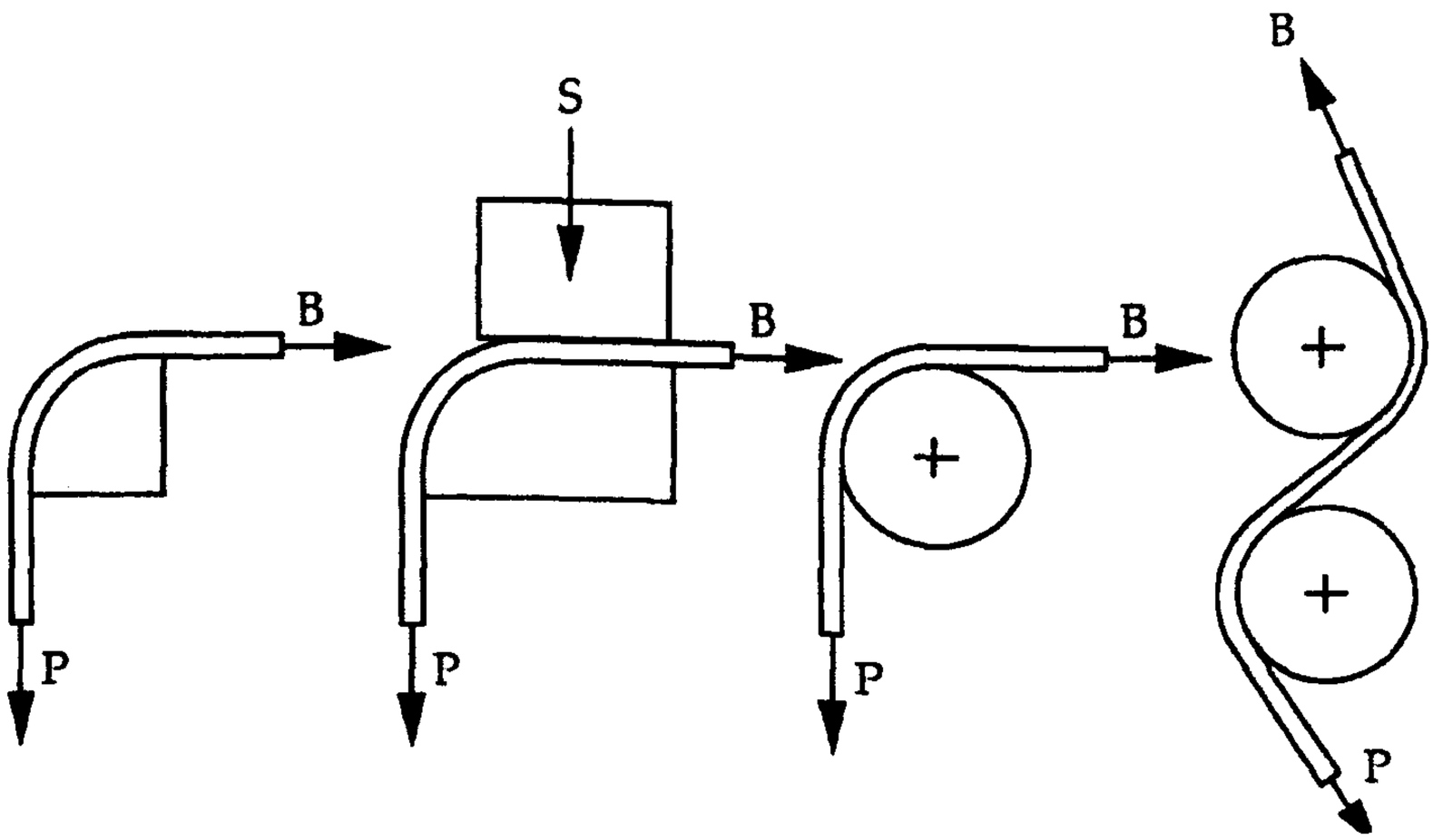

Figure 3.9 Bending-under-tension friction tests
(a) drawing over the quadrant die,
(b) drawing over the quadrant die with blank holder,
(c)&(d) drawing over the cylindrical pin/roller (Schey, 1983)

equipped with a specially designed grip fixture. The average friction coefficient can be calculated through Equation (3.1) using experimental data,

$$\mu = \frac{2}{\pi} \ln \frac{p_1}{p_2} \tag{3.1}$$

where, the die-wall force p_1 can be measured directly and the centre force p_2 can be obtained by utilizing the load-elongation curve of the side wall as illustrated in Figure 3.10 (b).

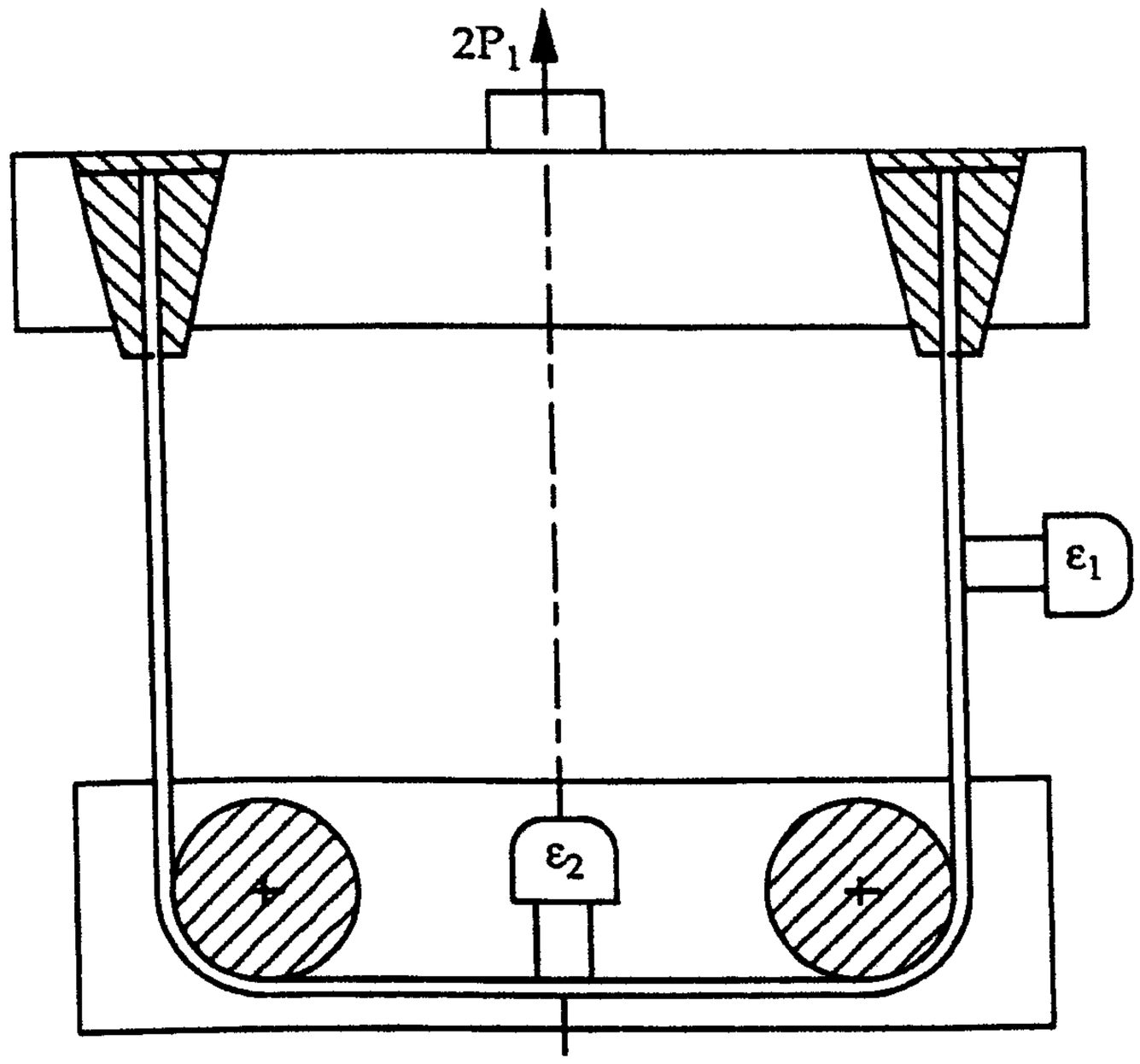

(a)

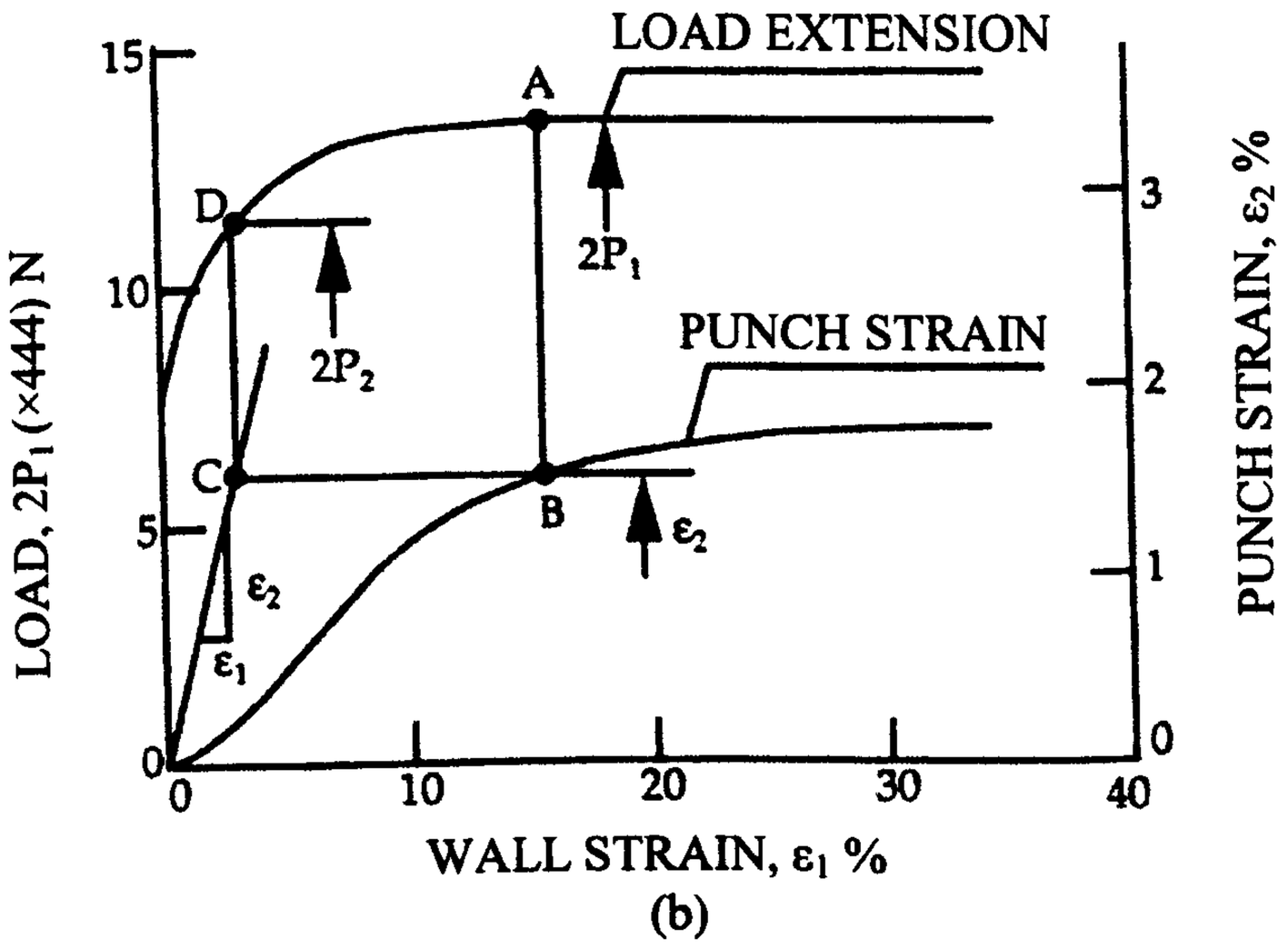

(b)

Figure 3.10 Illustrations of (a) the strip-tension friction test, and
(b) the methodology for friction calculation (Duncan et al, 1978)

Wagoner et al (1994) designed another improved device to study friction at a punch corner as shown in Figure 3.11. The friction coefficient is calculated from the force ratio and contact angle using following formula,

$$\mu = \frac{1}{\beta} \ln \frac{p_1}{p_2} \tag{3.2}$$

where p_1 and p_2 are the forces acting on the side wall and centre respectively, and β the contact angle. A limitation of this test is that the strip is bent to shape before testing. This will introduce some microstructure changes which will cause some effects on the measured results. Also the bending and unbending effects are not included in the calculation of the friction coefficient for the test.

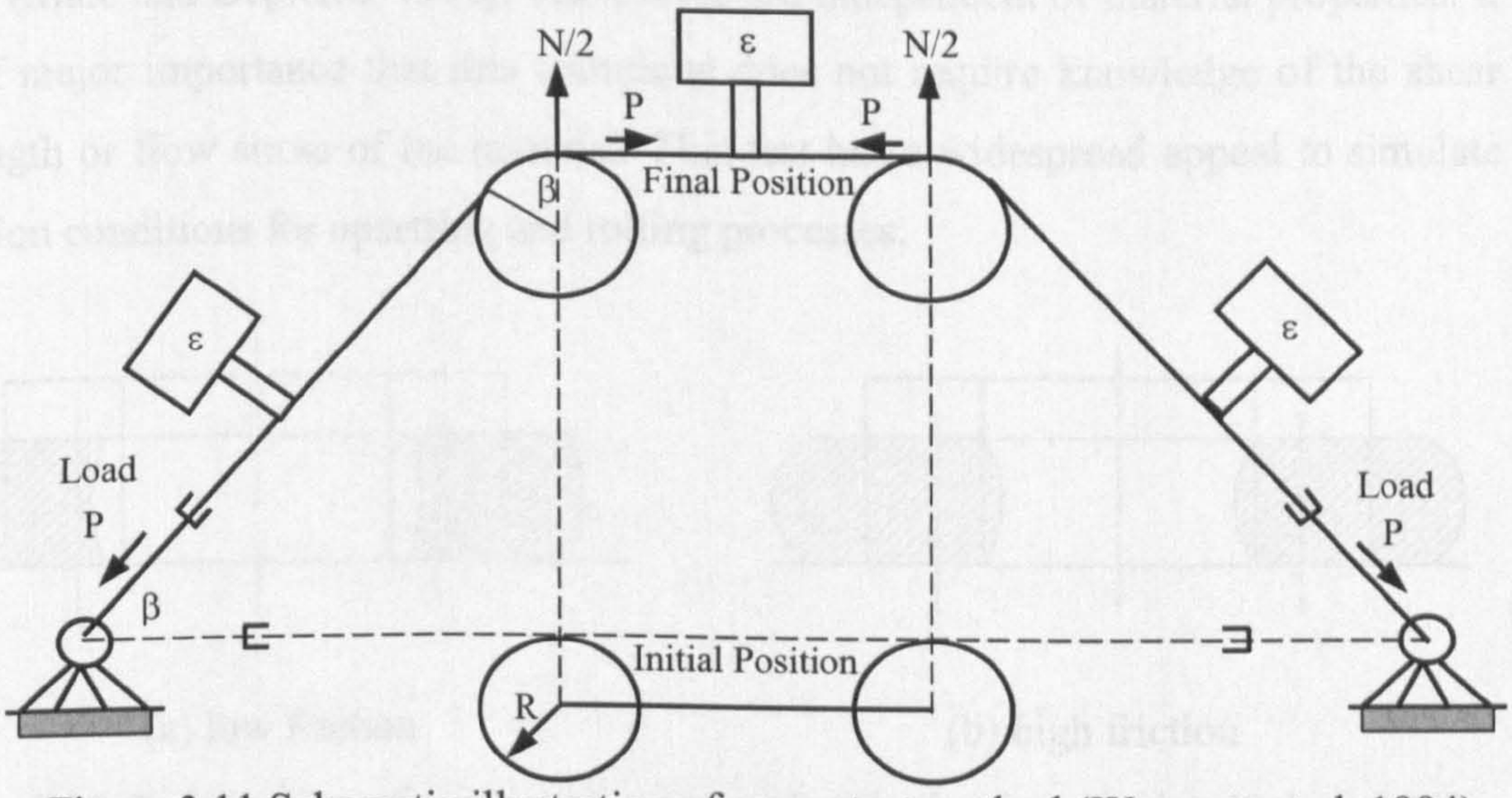

Figure 3.11 Schematic illustration of a new test method (Wagoner et al, 1994)

The ring compression test is a well established and widely used method for the determination of the friction conditions in bulk metal forming for a given combination of tool, material and lubricant. It is based on the fact that the changes of the ring geometry (especially of the inner equatorial diameter) during upsetting react sensitively to the friction condition at the interface between the die and ring specimen. The ring compression test was first proposed by Kunogi (1954) and Kudo (1955) and later further developed by Male and Cockcroft (1964) as well as several others (Schey, 1971; Foetz et al, 1991; Sahi et al, 1996; Rudkins et al, 1996 and Petersen et al. 1997). A standard ring with an initial ratio of 6:3:2 or 6:3:1 for the outside diameter, inside diameter and thickness is compressed plastically between two platens. As its height is reduced, the ring expands radially outward. If friction at the

interface is zero, both the inner and outer diameters of the ring expand as of it were a solid disk. When there is friction, the material's outward flow is retarded, the magnitude of which is dependent on the frictional conditions. When friction is significant, the retardation is also significant and the inner radius flows inwards while the outer radius grows, creating a neutral radius at which the radius velocity is zero. At a particular magnitude of friction the neutral radius coincides with the inner radius. When friction is smaller than that value, the inner radius will expand as the deformation proceeds as shown in Figure 3.12 (Schey, 1983). By measuring the change in the specimen's inner diameter it is possible to assess the level of friction at the specimen/tool interface, through the use of calibration curves as shown in Figure 3.13 (Male and Depierre, 1970). The curves are independent of material properties. It is of major importance that this technique does not require knowledge of the shear strength or flow stress of the material. This test has a widespread appeal to simulate friction conditions for upsetting and rolling processes.

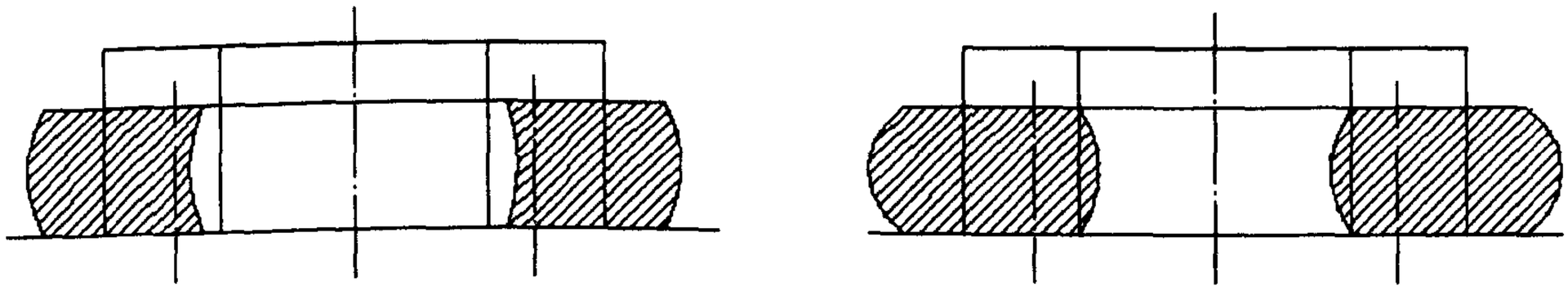

(a) low friction (b) high friction

Figure 3.12 Deformation of a ring and pressure distribution in upsetting (Schey, 1983)

These calibration curves, originally introduced by Male and Cockroft (1964), relate the percent reduction in height, shown on the abscissa to the percent change at the inner diameter, given on the ordinate. Several lines, each corresponding to a certain value of either the interfacial friction shear factor or the friction coefficient, are also plotted on the figure. Geometrical changes during a compression experiment are then placed on the curves, their locations identifying the frictional conditions at the contact surface. To provide accurate calibration curves for friction evaluation, most of the researchers adopted the upper bound method and assumed the existence of either a parallel velocity field (Male and Depierre, 1970; Avitzur, 1968) or that the cylindrical surface barrels outward (Avitzur, 1969; Hartley et al, 1979; Lee and Altan, 1972;

Nagpal et al., 1978). More recently finite element methods have been adopted (Petersen et al, 1997; Rudkins et al, 1996; Tan et al, 1998; Tan, 2001).

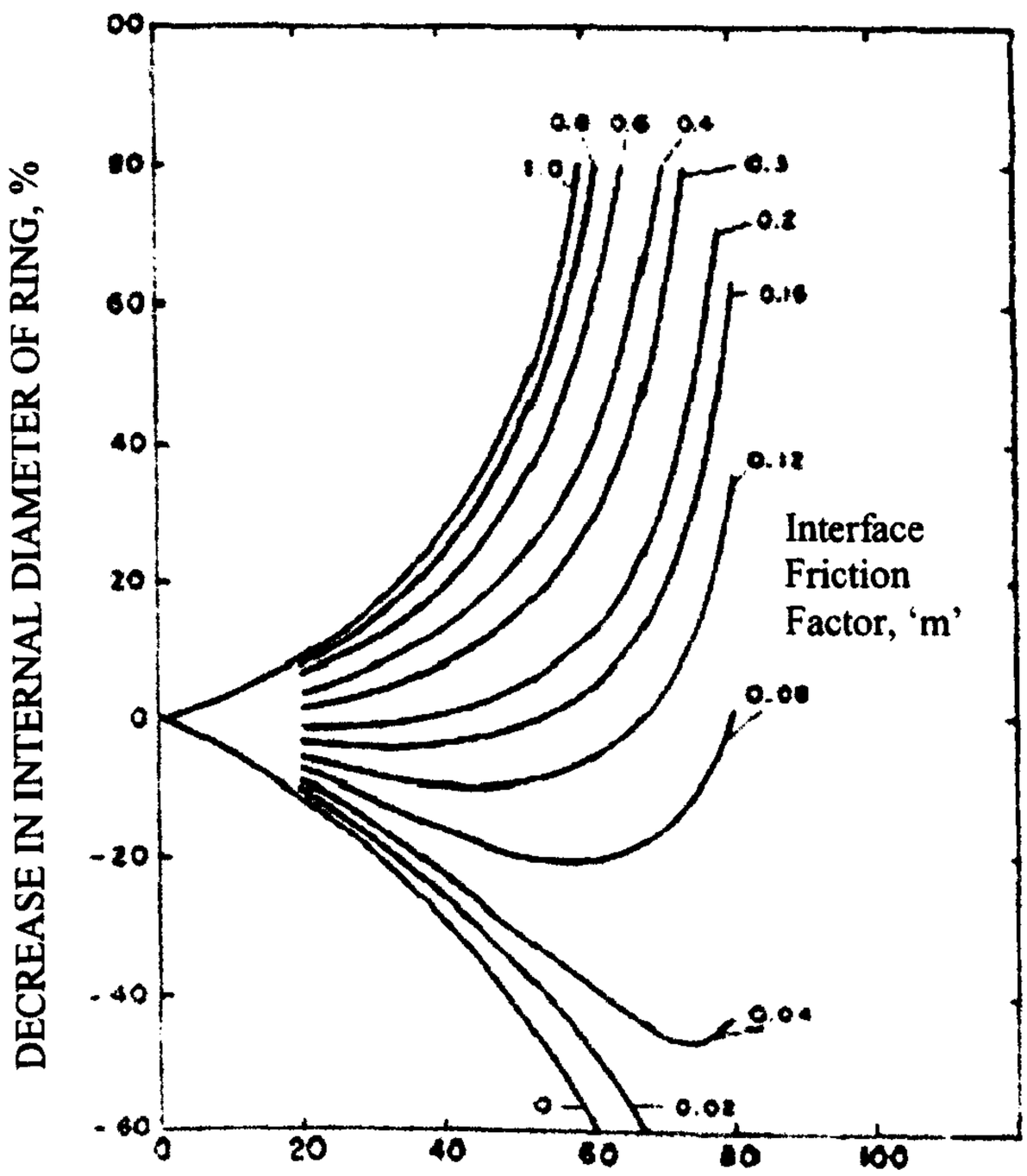

Figure 3.13 Calibration curves for ring test. (Male and Depierre, 1970)

Experimental studies of friction at high temperature using ring compression tests are not numerous. Direct comparison of the results was found to be difficult because of the very large number of variables and parameters involved in the experiments. Felder and Montagut (1980) completed a ring compression test at 1250°C and found that the tool velocity had a significant effect on friction, and it was shown that the friction reduces as the velocity increases. Wang and Lenard (1992) conducted a series of ring compression tests on steel specimens at strain rates between 0.005 and 5 s^{-1} in the temperature ranging from 900°C to 975°C using a glass based lubricant. The experimental results showed that the shear factor dropped from 0.35 to 0.1 with an increasing strain rate. Beynon et al (2000) summarized the application of the ring compression test under hot working conditions. It was reported that the quality and interpretation of the friction results depended critically upon the accuracy of the thermo-mechanical material description (Fletcher et al, 1998). A simple evaluation of hot friction from geometry alone is not meaningful without additional reference to the

thermal conditions and oxide scale. At high temperature, even with zero surface friction, there will be some barrelling of the ring because of the temperature-dependent flow stress and, less significantly, thermal expansion.

The NPL big friction rig is a newly developed high temperature friction test apparatus at National Physical Laboratory (Brooks and Loveday, 2000). The rig can be used with two sizes of cylindrical billets, of 30 and 50mm in diameter, which are pre-heated in a furnace up to 1000°C and then transferred to the yoke in the big friction rig. An axial load is applied using the press, and the load is monitored using a three column load cell. As the billets are compressed between platens they can be dragged horizontally up to 100mm between the platens. By recording the vertical and horizontal loads, the coefficient of friction can then be determined, an allowance being made for the fact that both the upper and lower surfaces of the billet are in contact with tool steel platens.

Flat compression test method for characterising the frictional condition in metal forming was developed by Pawelski et al (1998) and Wolff et al (2000). The test can be used to analyse friction conditions in the interface area between the die and the workpiece with regard to lubrication, surface microstructure, material properties, forming temperature and velocity as show in Figure 3.14. In the test a flat plate with asymmetric lubrication is compressed between two narrow punches. The transferred shear friction initiates bending of the plate because of different lubricants on the upper

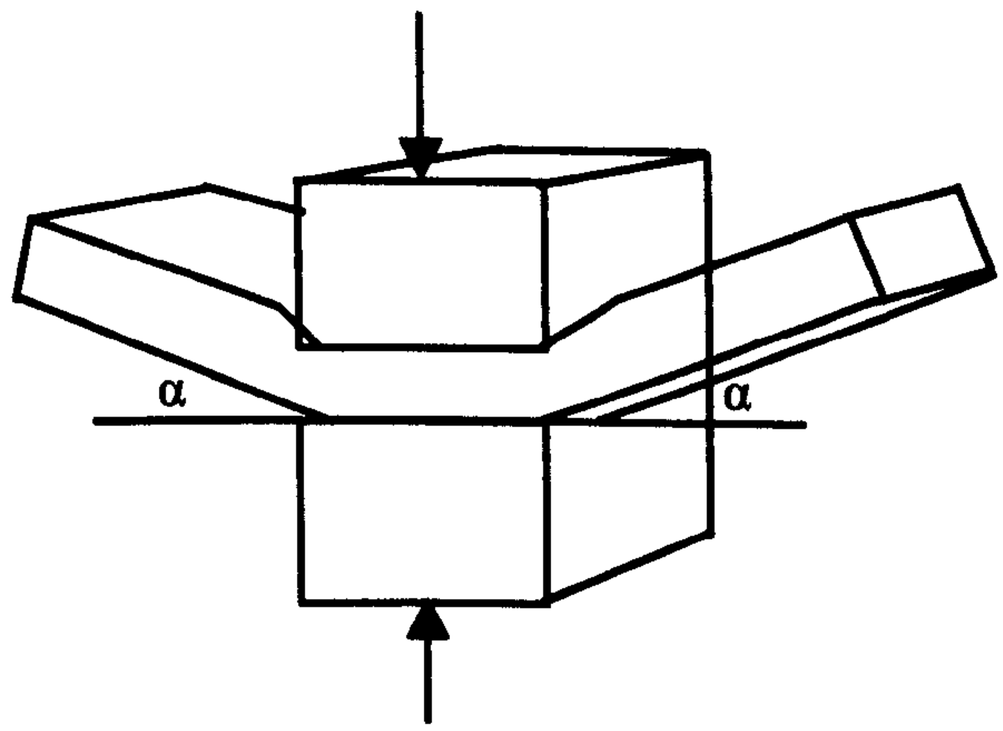

Figure 3.14 Asymmetric upsetting and top view of the billet with lateral spread (Pawelski et al, 1998)

and lower punch. The final deflection angle α is a measure for the shear friction difference between the upper and lower punch. The calibration curves of the deflection angle (α) dependent on the shear friction difference have to be established from either finite element simulation or theoretical calculation (using upper bound method) as shown in Figure 3.15 (Pawelski et al, 1998). This asymmetric upsetting method is applicable to simulate some metal forming operations, such as foil rolling, sheet rolling, cold and hot forging.

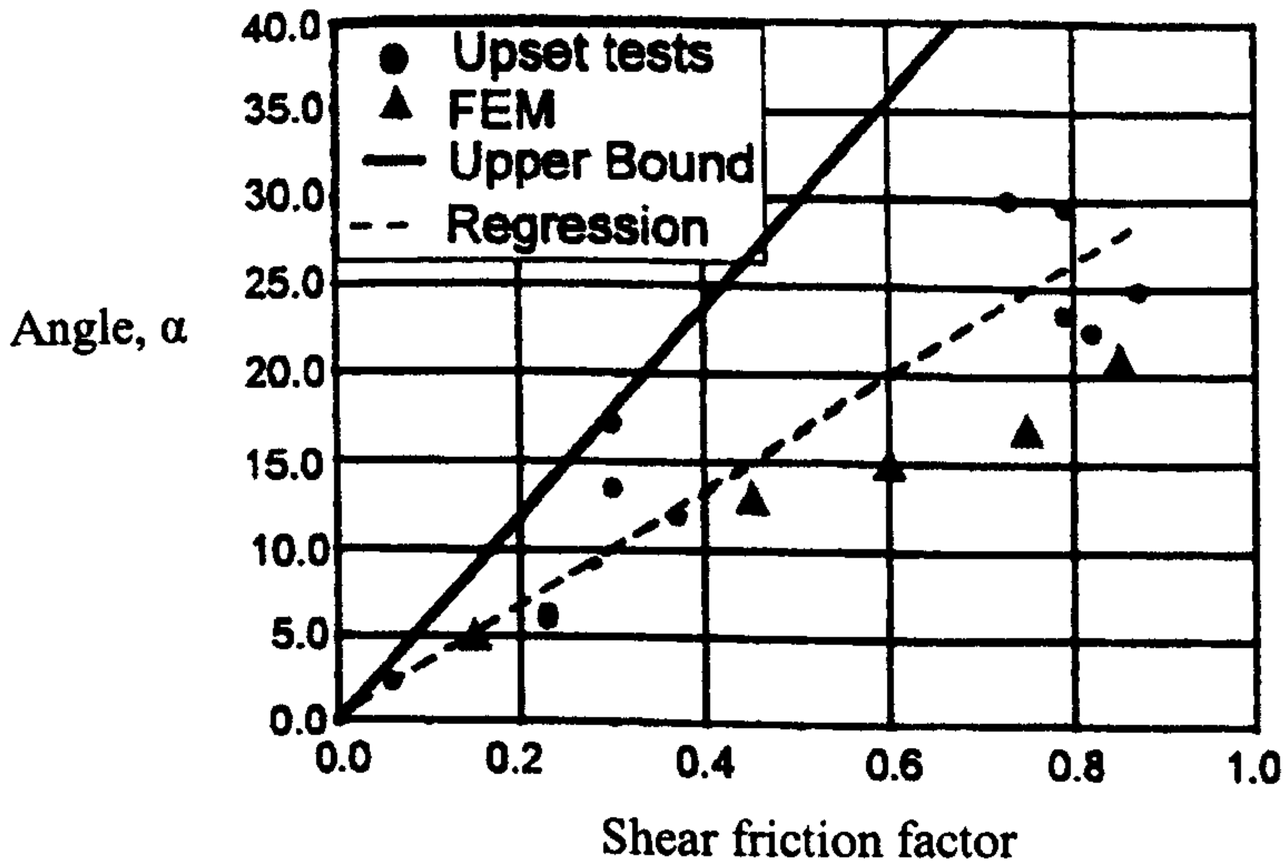

Figure 3.15 Angle dependence on friction difference (Pawelski et al, 1998)

3.4.2. Engineering Tests

There are relatively few engineering testing methods for friction measurement representative to the actual metal forming processes. This section briefly introduces the double cup extrusion test which has received most of attention.

The double cup extrusion (DCE) test is used to evaluate the frictional coefficient in extrusion processes. The test, originally proposed by Geiger (1976), was chosen because it produces a relatively high surface expansion and high pressure in comparison with the ring compression test, and thus it represents the actual situation in forward and backward extrusion tests (Ghobrial et al, 1993; Barcellona et al, 1996; Tan et al, 1998; Tiesler and Engel, 2000). The influence of friction, lubrication and reduction on metal flow for the test has been investigated (Baschhausen et al, 1992;

Ghobrial, 1993; Forcellese et al, 1994; Barcellona, 1995). The test uses a cylindrical billet that is placed in a die between a stationary and a moving punch of identical shape, and a stationary container bore, as shown in Figure 3.16. When the upper punch moves downwards, the material begins to flow and form the upper and lower cup. In the theoretical case of zero friction, both cups develop identically and thus have the same heights. Friction along the container wall slows down the development of the lower cup but increases the development of the upper one. The difference between the two cup heights increases with increasing friction. This behaviour results from the different relative velocities between the moving and stationary punch, die and billet. Therefore, small changes in friction can be detected by a significant change in cup heights, which is usually expressed by the cup height ratio. A set of calibration curves from finite element analysis, as shown in Figure 3.17, has to be determined to assess the experiment results from the test. However, Tan et al (1998) pointed out that the main disadvantage of this kind of test is that the significant difference for various lubricants was observed only at small to medium deformations and, at that stage, small errors in measuring the cup heights may lead to considerable discrepancy in the result.

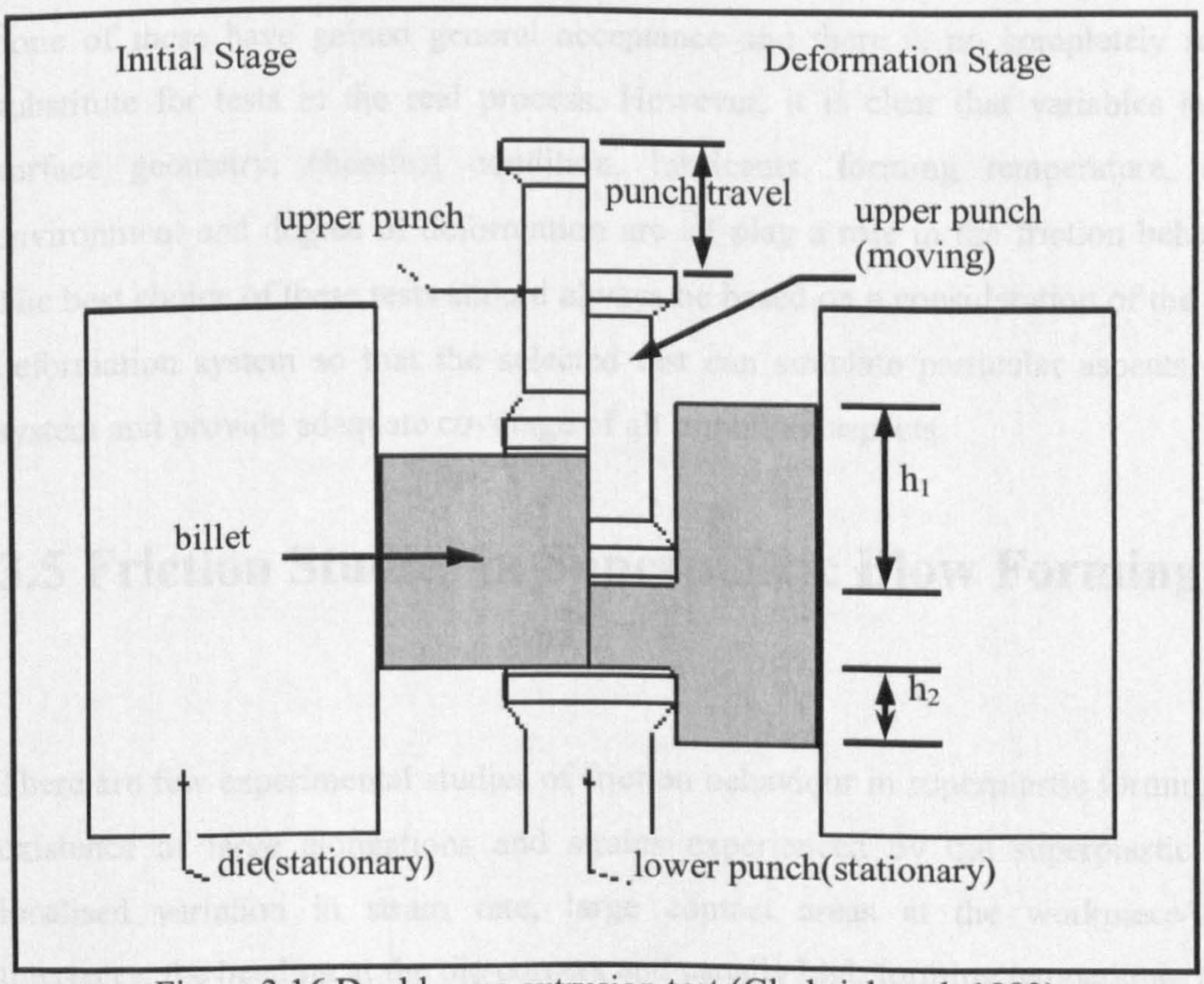

Figure 3.16 Double cup extrusion test (Ghobrial et al, 1993)

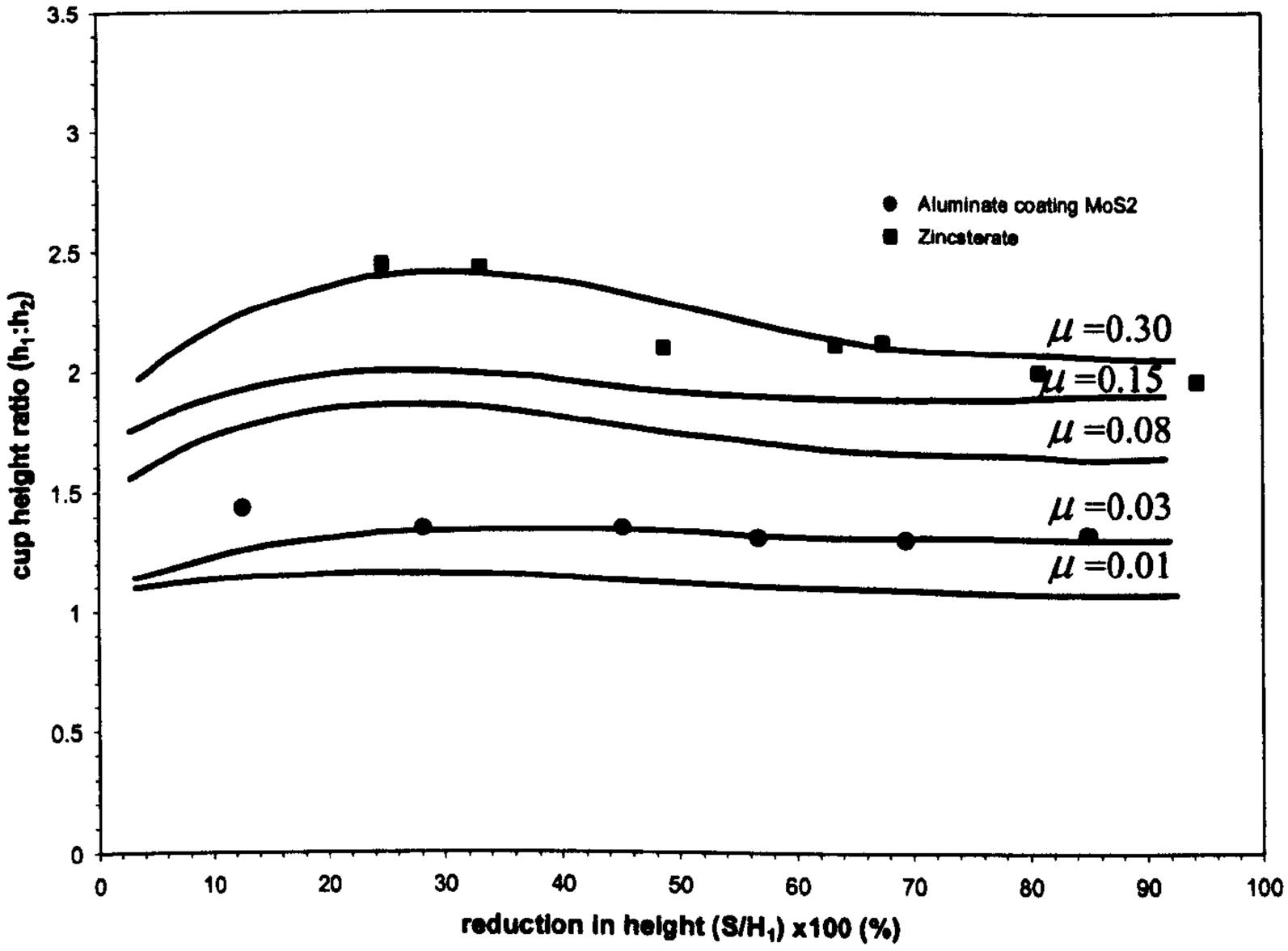

Figure 3.17 Calibration curves for double cup extrusion test (Ghobrial et al, 1993)

From the review of frictional test methods in metal forming processes, it seems that none of these have gained general acceptance and there is no completely reliable substitute for tests in the real process. However, it is clear that variables such as surface geometry, chemical condition, lubricants, forming temperature, speed, environment and degree of deformation are all play a role in the friction behaviour. The best choice of these tests should always be based on a consideration of the whole deformation system so that the selected test can simulate particular aspects of the system and provide adequate coverage of all important aspects.

3.5 Friction Studies in Superplastic Blow Forming

There are few experimental studies of friction behaviour in superplastic forming. The existence of large elongations and strains experienced by the superplastic sheet, localised variation in strain rate, large contact areas at the workpiece/tooling interfaces, the bending at the die corners and usually high forming temperature are the

characteristic conditions which make the frictional behaviour unique in superplastic blow forming.

The forming pressure for superplastic forming is usually below the level of the flow stress and the contact friction is largely limited to asperities (Chen and Thomson, 1996). In Figure 3.18, a schematic illustration of the contact relationship between the sheet and the die during blow forming operation is shown (Hwang et al, 1996), where P is the forming pressure. According to the contact situations between the sheet and the die, the bulged sheet is divided into four different regions: 1) the free bulged region; 2) the die entry contact region; 3) the side-wall contact region; 4) the bottom contact region, designated as regions I, II, III and IV, respectively. The forming operation is considered to occur in three geometrical phases: 1) phase I, in which the free bulged sheet is in contact with the die entry only; 2) phase II, in which, in addition to contact with the die entry, the sheet is also in contact with the die bottom or the side-wall or both simultaneously, and 3) phase III, in which the sheet is in contact with the entry, the bottom, and the side-wall of the die.

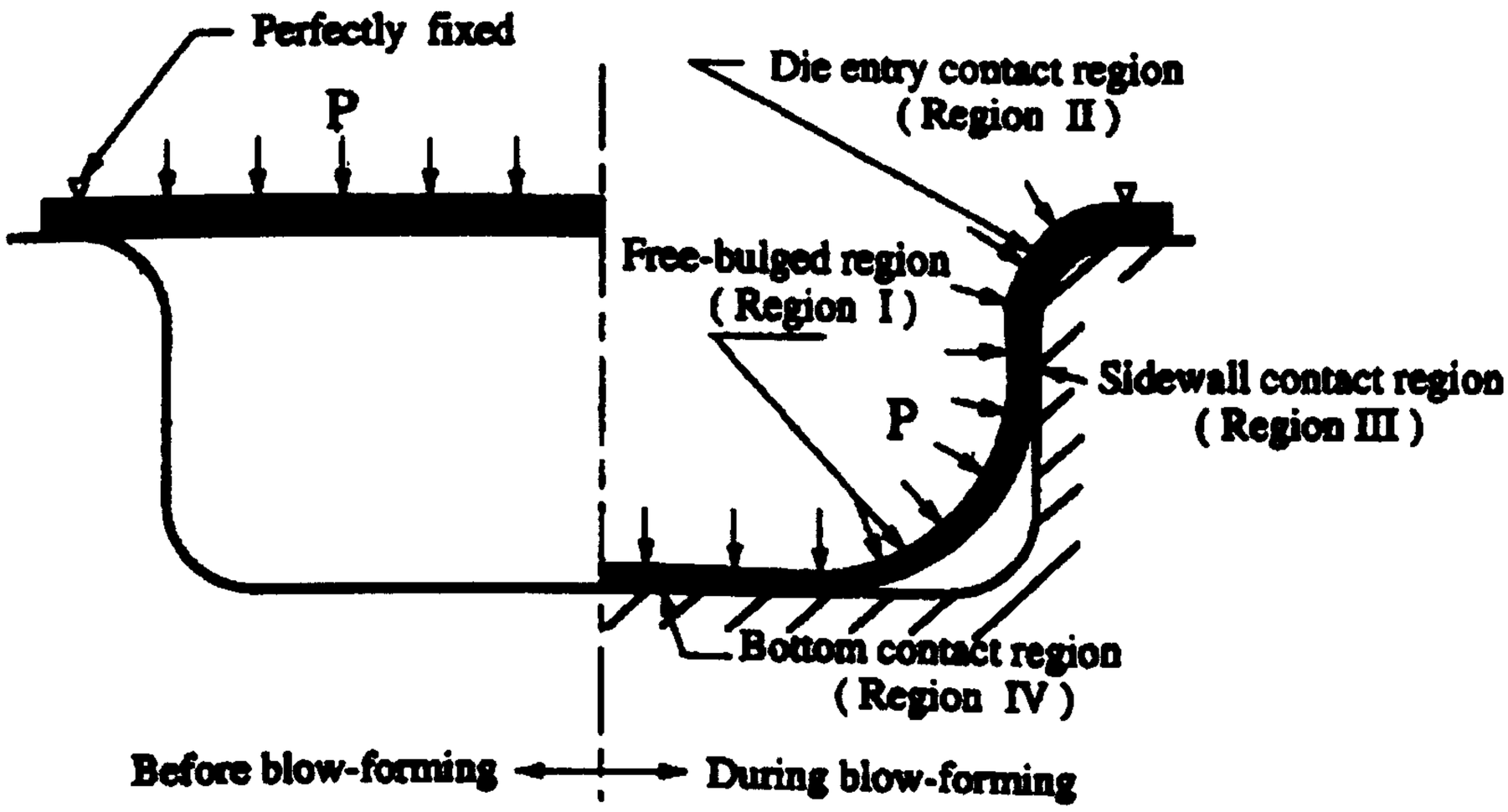

Figure 3.18 Schematic illustration of the contact relations between the sheet and the die during the blow-forming process (Hwang et al, 1996)

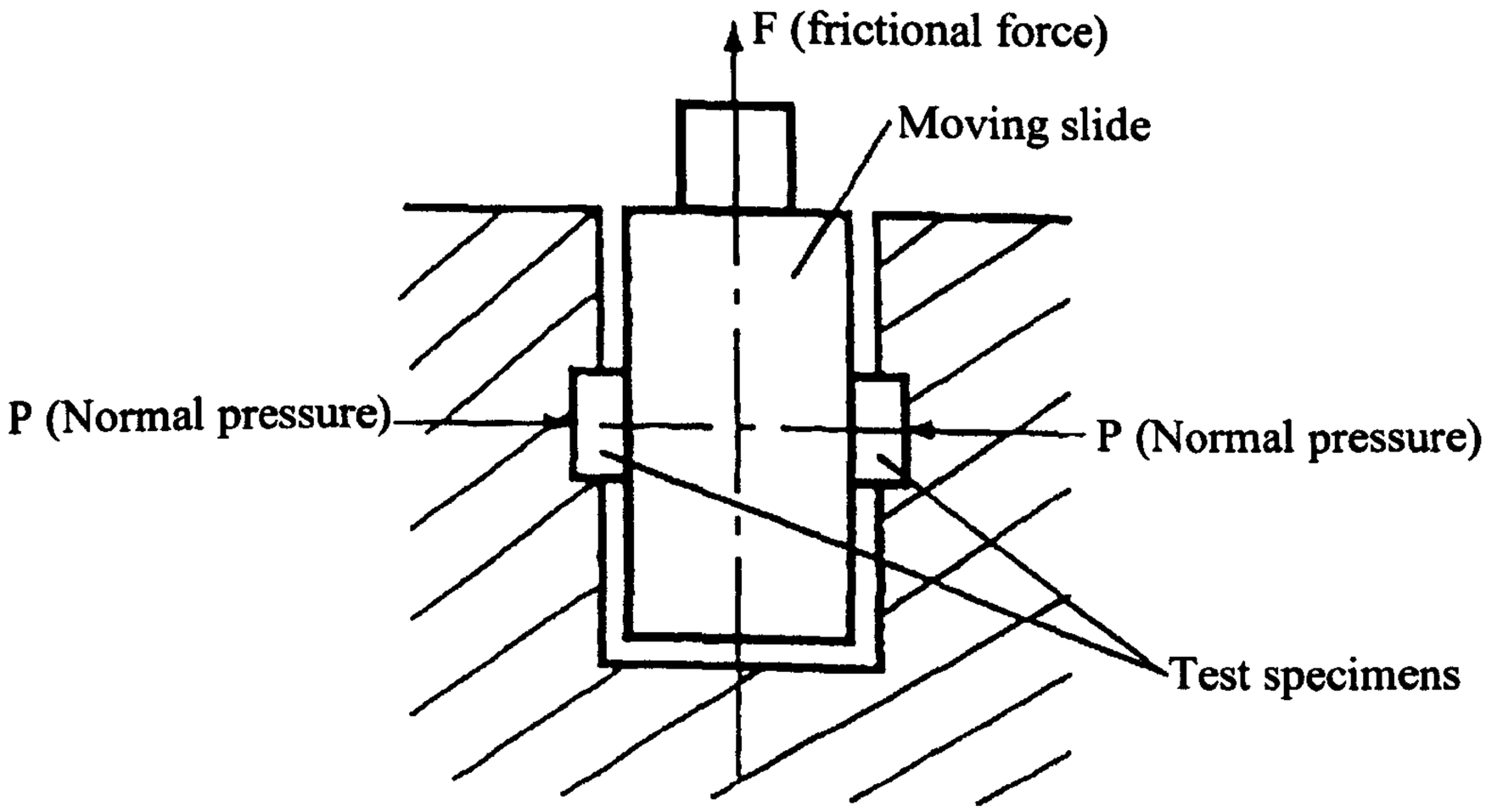

Figure 3.19 Experimental set-up of superplastic forming (Chen and Thomson, 1996)

A test rig was developed by Chen and Thomson (1996), as shown in Figure 3.19, which was installed on a test machine. The slide between the specimens was connected to the crossheads of the testing machine which was controlled by a computer; and the friction force was accurately recorded by the machine. The effect of temperature, strain rate, lubrication and normal pressure on the measured friction coefficients of aluminium sheets along the dies was investigated. It was found that lubrication and atmosphere conditions at the interface had little effect on the coefficient of Coulomb friction (Chen and Thomson, 1996). The coefficient of friction increased approximately exponentially as normal stress decreased and increased essentially linearly with strain rate. The most remarkable feature was the steep minimum in the coefficient of friction at the superplastic forming temperature.

3.6 Summary

Based on the analysis of the existing friction theories and friction testing methods, it appears that although a lot of research has gone into this area, little is still known about how the phenomenon actually operates and the exact causes. The complexity of friction phenomena occurring in metal forming processes is in contrast with the

simplicity of mechanisms and models available in the literature. It is evident that any attempt to obtain a quantitative description of friction for different forming processes, by utilizing a single friction test method is unrealistic.

The study of friction in superplastic blow forming is seldom investigated due to its unique characteristics such as large deformations, complex contact interaction with the dies and usually high forming temperatures. In order to understand thoroughly the friction behaviour in superplastic blow forming, a new testing technique which can produce reliable results while at the same time remaining as close as possible to realistic production conditions is necessary.

Chapter 4

Introduction to ABAQUS

4.1 Introduction

The finite element method (FEM) has been extensively used to model the superplastic blow forming process providing predictions of the deformation behaviour (Chandra, 1988; Bonet et al, 1990; Bonet et al, 1994; Wood, 1996; Kim et al, 1996). Finite element modelling of the superplastic blow forming process is a key component of this thesis, and is conducted using the general finite element package, ABAQUS (HKS, 2002). Therefore, a brief introduction to the finite element method and the ABAQUS package is given. In addition, several important aspects of the finite element modelling of the superplastic blow forming process are generally described.

4.2 About ABAQUS

ABAQUS is a suite of engineering simulation programs based on the finite element method, which is capable of solving problems ranging from relatively simple linear analysis to the most challenging non-linear simulations (HKS, 2002). ABAQUS contains an extensive library of elements that can virtually model any geometry. In addition, it has an equally extensive list of material models that can simulate the behaviour of most typical engineering materials.

In general, ABAQUS consists of two main analysis modules, i.e., ABAQUS/Standard and ABAQUS/Explicit. Because ABAQUS/Explicit is a special purpose analysis module that uses an explicit dynamic integration FE formulation, it is only suitable for short, transient dynamic problems such as impact. While ABAQUS/Standard is a

general purpose, production oriented FE analysis module designed for advanced analysis applications. In addition, it uses an implicit integration scheme, which provides a wide range of linear and non-linear solutions involving the static, dynamic and thermal response of a structure.

An important aspect of flexibility within ABAQUS is that it allows the user to step through the history to be analyzed. This is accomplished by defining analysis procedures. In general, analysis procedures are divided into two classes, i.e., general analysis and linear perturbation analysis. User-defined material and user subroutines are also available to give users more flexibility. A more detailed overview of the theory of ABAQUS can be found in the ABAQUS theory manual (2002).

4.3 Finite Element Method

In the last quarter century, the finite element method has experienced enormous growth in both theoretical development and applications (Zienkiewicz, 1977; Zienkiewicz and Taylor, 1989). Having been used since the early 1960s, it is certainly the most popular, flexible and powerful tool for superplastic forming research. Especially with the rapid development of powerful computers, large commercial finite element analysis packages such as ABAQUS have been developed. As the finite element method has been developed for many years and there are many books (Zienkiewicz, 1977; Owen and Hinton, 1980; Cook et al, 1989; Rao, 1989; Cheung etc, 1996) that give a detailed description of the method, only a brief review of FEM is presented here for discussion.

4.3.1 General Description of the Finite Element Method

While looking for a mathematical description of a physical phenomenon, the engineer derives a set of partial differential equations valid in a certain region and places boundary conditions on this system. For practical applications, only one solution for a particular set of numerical data is required. However, only the simplest forms of equations are capable of being solved exactly with the available mathematical methods. Therefore, numerical techniques, such as the finite element method, are considered for an approximate solution by changing the differential equations to a system of algebraic equations. The basic methodology of the finite element method is very simple. It requires a discretization of a region or body into an assembly of elements as shown in Figure 4.1. Each element is connected together at points referred to as nodes. A field variable, such as displacement, is assumed to act over each element in a predefined manner. The variable is often incorporated in the solution through a polynomial equation referred to as a shape function, which is defined in terms of the values of the field variable at the nodes.

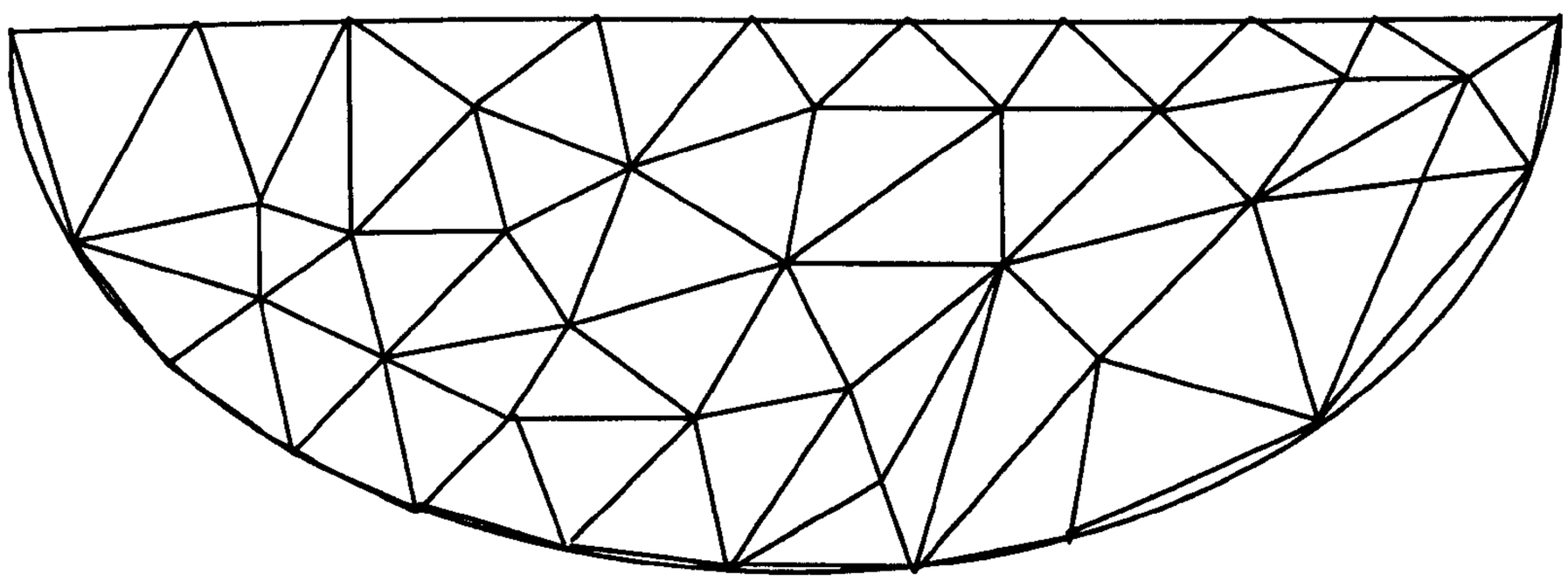

Figure 4.1 Discretization of a region into a number of finite elements

Once the problem has been discretized, the governing equations for each element are calculated and assembled to give the system equations, which describe the behaviour of the whole body. Usually it takes the following form,

$$[K]\{d\} = \{f\} \tag{4.1}$$

where, $[K]$ is a square matrix, known as the stiffness matrix, $\{d\}$ is the vector of unknown nodal displacements and $\{f\}$ is the vector of applied nodal forces. Equation (4.1) is analogous to the equilibrium of load-displacement relationship for a one-dimensional spring. To find the displacements developed by a given force, the equation is inverted and solved for $\{d\}$, provided boundary conditions are applied. It is noted that the solution to Equation (4.1) is not trivial in practice because the number of equations involved tends to be very large. Fortunately, the stiffness matrix is usually banded, and many techniques have been developed to store and solve the equations efficiently. After solving the unknown nodal values, it is straightforward to calculate the strain and stress from the prescribed displacements.

4.3.2 Performing a Finite Element Analysis

A finite element analysis can be considered to be a four-stage process for any type of problem, whether it is linear or non-linear, and is described as follows:

1. Description of operation – Obtain a complete mathematical description of the process or object in numerical form.

2. Pre-processing – Geometry, mesh, material properties, boundary conditions and initial state parameters.

3. Finite element calculation – Stiffness-matrix equation formulation, assemblage and computational algorithm to obtain the values of state parameters (i.e., displacement, strain and stress) and updated mesh geometry, state parameters and boundary conditions.

4. Post-processing – Output the results from the calculation in a format which can be easily interpreted.

4.4 Contact Interaction Modelling

Contact and friction modelling has attracted much attention of FEM code developers and numerical analysts in the last decade. For the successful modelling of the superplastic forming process with large deformation and complicated die surfaces, one of the most important and difficult problems is the treatment of contact interaction between the die and the deformed sheet. The superplastic forming process is normally non-stationary and the geometry of the sheet progressively changes. Therefore, to get reasonable and stable solutions, the surfaces of the dies which are in either direct or potential contact with the component must be defined, checked and modified according to the progress of the forming process.

ABAQUS/Standard (2002) has two different approaches to model the contact and surface interaction problems, i.e., surface-based contact simulation and element-based contact simulation.

Most contact problems are modelled by using surface-based contact. Interactions between two deformable bodies or between a deformable body and a rigid body are allowed. To define the contact between two structures in ABAQUS, the first step is to create the surfaces using the *SURFACE DEFINITION option. The *CONTACT PAIR option is then used to define the pair of surfaces that may interact each other. Each contact pair references a surface interaction definition, which is created using the *SURFACE INTERACTION option. The contact pair approach in ABAQUS provides two formulations for modelling the interaction between the surfaces in either two or three dimensions, namely small-sliding contact and finite-sliding contact. With the small-sliding formulation, the surfaces can only undergo small sliding relative to each other, but may undergo arbitrary rotation. With the finite sliding formulation, separation and sliding of finite amplitude, as well as an arbitrary rotation of the surfaces, may arise. When the contact pairs are defined, a "master-slave" concept is employed in ABAQUS (2002) to enforce the contact constraint. All nodes in the slave surface are constrained not to penetrate into the master surface. Consequently, the

contact direction is always normal to the master surface. However, the nodes in the master surface can, in principle, penetrate into the slave surface.

Various contact interactions, such as mechanical, thermal, electrical, pore pressure and pressure penetration interactions, can be modelled using the surface-based contact approach. For mechanical interaction modelling, the shear interaction can be modelled using a static or kinetic Coulomb friction model within ABAQUS (2002). The friction coefficient is dependent on the tangential slip velocity, contact pressure, average surface temperature, and field variables. For more complex response a user subroutine can be used to define the frictional behaviour. Contact surfaces can be bonded completely or allowed to debond according to a specified criterion defined. Various contact pressure-clearance relationships can be assigned to a surface interaction definition. The default is a hard contact behaviour, which instantaneously introduces contact pressure as points come into contact. Alternatively, a "softened" model allows either an exponential or a tabular relationship between the pressure and clearance. In addition, a clearance-dependent viscous damping relationship for contact pressure allows highly unstable contact conditions to be modelled.

There are several classes of problems for which the surface-based contact method cannot be used. ABAQUS provides a library of contact elements for these problems. Contact elements which can be used in such cases are gap elements, tube-to-tube, slide plane, slide line, interface, rigid surface, acoustic interface and underwater shock interface elements.

For superplastic forming applications the dies are rigid. Dies/sheet contact interaction can therefore be modelled as rigid surfaces and a deformable surface using the finite-sliding contact interaction formulation. It is a very complex calculation because ABAQUS needs constantly to determine which part of the master surface (die surface) is in contact with the slave (sheet) surface. At each integration point, the contact elements, which ABAQUS automatically generates according to the data defined using the *CONTACT PAIR option, measure the overclosure as well as relative shear sliding. These kinematic measures are then used, together with appropriate Lagrange multiplier techniques, to introduce the surface interaction theories.

4.5 Friction Algorithm

A Coulomb friction model with an additional limit on allowable shear stress is provided in ABAQUS to solve the frictional phenomena existing between any pair of contacting surfaces.

The model characterises the frictional behaviour between the surfaces using a coefficient of friction, μ. The product μp, where p is the contact pressure between the two surfaces, giving the limiting frictional shear stress for the contacting surfaces. The contacting surfaces will not slip (slide relative to each other) until the shear stress across their interface equals the limiting frictional shear stress μp.

Modelling the ideal friction behaviour can be very difficult; therefore, ABAQUS uses a penalty friction formulation with an allowable elastic slip shown by the dotted line in Figure 4.2. The elastic slip is the small amount of relative motion between the surfaces that occurs when the surfaces should be sticking. ABAQUS automatically choose the penalty stiffness (the slope of the dotted line) so that this allowable elastic slip is a very small fraction of the characteristic element length.

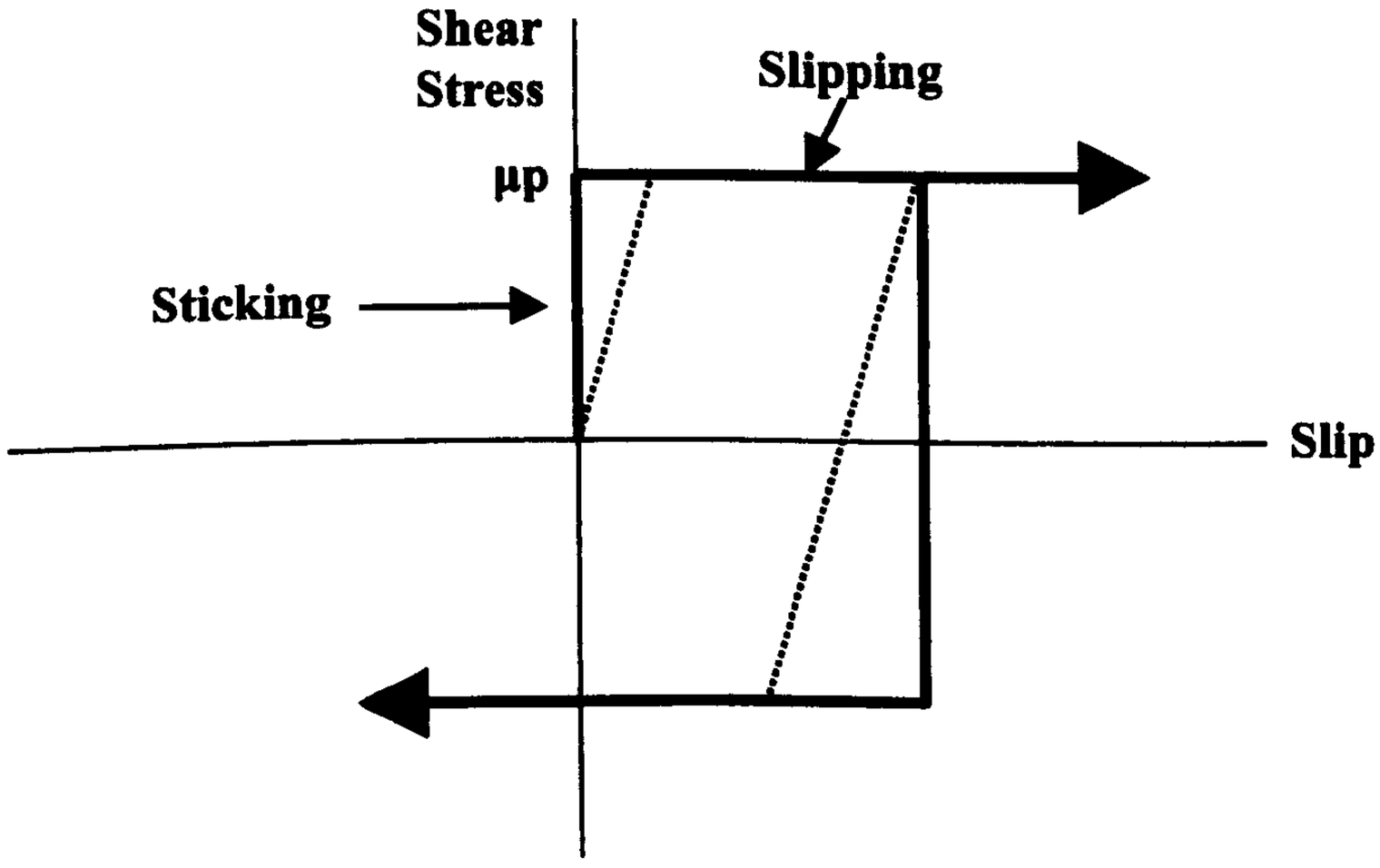

Figure 4.2 Frictional behaviour (ABAQUS Theory Manual, 2002)

To include a friction model as part of a surface interaction definition when using surface-based contact modelling in ABAQUS, the *FRICTION option is used in conjunction with the *SURFACE INTERACTION option, so that the coefficient of Coulomb friction can be defined.

4.6 Loading and Strain Rate Control Algorithm

The superplastic blow forming operation can usually be carried out with two kinds of gas pressure control. One is with constant forming pressure which is easy to achieve and control, thus it is also adopted in the following experiments and the simulations performed in Chapter 8 to interpret the experimental results. The disadvantage is that the variation of maximum strain rate of the blank which is undesired, however, cannot be avoided. The other is with variable pressure-time profile to maintain the strain rate within an optimum range throughout the whole forming process. Yang et al (1996) investigated experimentally the blow forming of 7475Al alloy under constant pressure and constant forming strain rate. It was concluded that forming under a variable pressure-time profile, reduced the forming time and resulted in a satisfactory thickness distribution in comparison with forming under constant pressure. Similar result was obtained by Akkus et al (1997). Thus constant strain rate loading fits superplastic forming process well, and is adopted in the preliminary simulation as described in Chapter 5.

The two loading schemes, i.e. constant pressure loading and constant strain rate loading, can be chosen within ABAQUS. In particular, the constant pressure scheme is relatively easy to understand. The constant-strain-rate loading scheme is achieved by adjusting the loading pressure schedule according to the difference between the maximum effective strain rate among all of the elements and the target strain rate at any point of time. ABAQUS provides this capability with automatically adjusted loading to obtain a controlled stain rate, which is explained as follows.

During an increment ABAQUS calculates r_{max}, the maximum value of the ratio of the equivalent creep strain rate to the target creep strain rate for any integration point in a

specified element set. If r_{max} is less than 0.2 or greater than 3.0 in a given increment, the increment is abandoned and restarted with the following load modifications,

$$\begin{aligned} r_{max} < 0.2 \quad & p = 2.0 p_{old} \\ r_{max} > 3.0 \quad & p = 0.5 p_{old} \end{aligned} \tag{4.2}$$

where p is the new load magnitude and p_{old} is the old load magnitude. If $0.2 \le r_{max} \le 3.0$, the increment is accepted; and at the beginning of the following time increment, the load magnitudes are modified as follows,

$$\begin{aligned} 0.2 \le r_{max} < 0.5 \quad & p = 1.5 p_{old} \\ 0.5 \le r_{max} < 0.8 \quad & p = 1.2 p_{old} \\ 0.8 \le r_{max} < 1.5 \quad & p = p_{old} \\ 1.5 \le r_{max} \le 3.0 \quad & p = p_{old} / 1.2 \end{aligned} \tag{4.3}$$

The *CREEP STRAIN RATE CONTROL option actives the above algorithm so that the loading in a superplastic forming process can be controlled. This option is also used to define a target equivalent creep strain rate. The *AMPLITUDE, DEFINITION=SOLUTION DEPENDENT is used to define the minimum and maximum limits of the loading. The *CREEP STRAIN RATE CONTROL option refers to the *AMPLITUDE option through the required AMPLITUDE parameter. With such features, ABAQUS can monitor the maximum strain rate and compare it with the target value during a loading procedure. The loading pressure will be adjusted on the basis of the comparison subsequently.

Chapter 5

Numerical Analysis of Superplastic Blow Forming

5.1 Introduction

Superplastic forming is characterised as strain-rate sensitive and superplasticity is achieved only in a narrow range of strain-rate with an optimum value dependent on the material. The factors that affect formability in a superplastic forming process generally include geometric parameters (die geometry, shape of the sheet etc), material parameters (sheet thickness, strain rate sensitivity index m, material constant K etc) and process parameters (forming pressure profile, friction coefficient etc). It is therefore crucial to understand the effects and interactions of all the parameters on the formability in order to produce a SPF part successfully. With this knowledge, engineers would be able to design manufacturable components with a minimum number of modifications and trials.

From a practical point of view, to produce maximum ductility in the superplastic blow forming process, it is desirable to find a varying forming pressure cycle that will maintain the overall strain rate within an optimum range throughout the whole forming process. Friction between the die and the sheet is found to significantly affect thinning of the component during the blow forming process (Lee, 1997). Severe thinning will lead to failure of the component. Furthermore, it is important to be able to predict the final thickness distribution of the component. It is with respect to these problems that the predictive capabilities of the finite-element method make an important contribution to the design of SPF manufacturing process.

Compared to costly experimental methods, the finite element method (FEM) has proved to be a powerful investigative tool in the design of the SPF process, because it can provide a valuable insight into the effects of various process parameters on the product quality and tool design, reduce the number of tests or even eliminate the need for expensive trial-and-error testing (Zienkiewicz and Taylor, 1989; Carrino and Giuliano, 1997). It has been demonstrated that functions of the processing parameters, such as the forming pressure-time cycle and final thickness distribution, can be successfully predicted by FEM (Chandra, 1988; Rama and Chandra, 1991). Also it is found that the accuracy of a numerical simulation is strongly influenced by the die-sheet interface frictional conditions, while the frictional phenomenon, which is the main concern in this project, is the least understood factor in the blow forming process.

In this chapter, a preliminary FEM study was carried out to understand the blow forming process. A simple cylindrical cup and a complex reverse formed component were modelled. The cylindrical cup was chosen for analysis because it is one of the most common features on products, and thus characterises the most relevant design geometries. The complex component design sample, supplied by Rolls Royce Plc, was formed by a superplastic reverse blow forming technique. Material properties and simulation procedures are discussed in the following sections. The main objective of this chapter is to understand the superplastic forming process with particular attention to how friction affects the superplastic forming.

5.2 Superplastic Blow Forming of a Cylindrical Cup

5.2.1 Modelling Description

Superplastic blow forming is a complicated system governed by large strains, large deformations, highly non-linear material behaviour and, usually, deformation dependent boundary conditions. Consequently the numerical analysis of such a highly non-linear process involves formidable computational problems. Fortunately, the superplastic behaviour of materials is characterised by the dependency of the flow

stress upon the strain rate, which allows the material to be described as incompressible, non-linear and with rigid viscoplasticity. Large deformation problems need non-linear solutions, since force-displacement relationships depend on the particular material characteristics in the current state of the particular deformation step.

A schematic diagram of a Ti-6Al-4V cylindrical cup studied in this preliminary investigation is shown in Figure 5.1. The diameter of the circular sheet is 200 mm, of which the 10 mm outer rim is clamped between the upper die and the lower die. The initial thickness of the sheet is 1.25 mm. According to the geometry of the component and the loading conditions, the problem can be simplified as an axisymmetric case.

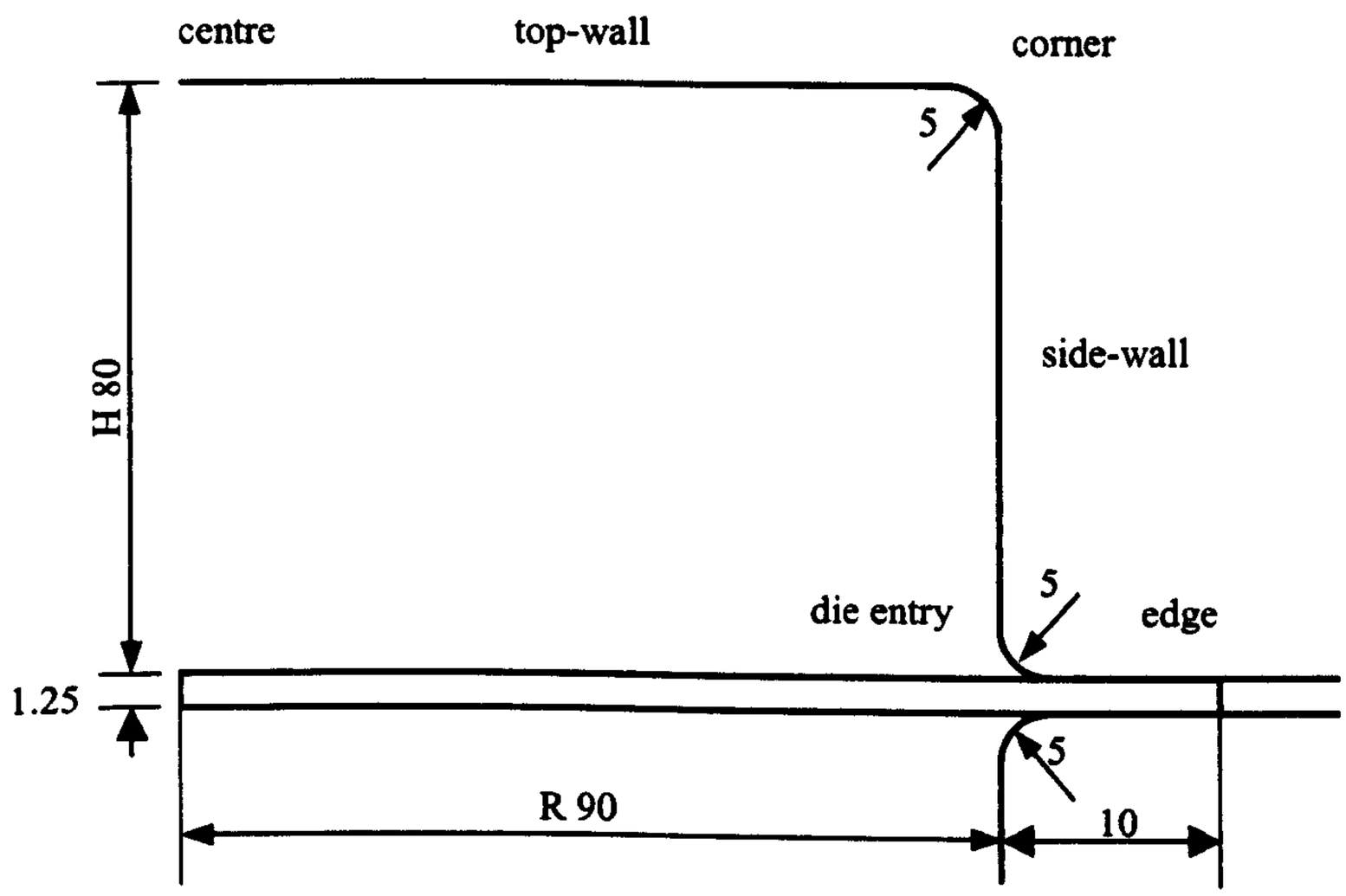

Figure 5.1 Geometry of dies and sheet (unit: mm)

The simulation was performed in accordance with the actual experimental process (Cheng, 1996). The finite element formulation includes a contact algorithm and a pressure control algorithm for the optimisation of the forming time. The calculation deals with the maximisation of the strain-rate sensitivity, the changing of the deformation shape and the consistency of the desired strain rate. An iterative Newton-Raphson solution scheme was chosen to solve the non-linear equations within ABAQUS. The above procedures enabled the FE program to model the superplastic blow forming process.

5.2.1.1 Material Constitutive Behaviour

The material being studied in the simulation is Ti-6Al-4V alloy which has been widely applied in the aerospace industry because of its superior properties such as high strength-to-weight ratio, high temperature tolerance and excellent corrosion resistance. The material properties of Ti-6Al-4V alloy, which are taking from Cheng (1996), are summarized in Table 5.1 for the numerical simulation of superplastic blow forming process

Table 5.1 Material properties (Cheng, 1996)

Material Property	Value
Young's modulus E (GPa)	20
Poisson's ratio γ	0.3
Material Constant K (MPa)	1030.78
Strain Rate Sensitivity Index m	0.61305

The material constitutive behaviour of the component is very crucial for an accurate prediction of the thickness distribution during a SPF process. The material constitutive behaviour modelled in the simulation can be described by the following empirical equation (Arieli and Mukherjee, 1982; Pilling and Ridley, 1989; Rebelo et al, 1990; Kim et al, 1996; Cheng, 1996; Hwang et al, 1998; Carrino & Giuliano, 2001)

$$\sigma = K\dot{\varepsilon}^m \tag{5.1}$$

Where σ is the flow stress, $\dot{\varepsilon}$ is the strain rate, K is a material constant and m is the strain rate sensitivity index. Equation (5.1) defines that the flow stress is governed by the index m. In the simulation, the constitutive equation has been implemented using the isotropic creep material model within ABAQUS. As discussed in Section 4.6, deformation under constant strain rate results in a better thickness distribution compared with that under constant pressure loading, thus the constant strain rate forming process is considered here. A special solution dependent magnitude scheme of pressure control is employed in the finite element program to maintain an

approximate constant strain rate in the simulation (ABAQUS User Manual, 2002). The target strain rate is set at 10^{-3} /s in the simulation.

5.2.1.2 Element and Mesh Study

Numerical analysis of the superplastic blow forming process is generally carried out with membrane element (Bonet et al, 1990; Chenot and Bellet, 1992; Lee, 2001), shell element (Bonet and Wood, 1987) or continuum element (Chandra, 1988; Rebelo et al, 1990). In particular, Bonet et al (1990) developed a general three-dimensional finite element formulation by using a 3-node triangular membrane element. A strain rate constraint equation was also introduced to control the gas pressure to maintain an optimum strain rate during the superplastic forming process. Chenot and Bellet (1992) developed an isoparametric membrane element approach for the 3D simulation and a plane-strain element formulation for a 2D circumstance. Chandra (1988) investigated an isoparametric continuum element formulation which can model the effects of bending and shear stress. Hence, the question of which element will be the most suitable one arises and this is addressed in the following section.

Simulations of sheet forming are performed dominantly using a membrane element because of the reduced computational cost. However, a membrane element is a surface element that only transmits the in-plane force without considering moments and bending stiffness. Membranes do not show bending resistance out of their plane, so although they fit perfectly in the die, buckling will occur if the friction coefficient is high enough. Under these conditions, the program will not be able to reach convergence, because of the numerical singularities that appear. In a general superplastic sheet forming process, the sheet thickness may not be smaller than the other dimensions to neglect the bending effect (Lee & Huh, 2001). Similarly, a shell element is proposed as a substitution for the membrane element. Both membrane and shell formulations assume that the thickness strain can be computed as a function of the in-surface deformation due to material incompressibility (Rebelo et al, 1990). This simplified assumption does not allow for the development of stress in the thickness direction of the sheet. In fact, both sides of the sheet will be in contact with the rigid

dies during a SPF process. It is difficult for either a membrane or a shell element to model this type of contact because they cannot accommodate the stress in the thickness direction. Therefore, a continuum element is necessary for the capabilities to consider these effects and model the complicated non-linear analysis which involves contact and large deformation (Chandra, 1988; Rebelo et al, 1990).

In order to further clarify the most suitable element for the simulation of superplastic blow forming, a detailed element type study has been performed and a comparison among these different elements is presented. The elements studied include the four-node reduced integration axisymmetric quadrilateral continuum element (CAX4R), the first-order axisymmetric shell element (SAX1), and the first order axisymmetric membrane element (MAX1) (ABAQUS, 2002). In addition, deferent mesh densities are generated according to the deformed configuration in order to obtain an accurate prediction with an optimum computational cost. Generally, the mesh should be refined in the sheet where severe distortion and excessive thinning occur in order to model accurately the SPF process. This is further discussed in more detail in Section 5.2.2.

5.2.1.3 Contact and Friction Algorithms

During a superplastic blow forming process, contact between the sheet and the die results in friction. An important consideration in modelling the process is how to simulate the friction effect since the friction force strongly influences the blow forming process especially on the localization of the thickness variance. In this research, the contact interaction was simulated by means of a rigid die surface and a deformable sheet surface (ABAQUS Example Manual, 2002). In order to avoid having points falling-off the rigid die surface during the numerical simulation of the forming process, the rigid surfaces are extended far enough so that contacting nodes will not slide off the master surfaces (ABAQUS Example Manual, 2002). Associated with the contact pairs, the Coulomb friction formulation (ABAQUS Theory Manual, 2002) was employed to model the friction effect characterised by a friction coefficient. The automatic shrink fit option specified in the ABAQUS input file was

used to solve the common problem of overclosure during the contact (ABAQUS Theory Manual, 2002). For membrane and shell elements, the contact problems were resolved by using the softened contact model to impose the clamping pressure in the thickness direction (ABAQUS User Manual, 2002).

5.2.1.4 Loading Steps

The following procedures are generally carried out in a practical blow forming operation (Hwang et al, 1996). The sheet is first heated to the required temperature range. The sheet is then clamped around its periphery and gas (normally argon) pressure is applied to inflate the sheet against the die configuration. Accordingly, several loading steps corresponding to each operational procedure are modelled to obtain an accurate simulation of superplastic blow forming in ABAQUS. Section 1.1 of Appendix 1 shows the ABAQUS code for the simulation of blow forming of a cylindrical cup. To avoid rigid body motion and contact status oscillation, in the first step a very small displacement is assigned to the upper die to establish a firm contact between the sheet and the dies. A force is then applied to the upper die to clamp the rim of the sheet as in a practical SPF process. A gas pressure is imposed on the bottom of the sheet, causing it to flow into the upper die geometry gradually. It should be noted that the sheet is fixed at the outside edge to avoid it slipping into the dies throughout the process. This effect is achieved in reality, by the gas sealing beads acting as grips.

5.2.2 Validation with Experimental Data

The algorithms described above have been implemented in the finite element program within ABAQUS to simulate the superplastic blow forming process. In order to evaluate the accuracy of the proposed FEM analysis, comparisons were performed with experimental data (Kim et al, 1996). The component in the experiment was an aluminium SUPRAL 150 alloy sheet of 0.88 mm initial thickness, which was bulged into a cylindrical cup of 30 mm in height and 100 mm in diameter with a fillet radius

of 4 mm. The experimental material constitutive relationship was fitted into an empirical expression of $\sigma = K\dot{\varepsilon}^m$ in reference (Kim et al, 1996), with the material parameters summarized in Table 5.2. The optimum strain rate during the whole forming process was set to be $6.93\times10^{-3}/s$ (Kim et al, 1996). The comparison was made possible by the fact that the simulation in this section modelled the same geometry, the same material characteristics and the same friction contact as those occurred in the reference (Kim et al, 1996). The friction coefficient modelled in the simulation was assumed to be uniform with a value of 0.4 (Kim et al, 1996). In addition, an element study, in terms of its ability to accurately predict the thickness distribution of the component, was performed and evaluated in comparison with the experimental data.

Table 5.2 Material parameters from experiment (Kim et al, 1996)

Material Parameters	Value
Material Constant K (MPa)	105.9
Strain Rate Sensitivity Index m	0.4

An initial comparison in terms of the computational time with different elements is given in Table 5.3. It is shown that the membrane formulation was the most economical approach, as only 268 seconds was needed. While for the continuum and shell elements, approximately three times more time was used. For a continuum element with a refined mesh pattern (CAX4R-b), more computational time was expected.

Table 5.3 Element type and mesh density

Label	Element type	Element Description	Element layers	CPU time (sec.)
CAX4R-a	CAX4R	Continuum Element	2	794
CAX4R-b	CAX4R	Continuum Element	4	885
SAX1	SAX1	Shell Element	1	788
MAX1	MAX1	Membrane Element	1	268

The predicted thickness distributions from different elements in comparison with the experiment are illustrated in Figure 5.2 with labels cross referenced in Table 5.3. A Fortran code to calculate the thickness distribution in a blow forming of cylindrical cup from ABAQUS data output is shown in Section 2.1 of Appendix 2. A fairly good

agreement between the predictions and experimental results was obtained with the maximum discrepancy within 25%, which demonstrated that the proposed finite element modelling could give a satisfactory prediction. In addition, the experiment indicated a greater thinning occurred at the corner of the upper die, which was demonstrated in accordance with the predicted thickness variation trend in all simulations. Although the least computational time was needed, the maximum discrepancy was found to be that with the membrane element in comparison with the experiment as shown in Figure 5.2. Furthermore, it was shown that the prediction from the continuum element was the most accurate in comparison with those from shell and membrane elements, possibly because the membrane and shell elements are constructed with simple assumptions which are not valid in a superplastic blow forming process as described in Section 5.2.1.2. Moreover, from the mesh study it was found that there was no difference between the thickness predictions from four-layer and two-layer continuum element mesh patterns, although a simulation with a two-layer mesh took less computing time, as shown in Table 5.3. It is therefore concluded that simulation using the continuum element gives the most accurate prediction, although more computational time may be necessary. On the basis of the above comparison, the continuum element with two layers mesh density was chosen to carry out the following parametric studies.

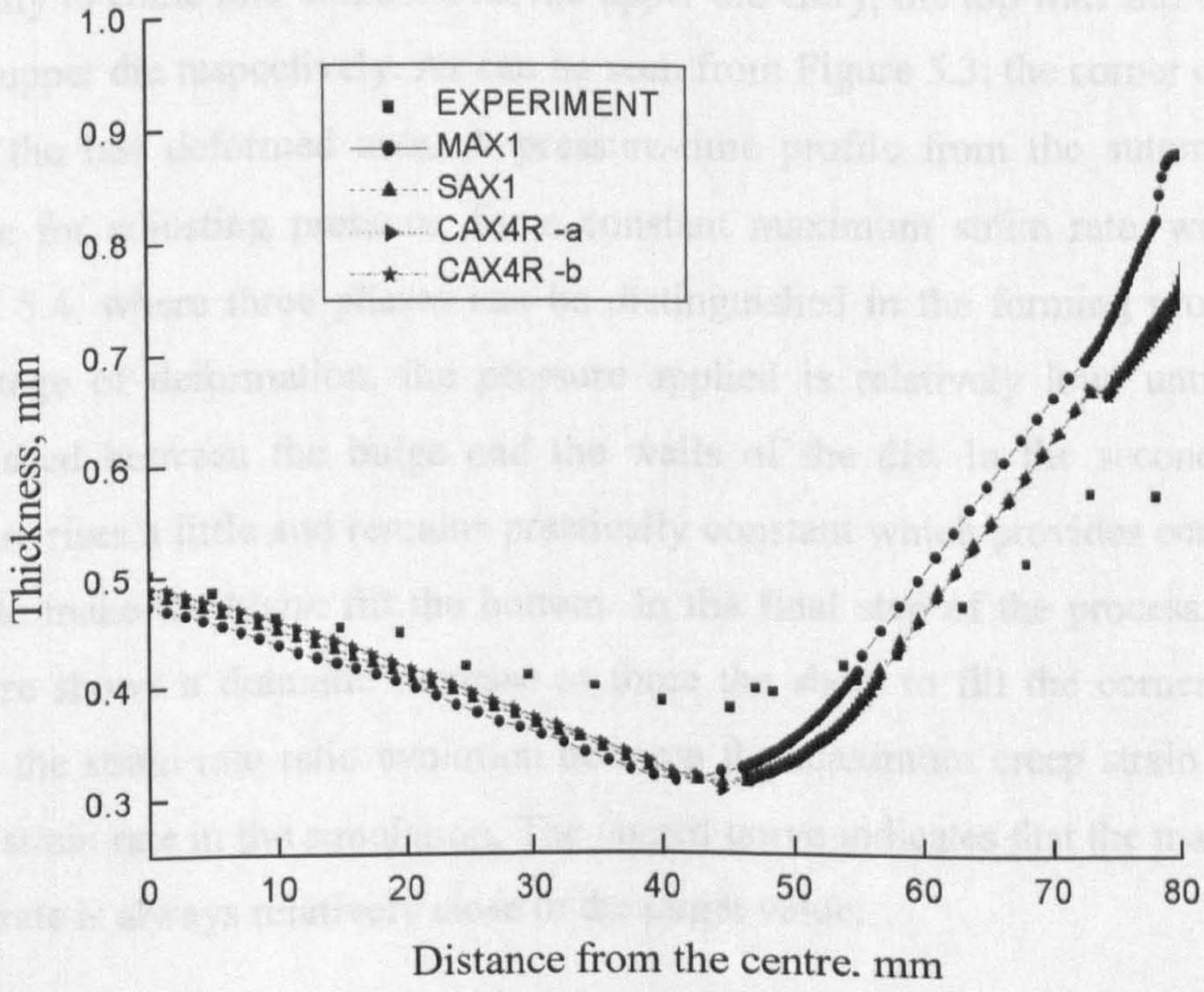

Figure 5.2 Comparison of thickness distribution of different element types with experiments

5.2.3 Results and Discussions

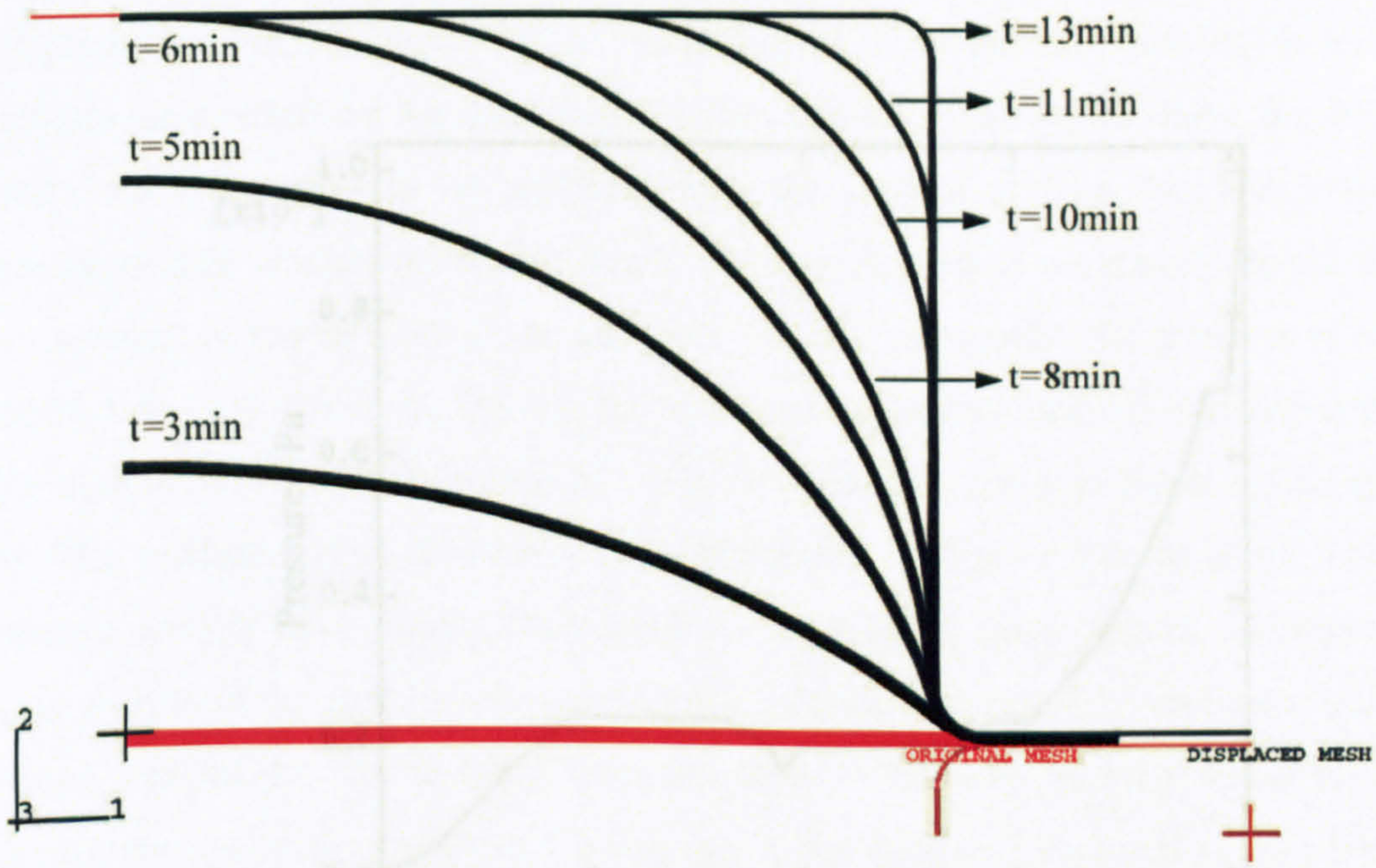

Figure 5.3 Different deformation processes with time from FEM

Typical deformation of the sheet in a superplastic blow forming process was predicted as shown in Figure 5.3. With an increase in the forming time, the sheet inflated gradually to come into contact with the upper die entry, the top wall and the side-wall of the upper die respectively. As can be seen from Figure 5.3, the corner of the upper-die is the last deformed area. A pressure-time profile from the automatic control scheme for adjusting pressure, for a constant maximum strain rate, was shown in Figure 5.4, where three phases can be distinguished in the forming process. At the first stage of deformation, the pressure applied is relatively low, until contact is established between the bulge and the walls of the die. In the second phase, the pressure rises a little and remains practically constant which provides enough driving force to make the blank fill the bottom. In the final step of the process, the applied pressure shows a dramatic increase to force the sheet to fill the corner. Figure 5.5 shows the strain rate ratio evolution between the maximum creep strain rate and the target strain rate in the simulation. The jagged curve indicates that the maximum peak strain rate is always relatively close to the target value.

The effects of the friction coefficient, the strain rate and the strain rate sensitivity index on the thickness distribution in the superplastic blow forming process have been investigated and are presented in the following sections.

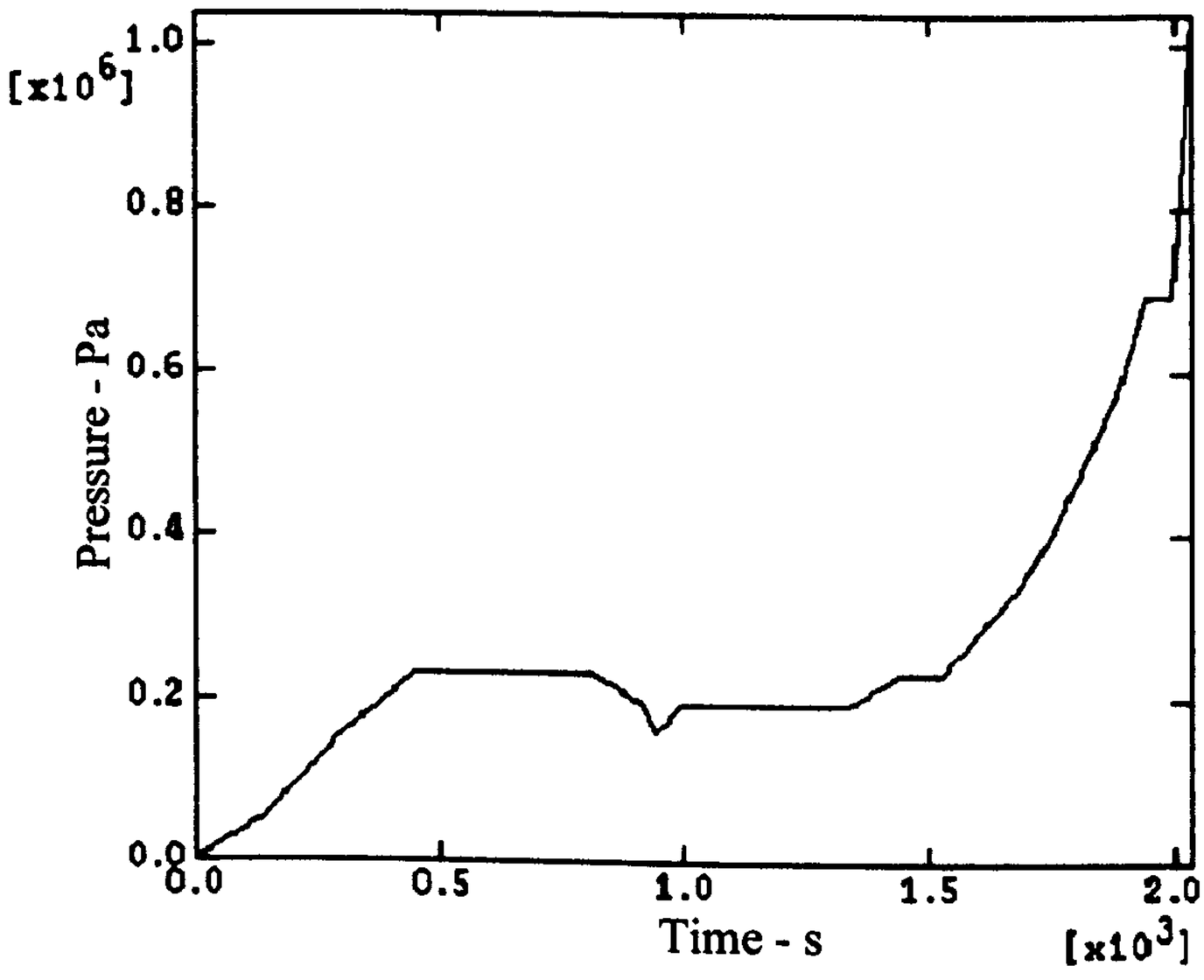

Figure 5.4 Pressure profile of superplastic blow forming

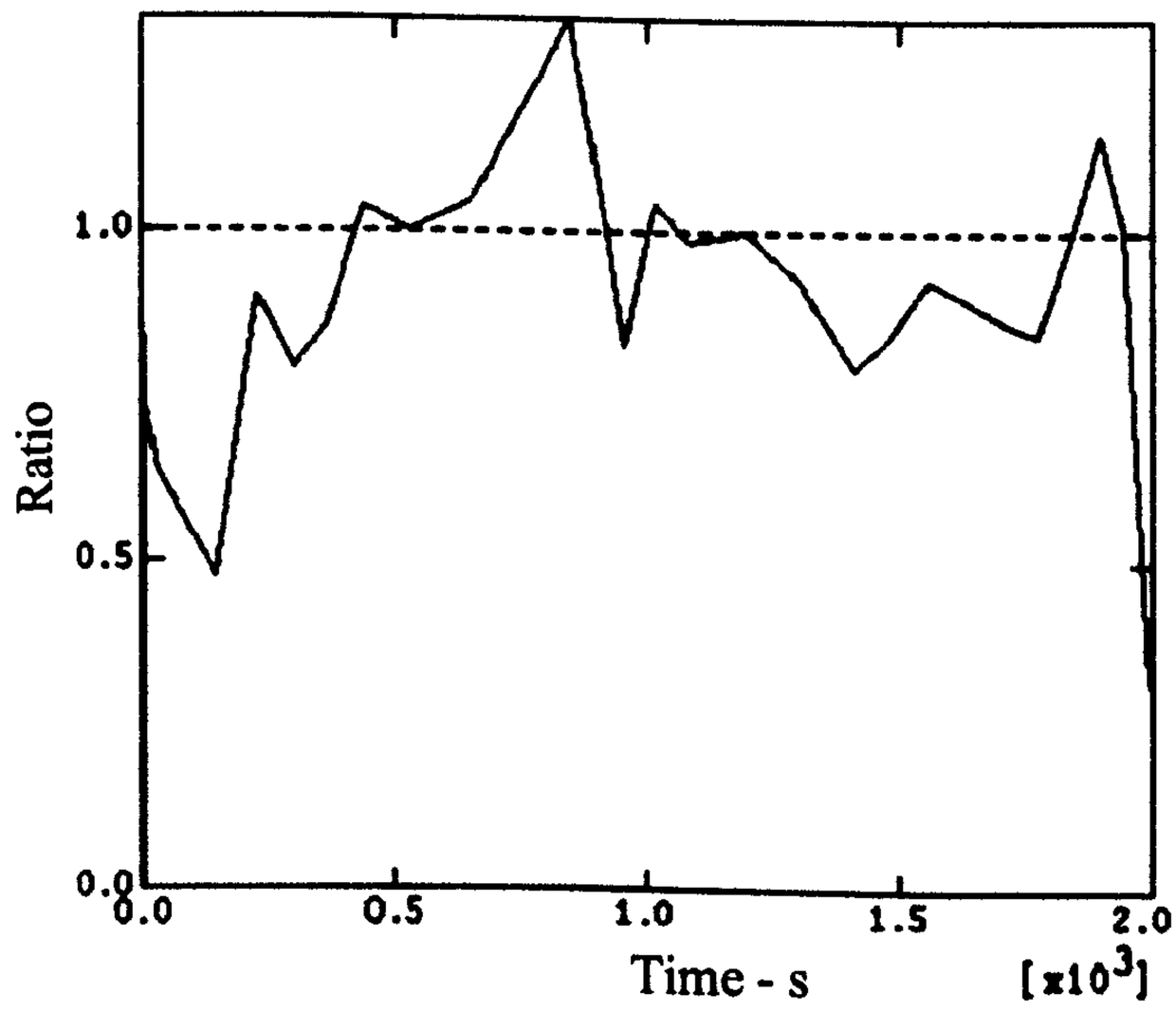

Figure 5.5 History of ratio between the maximum creep strain rate and target creep strain rate

5.2.3.1 The Effect of Friction Coefficient

Friction is widely recognized as an important factor affecting thinning of SPF components. A crucial factor in the modelling of blow forming problem is how to simulate the contact and the associated friction effects. As an initial study, the friction coefficient is assumed to be uniform along the contact surface. No lubrication is considered and changes in friction due to changes in surface roughness are not taken into account in the simulation. In addition, the friction coefficient is select to range from 0.1 to 0.9. Therefore, the effects of friction upon the forming pressure and the quantitative thickness distribution of the component are shown in Figures 5.6 (a) and (b). The predicted pressure-time curves illustrated in Figure 5.6 (a) show that the pressure initially rises rapidly, followed by a comparably stable region, and increases again sharply at the end, (the same trend as described before). With an increase in the friction coefficient, the forming time increases, while the corresponding forming pressure decreases. From Figure 5.6 (b), the thickness at the edge and at the centre of the upper die is relatively greater than that elsewhere, while the minimum section is located at the corner of the upper die, regardless of the friction coefficient. From Figure 5.6 (b), it can be seen that a lower friction coefficient results in a more uniform thickness distribution through the component.

The above observations can be explained as follows. During the initial stage of inflation, because the sheet is not in contact with the upper die except at the flange area, deformation of the sheet is concentrated at the centre and consequently this region shows the greatest strain because of higher stresses at centre. Once the sheet comes into contact with the centre of the upper-die and spreads progressively to the top-corner, friction tends to resist further deformation. Due to the symmetry constraint and tensile nature of load in plane of sheet, the material can only flow from the centre to the corner of the upper die. With the outer edge being assumed fixed in the simulation, the material can only flow from the die entry to the corner of the upper die. The remaining free regions of the sheet continue to deform making the formed section more uniform. The lower the coefficient of friction, the more volume flows into the corner, which reduces severe thinning around the corner and greater forming pressure is needed to fill the corner. Since the corners of the die are usually the last

regions to be filled, the greatest strain is developed at these points. The minimum thickness is generally at corners where rupture may occur during superplastic forming. Since the maximum thinning is observed at these critical zones, the material behaviour in these zones plays an important role in obtaining components of high quality.

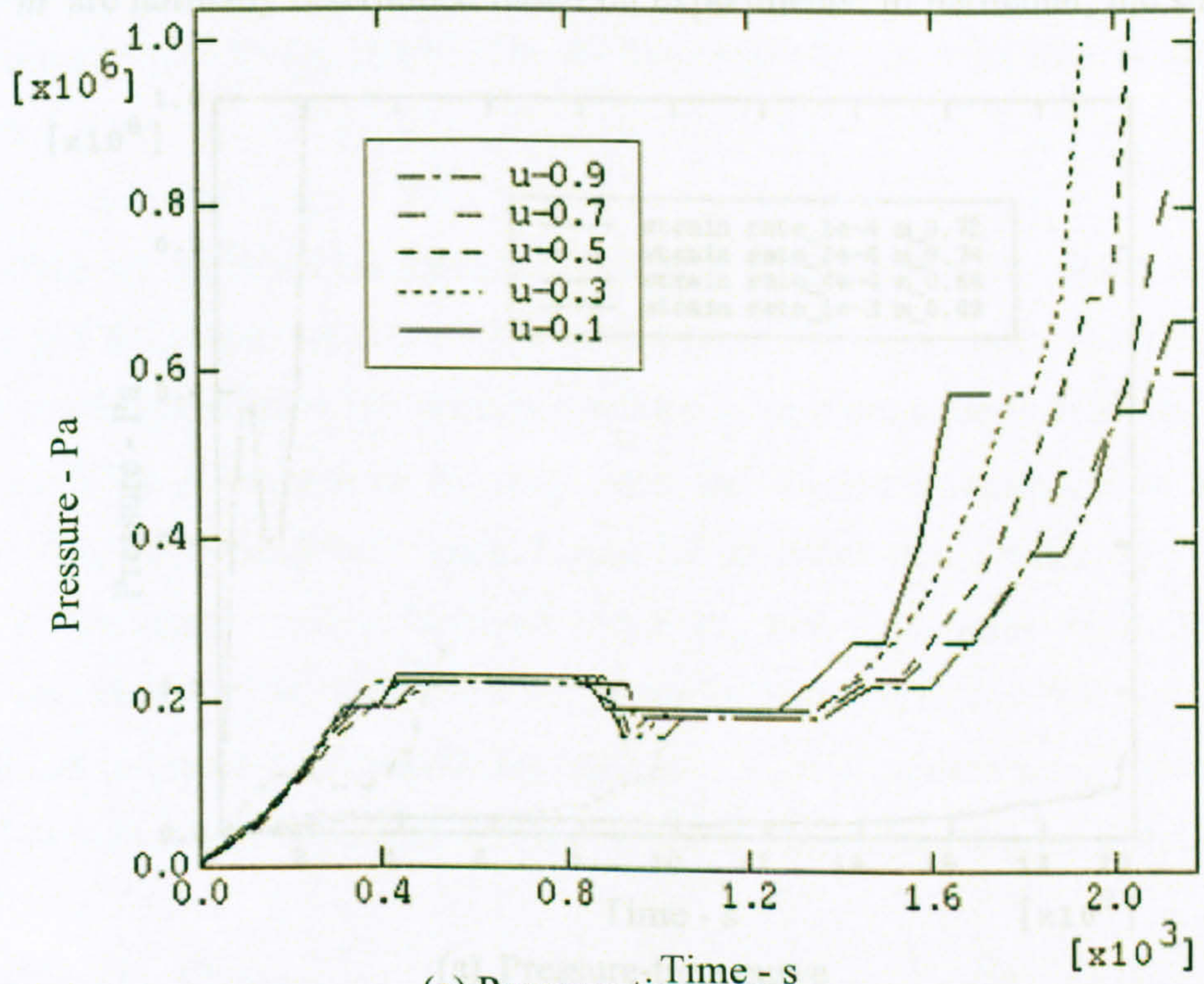

(a) Pressure-time curve

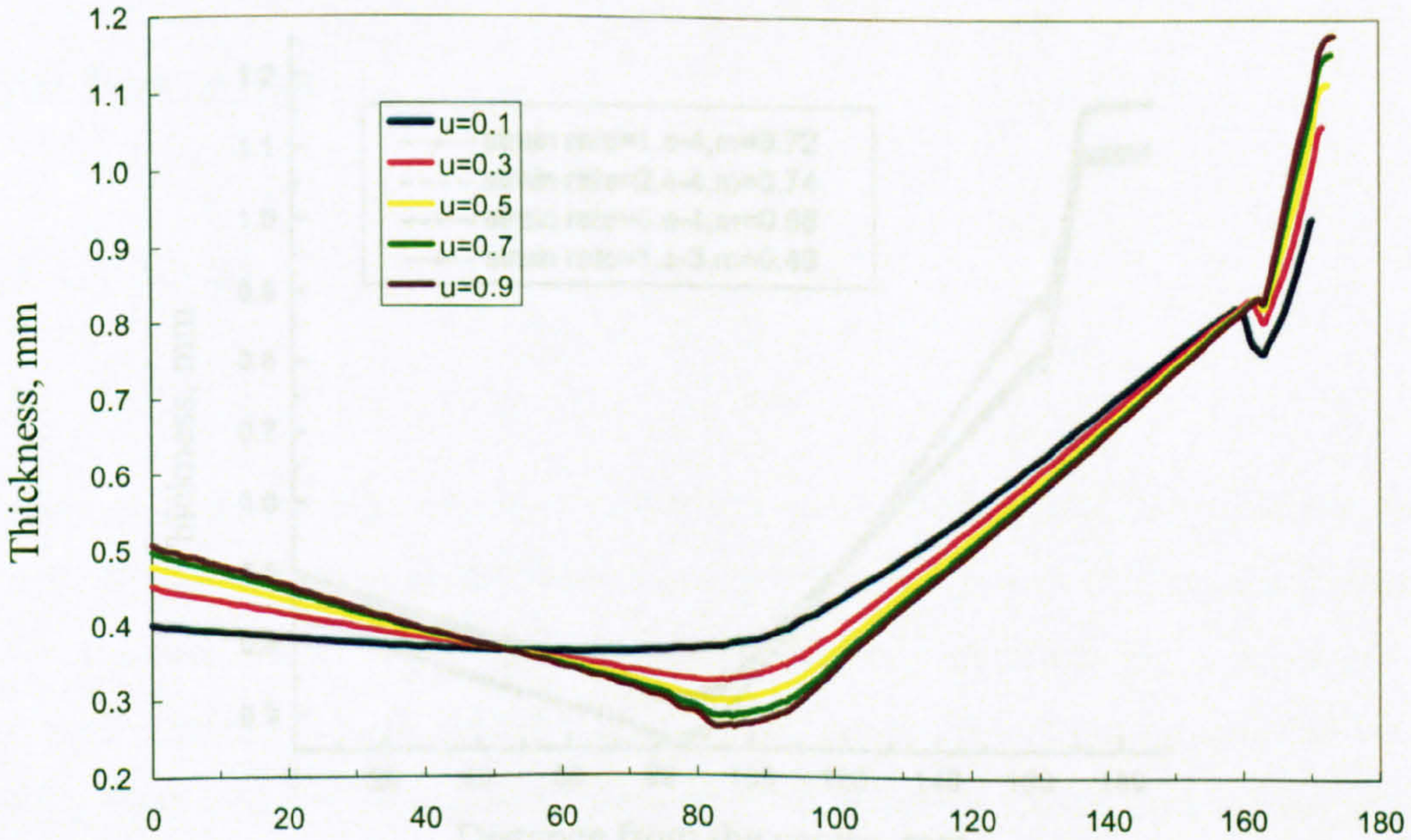

(b) Thickness distribution

Figure 5.6 Effects of friction of coefficient

5.2.3.2 The Effect of the Strain Rate and the Strain Rate Sensitivity Index

Material parameters such as the material constant K and the strain rate sensitivity index m are normally determined based on experiments. In particular, the strain rate

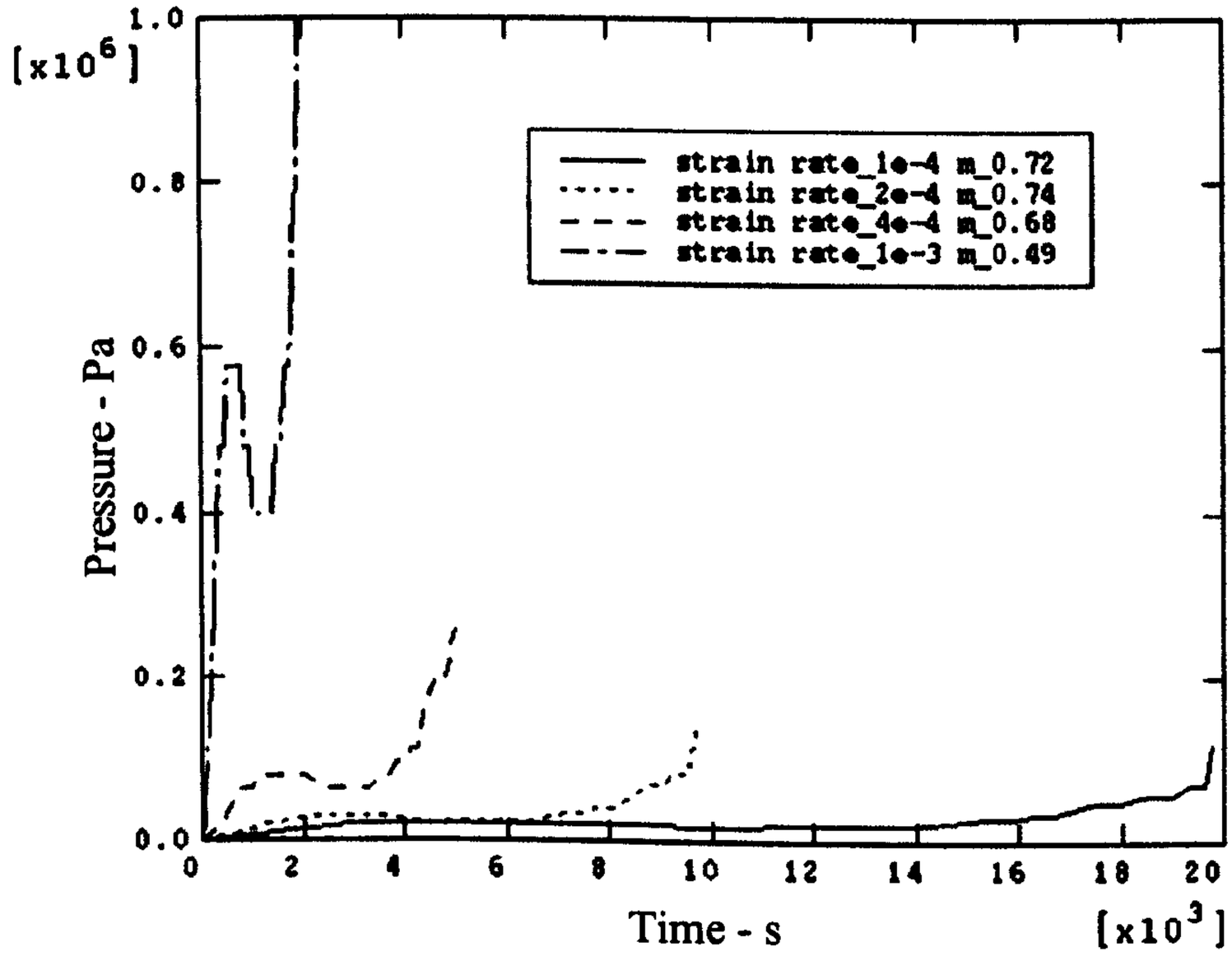

(a) Pressure-time curve

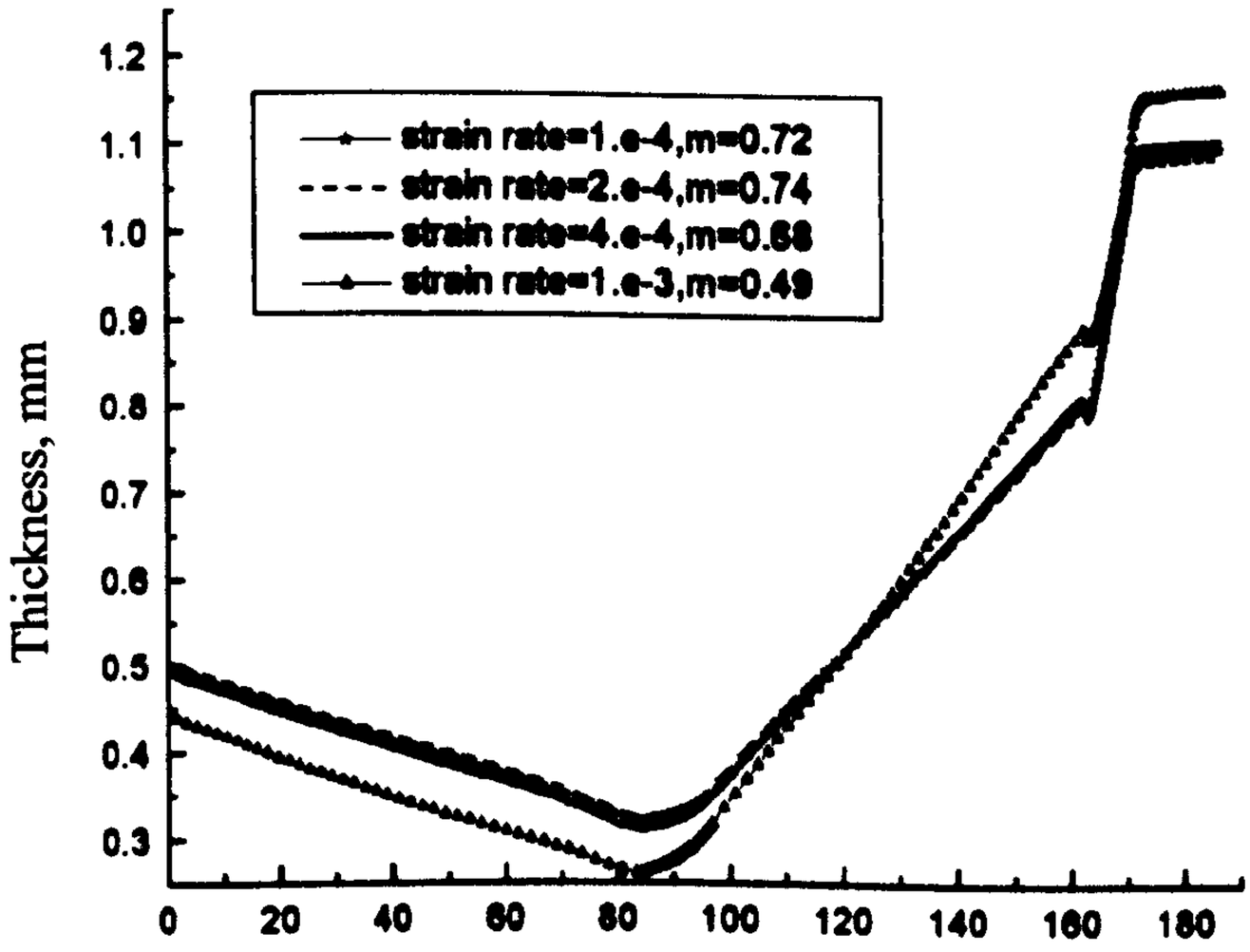

(b) Thickness distribution

Figure 5.7 Effects of the strain rate and the strain rate sensitivity index

sensitivity index m is sensitive to the strain rate, which has a maximum value at an optimum strain rate. In this analysis, the relationship between m and the strain rate $\dot{\varepsilon}$ of Ti-6Al-4V alloys at $T = 900\,°C$ is taken from experiments (Stephen, 1986). As for the material constant K, it is proposed to be a function of the structure, temperature T and the strain rate $\dot{\varepsilon}$ (Arieli and Mukherjee, 1982). However, since this relationship is not readily available from experiment, K is assumed to be a constant in accordance with Cheng (1996). The friction coefficient is assumed to be 0.5 in this section.

The effects of the strain rate and the strain rate sensitivity index upon the pressure profile and thickness variation are shown in Figures 5.7 (a) and (b). From Figure 5.7 (a), it can be seen that a low value of m results in a dramatic increase in forming pressure. With a decrease in the strain rate, the necessary forming time increases greatly. The thickness distribution in Figure 5.7 (b) shows that a better, homogeneous thickness distribution can be obtained with a relatively high value of m. When the strain rate sensitivity is close to the maximum m value, it is expected that it has no significant influence on the thickness variation. This is because a high value of m confers a high resistance to neck development and, thus results in good material flow.

5.3 Finite Element Analysis of Superplastic Reverse Blow Forming

5.3.1 General

The reverse blow forming method is nowadays recognized as an effective technique of obtaining a good thickness distribution in complex components (Pilling and Ridley, 1989). However, little is available in the published literature for a reasonable interpretation of the good thickness control in the reverse blow forming process. This study has been initiated and guided by the need to establish a clear understanding of the thickness control mechanism in the reverse forming process.

Generally reverse blow forming process consists of two operations starting from an initial sheet. As shown in Figure 5.8, in the first operation gas pressure is imposed on the top of the heated sheet. After producing the pre-forming shape, the forming pressure is reversed, forcing the material to flow into the final tool (Vieilledent and Fourment, 2000). This method requires an optimisation for the shape of a pre-forming tool during a two-step operation for which the shape of a second operation is known. An optimal shape of the pre-forming tool is designed so that a prescribed thickness distribution in the final component can be obtained. Such a design has been traditionally conducted by skilled experts who, based on their past experience and intuition, build a pre-forming prototype and modify it by trial-and-error experiments. However, such a design procedure has turned out to be costly and time consuming. Therefore, finite element based process simulation is adopted efficiently to optimise process design.

The candidate component design for the simulation of the reverse blow forming process was supplied by Rolls-Royce Plc at Derby. In the following sections, the superplastic reverse forming of a Ti-6Al-4V sheet into the shaped component is described. To understand the thinning control mechanism, a simulation of the same structure under a non-reverse forming process was also carried out and a comparison made between the reverse forming and the non-reverse forming. Furthermore, the effect of friction coefficients was evaluated and discussed.

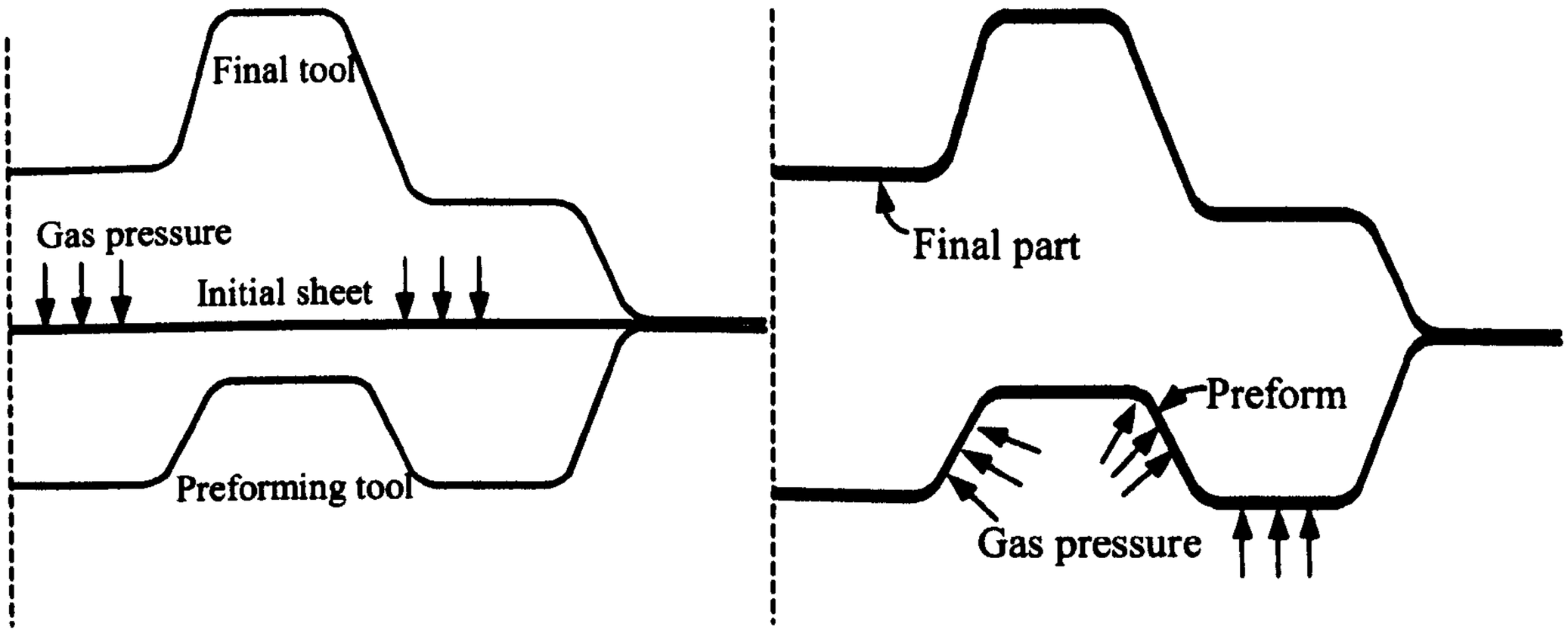

Figure 5.8 Schematic diagram of reverse forming

5.3.2 Modelling Description

The reverse forming tool design studied in the simulation is shown in Figure 5.9, including a pre-forming upper die and a final forming lower die. A circular sheet of 3 mm in thickness and 330 mm in diameter, of which the periphery is clamped between the two dies, is subjected to gas pressure. The simulation of the reverse blow forming of the sheet can be simplified as an axisymmetric case. An axis symmetric cross section of the dies and the sheet assembly was modelled.

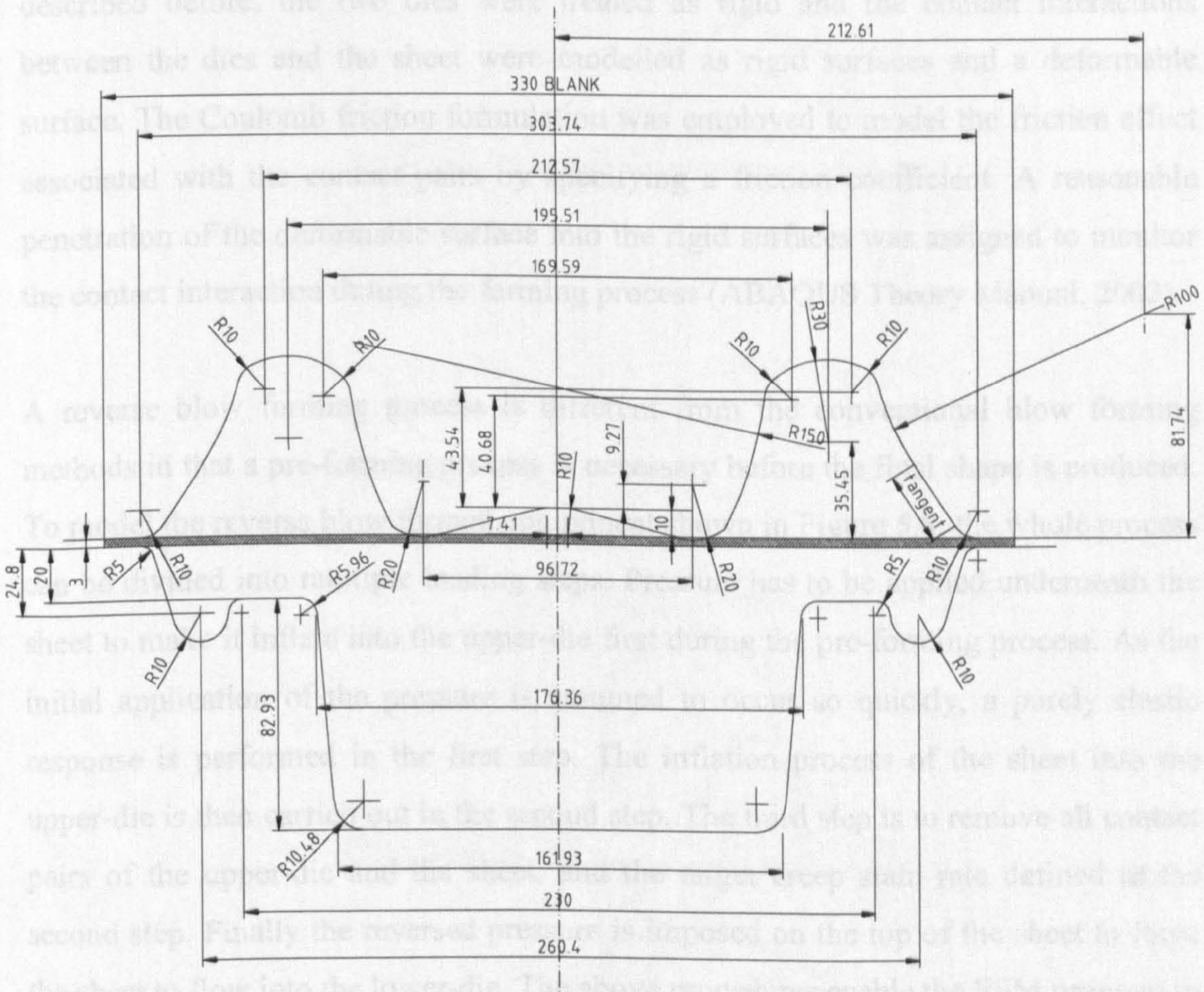

Figure 5.9 Geometry of the reverse forming tool for a complex component (unit: mm)

The material used in the simulation is a Ti -6Al-4V alloy sheet with the material properties shown in Table 5.1 (Cheng, 1996). The material properties were implemented into an isotropic creep model within ABAQUS as described in Section 5.2.1.1. From the element study described in Section 5.2.2, a continuum element was

selected to model the blow forming process. In addition, the regions where stress concentrations are significant were constructed with finer meshes. To model the superplastic deformation, an iterative Newton-Raphson solution technique was employed to solve the governing nonlinear equations. The imposed gas pressure was controlled by a special solution dependent magnitude scheme (ABAQUS, 2002) to maintain an approximately constant strain rate of 0.001/s in the simulation.

The friction associated with the contacts between the sheet and the dies is very important for superplastic reverse blow forming process. An important factor in modelling of the process is how to simulate the friction effect due to contact. As described before, the two dies were treated as rigid and the contact interactions between the dies and the sheet were modelled as rigid surfaces and a deformable surface. The Coulomb friction formulation was employed to model the friction effect associated with the contact pairs by specifying a friction coefficient. A reasonable penetration of the deformable surface into the rigid surfaces was assigned to monitor the contact interaction during the forming process (ABAQUS Theory Manual, 2002).

A reverse blow forming process is different from the conventional blow forming methods in that a pre-forming process is necessary before the final shape is produced. To model the reverse blow formed component shown in Figure 5.8, the whole process can be divided into multiple loading steps. Pressure has to be applied underneath the sheet to make it inflate into the upper-die first during the pre-forming process. As the initial application of the pressure is assumed to occur so quickly, a purely elastic response is performed in the first step. The inflation process of the sheet into the upper-die is then carried out in the second step. The third step is to remove all contact pairs of the upper-die and the sheet, and the target creep stain rate defined in the second step. Finally the reversed pressure is imposed on the top of the sheet to force the sheet to flow into the lower-die. The above procedures enable the FEM program to model the reverse forming process. Section 1.2 of Appendix 1 shows the ABAQUS code for the simulation of the reverse formed component.

5.3.3 Results and Discussions

5.3.3.1 Reverse Blow Forming

It is important that a good FEM model is capable of predicting the reverse blow forming behaviour. The deformation configuration in the reverse forming process has been predicted, as shown in Figure 5.10. In particular, Figure 5.10 (a) shows the

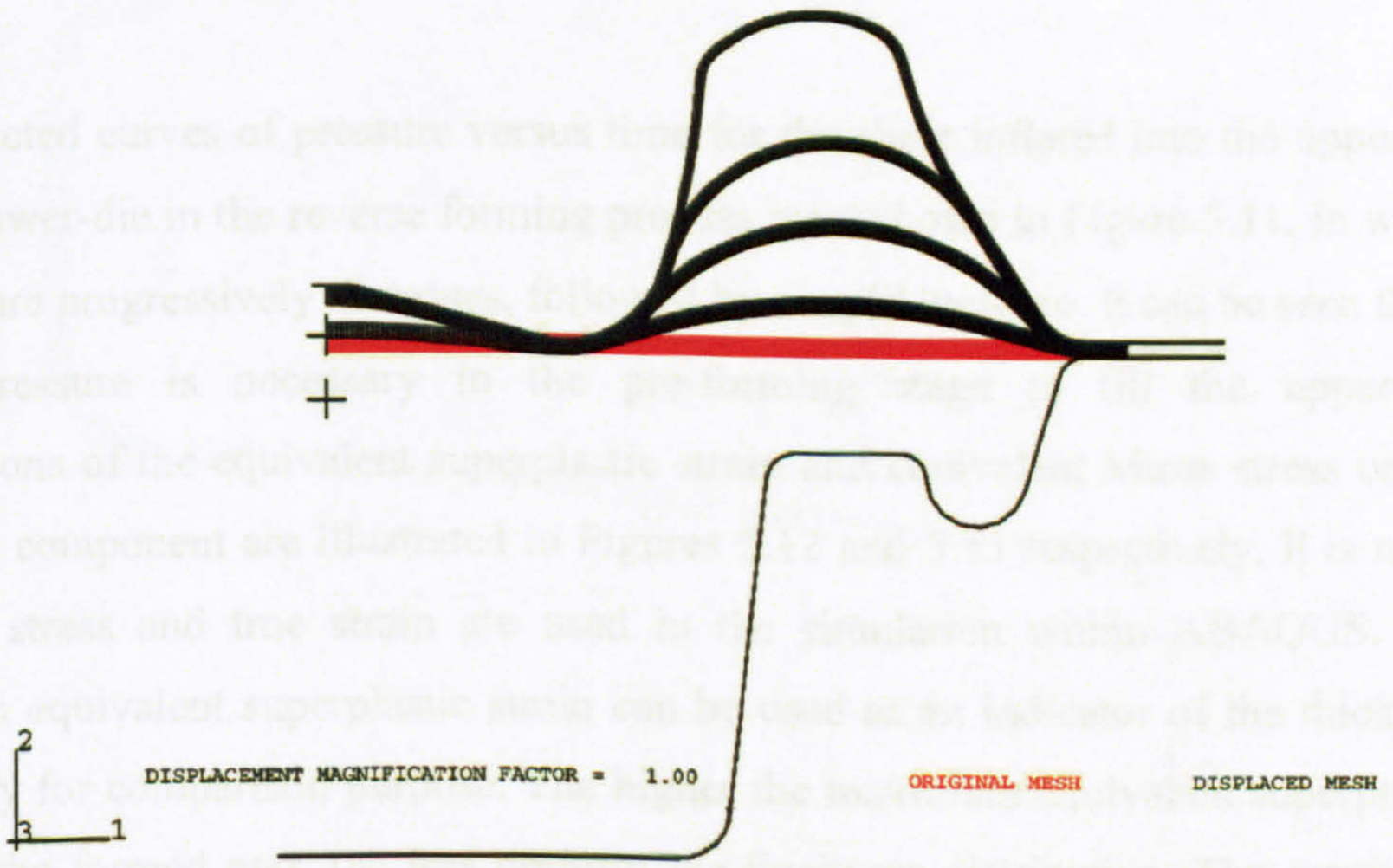

(a) To the Pre-forming die

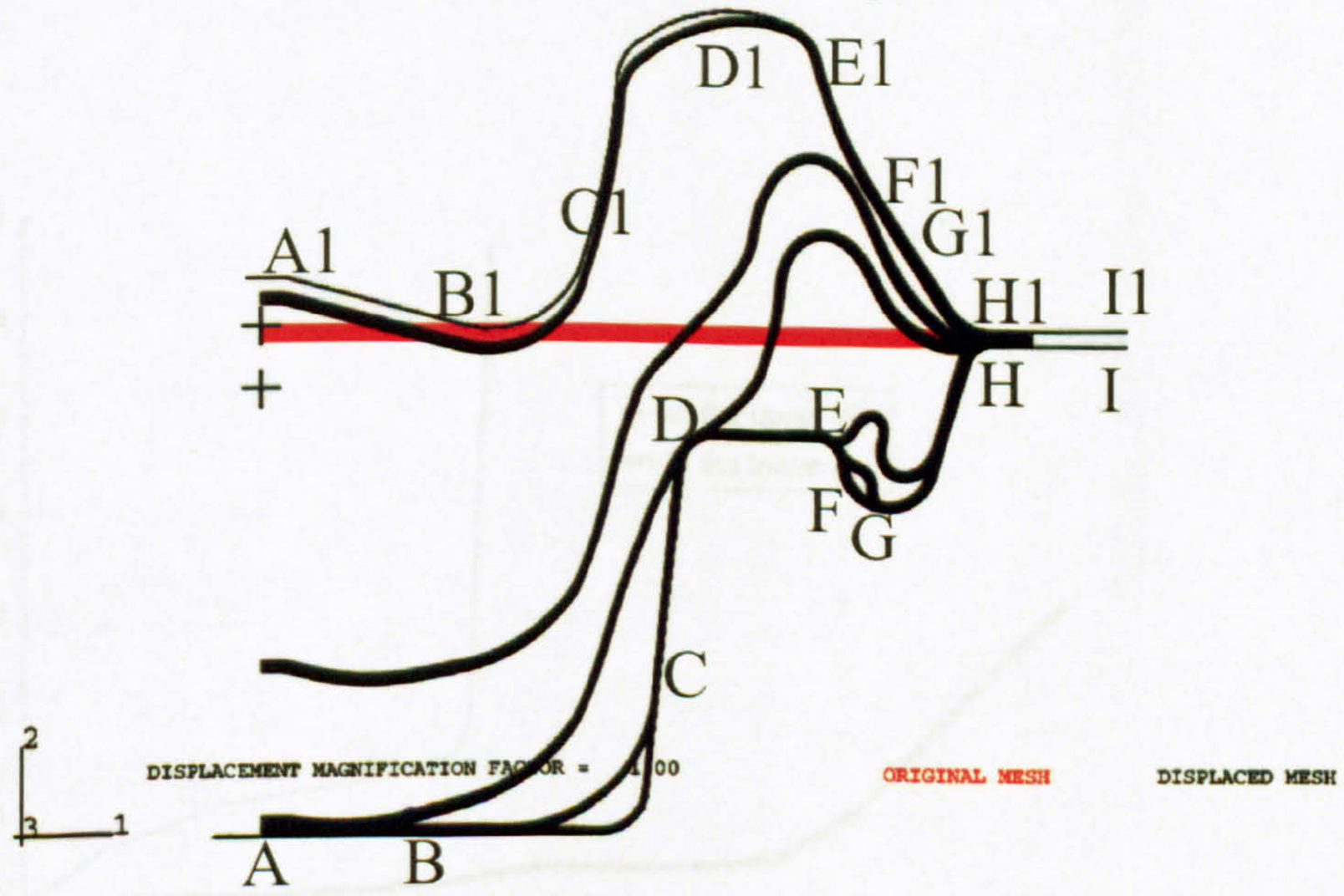

(b) Reverse forming to the lower-die

Figure 5.10 Finite element simulation of reverse blow forming process

process of the sheet bulging into the pre-forming die, i.e., the upper-die, whilst in Figure 5.10 (b) shows the reverse process into the final die. For the convenience of description, let points ranging from A1 to I1 represent the deformation instants to the upper-die, whilst points A to I represent the corresponding instants where the material flow into the lower-die. It can be seen that large deformation is concentrated around the bubble area (region C1 to H1) in the pre-forming process, resulting in a thickness profile in which the centre and the clamped area are thicker than the bubble area. After filling the upper-die, the sheet moves downward gradually to the bottom AB, region DE and the bottom corner BC respectively.

The predicted curves of pressure versus time for the sheet inflated into the upper-die and the lower-die in the reverse forming process were shown in Figure 5.11, in which the pressure progressively increases, followed by a rapid increase. It can be seen that a higher pressure is necessary in the pre-forming stage to fill the upper-die. Distributions of the equivalent superplastic strain and equivalent Mises stress on the deformed component are illustrated in Figures 5.12 and 5.13 respectively. It is noted that true stress and true strain are used in the simulation within ABAQUS. The maximum equivalent superplastic strain can be used as an indicator of the thickness uniformity for comparison purpose. The higher the maximum equivalent superplastic strain in the formed part, the less uniform the thickness distribution. The maximum strain and maximum stress both occur at the small corner in the reverse forming process.

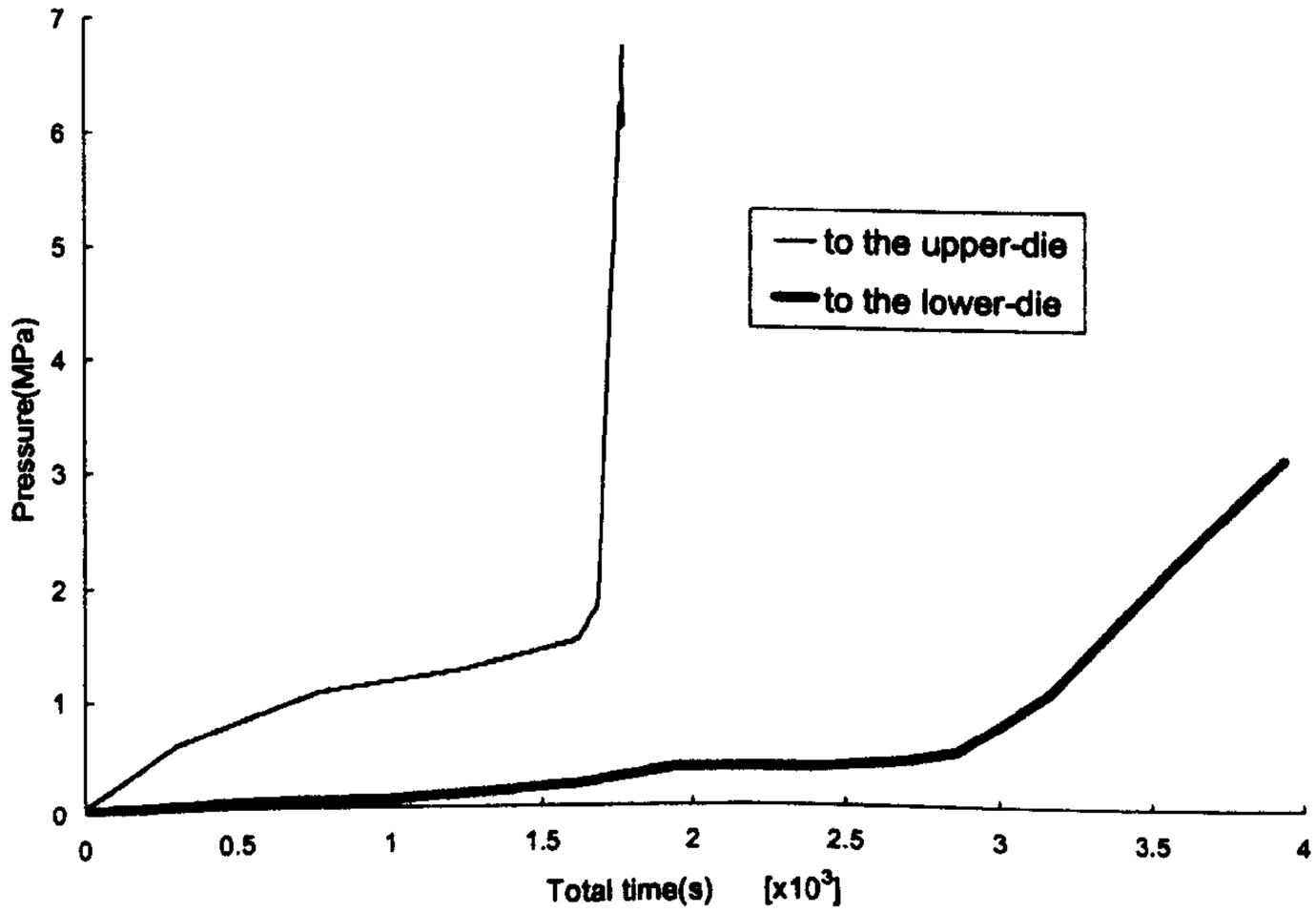

Figure 5.11 Pressurisation curves in the reverse forming process

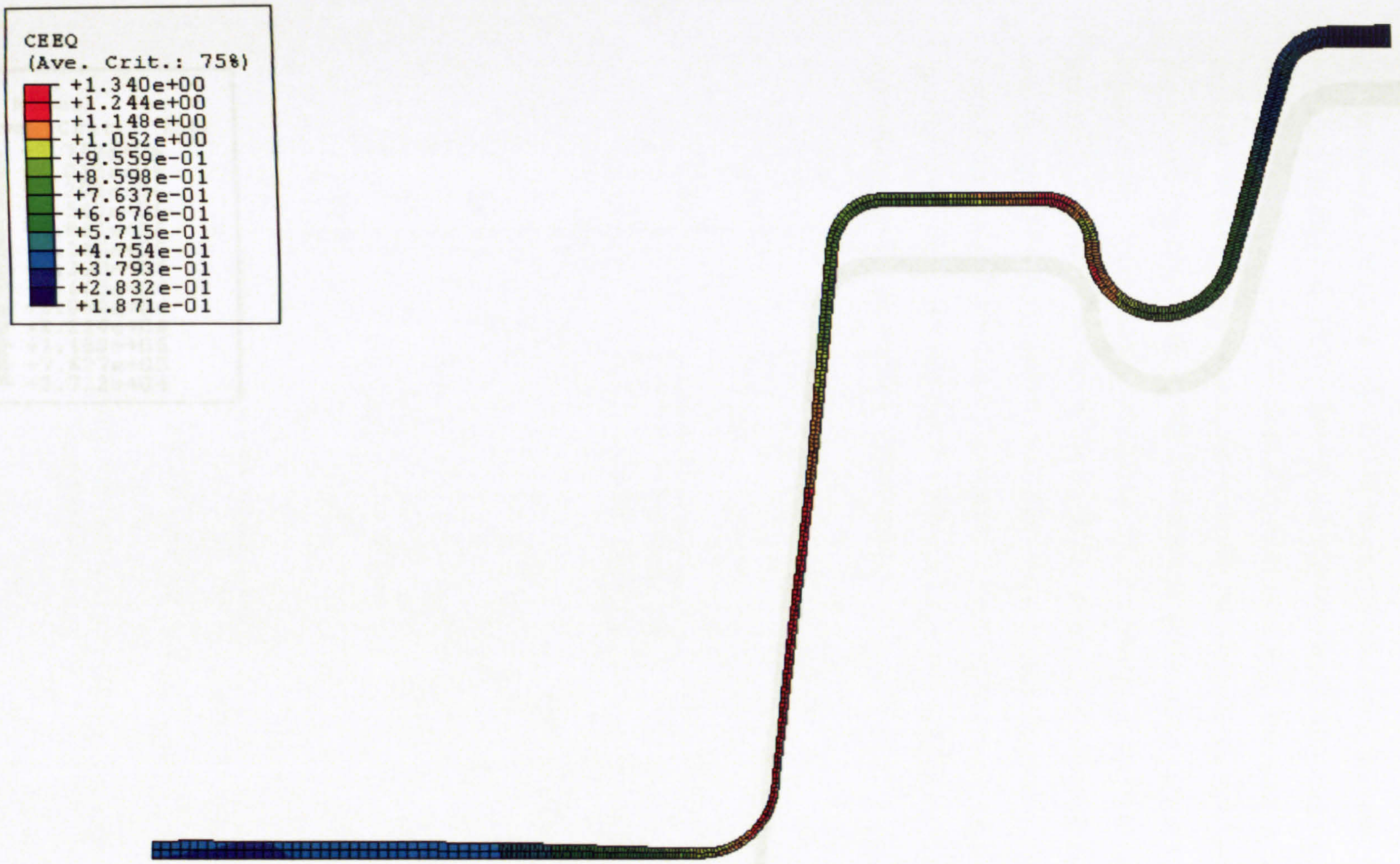

Figure 5.12 Equivalent strain distribution in reverse forming

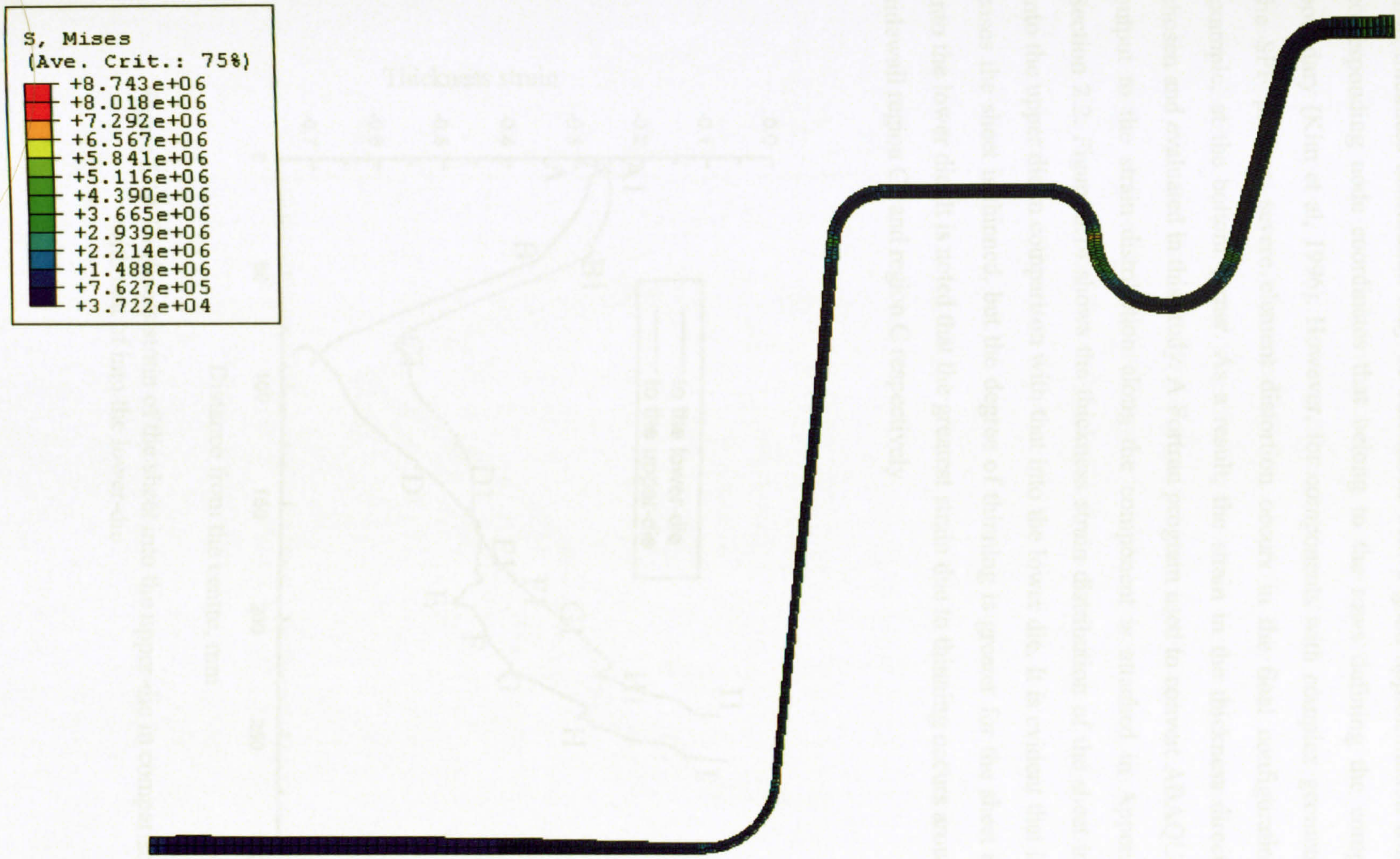

Figure 5.13 Mises stress distribution in reverse forming

The thickness distribution along the component is essential to evaluate whether the formed component is successful or not. For components with simple geometries, the final thickness distribution may be calculated with a good approximation using the corresponding node coordinates that belong to the rows defining the component boundary (Kim et al, 1996). However, for components with complex geometries in the SPF process, severe element distortion occurs in the final configuration, for example, at the bottom corner. As a result, the strain in the thickness direction is chosen and evaluated in this study. A Fortran program used to convert ABAQUS data output to the strain distribution along the component is attached in Appendix 2, Section 2.2. Figure 5.14 shows the thickness strain distribution of the sheet inflated into the upper die in comparison with that into the lower die. It is evident that in both cases the sheet is thinned, but the degree of thinning is greater for the sheet bulged into the lower die. It is noted that the greatest strain due to thinning occurs around the sidewall region C1 and region C respectively.

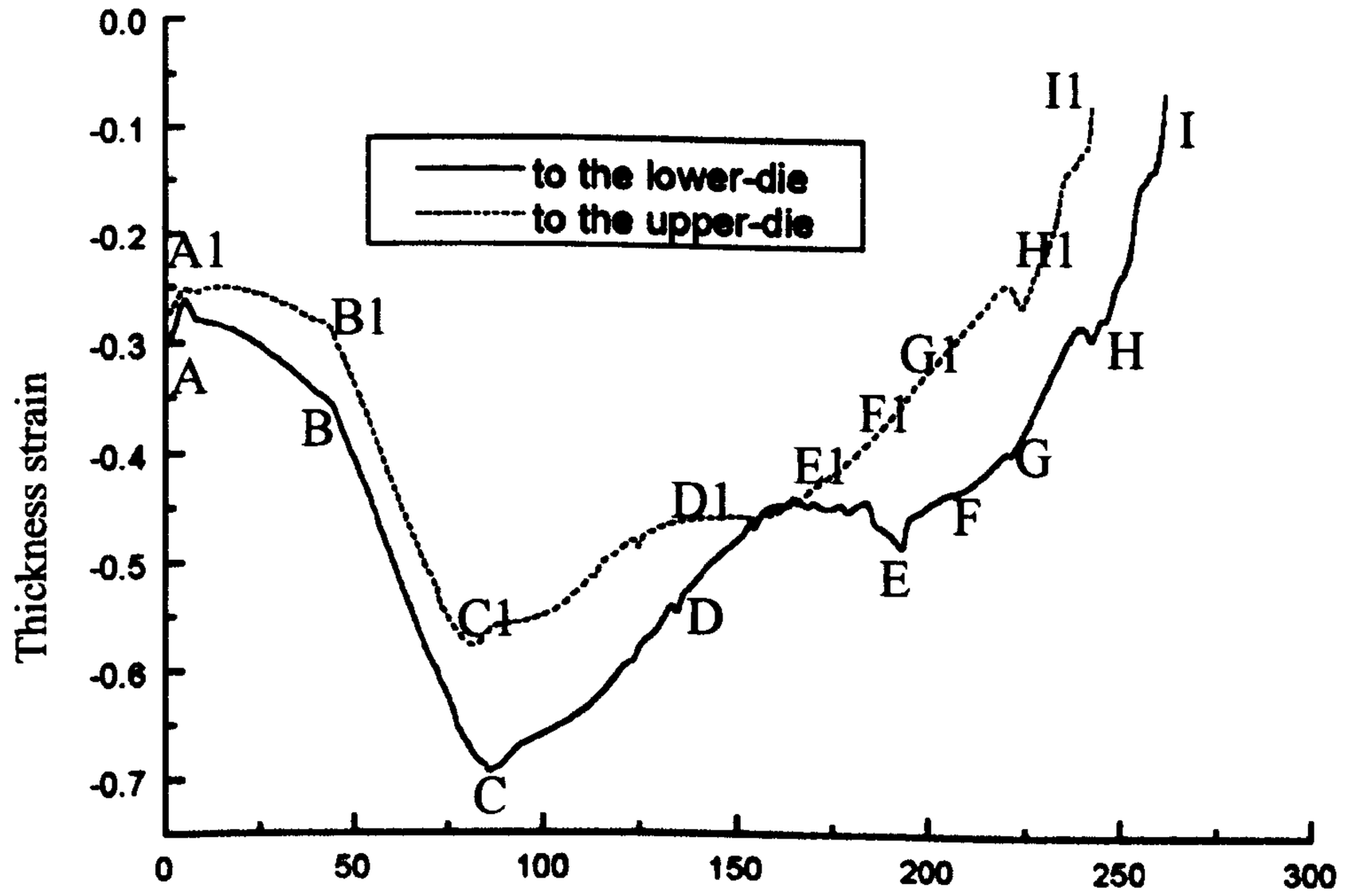

Figure 5.14 Thickness strain of the sheet into the upper-die in comparison with that of into the lower-die

The effect of friction on the thinning of a component in the reverse blow forming process was studied, in which the friction coefficient was assumed to be uniform along the contact surface, varying from 0.1 to 0.5 in the simulation. The distributions of thickness strain under different friction coefficients are illustrated in Figure 5.15. Again, greater thinning occurs around the side-wall region C of the lower die for all values of the friction coefficient studied. The lower the friction coefficient, the more uniform thickness distribution along the component. It is noted that when the friction coefficient is greater than 0.4, the thickness strain sharply changes around the outside corner (region EG) as illustrated in Figure 5.15. This is mainly because higher friction force resists material flow in contact regions and thus results in sharp thickness variations in the simulation.

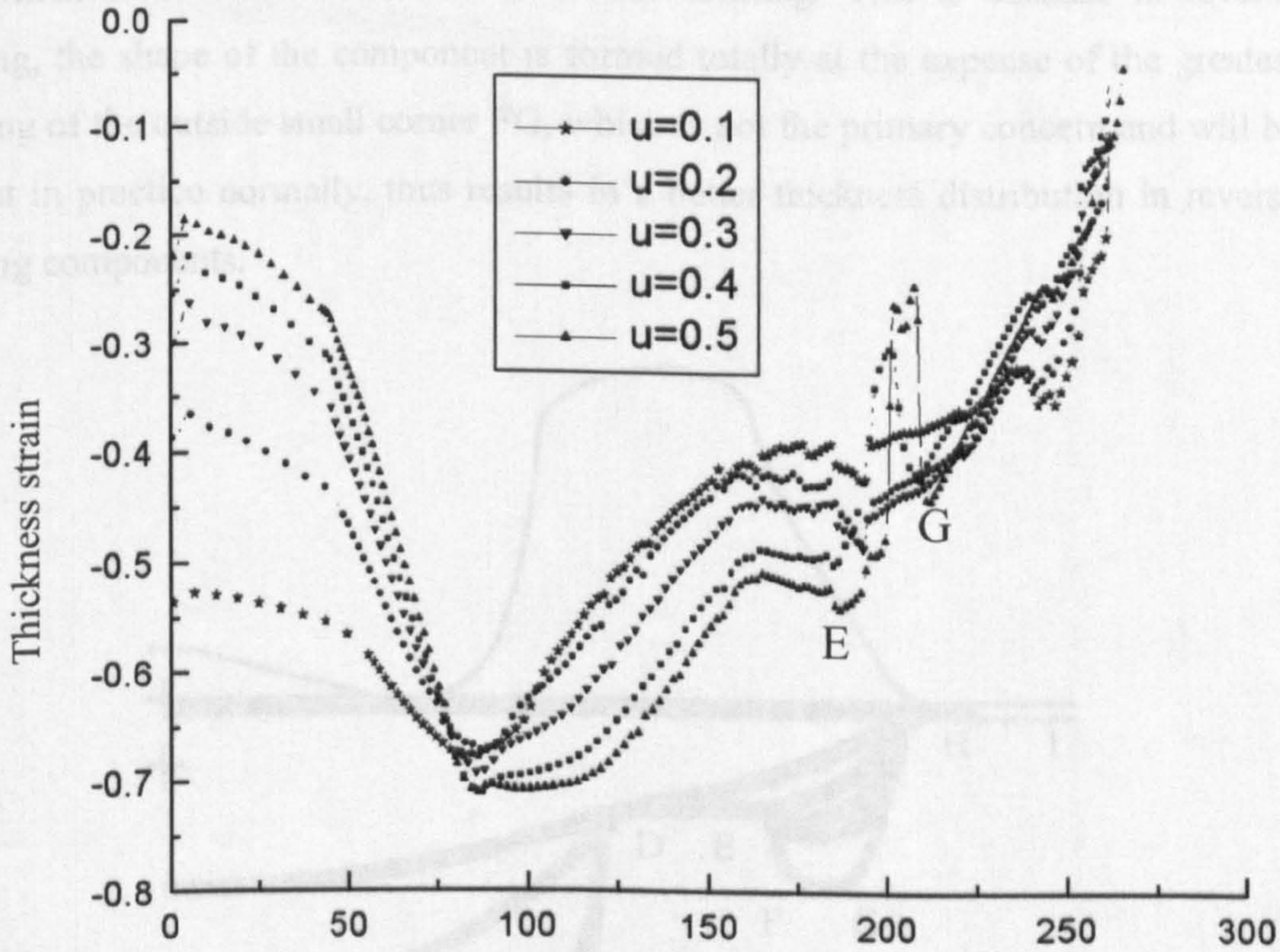

Figure 5.15 Effect of the friction coefficient

5.3.3.2 Comparison of Reverse Forming and Non-reverse Forming

To further understand the effect of reverse forming on the component thickness distribution, simulation of a non-reverse forming process for the same sheet was also conducted for a comparison with that of reverse forming. Similar to reverse forming, the deformation configuration of non-reverse forming is presented in Figure 5.16, showing the sequences of contact with bottom region AB, region DE and the bottom corner BC respectively. In addition, in Figures 5.17 and 5.18 the equivalent strain and the Mises stress distributions in a non-reverse forming process are shown. It is shown that the maximum stress locates in the small corner in the deformation configuration, which is the same as that in a reverse forming process. However, the maximum equivalent strain distribution in non-reverse forming is at the bottom corner region BC, which is different from that of reverse forming. This is because in reverse forming, the shape of the component is formed totally at the expense of the greatest thinning of the outside small corner FG, which is not the primary concern and will be cut out in practice normally, thus results in a better thickness distribution in reverse forming components.

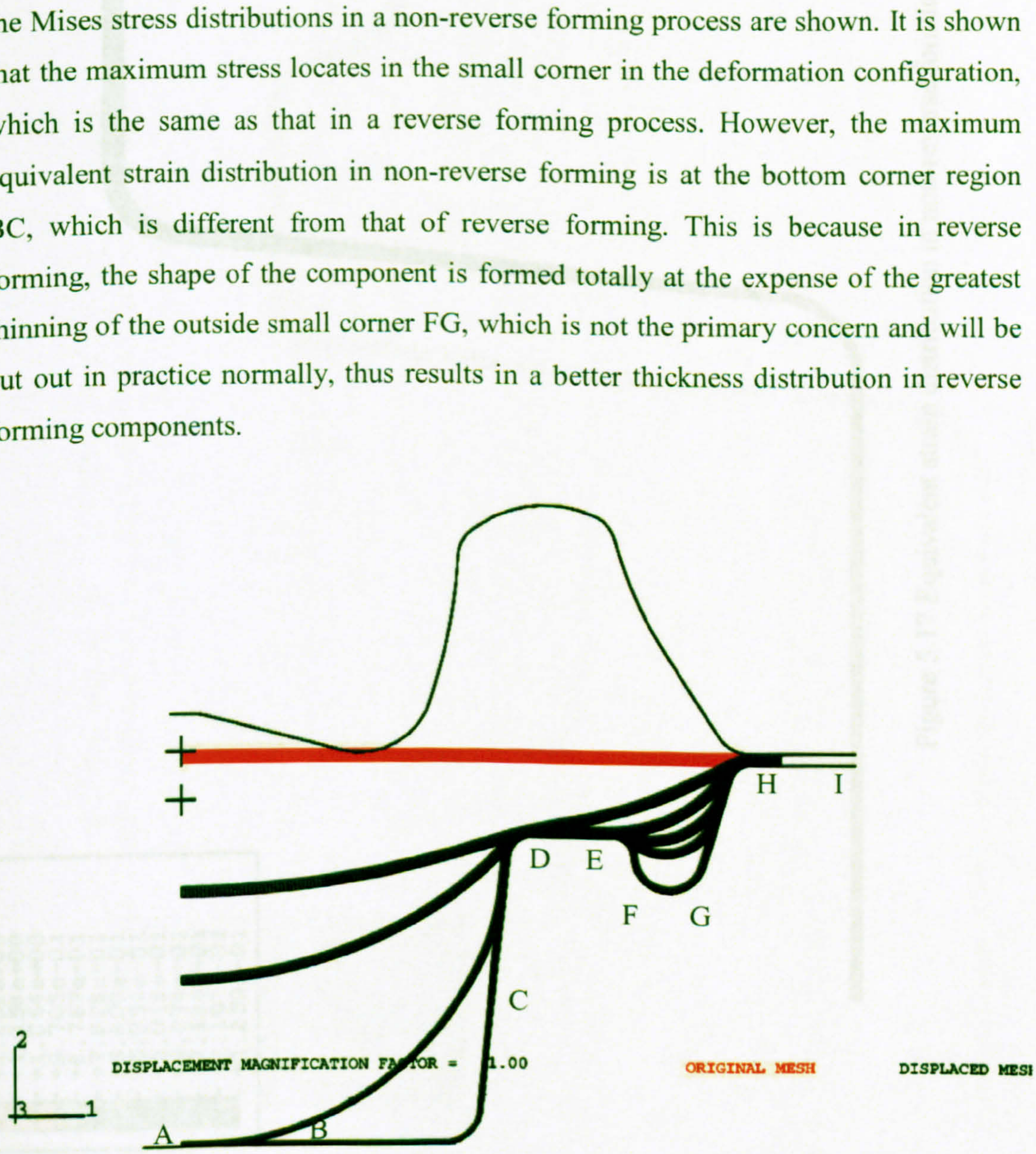

Figure 5.16 non-reverse forming processes

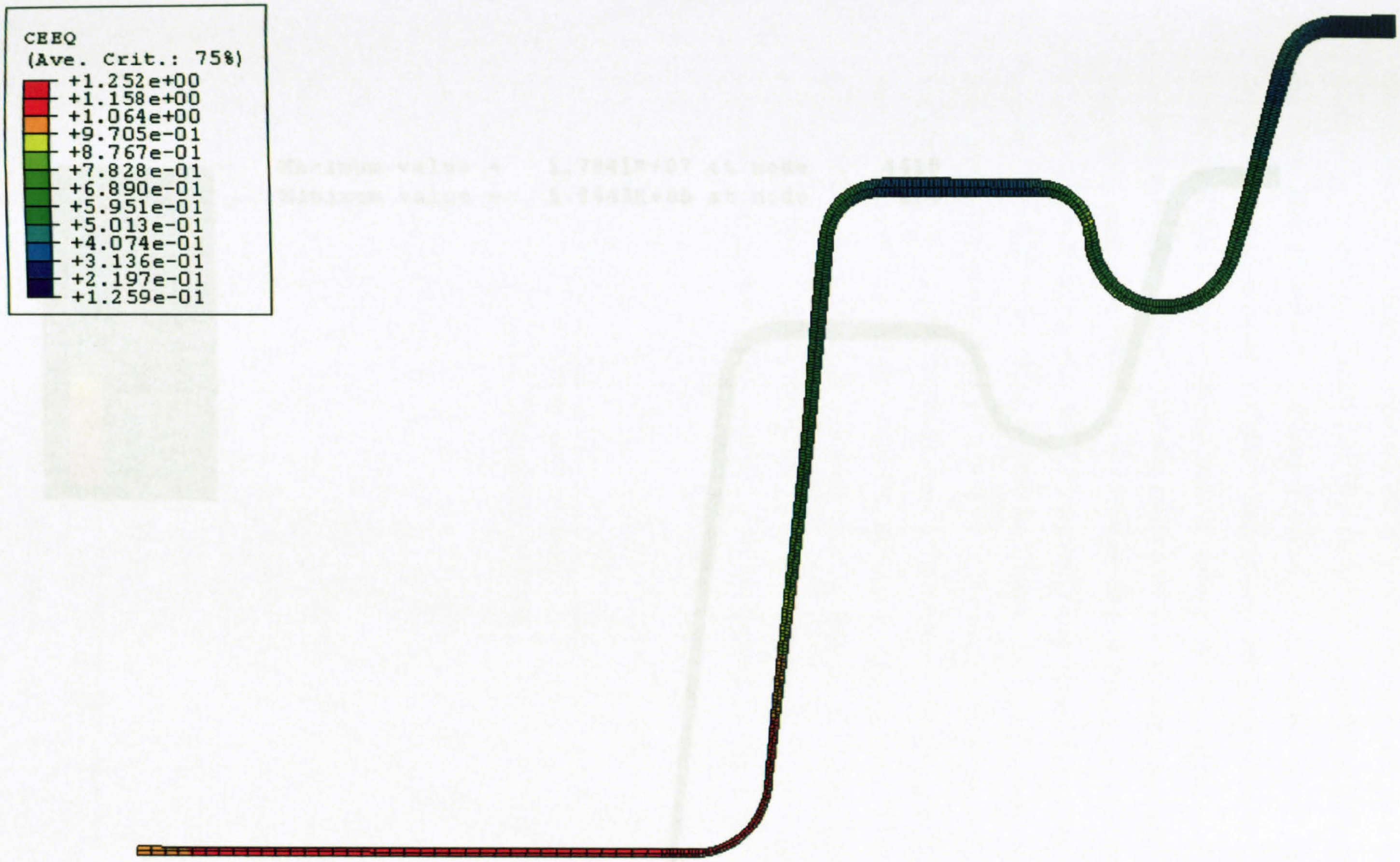

Figure 5.17 Equivalent strain distribution in non-reverse forming

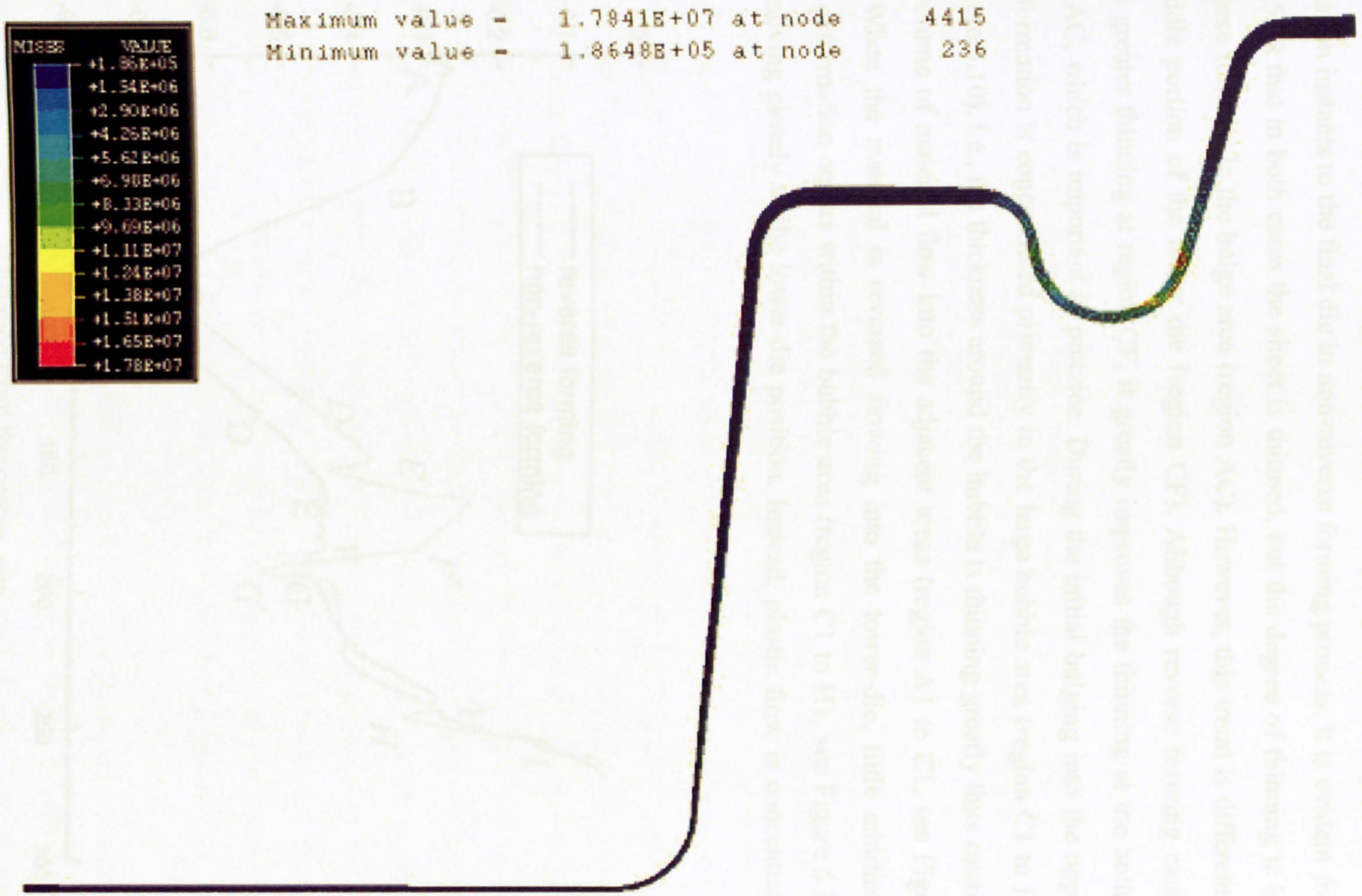

Figure 5.18 Equivalent Mises stress distribution in non-reverse forming

To illustrate the good thickness distribution of reverse forming, thickness strain distributions of the final component for a reverse forming and non-reverse forming process are compared in Figure 5.19. Points A-I represents the deformation instants to the final die in reverse forming process, whist points A'-I' represents the deformation instants to the final die in non-reverse forming process. It is evident from Figure 5.19 that in both cases the sheet is thinned, but the degree of thinning is less for reverse forming in the bulge area (region AC). However, this trend is different in the middle portion of the lower die (region CF). Although reverse forming causes slightly greater thinning at region CF, it greatly improves the thinning at the bottom region AC, which is important in practice. During the initial bulging into the upper-die, deformation is concentrated primarily in the large bubble area (region C1 to H1, see Figure 5.10), i.e., the thickness around the bubble is thinning greatly thus causing more volume of material flow into the adjacent areas (region A1 to C1, see Figure 5.10). When the material is reversed flowing into the lower-die, little additional plastic deformation occurs within the bubble area (region C1 to H1, see Figure 5.10) when moving closely to the lower-die position. Instead, plastic flow is concentrated

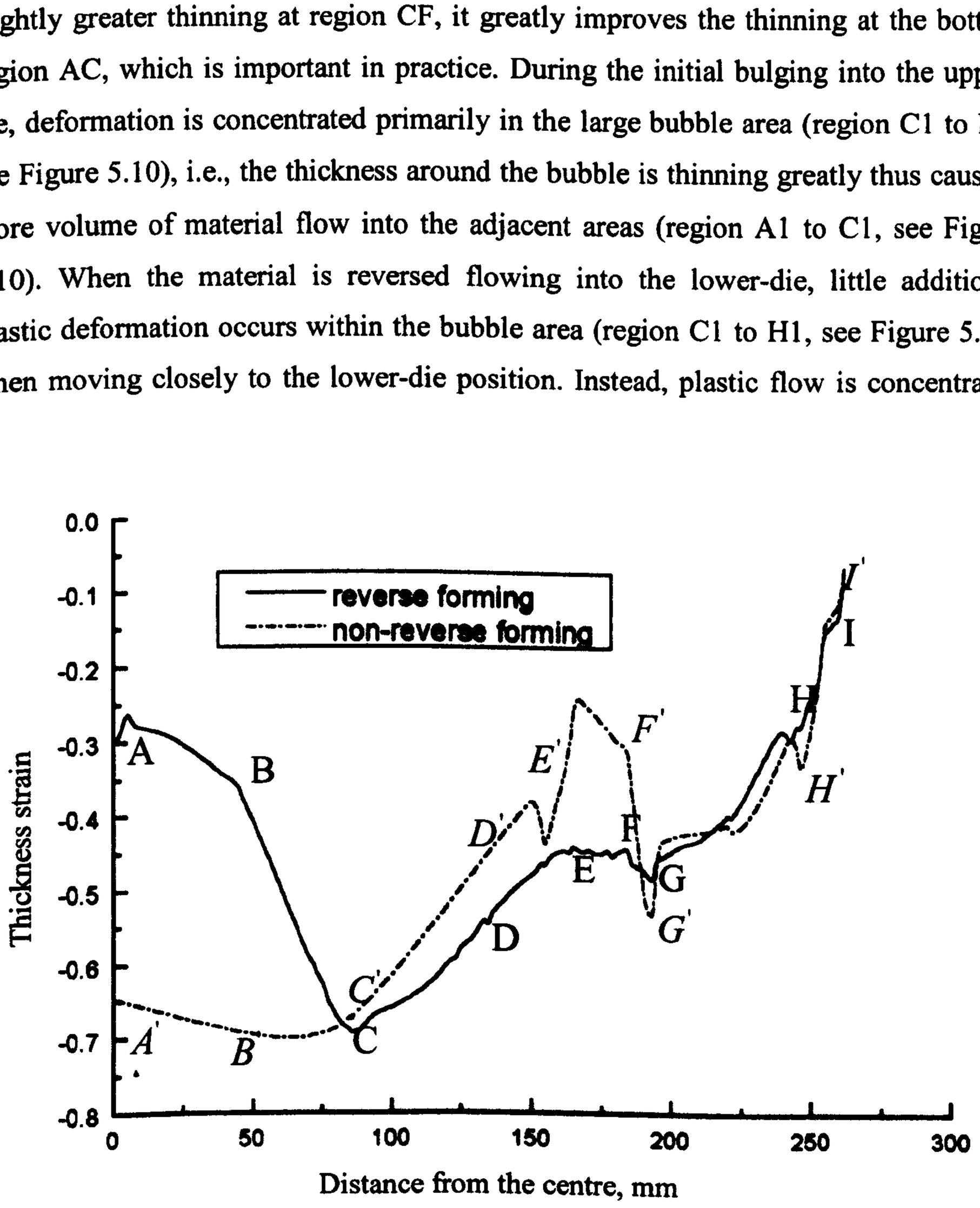

Figure 5.19 Thickness strain distribution comparison between reverse and non-reverse forming

within region A to C. Because of the material deformation and flow during initial bulging step in the reverse forming process, there is more volume in the region A to C in reverse forming than that in non-reverse forming, which results in less thinning in reverse forming than could be obtained in non-reverse forming as demonstrated in Figure 5.19.

5.4 Summary

A preliminary study of superplastic blow forming and the role of friction, applied to the two examples of a simple cylindrical cup and a complex reverse formed component, are discussed in this chapter.

An FEM model was proposed to simulate the superplastic blow forming process of a Ti-6Al-4V sheet into a cylindrical cup as well as a more complicated shaped component. To verify the accuracy and reliability of the proposed FE model, the numerical prediction has been validated by experimental data from reference (Kim et al, 1996). In addition, an element type study, in terms of the ability to predict the thickness distributions of the component, was performed and evaluated in comparison with the experimental data. It was found that the best prediction can be achieved using the continuum element with two layers in the thickness direction. Major factors such as the friction coefficient and the strain rate sensitivity index have been investigated. A multi-step loading method was employed in the simulation of the complex component during reverse blow forming to understand the thickness control mechanism. Comparisons between reverse blow forming and non-reverse forming demonstrate that reverse blow forming results in less thinning in the thickness of the formed component than can be obtained from a non-reverse forming process.

The results obtained from the two examples show that two of the primary industry concerns, i.e., the pressure versus time profile and the thickness distribution, can be obtained through FEM analysis of the superplastic forming process. The pressure-time profile is a design parameter to determine whether a superplastic forming process is close to the optimum or near-optimum strain rate condition. The thickness

distribution is a major consideration in determining whether a superplastic forming process is successful or not. Although the friction and contact algorithms within ABAQUS are capable of predicting the superplastic deformation in the two examples, the friction coefficients are limited to uniform values and lack of practical significance. This indicates the friction behaviour can be further improved. As a result, the real physical friction coefficient and deformation behaviour in a superplastic blow forming experiment are investigated and reported in the next chapter.

Chapter 6

Theoretical Calculation of the Friction Coefficient in Superplastic Forming

6.1 Introduction

The friction coefficient is assumed to be uniform in almost all the publications. However, from a tribological point of view, a global constant coefficient of friction in a frictional model does not correspond to practice (Schey, 1983; Schipper, 1988; Petty, 1994; Carleer et al, 1996). According to Schey (1983) and Schipper (1988), there are several different contact situations between the sheet and tools, and these contacts keep changing during a metal forming process. As the value of the friction coefficient depends on the local contact conditions, it may have different values for each contact region. Wang (1994) also pointed out that, although the strain distribution in a deformed component is mainly controlled by the tool geometry and material properties, friction can alter the straining pattern within the workpiece, and determine the magnitude and location of the maximum strain. Because the applied normal pressures and sliding velocities are quite different at distinct contact regions, the characteristics of friction in each region are different. It is therefore more practical if the friction model can incorporate different characteristics of contact conditions. In this chapter a set of theoretical friction calculations are derived, with respect to the analysis of different contact regions in a superplastic blow forming process.

6.2 Calculation of Friction Coefficients at Different Contact Regions

As discussed previously in Section 3.5, an alloy sheet blow formed into a cylindrical cup consists of four different regions based on different contact situations between the sheet and the die, as shown in Figure 6.1, i.e., free bulged bottom corner region BC, bottom contact region AB, side-wall contact region CD and die entry contact region DE. During the blow forming process, the sheet undergoes three different stages of deformation resulting in different frictional situations in the four different contact regions. The calculation of the corresponding friction coefficient with respect to each contact region is derived in the following sections.

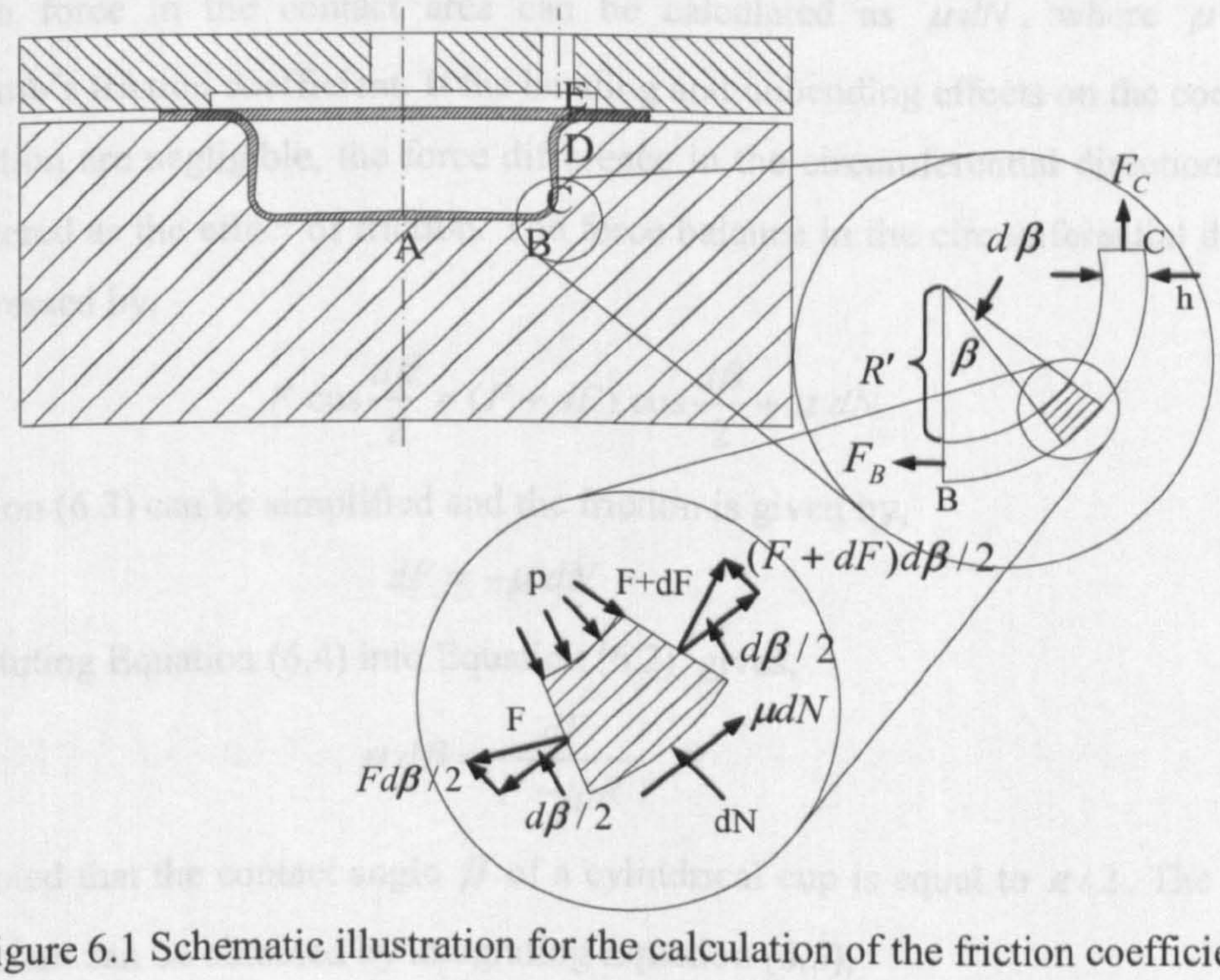

Figure 6.1 Schematic illustration for the calculation of the friction coefficient

6.2.1 Bottom Corner Region BC

A schematic illustration of the friction analysis and stress state in the bottom corner region BC is shown in Figure 6.1. As described in Section 5.2.3.1, this region of

interest is the last filled area during the blow forming operation and usually the largest thinning occurs. Let the force acting on the bottom section of the sheet be denoted F_B, and the force acting on the side wall section denoted F_C, the force equilibrium for a small element in the thickness direction at region BC can be expressed as follows,

$$pR' d\beta\, l = dN + F\frac{d\beta}{2} + (F + dF)\frac{d\beta}{2} \tag{6.1}$$

Ignoring the infinite small term of $dF\frac{d\beta}{2}$, the normal force can be described by,

$$dN = (l\ p\ R' - F)\, d\beta \tag{6.2}$$

Where β is the contact angle, F is the tension force on the element, p is the forming pressure, R' is the average distance between the centre of the corner and the sheet, and l is the cross section length. By assuming Coulomb friction law, the friction force in the contact area can be calculated as μdN, where μ is the Coulomb's friction coefficient. If the bending and unbending effects on the coefficient of friction are negligible, the force difference in the circumferential direction can be considered as the effect of friction. The force balance in the circumferential direction is expressed by,

$$F\cos\frac{d\beta}{2} = (F + dF)\cos\frac{d\beta}{2} + \mu\, dN \tag{6.3}$$

Equation (6.3) can be simplified and the friction is given by,

$$dF = -\mu\, dN \tag{6.4}$$

Substituting Equation (6.4) into Equation (6.2), gives,

$$\mu\, d\beta = \frac{dF}{F - lpR'} \tag{6.5}$$

It is noted that the contact angle β of a cylindrical cup is equal to $\pi/2$. The friction coefficient can be obtained by integrating Equation (6.5),

$$\mu = \frac{2}{\pi}\ln\frac{F_C - lpR'}{F_B - lpR'} \tag{6.6}$$

In order to calculate the friction coefficient, the forces F_B and F_C acting on the two opposite cross sections of the sheet around the bottom corner region must be obtained. As the forces F_B and F_C are given by the product of the applied stresses and the corresponding cross sectional areas, Equation (6.6) can be simplified as follows,

$$\mu = \frac{2}{\pi} \ln \frac{\sigma_C h_C - pR'}{\sigma_B h_B - pR'} \tag{6.7}$$

Where σ_B denotes the stress on the bottom, σ_C denotes the stress on the side-wall, and h_C, h_B are the corresponding thickness. The calculation of the friction coefficient is dependent on the stresses at both the bottom section (σ_B) and the side-wall (σ_C) section of the sheet, and the corresponding thickness.

6.2.2 Bottom Region AB

Similar to the analysis at the bottom corner region BC, the friction analysis at the bottom wall contact region AB is illustrated in Figure 6.2. Let the force acting on the central line be denoted F_A and the force acting near the bottom corner denoted F_B, the force equilibrium in the horizontal direction is expressed by,

$$F + \mu dN = F + dF \tag{6.8}$$

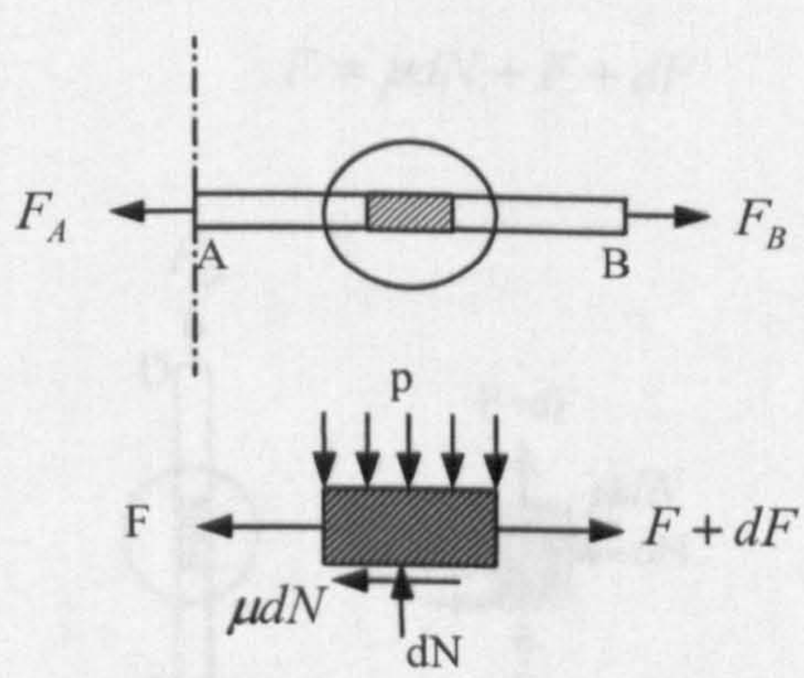

Figure 6.2 Schematic illustration of friction analysis at the bottom contact region AB

Thus gives,

$$dN = \frac{dF}{\mu} \tag{6.9}$$

A force balance in the thickness direction is given by,

$$pldx = dN \tag{6.10}$$

Where dx is the length of an element. Substituting Equation (6.9) into equation (6.10), and integrating,

$$\mu = \frac{F_B - F_A}{plx_0} \tag{6.11}$$

Similarly after simplification, Equation (6.11) gives,

$$\mu = \frac{\sigma_B h_B - \sigma_A h_A}{px_0} \tag{6.12}$$

where x_0 denotes the distance between the central line to the bottom corner.

6.2.3 Side-Wall Region CD

A schematic illustration of the friction analysis at the side-wall contact region CD is shown in Figure 6.3. In a manner similar to the previous sections, the force balance provides a differential equilibrium equation in the thickness direction for an element,

$$pldx = dN \tag{6.13}$$

While the force balance in the vertical direction of an element in the side-wall region is given by,

$$F = \mu dN + F + dF \tag{6.14}$$

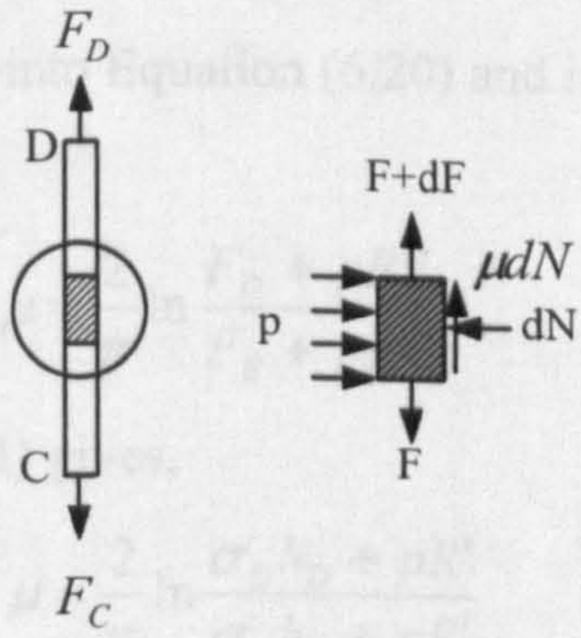

Figure 6.3 Schematic illustration of friction calculation at the side-wall

Thus gives,

$$dN = -\frac{dF}{\mu} \tag{6.15}$$

Substituting Equation (6.15) into Equation (6.13) and integrating to give,

$$\mu = \frac{F_C - F_D}{plx_1} \tag{6.16}$$

which can be similarly simplified and expressed,

$$\mu = \frac{\sigma_C h_C - \sigma_D h_D}{p x_1} \tag{6.17}$$

where x_1 is the vertical length of the side-wall.

6.2.4 Die Entry Region DE

The friction analysis in the die entry contact region DE is shown in Figure 6.4. The force equilibrium equation in the thickness direction of an element is expressed as,

$$pR'ld\beta + F\frac{d\beta}{2} + (F + dF)\frac{d\beta}{2} = dN$$
$$dN = pR'ld\beta + Fd\beta \tag{6.18}$$

The force balance in the circumferential direction of an element is,

$$F\cos\frac{d\beta}{2} = (F + dF)\cos\frac{d\beta}{2} + \mu\, dN \tag{6.19}$$

Thus,

$$dF = -\mu dN \tag{6.20}$$

Substitute Equation (6.18) into Equation (6.20) and integrate to give the friction coefficient as,

$$\mu = \frac{2}{\pi}\ln\frac{F_D + pR'l}{F_E + pR'l} \tag{6.21}$$

Simplifying Equation (6.21) gives,

$$\mu = \frac{2}{\pi}\ln\frac{\sigma_D h_D + pR'}{\sigma_E h_E + pR'} \tag{6.22}$$

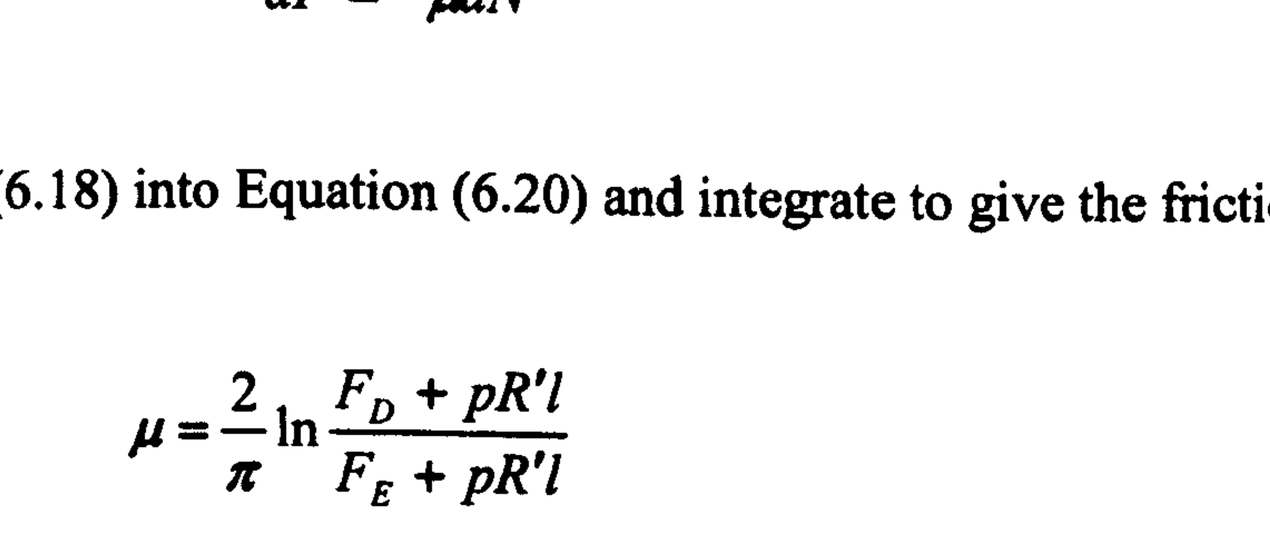

Figure 6.4 Schematic illustration of friction calculation at the die entry contact region DE

6.3 Derivation of Friction Coefficient Equations in Superplastic Blow Forming

As described in Section 6.2, the calculation of the friction coefficient during the superplastic blow forming mainly depends on the measurement of the stress and thickness across the contact region. During a superplastic blow forming operation, the thickness of each element keeps changing. In addition, the entire state of stresses can be converted to strain rate through the constitutive equation of superplastic forming. If the strain rate and thickness in the contact areas can be sensitively measured, it is possible to calculate the friction coefficient at each contact region.

There have been some attempts in establishing analytical modelling to give a detailed and accurate simulation of superplastic blow forming as described in the literature review in Section 2.5. In this investigation, the following assumptions are adopted to simplify the analysis (Ghosh and Hamilton, 1980; Dutta and Mukherjee, 1992; Guo and Ridley, 1989; Enikeev and Kruglov, 1995; Hwang et al, 1996 and 1997):

(1) The material being bulged is isotropic and incompressible;

(2) The material obeys Levy-Mises flow rule;

(3) The elastic strain is negligible;

(4) The strain-hardening effect is ignored.

The friction calculations of different regions are thus derived as follows.

6.3.1 Stress and Strain States at the Pole

The schematic diagram for the blow forming in the cylindrical die is shown in Figure 6.5. The stress state at the pole for the superplastic deformation of a thin sheet is approximately equi-biaxial plane stress state (Hwang et al, 1997), i.e.,

$$\sigma_r = \sigma_\theta$$
$$\sigma_h = 0 \qquad (6.23)$$

where subscripts r, θ and h represent the meridional, circumferential, and thickness directions respectively.

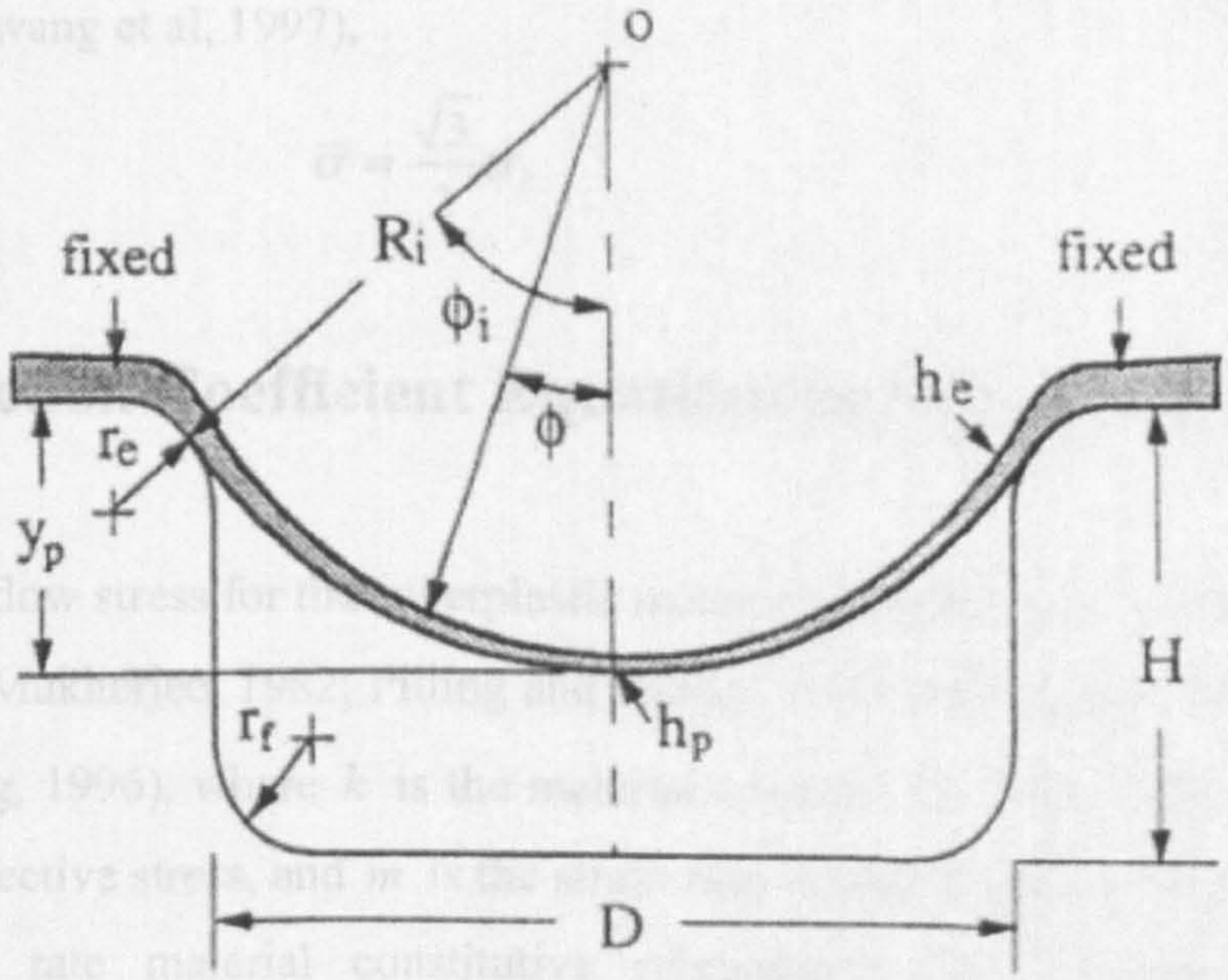

Figure 6.5 Schematic illustration of superplastic blow forming (Hwang et al, 1997)

According to the Von-Mises yield criterion, the effective stress $\bar{\sigma}$ can be obtained as,

$$\bar{\sigma} = \sigma_r = \sigma_\theta \tag{6.24}$$

According to volume constancy and Levy-Mises flow rule (Johnson and Meller, 1985),

$$\begin{aligned} \dot{\varepsilon}_r &= \dot{\varepsilon}_\theta \\ \dot{\varepsilon}_h &= -2\dot{\varepsilon}_r \end{aligned} \tag{6.25}$$

Hence the effective strain rate $\bar{\dot{\varepsilon}}$ is obtained,

$$\bar{\dot{\varepsilon}} = 2\dot{\varepsilon}_r = -\dot{\varepsilon}_h \tag{6.26}$$

6.3.2 Stress and Strain States at the Edge

Owing to the constraint at the edge, an approximate plane strain state is involved at this region, i.e., $\dot{\varepsilon}_\theta = 0$. From Levy-Mises flow rule and volume constancy,

$$\dot{\varepsilon}_r = -\dot{\varepsilon}_h \tag{6.27}$$

Hence the effective strain rate $\bar{\dot{\varepsilon}}$ is,

$$\bar{\dot{\varepsilon}} = \frac{2}{\sqrt{3}}\dot{\varepsilon}_r = -\frac{2}{\sqrt{3}}\dot{\varepsilon}_h \tag{6.28}$$

Ignoring the thickness stress, the effective stress for a plane strain problem can be obtained (Hwang et al, 1997),

$$\bar{\sigma} = \frac{\sqrt{3}}{2}\sigma_r \tag{6.29}$$

6.3.3 Friction Coefficient Equations in Superplastic Forming

The plastic flow stress for the superplastic material is generally described as $\bar{\sigma} = k\bar{\dot{\varepsilon}}^m$ (Arieli and Mukherjee, 1982; Pilling and Ridley, 1989; Rebelo et al, 1990; Kim et al, 1996; Cheng, 1996), where k is the material constant, $\bar{\dot{\varepsilon}}$ is the effective strain rate, $\bar{\sigma}$ is the effective stress, and m is the strain rate sensitivity index. On the basis of the stress-strain rate material constitutive relationship, the calculation of friction coefficient in a superplastic forming process is derived as follows.

6.3.3.1 Die Entry Region DE

As the die entry radius is generally smaller than the diameter of the die, the deformation in the die entry region DE can be assumed as a plane strain problem (Hwang et al, 1997). As a result, σ_D and σ_E are expressed as,

$$\begin{aligned}
\sigma_D &= \frac{2\bar{\sigma}_D}{\sqrt{3}} = \frac{2}{\sqrt{3}}(k\bar{\dot{\varepsilon}}_D{}^m) = \frac{2}{\sqrt{3}}\left[k(-\frac{2}{\sqrt{3}}\dot{\varepsilon}_{h_D})^m\right] \overset{or}{=} \frac{2}{\sqrt{3}}\left[k(\frac{2}{\sqrt{3}}\dot{\varepsilon}_{r_D})^m\right] \\
\sigma_E &= \frac{2\bar{\sigma}_E}{\sqrt{3}} = \frac{2}{\sqrt{3}}(k\bar{\dot{\varepsilon}}_E{}^m) = \frac{2}{\sqrt{3}}\left[k(-\frac{2}{\sqrt{3}}\dot{\varepsilon}_{h_E})^m\right] \overset{or}{=} \frac{2}{\sqrt{3}}\left[k(\frac{2}{\sqrt{3}}\dot{\varepsilon}_{r_E})^m\right]
\end{aligned} \tag{6.30}$$

Substituting the stresses Equation (6.30) into Equation (6.22), the calculation of friction coefficient in the die entry region can be obtained,

$$\mu = \frac{2}{\pi}\ln\frac{\frac{2}{\sqrt{3}}\left[k(\frac{2}{\sqrt{3}}\dot{\varepsilon}_{r_D})^m\right]h_D + pR'}{\frac{2}{\sqrt{3}}\left[k(\frac{2}{\sqrt{3}}\dot{\varepsilon}_{r_E})^m\right]h_E + pR'} \overset{or}{=} \frac{2}{\pi}\ln\frac{\frac{2}{\sqrt{3}}\left[k(-\frac{2}{\sqrt{3}}\dot{\varepsilon}_{h_D})^m\right]h_D + pR'}{\frac{2}{\sqrt{3}}\left[k(-\frac{2}{\sqrt{3}}\dot{\varepsilon}_{h_E})^m\right]h_E + pR'} \tag{6.31}$$

where h_D and h_E are the final thickness of the component.

6.3.3.2 Bottom Region AB

In the bottom contact region AB, an equi-biaxial stress state can be assumed (Hwang et al, 1997). Therefore, the stresses σ_A and σ_B can be expressed as,

$$\begin{aligned} \sigma_A = \bar{\sigma}_A = k\bar{\dot{\varepsilon}}_A^{\,m} = k(-\dot{\varepsilon}_{h_A})^m \overset{or}{=} k(2\dot{\varepsilon}_{r_A})^m \\ \sigma_B = \bar{\sigma}_B = k\bar{\dot{\varepsilon}}_B^{\,m} = k(-\dot{\varepsilon}_{h_B})^m \overset{or}{=} k(2\dot{\varepsilon}_{r_B})^m \end{aligned} \tag{6.32}$$

Substituting Equation (6.32) into Equation (6.12), the calculation of friction coefficient in the bottom region can be derived,

$$\mu = \frac{k(2\dot{\varepsilon}_{r_B})^m h_B - k(2\dot{\varepsilon}_{r_A})^m h_A}{px_0} \overset{or}{=} \frac{k(-\dot{\varepsilon}_{h_B})^m h_B - k(-\dot{\varepsilon}_{h_A})^m h_A}{px_0} \tag{6.33}$$

where h_A and h_B are the final thickness of the component, x_0 is the distance between the central line and bottom corner.

6.3.3.3 Side-wall Region CD

In the side-wall region CD, the plastic deformation can be assumed as plane strain (Hwang et al, 1997). Similar to the derivation at the die entry region, the friction coefficient can be calculated according to Equation (6.17),

$$\mu = \frac{\frac{2}{\sqrt{3}}k(\frac{2}{\sqrt{3}}\dot{\varepsilon}_{r_C})^m h_C - \frac{2}{\sqrt{3}}k(\frac{2}{\sqrt{3}}\dot{\varepsilon}_{r_D})^m h_D}{px_1} \overset{or}{=} \frac{\frac{2}{\sqrt{3}}k(-\frac{2}{\sqrt{3}}\dot{\varepsilon}_{h_C})^m h_C - \frac{2}{\sqrt{3}}k(-\frac{2}{\sqrt{3}}\dot{\varepsilon}_{h_D})^m h_D}{px_1} \tag{6.34}$$

where h_C and h_D are the final thickness of the sheet, x_1 is the vertical length of the side-wall.

6.3.3.4 Bottom Corner Region BC

As an equi-biaxial stress state is assumed in the bottom region AB and a plane strain state is assumed in the side-wall region CD, the stresses σ_B and σ_C in the bottom corner region BC can be expressed respectively as,

$$\sigma_B = \bar{\sigma}_B = k\dot{\bar{\varepsilon}}_B^{\,m} = k(-\dot{\varepsilon}_{h_B})^m \overset{or}{=} k(2\dot{\varepsilon}_{r_B})^m \tag{6.35}$$

$$\sigma_C = \frac{2\bar{\sigma}_C}{\sqrt{3}} = \frac{2}{\sqrt{3}}(k\dot{\bar{\varepsilon}}_C^{\,m}) = \frac{2}{\sqrt{3}}\left[k(-\frac{2}{\sqrt{3}}\dot{\varepsilon}_{h_C})^m\right] \overset{or}{=} \frac{2}{\sqrt{3}}\left[k(\frac{2}{\sqrt{3}}\dot{\varepsilon}_{r_C})^m\right] \tag{6.36}$$

Substituting the above equations to Equation (6.7), the friction coefficient at the bottom corner region is expressed as follows,

$$\mu = \frac{2}{\pi}\ln\frac{\frac{2}{\sqrt{3}}\left[k(\frac{2}{\sqrt{3}}\dot{\varepsilon}_{r_C})^m\right]h_C - pR'}{k(2\dot{\varepsilon}_{r_B})^m h_B - pR'} \overset{or}{=} \frac{2}{\pi}\ln\frac{\frac{2}{\sqrt{3}}\left[k(-\frac{2}{\sqrt{3}}\dot{\varepsilon}_{h_C})^m\right]h_C - pR'}{k(-\dot{\varepsilon}_{h_B})^m h_B - pR'} \tag{6.37}$$

where h_B and h_C are the final thickness of the component.

6.4 Summary

In this chapter the theoretical calculations of the friction coefficients at different contact regions during a superplastic blow forming process were discussed. The friction coefficient depends not only on the material properties, i.e., K and m values, but also on the strain rate in the meridional or thickness direction and final thickness distribution of the component sheet. The material properties can be obtained from the material tests in the following chapter and the final thickness distribution can be measured after the superplastic forming process. However, the strain rate $\dot{\varepsilon}$, which varies during the superplastic deformation, is difficult to measure directly due to the high pressure, high temperatures, harsh environment, contaminants and high abrasion in a superplastic forming process. To avoid the difficulty in directly measuring the strain rate $\dot{\varepsilon}$, an indirect method is proposed and the experimental devices are

designed in order to investigate the friction behaviour in a superplastic blow forming process, which are described in detail in the following chapter.

Chapter 7

Experimental Friction Study in Superplastic Blow Forming

7.1 Introduction

It is necessary to understand the friction behaviour in a superplastic forming process in terms of the formability of the sheet, because the thickness distribution of a superplastic formed component is significantly altered by the different frictional factors. There is, however, relatively little work on the experimental investigation of the frictional behaviour in the superplastic blow forming process. In the previous chapter, theoretical formulations of frictional behaviour at different regions in a superplastic blow forming process were presented to provide a theoretical background for the experimental study. The objective of this chapter is to propose a methodology to investigate the frictional behaviour experimentally under a superplastic blow forming process, using the derived theoretical equations at different contacting areas. To achieve the objective, efforts have been made to design and build an easy-to-control laboratory testing rig which is capable of producing reliable results, while at the same time remaining as close as possible to the realistic superplastic blow forming conditions so that the frictional behaviour can be evaluated experimentally. The experiments will provide validations for the friction behaviour predicted by simulation using ABAQUS, in return, the validated FE model is capable of predicting the final thickness distribution of a component accurately if all parameters are known.

The design of the experimental rig is first presented in Section 7.2. Attention is next turned to the experiment of a cylindrical cup to obtain an initial impression of the frictional behaviour during a SPF process. The effects of the parameters including the

temperature and forming pressure on the friction coefficient were investigated. Particular attention is paid to the experimental friction investigation of a reverse formed component with complex configuration. Finally, a realistic and closely simulative experimental method to evaluate friction in the superplastic blow forming process is given.

7.2 Experimental Device Design

7.2.1 General Requirements

To study the frictional behaviour at different contact regions, a laboratory friction measurement device was designed to simulate the superplastic blow forming. The goal of the design is to closely simulate the industrial superplastic blow forming process and, at the same time, keep the whole experimental process simple and easy to operate. To carry out a superplstic blow forming, there are many important parameters to be considered, including operational parameters such as gas pressure and forming temperature, the mechanical and thermal properties of the superplastic material, the geometrical properties of the forming dies. These parameters form a range of requirements which must be met by the experimental device in order to perform a representative experiment. The main requirements for the experimental device design are as follows,

(1) Controllable forming pressure;

(2) Controllable forming temperature;

(3) Remove-ability of the sheet and the dies after experiment completion;

(4) Measurement of the strain rate;

(5) Ability to simulate the state of contact interaction under industrial process conditions;

(6) Operation under combined process parameters.

Among the above requirements, one of the main concerns in the experimental design was how to realise the controllable forming pressure. Since the forming of a sheet into a cavity by hydraulic pressure is in principle similar to the case of a superplastic

forming process by gas pressure (Siegert et al, 2000; Zhang, 1999), it was proposed to apply hydraulic pressure to make superplastic material flow into the die as in the conventional SPF process in this research. Therefore, a constant hydraulic pressure which is easy to achieve and control was adopted in the experiment, and subsequently eliminated the elaborate control system needed to vary the gas pressure with time in order to maintain the constant strain rate required for an optimum superplastic forming (Thiruvarudchelvan and Lewis, 1999). As described in Chapter 6, measurement of the strain rate is very important for the calculation of friction coefficient because a small deviation in the strain rate may cause a significant error in the friction coefficient. Therefore measuring the strain rate effectively was critical. The direct method is to use a strain gauge, measuring the strain and converting to strain rate. However it was not possible to measure the deformation with a strain gauge because of the space restriction of the die and the very large deformation exceeding the measuring capacity of a strain gauge. A method of indirect measuring of strain rate was developed to avoid interference with the contact area. As the strain rate is proportional to the deforming length, if the deforming length can be recorded and obtained, the strain rate can be measured indirectly. This indirect method turned out to be applicable and is described in details in Appendix 3.

7.2.2 Material and Tensile Tests

7.2.2.1 Material

Most of the superplastic materials used in the industrial process are characterised by the high deformation temperatures ranging from 700 K to 1200 K. Carrying out forming at such high temperatures necessitates complex and costly experimental system. To avoid such high temperature requirements in the current frictional device design, Pb-Sn alloy, which has been well known for an outstanding superplasticity at room temperature (Ahmed and Langdon, 1977; Grivas et al, 1979; Alden, 1987; Mayo and Nix, 1988; Ma and Langdon, 1994), was chosen in the experiment. This material characteristic minimises the cost of experimental facilities over Al or Ti alloys which require high forming temperatures.

The Sn-34%Pb eutectic alloy, used in the experiment, was prepared by melting in air above 200°C and casting into a mould of dimension of 100 mm×100 mm×14 mm. After cooling to room temperature, the sample sheets were prepared from the cast ingots by first machining the casting along the thickness direction to eliminate possible surface defects. The machined castings were then pressed in two directions and rolled successively at room temperature into the final thickness sheets. With each rolling pass, the sheet was rotated through 90°.

The resulting microstructure was examined using scanning electron microscopy (SEM). As clearly shown in Figure 7.1, there are two phases with the light phase being lead-rich and dark phase being tin-rich. Detailed percentages are shown in Table 7.1. The sample microstructure is characterised by equiaxed grains, with an average grain size of 1.85~2 μm measured using the mean linear intercept method. The measured grain size confirmed that processing by pressing and rolling led to a grain refinement to satisfy the requirements of a superplastic material.

Table 7.1 Phase analysis of Sn-Pb alloys

Phase	Pb Percentage (%)	Sn Percentage (%)
Light phase (α)	88.5	11.5
Dark phase (β)	2.9	97.1

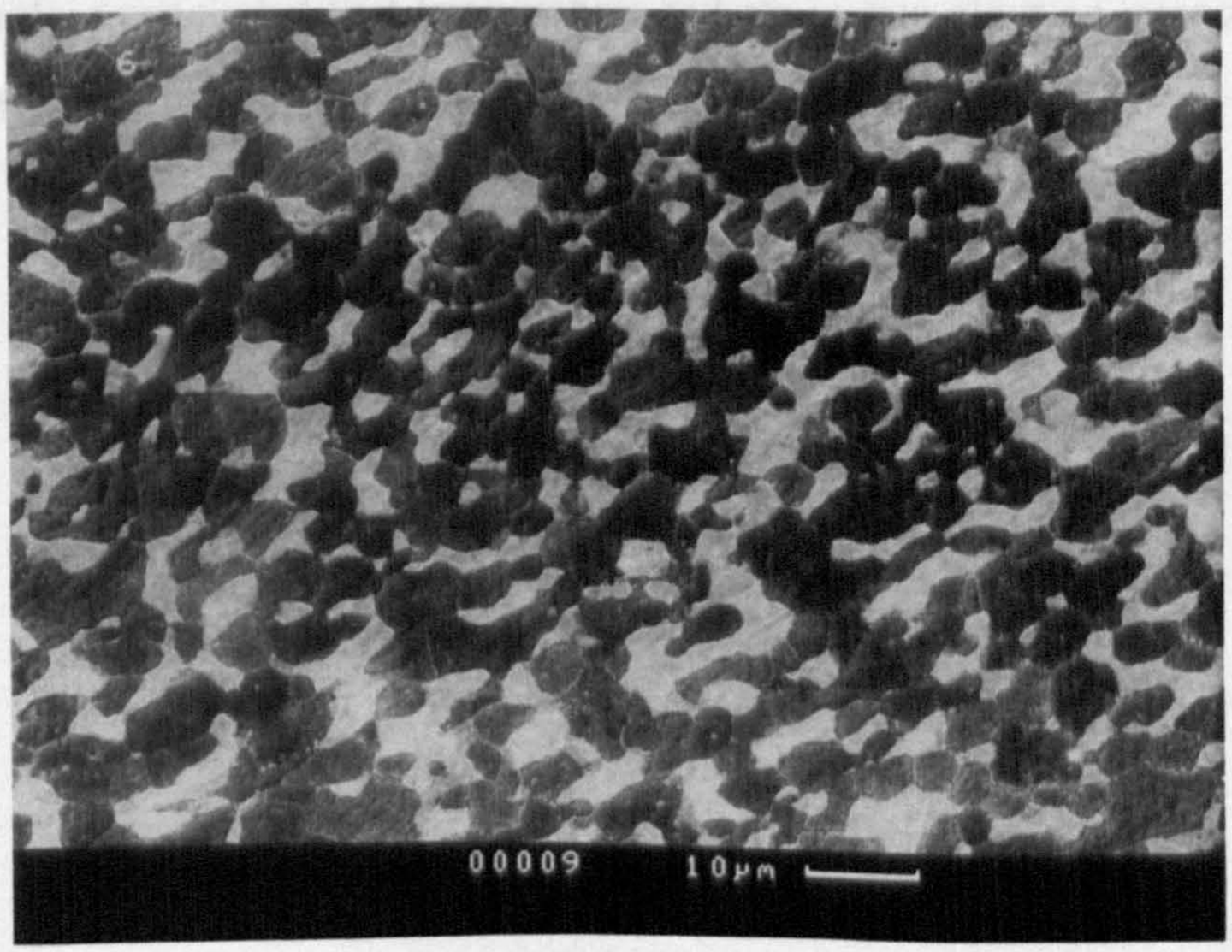

Figure 7.1 Typical microstructure of rolled and pressed Sn-Pb sheet (×1k)

7.2.2.2 Material Test

In order to verify the superplasticity of the Sn-Pb alloy sample, a series of tensile tests were carried out at a constant rate of crosshead speed on a Hounsfield tensometer before the superplastic blow forming experiment. The tensile samples were machined from the rolled sheets. The geometry of an undeformed tensile specimen is shown in Figure 7.2 with a gauge length of 10 mm and thickness of 2 mm. The specimens were pulled to failure at three different testing temperatures of 293 K, 308 K, 353 K and three different initial strain rates of $1.38\times10^{-3}s^{-1}$, $7.17\times10^{-4}s^{-1}$, $3.83\times10^{-4}s^{-1}$, as shown in Figure 7.3. Test results were recorded and sampled at a rate of 10 points per second. The elevated temperature was obtained using a heater. Because of the short gauge length, the specimens can be considered to be kept in a relatively uniform temperature zone. The appearance of the specimens after the tension test is shown in Figure 7.3 and confirms that the Sn-Pb alloy exhibited the fundamental characteristics of superplastic flow, i.e., uniform deformation within the gauge lengths and an absence of visible localized necking with the specimens pulling down to fine points at failure. A slower crosshead speed and a higher temperature resulted in a higher elongation. This is illustrated in Figure 7.4, where the elongations to failure are plotted against the initial strain rate. The highest elongation achieved in the test was 830% at an elevated temperature of 353 K with an initial strain rate of $3.83\times10^{-4}s^{-1}$. It can be therefore concluded that temperature and strain rate plays an important role in a superplastic forming process.

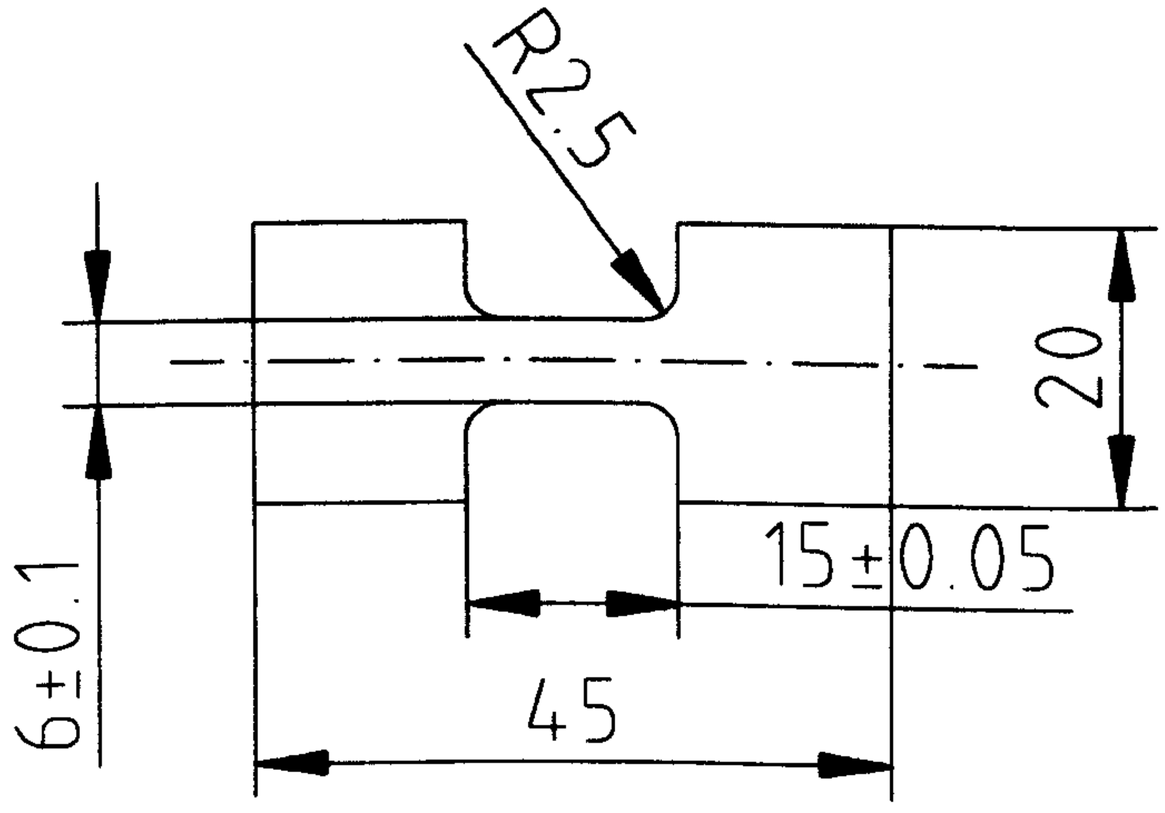

Figure 7.2 Geometry of the tensile specimen of 2 mm thickness

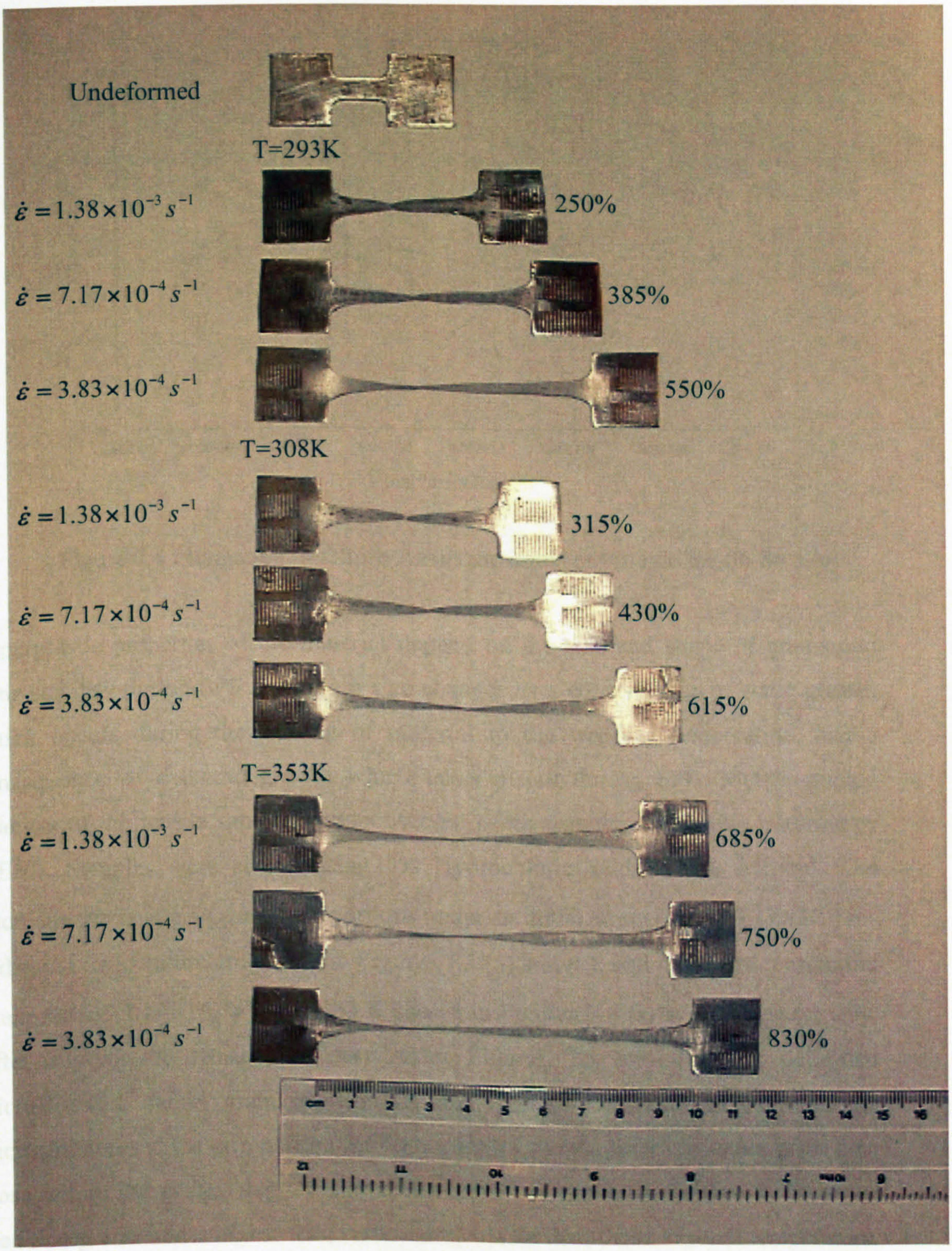

Figure 7.3 Deformed tensile specimens of Sn-Pb alloys

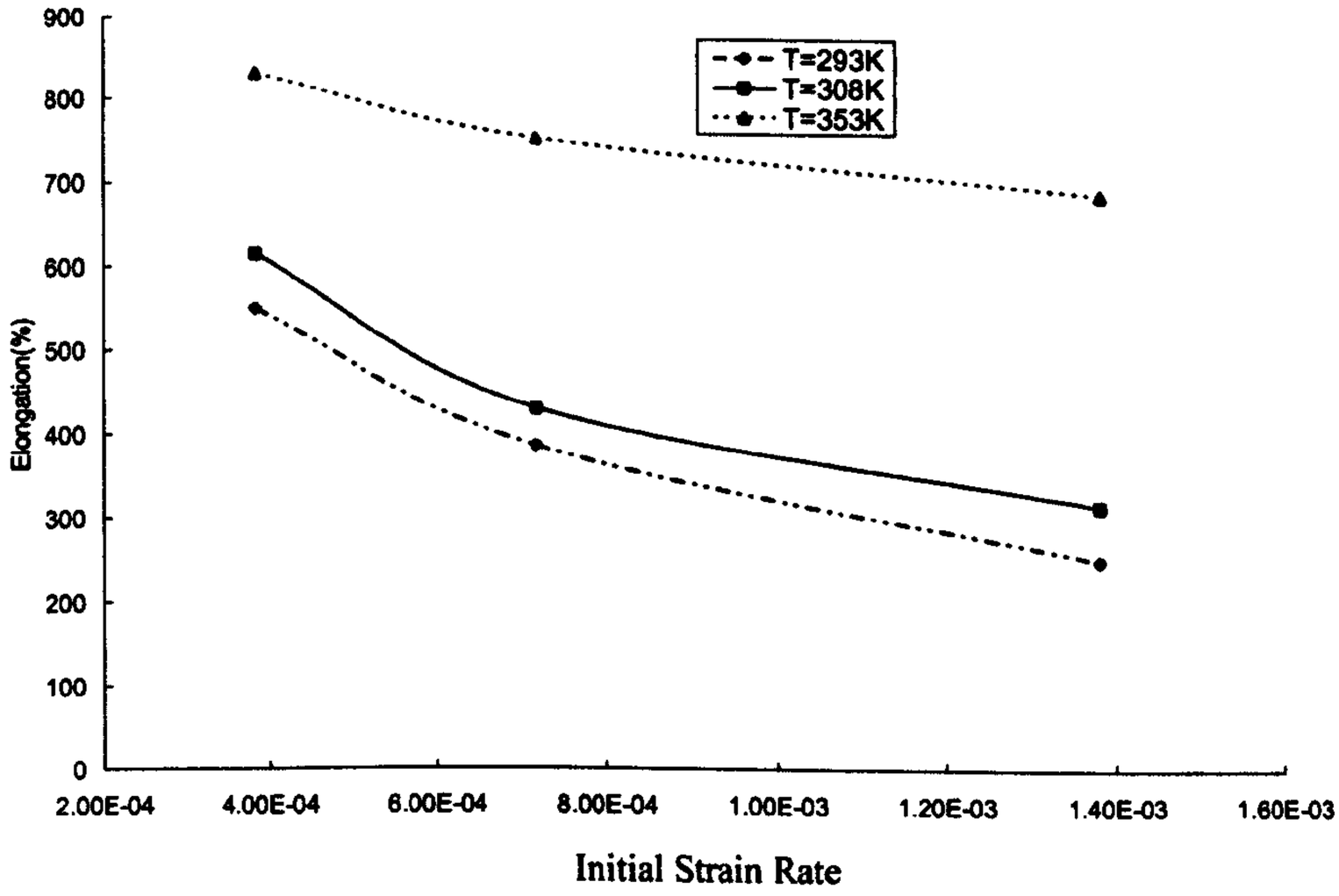

Figure 7.4 Elongation to failure versus the initial strain rate for Pb-Sn alloy

Superplastic properties of the material depend on the size and shape of grains and their stability during SPF. The grain size changes as a consequence of static growth which occurs during the heating of material to the working temperature, and a consequence of dynamic growth which takes places during SPF. Metallographic changes of the tensile samples were observed using scanning electronic microscopy (SEM). Samples were etched using 5% Hydrochloric acid – 95% Alcohol. The microstructures at gauge and grip portions under an initial strain rate of $7.17\times10^{-4}s^{-1}$ and room temperature are shown in Figures 7.5 (a) and (b), and those under an initial strain rate of $7.17\times10^{-4}s^{-1}$ and 353 K shown in Figures 7.6 (a) and (b) respectively. After superplastic tension, as seen from Figures 7.5 and 7.6, the deformed microstructure shows grain growth but still remains equiaxed. In addition, the microstructures at the grip portion for both samples show a finer equiaxied grain than those within the gauge. A grain size measurement is shown in Table 7.2. It can be seen that grains under higher temperature are coarser than those at room temperature. Such dynamic grain coarsening can be mainly attributed to the enhanced diffusivity at high temperature.

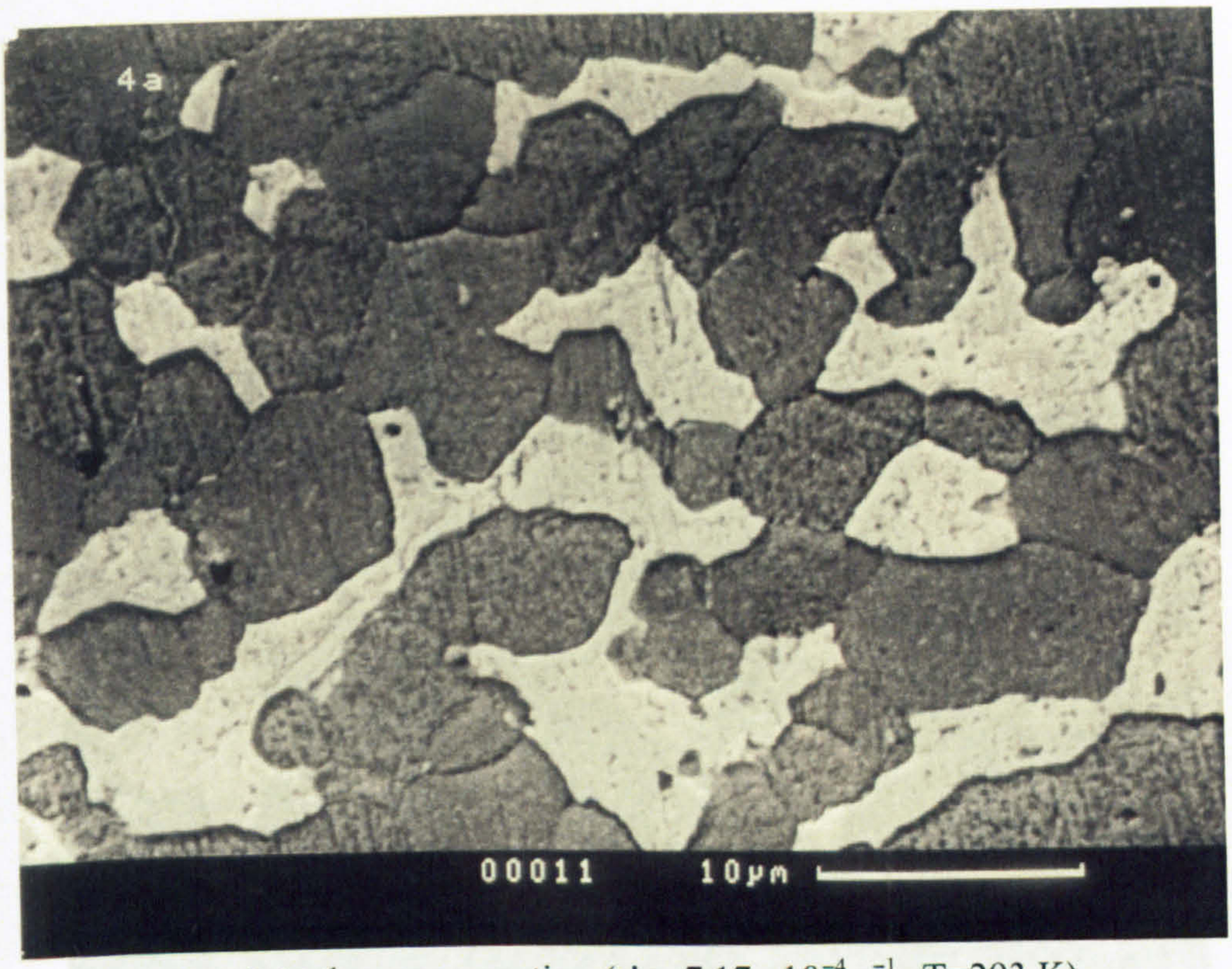

a) At the gauge portion ($\dot{\varepsilon} = 7.17 \times 10^{-4}\, s^{-1}$, T=293 K)

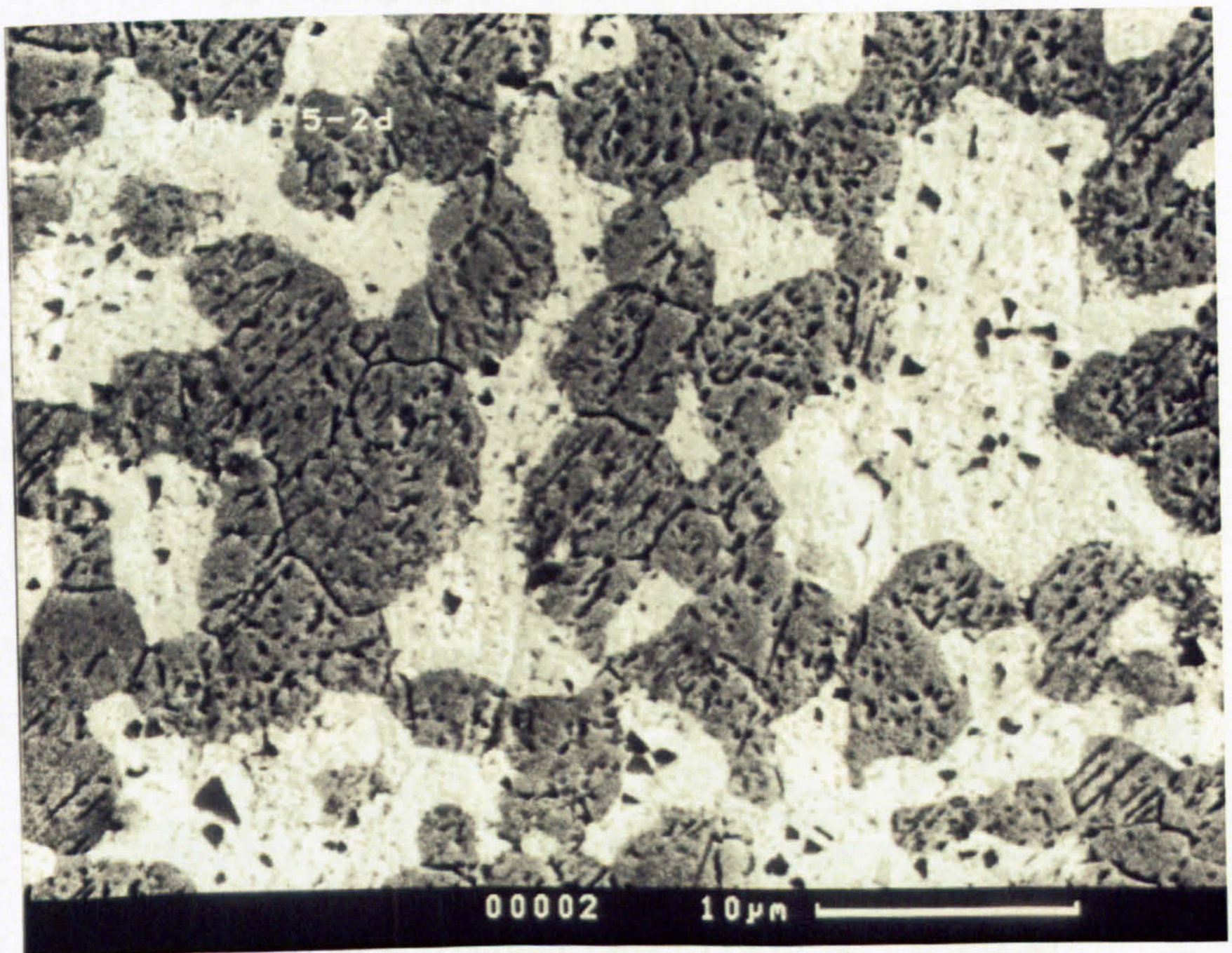

b) At the grip portion ($\dot{\varepsilon} = 7.17 \times 10^{-4}\, s^{-1}$, T=293 K)

Figure 7.5 Microstructures of tensile samples

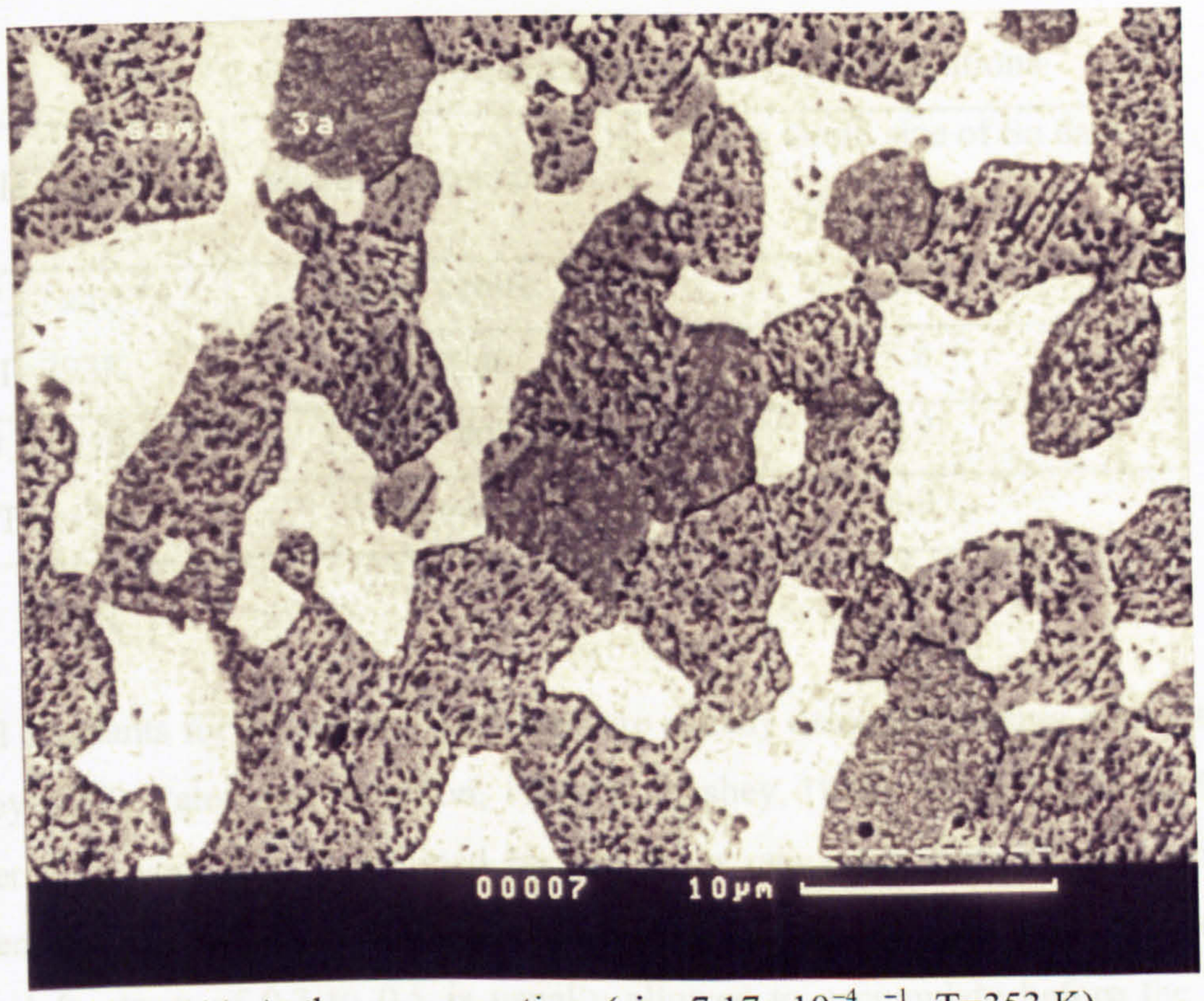

(a) At the gauge portion, ($\dot{\varepsilon} = 7.17 \times 10^{-4} s^{-1}$, T=353 K)

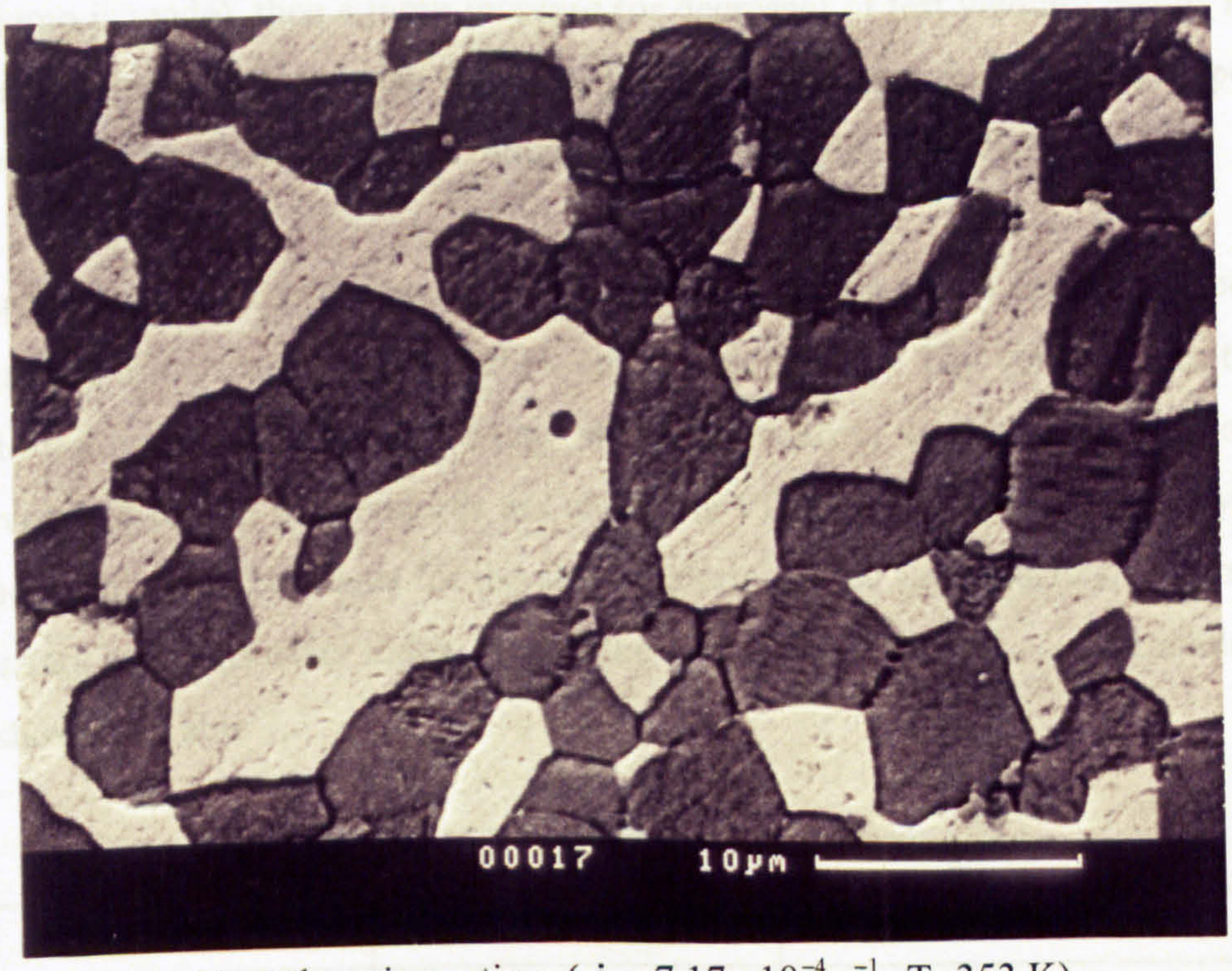

(b) At the grip portion, ($\dot{\varepsilon} = 7.17 \times 10^{-4} s^{-1}$, T=353 K)

Figure 7.6 Microstructures of the tensile samples

Table 7.2 Grain size measurement under tensile conditions

Tensile conditions	Micro-section potion	Mean Grain size of Sn dark phase (μm)
$\dot{\varepsilon} = 7.17\times10^{-4}\,s^{-1}$ T=293K	Gauge centre	4.2
	Grip edge	3.8
$\dot{\varepsilon} = 7.17\times10^{-4}\,s^{-1}$ T=353K	Gauge centre	4.9
	Grip edge	4.0

Material constants for superplastic materials are usually determined using tensile tests (Smirnoy, 1979; Paton and Hamilton, 1982; Kaibyshey, 1984). The superplastic flow characteristics were then determined by the strain rate jump method proposed by Backofen et al (1964). The test starts with a constant velocity until a steady load is registered (a strain of 0.3 to 0.5 is usually allowed to accumulate before the first velocity jump is made), then a jump increase (or decrease) of test velocity results in a higher (or lower) steady load state. Repeated incremental increases in crosshead speed allow the load to be measured over a range of strain rates (Ghosh, 1982).

In the current material test, the specimen was initially tensioned at a constant velocity of 0.2 mm per minute until a steady flow stress was reached. The velocity was then jumped to 0.5 mm per minute and a new steady flow stress was reached. The load-time curves at different temperatures are shown in Figures 7.7 and 7.8 respectively. The values of material constants for the sheet materials to be superplastically formed, i.e., the strain rate sensitivity index m and the material constant K, were calculated and are shown in Table 7.3.

Table 7.3 Material parameters of Sn-Pb alloy

Parameter	m value	K value (MPa)
Room temperature (293K)	0.37	277.3
High temperature (353K)	0.46	180.5

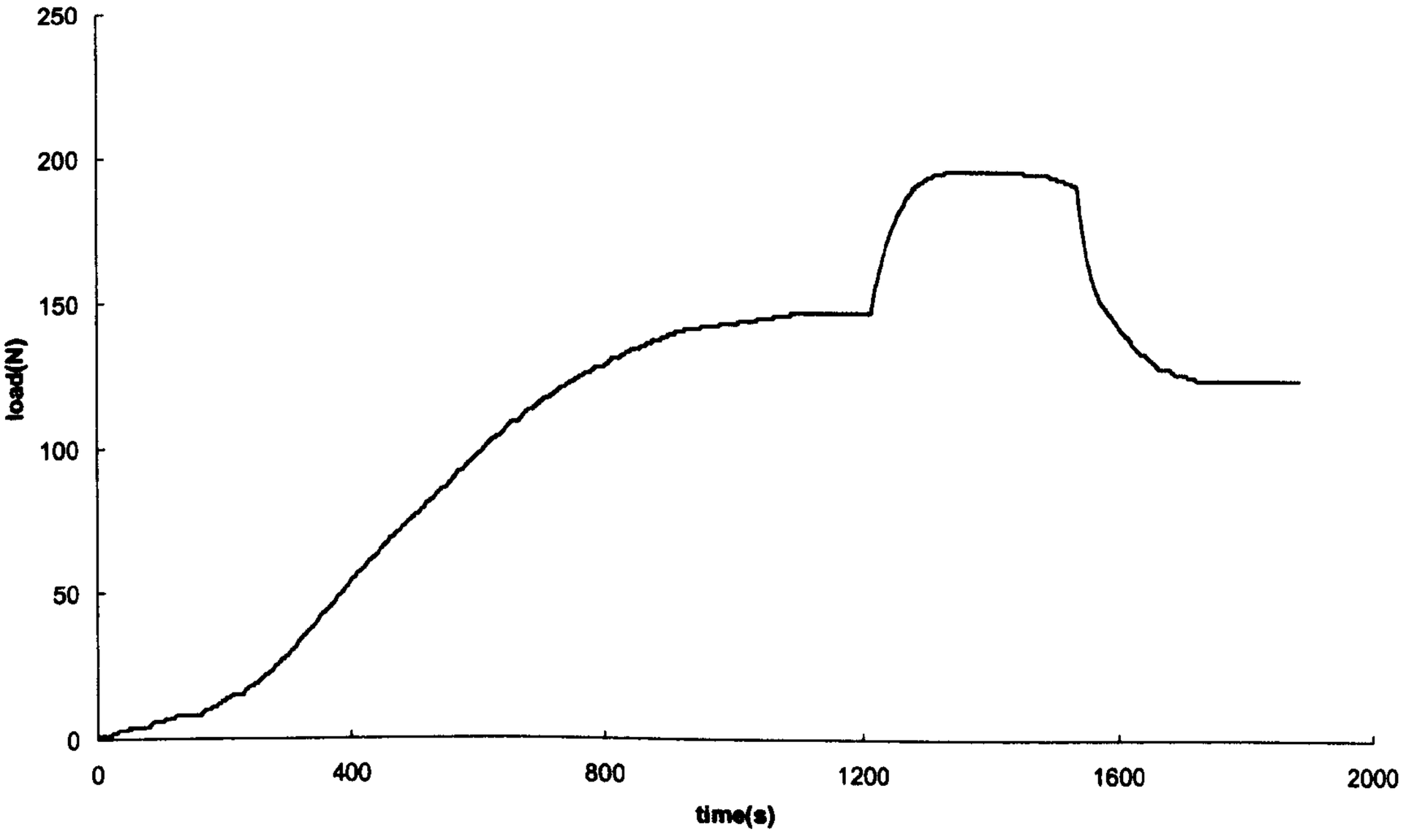

Figure 7.7 Velocity jump test from 0.2 mm/min to 0.5 mm/min (temperature: 293K)

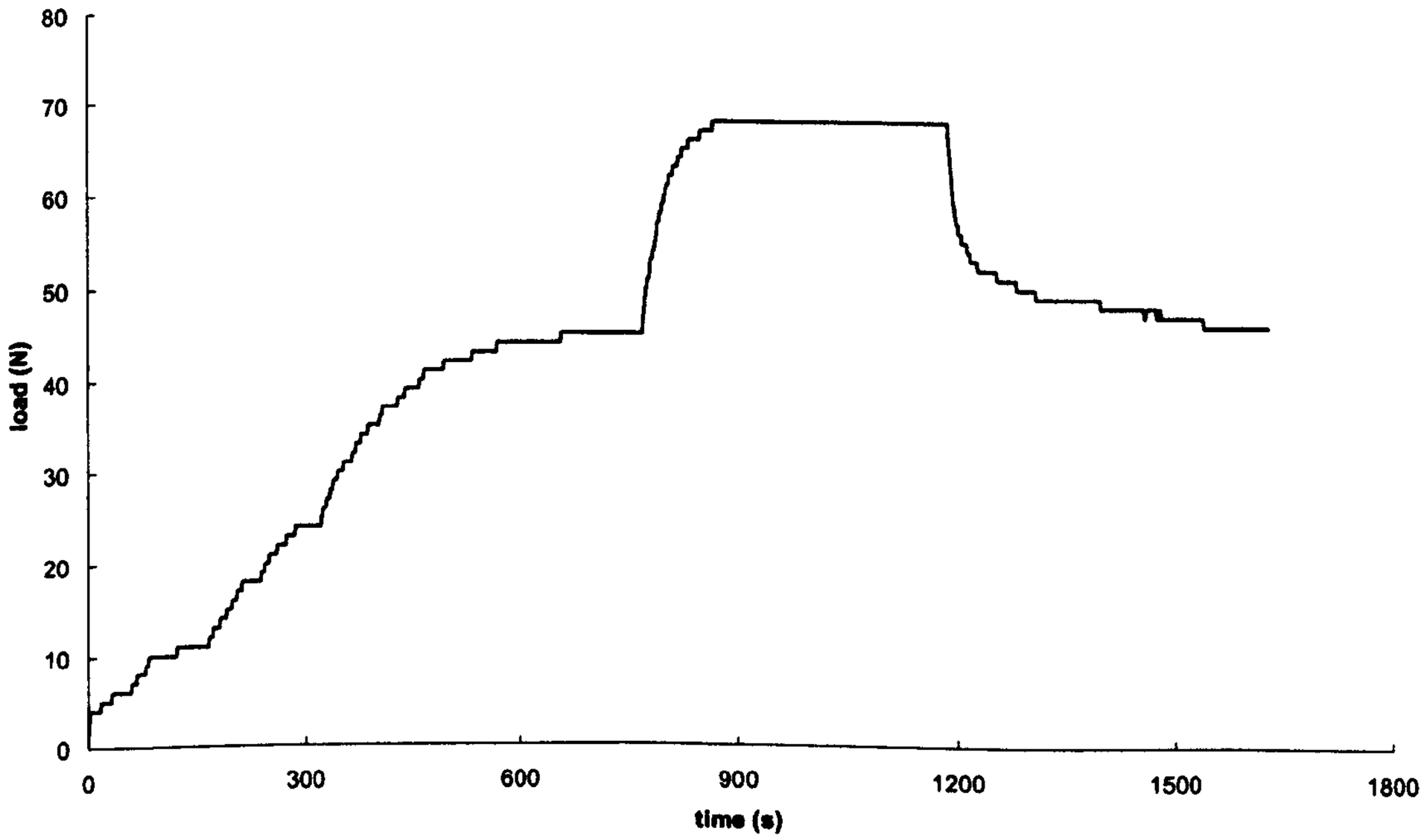

Figure 7.8 Velocity jump test from 0.2 mm/min to 0.5 mm/min (temperature: 353K)

7.2.3 Overall Description of Experimental Rig

The primary requirements, which have to be met by the experimental device, for measuring the frictional behaviour of sheet/die contacts under superplastic blow forming were presented in Section 7.2.1. The emphasis for the experimental device lies in applying controlled superplastic deformation while effectively measuring the stain rate for the calculation of friction coefficients using the equations derived in Chapter 6.

In practice a superplastic blow forming process consists of three main parts, i.e., gas control system, temperature control system and the forming tools. The forming of a sheet into a cavity can be done by hydraulic pressure in principle (Siegert et al, 2000). In addition, it is clear from the tensile tests that, the Sn-Pb alloys tested in the current study exhibit good superplasticity at room temperature, and a higher temperature results in considerable higher potential for superplastic deformation. The first idea of using hydrostatic pressure in SPF can be traced back to Alnaib and Duncan (1970). Therefore, a laboratory hydraulic blow forming rig using hot water as forming pressure instead of gas with temperature and forming pressure controllable was designed and built. According to the general requirements described in Section 7.2.1, a constant forming pressure was chosen because the operational procedure was relatively easy and no complicated control systems were required for the forming equipment. The basic features of the forming rig are described as follows.

A schematic illustration of the designed experimental device is shown in Figure 7.9. The basic system comprises three parts, i.e., the water temperature control circuit (part I), the forming pressure circuit (part II) and the pressure forming die set (part III). Simplicity and cost effectiveness were emphasized throughout the design process.

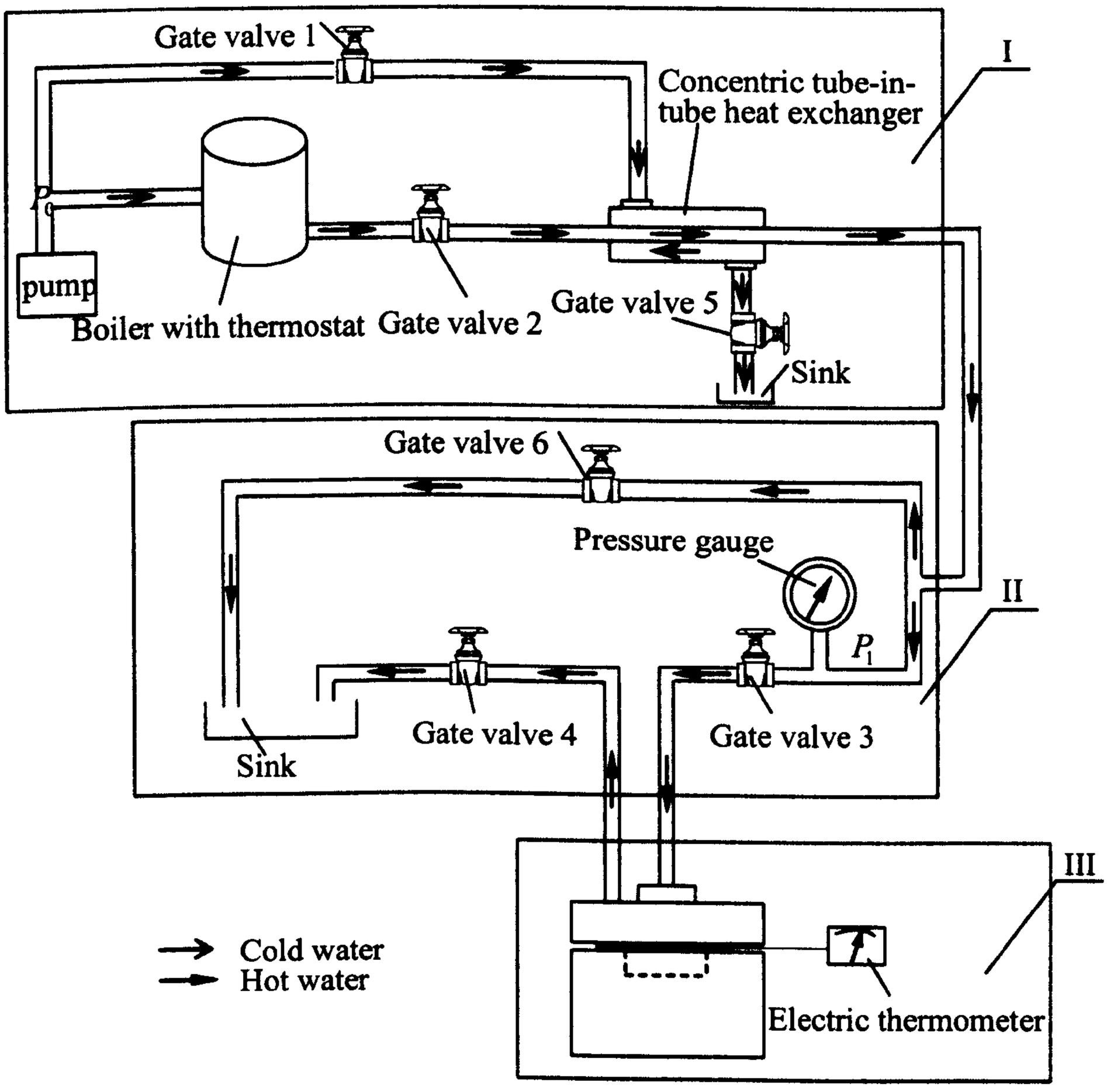

Figure 7.9 Schematic diagram of the experimental rig set.

Part I is used to control the water temperature at which the forming is conducted. Cold mains water flows into part I using an air-assisted pump to generate a pressure P_0 of up to 400 kPa. Part of the main water flows into the boiler, where the water is heated up to 100°C, and then goes through an internal tube of the concentric tube-in-tube heat exchanger. A gate valve No 2 is used to adjust the hot water flow in the internal tube. The other part of the main cold water flows through the external tube of the heat exchanger. The cold water flow in the external tube is adjusted by another gate valve

No 1, so that the temperature of the hot water can be set stable within a certain range. In such a way, the temperature can be adjusted by the concentric tube-in-tube heat exchanger to cool down the hot water. Heat loss does occur while hot water is flowing through part II and part III. However this loss will not lead to much difference of the forming process. During the whole forming process, the temperature variation can be maintained within $\pm 2°C$ to prevent localised deformation.

Part II is the hydraulic pressure system to control the forming pressure applied to the sheet. There are two routes where the hot water can flow through, one is through part III and the other is through gate valve No. 6. Moderate water flow is required to go through part III. This is because less water flow will not keep the desired forming pressure and temperature, on the other hand over flow is a waste of water resource. Desired pressure P_1 can be achieved by adjusting gate valve No. 3, gate valve No. 4 and gate valve No. 6 together. The pressure value of P_1 applied can be read from the pressure gauge directly.

Part III is the pressure forming die set where the sheet is formed into the configuration of the die by the fluid pressure. It is worth noting that the temperature of the forming sheet can be read directly and accurately through an electric thermometer as shown in Figure 7.9.

7.3 Friction Test for the Superplastic Cylindrical Cup

7.3.1 General

A schematic drawing of the geometric shape of the forming die is shown in Figure 7.10. The cylindrical cup to be formed has a radius of 30 mm with a height of 20 mm as well as a fillet radius of 5 mm. The forming chamber is made of a transparent perspex block in order to observe the forming process clearly from outside for the measurement of the strain rate. As described in Section 7.2.1, if the whole forming process can be recorded, the feature of deforming length can be extracted from the

recorded images. With the help of an image processing technique, deformation can be obtained so that the strain rate can be calculated.

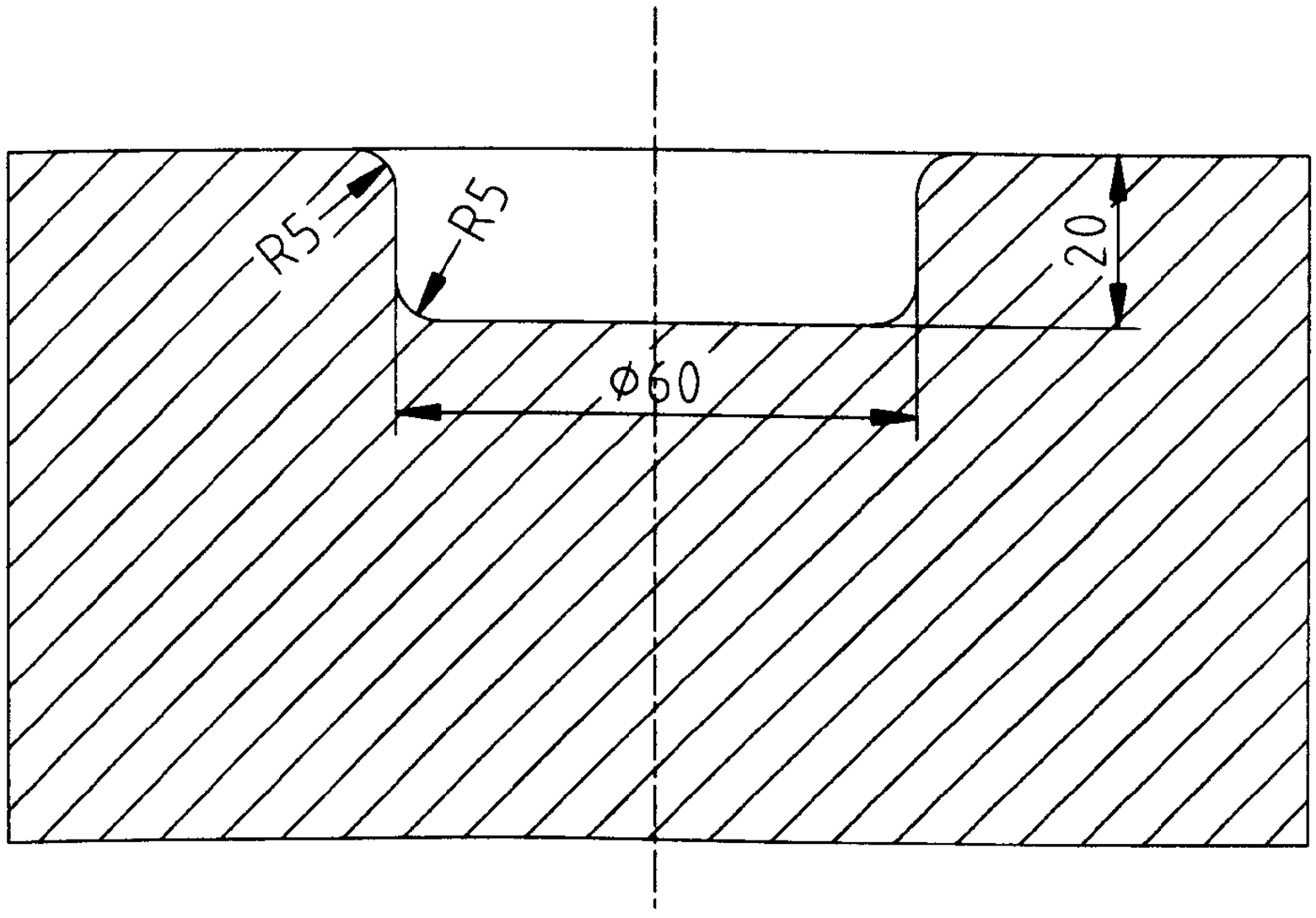

Figure 7.10 Geometry of the forming die (unit mm)

An assembly of the pressure forming die set is shown in detail in Figure 7.11, comprising of the inlet and outlet water connections, an aluminium pressure head, the forming sheet, the forming die, bolts and nuts. The aluminium pressure head is connected to the forming die block by four sets of bolts and nuts, with the forming sheet being clamped between them. Although it is not visibly seen, there are three concentric ring-shape teeth on the down side of the aluminium pressure head. When the nuts are tightened up, these teeth will 'bite' into the Sn-Pb sheet. Their purposes are twofold, i.e., to hold the sheet in place to prevent draw-in, and to seal up the chamber enclosed by the pressure head and the forming sheet, so that an effective seal of water inside the pressure container can be attained. There are two bleeding holes, 2 mm in diameter, with one at the centre of the Perspex forming die and the other located close to the bottom corner of the cup. Both holes are employed to bleed off the air in the chamber enclosed by the sheet and the cavity during the forming process.

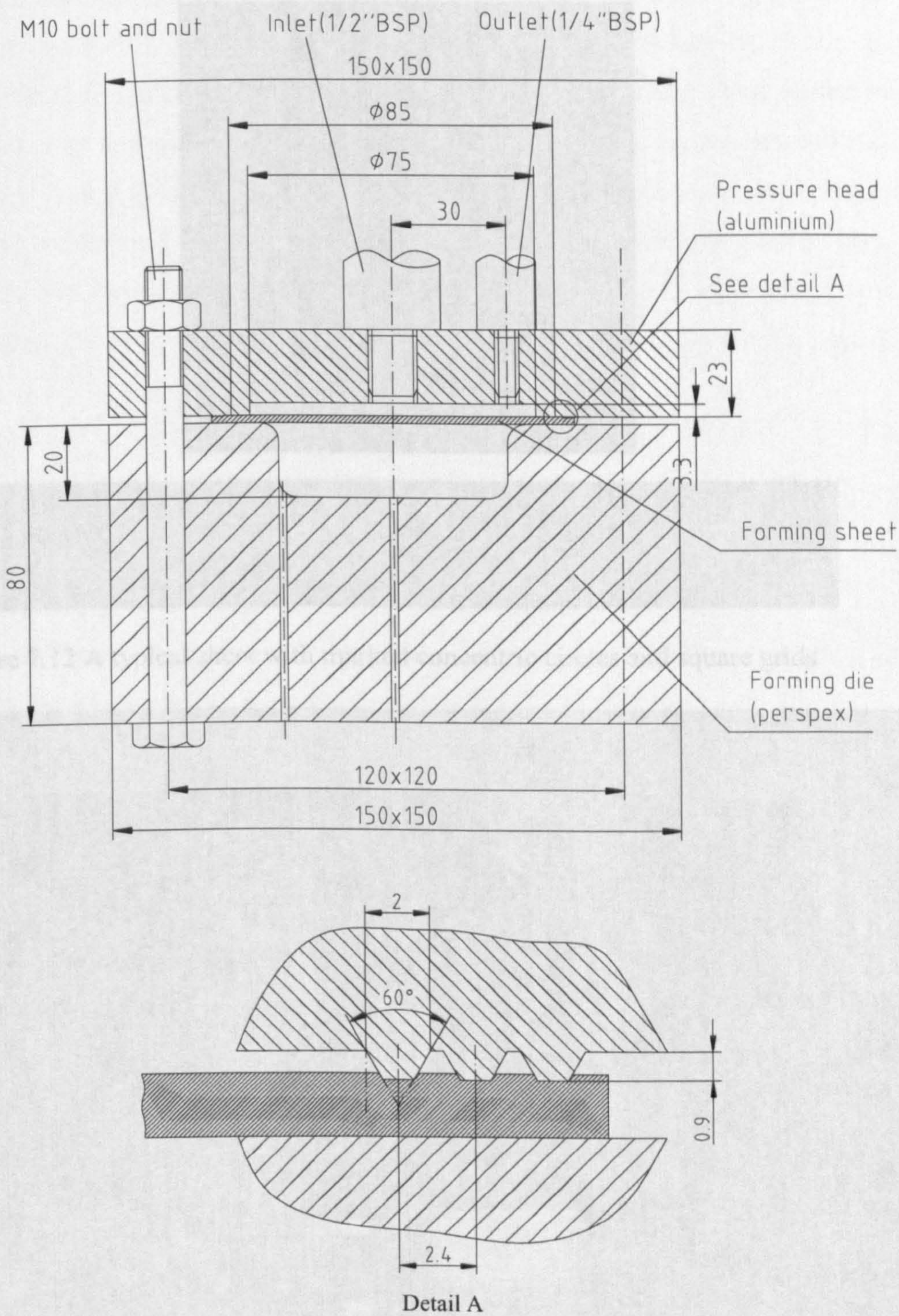

Detail A
Scale 10:1

Figure 7.11 Details of the pressure forming die set (unit: mm)

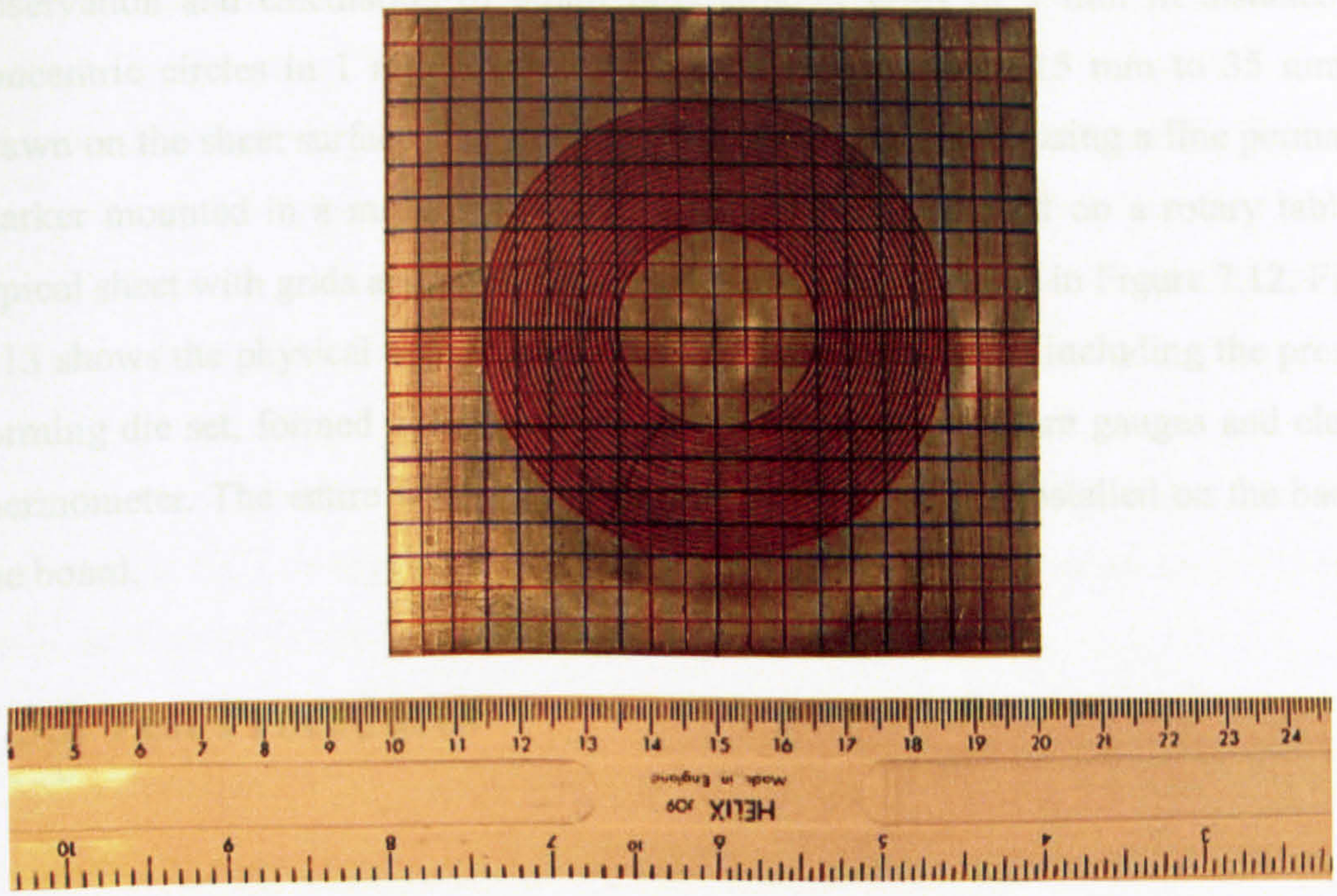

Figure 7.12 A typical sheet with marked concentric circles and square grids

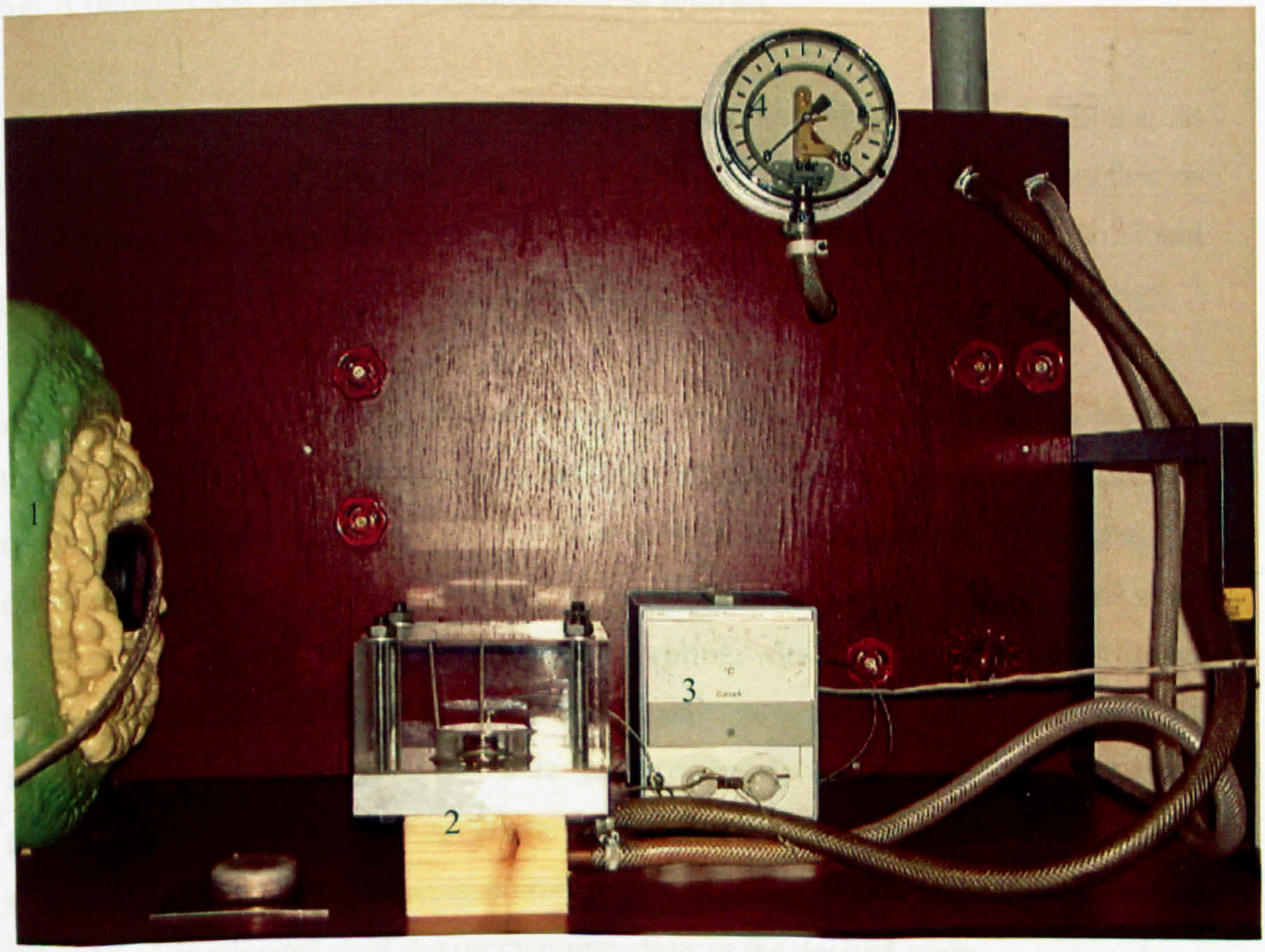

Figure 7.13 The whole experimental rig
(1 - tank, 2 - forming die assembly, 3 - electric thermometer, 4 - pressure gauge)

The blank sheet is 100 mm × 100 mm with 2 ± 0.02mm in thickness. For the observation and calculation of strain rate, straight grids of 5 mm in distance and concentric circles in 1 mm interval with radii ranging from 15 mm to 35 mm are drawn on the sheet surface. The concentric circles were drawn using a fine permanent marker mounted in a milling machine, with the sheet fastened on a rotary table. A typical sheet with grids and circles before deformation is shown in Figure 7.12. Figure 7.13 shows the physical appearance of the experimental rig set including the pressure forming die set, formed component, boiler, gate valves, pressure gauges and electric thermometer. The entire water pipe system of control unit is installed on the back of the board.

7.3.2 Test Procedures

The forming tests were performed using the aforementioned laboratory forming test rig. A detailed test procedure is summarized as follows.

The test rig has to be pre-heated in order to maintain steady forming conditions. At the beginning of each experiment, gate valves No. 1, 3, 4 and 5 are closed, so that no hot water flows through the forming die set at this stage. While gate valves No. 2 and 6 are opened to allow moderate hot water flowing through the part II of the test rig.

After pre-heating the test rig, a sheet is placed on the top of the aluminium pressure head in such a way that its centre is coincident with the centre of the dies. The perspex die is then placed on top of the sheet with four bolts and nuts screwed to keep the two die blocks together. The sheet is squeezed slightly and held in place by the teeth rings so that the sheet will not slip out during the forming, which also provides an effective seal of fluid inside the pressure container. At this stage, gate valves No. 3 and 4 are fully open, while gate valve No. 6 is gently tuned to make sure that there is no pressure in the forming die set. When the required water temperature is attained as revealed from the electric thermometer, gate valves No 1 and 5 are opened, where valve No. 1 is adjusted until the temperature stays in the desired scale.

When the forming temperature is kept stable to the desired scale, gate valve No. 6 is set to be approximately 99% closed so that there is still some hot water flowing through to the sink. This is to ensure a water circulation so that the forming temperature can be kept relatively stable. The pump is now started and the gate valve No. 4 tuned down until the pressure accumulated in the die set reaches a preset forming pressure value. Hence the sheet is slowly inflated into the configuration of the perspex die under the desired forming conditions.

After the component is completely formed, gate valves No. 1 and No. 2 are turned off to terminate the forming process. The bolts are unscrewed to remove the perspex die. Now the formed component can be removed safely.

Temperature variation of $\pm 2^0$C and pressure variation of ± 0.1 bar can be corrected by tuning the gate valves 1 and 6 respectively. The completion of the forming process can be determined by direct observation through the transparent die or using a depth probe.

7.3.3 Pilot Experiments

As the unique superplastic behaviour of an alloy occurs in narrow ranges of temperature and strain rate, an accurate control of temperature and forming speed in a superplastic forming process is much more demanding than the corresponding requirements for conventional forming processes. Therefore, a series of pilot experiments were conducted to determine the desired forming conditions before carrying out the formal experiments.

With different forming pressure and temperature, the formed components were observed and interpreted in terms of the forming time and thickness distribution. It was found from the pilot experiments that if the forming pressure was lower than 200 kPa, the component could not be fully formed. In addition, due to the capacity limitation of the pump, the highest forming pressure that could be attained was 400 kPa. Forming temperature is another important variable in superplastic forming. As

illustrated in Section 7.2.2.2, a higher temperature is beneficial to superplastic forming. Limited by the heater employed in the experimental setup, the maximum forming temperature in the experiments that could be obtained was 85°C. The temperature variation can be kept within ±2 °C. The pilot experiments also showed that the forming process might last for up to 6.5 hours depending on the applied forming pressure, the temperature and the sheet thickness profile. Based on these pilot experiments and the melting point of Pb-Sn material, a forming pressure ranging from 200 kPa to 360 kPa and a temperature of around 80°C were taken as the forming conditions for the formal experiments.

Figure 7.14 shows a typical superplastic formed cylindrical cup of Pb-Sn alloy. It can be seen that the material in the clamped region is less deformed and the square grids remain; while the material corresponding to the cup cavity has been stretched a lot and resulted in deformation of the grids.

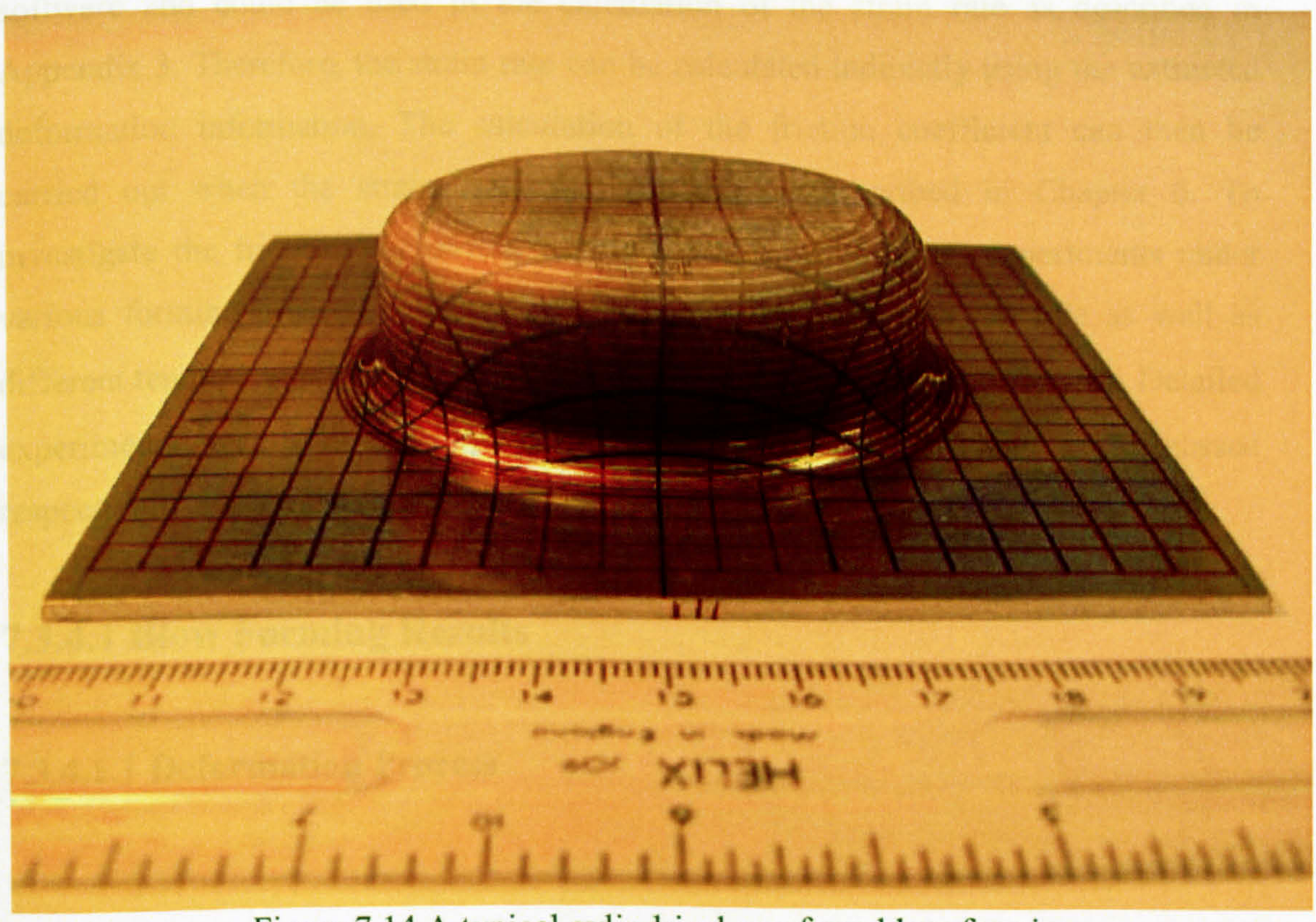

Figure 7.14 A typical cylindrical cup from blow forming

7.3.4 Experimental Results and Discussions

The main function of the above described experimental device is to meet the requirement of applying a superplastic blow forming process while measuring friction coefficient during the contact between the sheet and the dies. For the calculation of friction coefficient, a digital camera was employed to acquire the deformation process through the transparent perspex die. The deformation feature can be extracted at each deforming stage if an image processing technique is employed. In this research, Windig (WinDIG 2.5, 2002) software was adopted to obtain deforming length. The software defines the mapping of the coordinates system and digitizes data from the recorded deformation pictures. Each deformation instance from the digital camera was firstly loaded into the software Windig. After the mapping of the coordinates system was defined, numerical values for that deformation instance were obtained by the software and could be used in the calculation of the strain rate as described in Appendix 3. Therefore, the strain rate can be calculated indirectly using the extracted deformation information. The calculation of the friction coefficient can then be carried out when the strain rates are available as described in Chapter 6. To investigate the frictional behaviour during superplastic forming, experiments under various forming pressures of 360 kPa, 300 kPa, 250 kPa and 200 kPa as well as different temperatures of 80°C, 70°C and 60°C were carried out in this study. Detailed experimental results of the blow forming and frictional coefficient are discussed respectively in the following sections.

7.3.4.1 Blow Forming Results

7.3.4.1.1 Deformation Process

The deformation process is recorded from the side of the transparent die using a digital camera. A typical inflating sequence is shown in Figure 7.15. It is noted that the formed cup is scaled down in the middle of the die due to optical refraction when recorded by the camera. With the increase of the forming time, the sheet is formed

slowly into the die cavity. The sheet comes into contact first with the die entry corner, and gradually touches the top centre of the die. Following that, the contact is spread progressively to the top wall and the side-wall of the die until the final corner is filled at the end of the loading period.

For the demonstration of the deformation process, a KODAK motion recorder analyzer (KODAK, 2000) was employed to record the whole process with a speed of one frame per ten seconds. The images of the whole forming processes were analysed and an animation movie was made, shown in Appendix 4, which provided the same forming sequences as recorded by the digital camera.

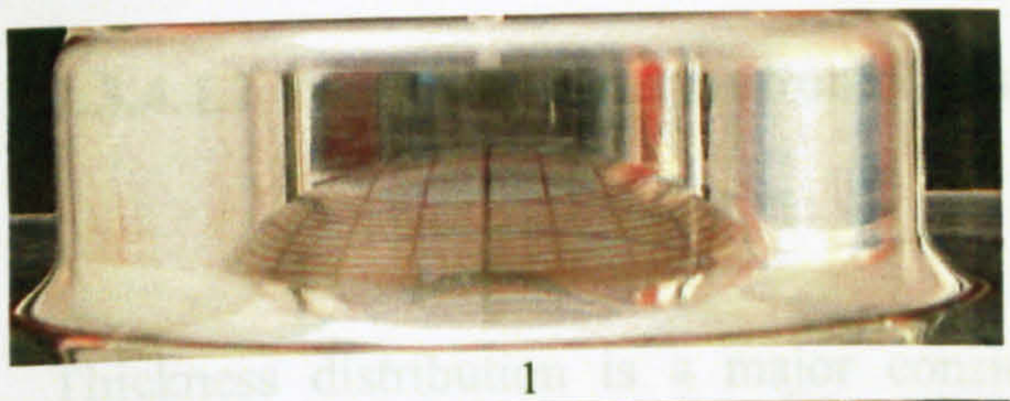

1

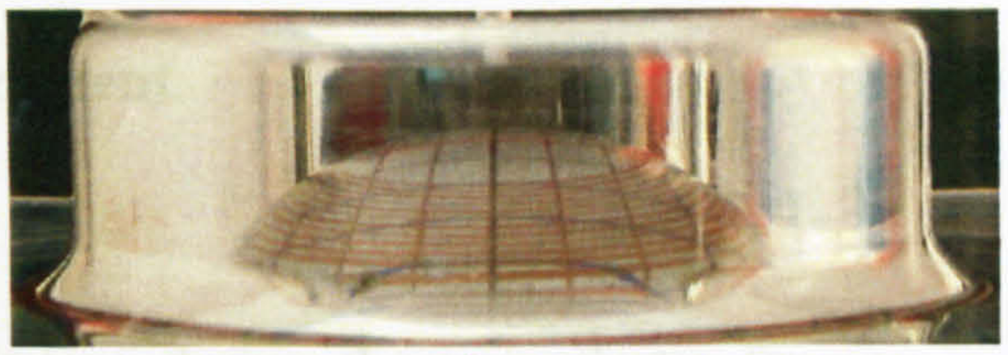

2

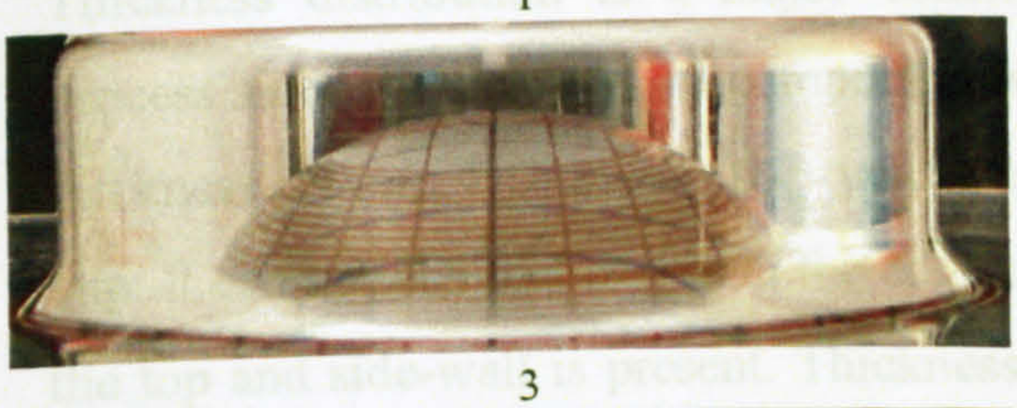

3

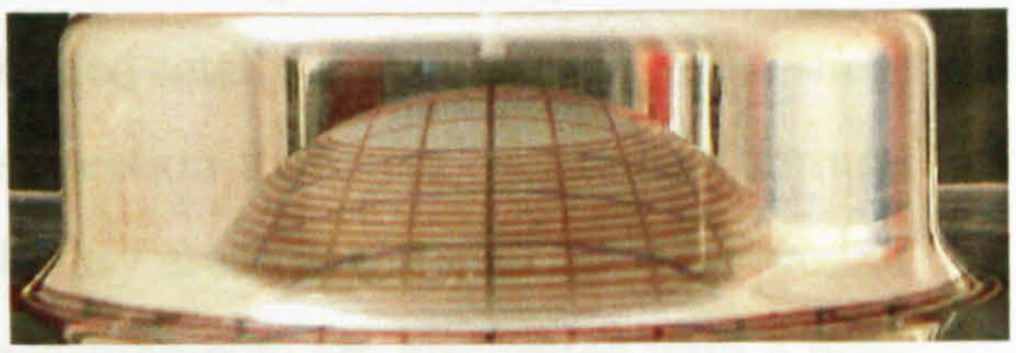

4

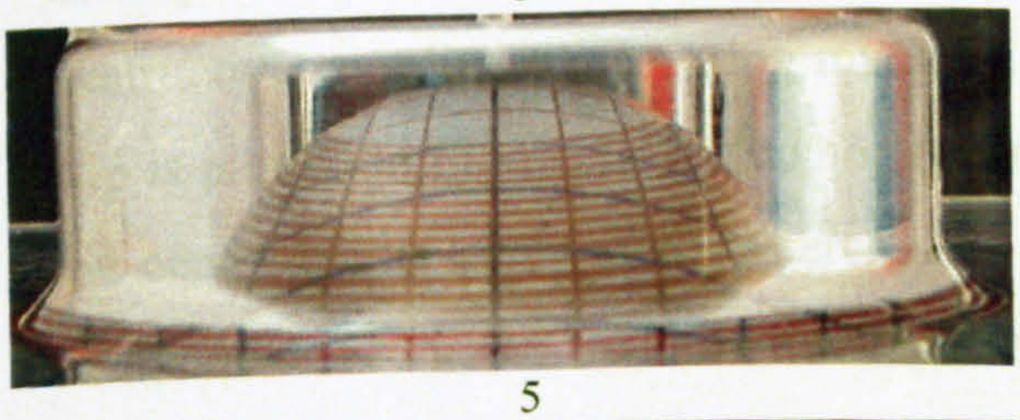

5

6

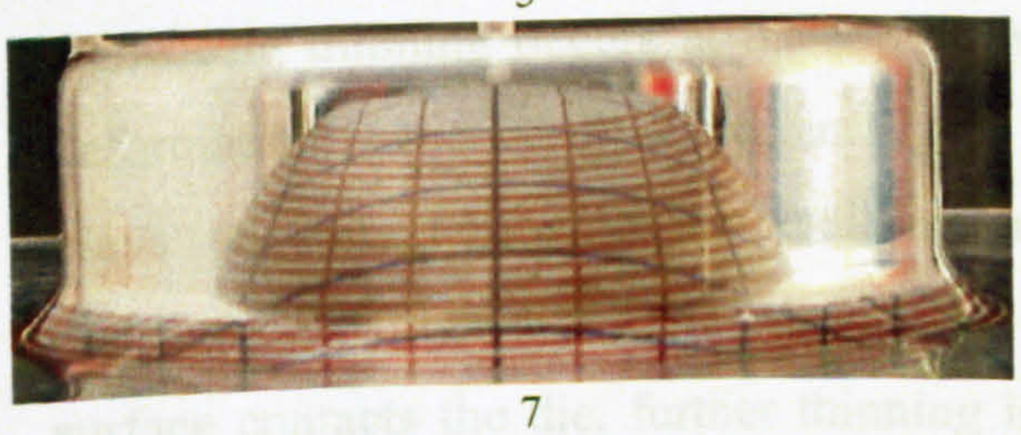

7

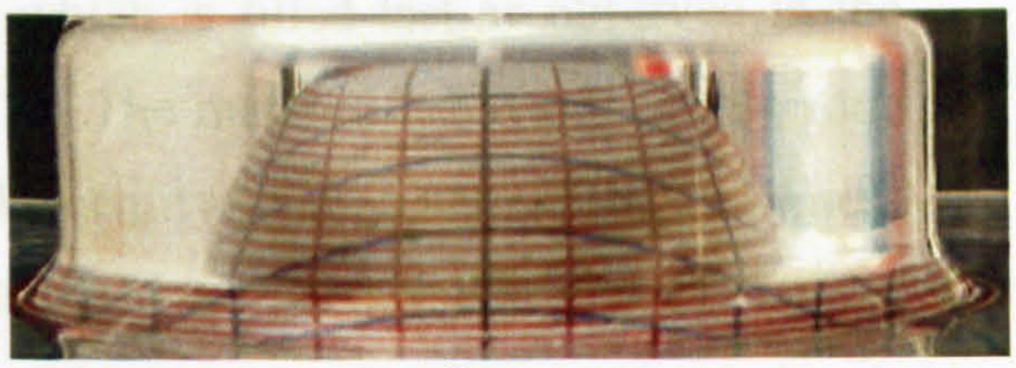

8

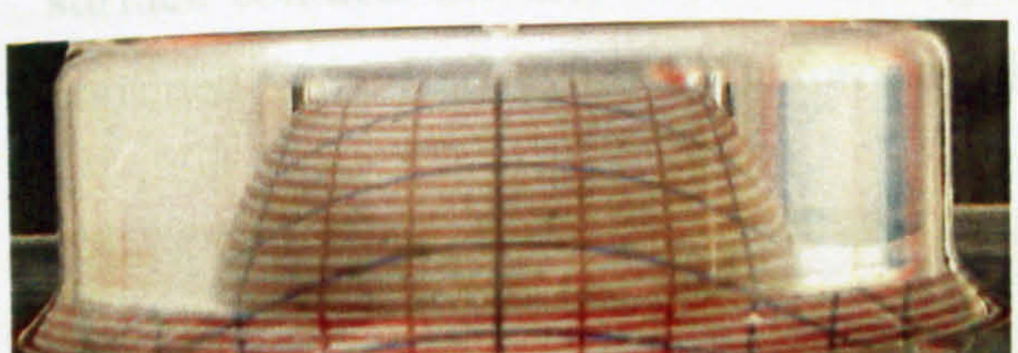

9

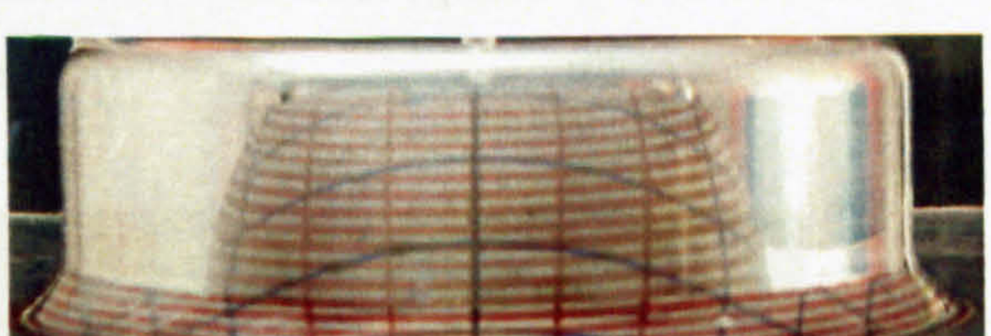

10

11

12

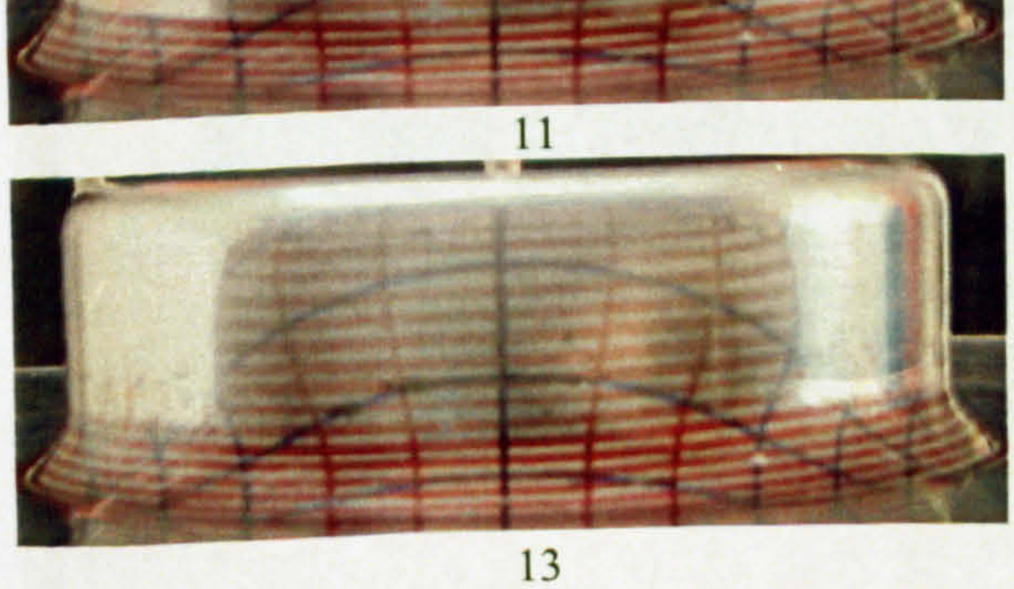

13

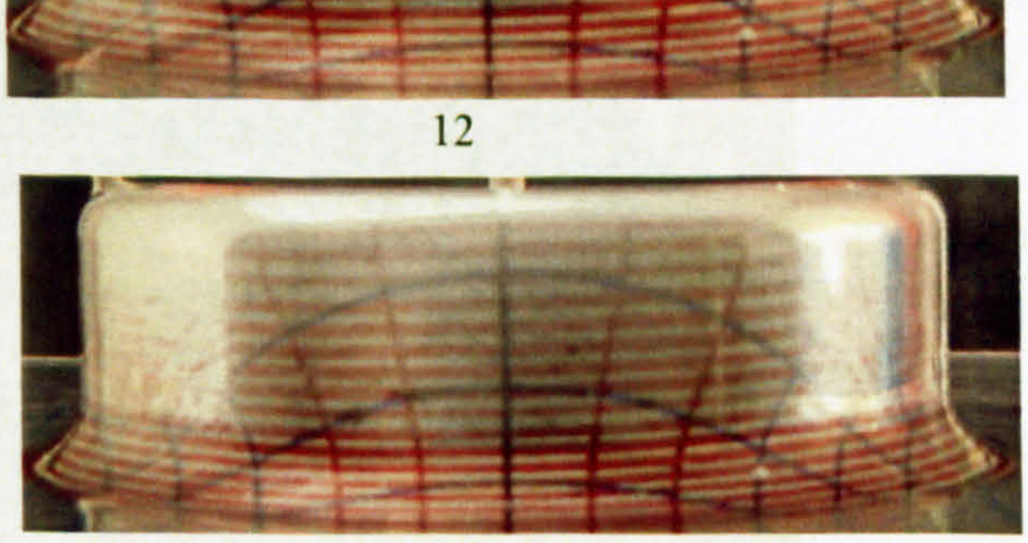

14

Figure 7.15 The deformation processes recorded from blow forming experiment

7.3.4.1.2 Thickness Distribution Measurement

Thickness distribution is a major consideration during the superplastic forming process since the shape of the component is formed totally at the expense of the sheet thickness. Figure 7.16 shows the typical cross-section thickness profile of a formed cup. It can be seen that except at the edge and entry areas, significant thinning around the top and side-wall is present. Thickness measurements are performed with a non-destructive coordinate measuring machine. A typical thickness distribution of a half cup is plotted in Figure 7.17. The horizontal coordinate is the arc length starting from the centre of the component, whereas the vertical coordinate is the thickness of the component. From the trend of the measured thickness distribution, it is shown that significant thinning occurs at the top corner which is filled last as observed in the deformation sequence illustrated in Figure 7.15. The material behaviour in this zone plays an important role in obtaining high quality components. The thickness distribution pattern along the cup can be attributed to the fact that when the sheet surface contacts the die, further thinning is inhibited and subsequent deformation is confined to the free region of the forming sheet.

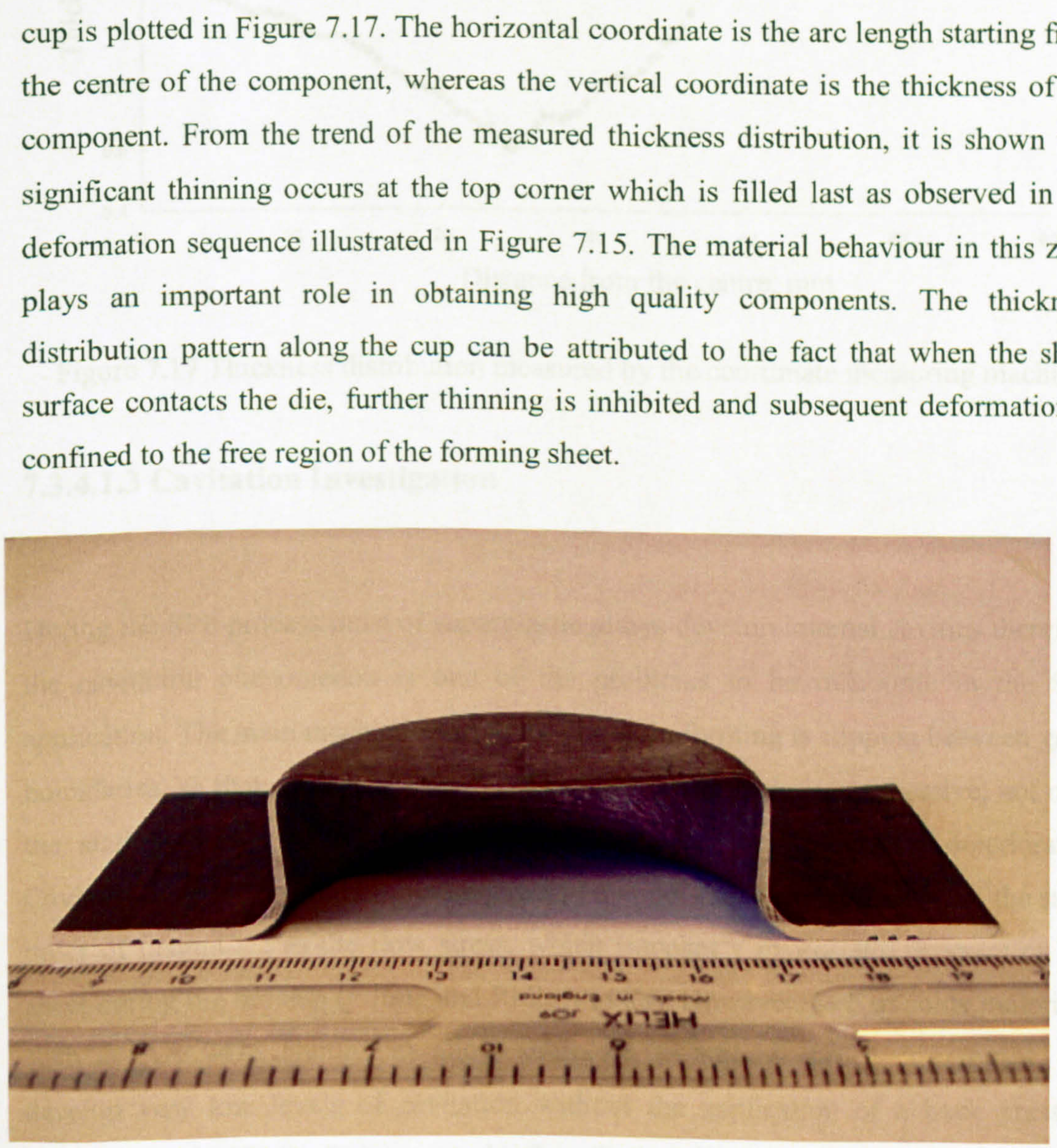

Figure 7.16 Final thickness distribution of a blow formed component

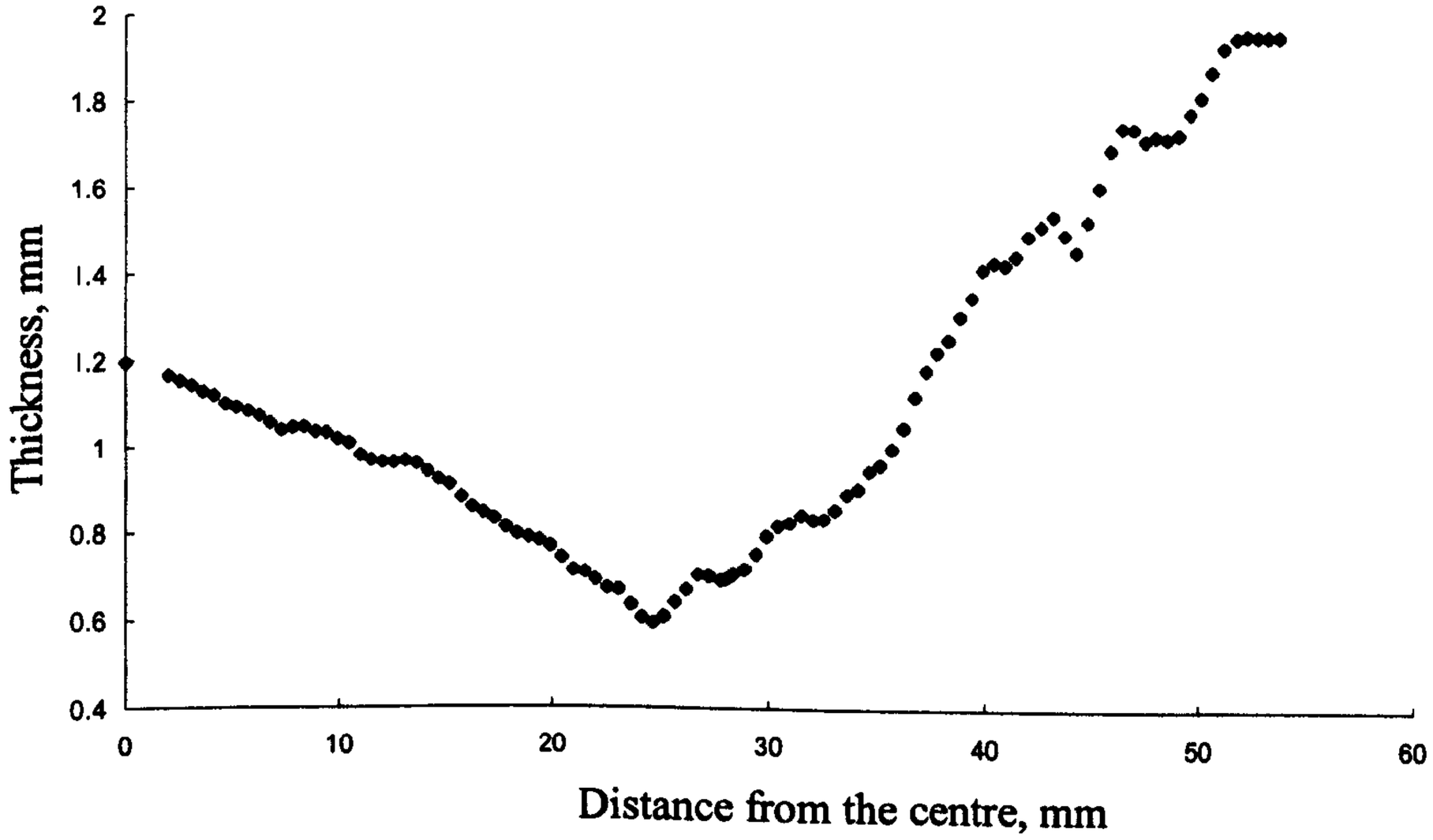

Figure 7.17 Thickness distribution measured by the coordinate measuring machine

7.3.4.1.3 Cavitation Investigation

During the SPF process most of superplastic alloys develop internal cavities therefore the cavitation phenomenon is one of the problems to be overcome in the SPF application. The main mechanism of deformation in forming is slipping between grain boundaries, so that cavities are produced there. If the cavities are excessive, not only the static strength of the material but also the fatigue strength is deteriorated. Cavitation can also be reduced or suppressed by applying a back pressure, of the same order of magnitude as the flow stress, which imposes a hydrostatic pressure on the sheet during the process (Pilling and Ridley, 1988). However, SPF of some materials, such as AA 7475 aluminium alloy, subjected to suitable processing routes, can develop very low levels of cavitation without the application of a back pressure (Mahon et al, 1994). Strict control of cavitation is required to enable adequate mechanical properties to be obtained in a cost-effective manner. Since the void volume fraction usually decreases with increasing temperature, decreasing strain and

strain rate, proper control of the forming conditions can be effective in reducing or preventing the formation of cavities (Pilling and Ridley, 1988).

Microstructures of the formed components were carefully examined by scanning electron microscopy (SEM), with a typical one shown in Figure 7.18. It can be seen that the grains still remain equiaxed. There is no obvious cavitation found between the grain boundaries.

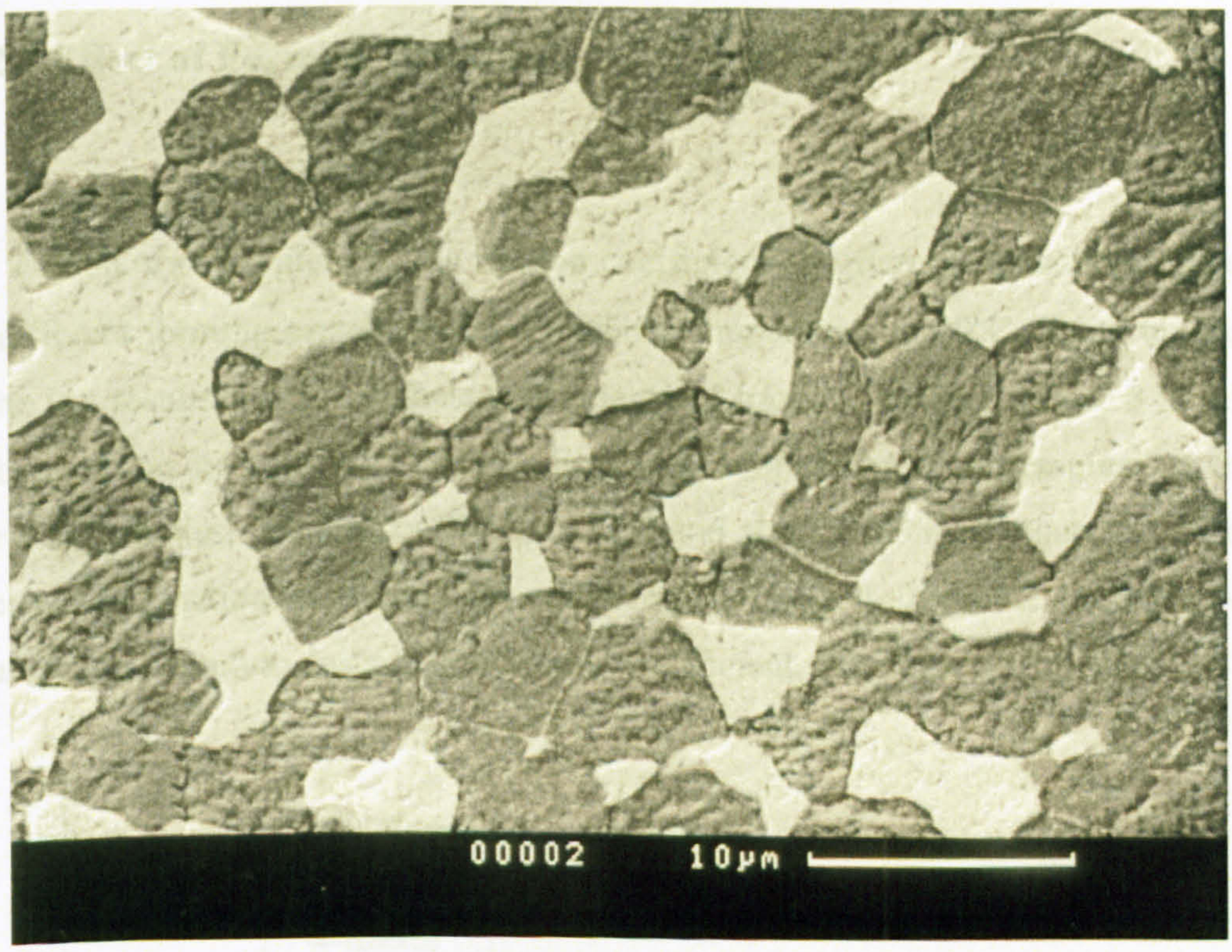

Figure 7.18 Microstructure of a typical blow formed component

7.3.4.2 Results of Friction Coefficient Measurements

In a real forming process, different sliding will occur at different regions of the contact between the tool and the workpiece. It can be expected that the frictional contact area will vary because of this. As a result, friction coefficients vary at different contact regions. In the experiment, various test conditions have been employed by changing the forming pressure and temperature as listed in Table 7.4.

The effect of forming pressure and temperature on the friction behaviour of Pb-Sn alloys is discussed as follows.

Table 7.4 Test Conditions for Friction Coefficients

Test No	1	2	3	4	5	6
Pressure (KPa)	360	300	250	200	360	360
Temperature (°C)	80	80	80	80	70	60

7.3.4.2.1 Effect of Forming Pressure

Figure 7.19 shows the values of the friction coefficient at different contacting regions under different forming pressures and a forming temperature of 80^0C. It can be seen from the test results that the highest coefficients of friction, ranging from 0.8 to 0.9, were found at the die entry area DE (see Figure 6.1) for all forming pressures. On the contrary, the smallest friction coefficient was found at area AB (see Figure 6.1). The coefficients of friction at other contacting regions ranged from 0.2 to 0.35. No obvious trend is found to describe the friction coefficient with forming pressure.

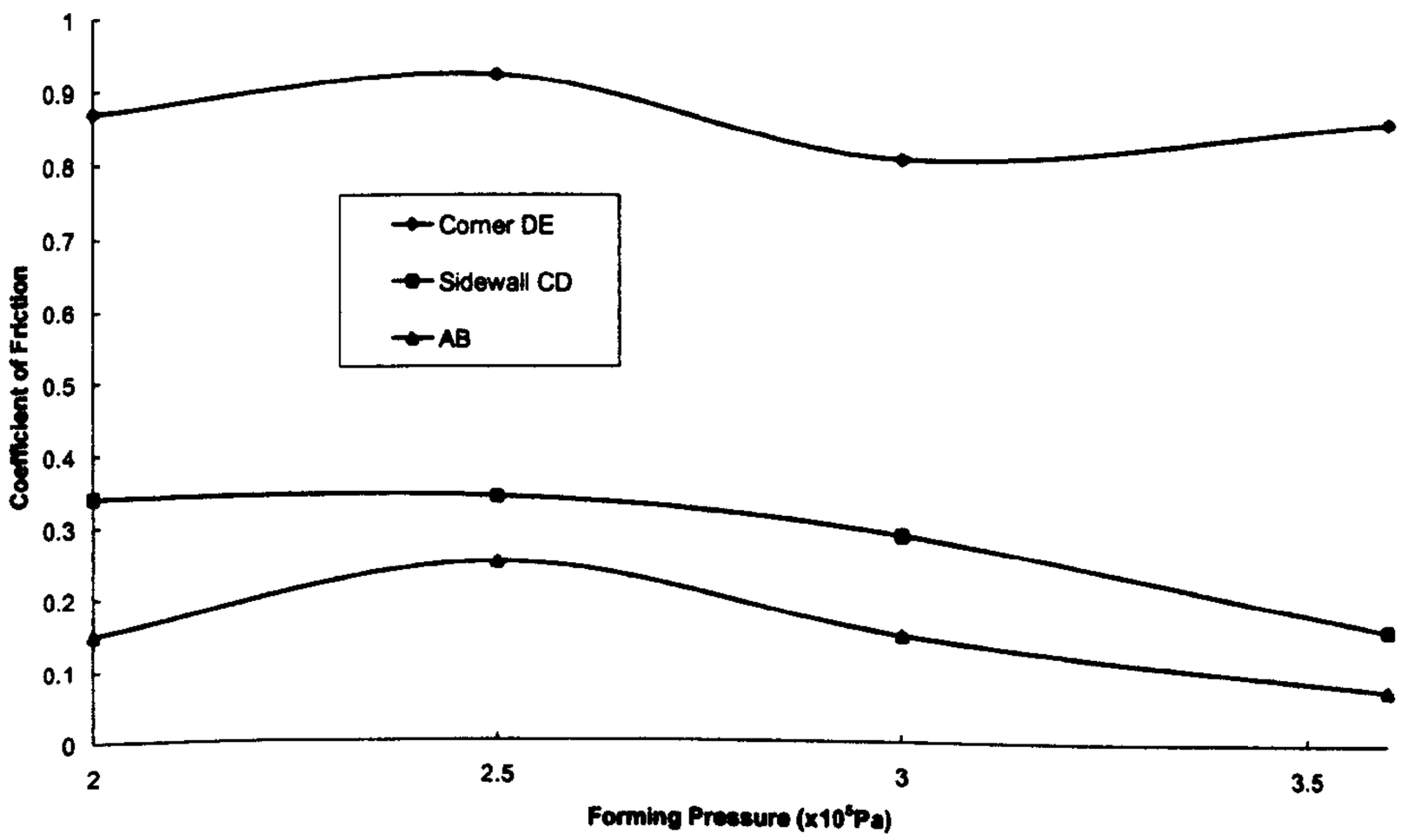

Figure 7.19 Friction coefficients at different forming pressures

The surfaces of the tested specimens were examined by a surface profilometer. Surface roughness is generally described by R_a, which is defined as the arithmetic average of the departures from the mean line over a single sampling length. Figure 7.20 shows results of peak height R_a at different contacting regions under different forming pressures. Before blow forming testing, the starting value of R_a of the sheet material was about 0.44 μm. The contact surfaces of specimens became rougher after the test, representing severe interaction between surfaces of specimen and dies. The R_a value at die entry corner DE is the smallest which is consistent with the observation in Figure 7.14.

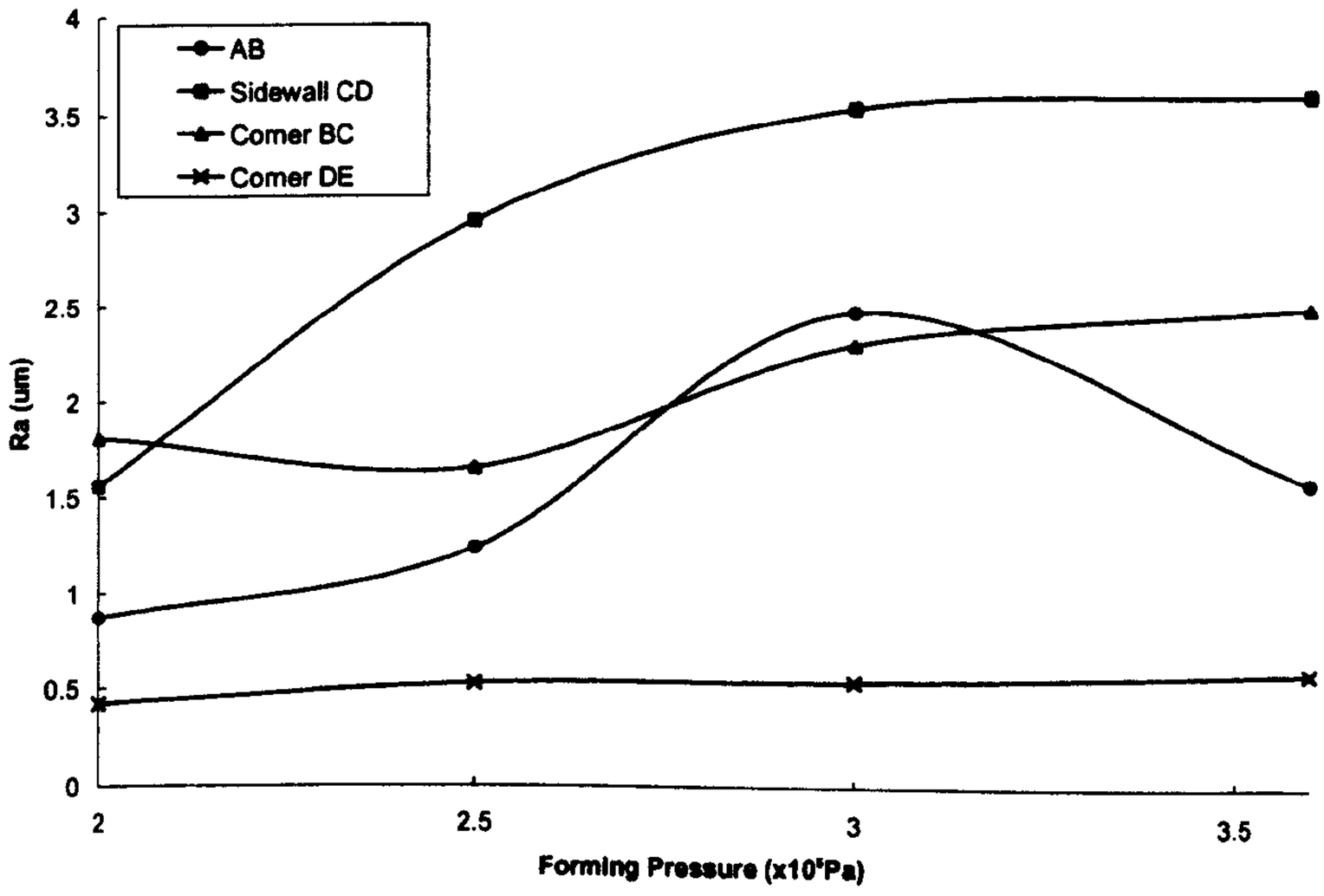

Figure 7.20 Surface roughness under different forming pressures

7.3.4.2.2 Effect of Forming Temperature

The coefficients of friction at temperatures ranging from 60°C to 80°C and a forming pressure of 360 kPa are shown in Figure 7.21. It can be seen that the die entry corner DE has the highest friction coefficient while region AB has the smallest value. The values of R_a corresponding to different temperatures of the friction test are shown in

Figure 7.22. The surface at the die entry corner DE remains relatively smooth at all forming temperatures, which is consistent with the experimental observation.

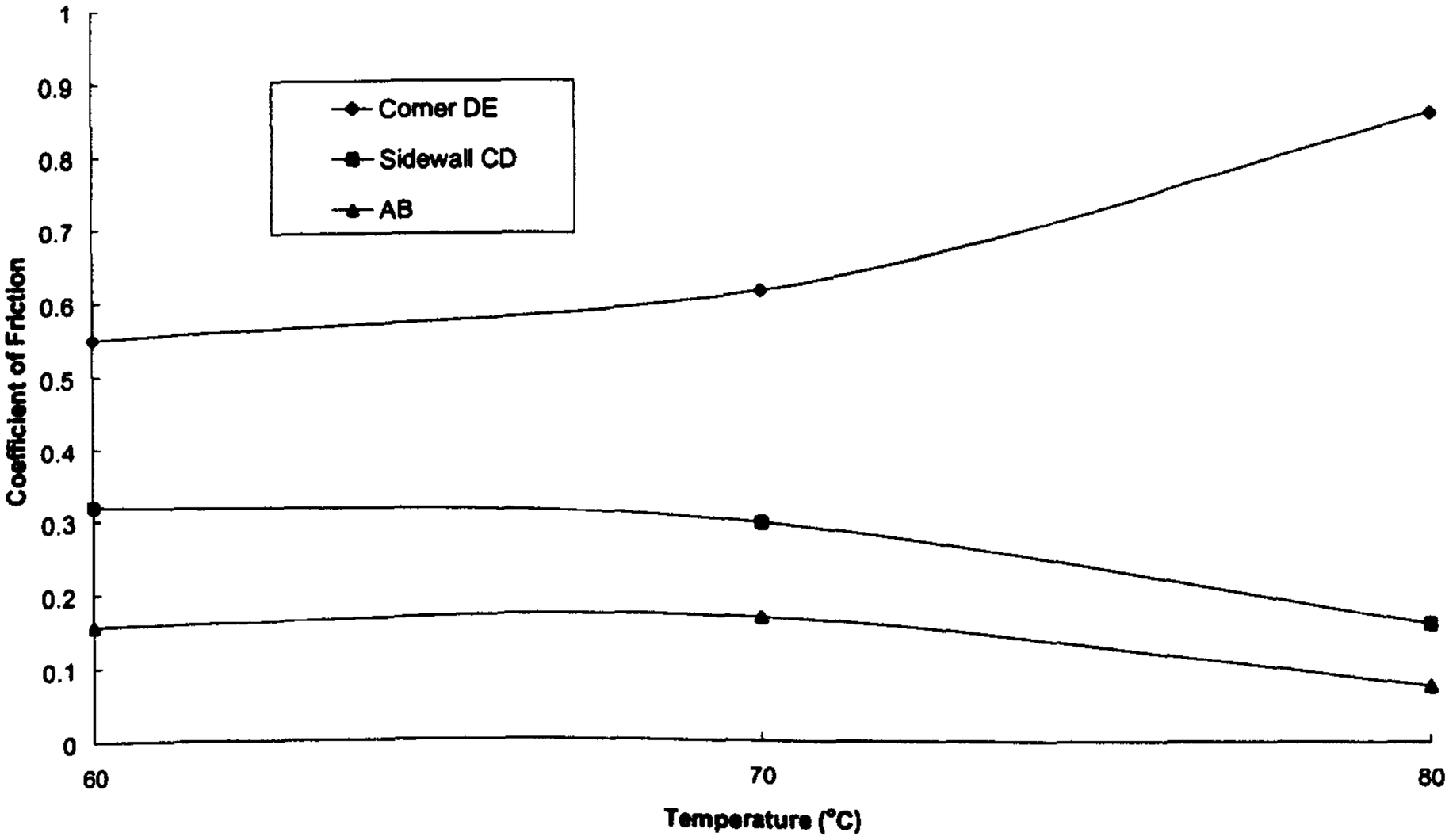

Figure 7.21 Friction coefficients at different forming temperature

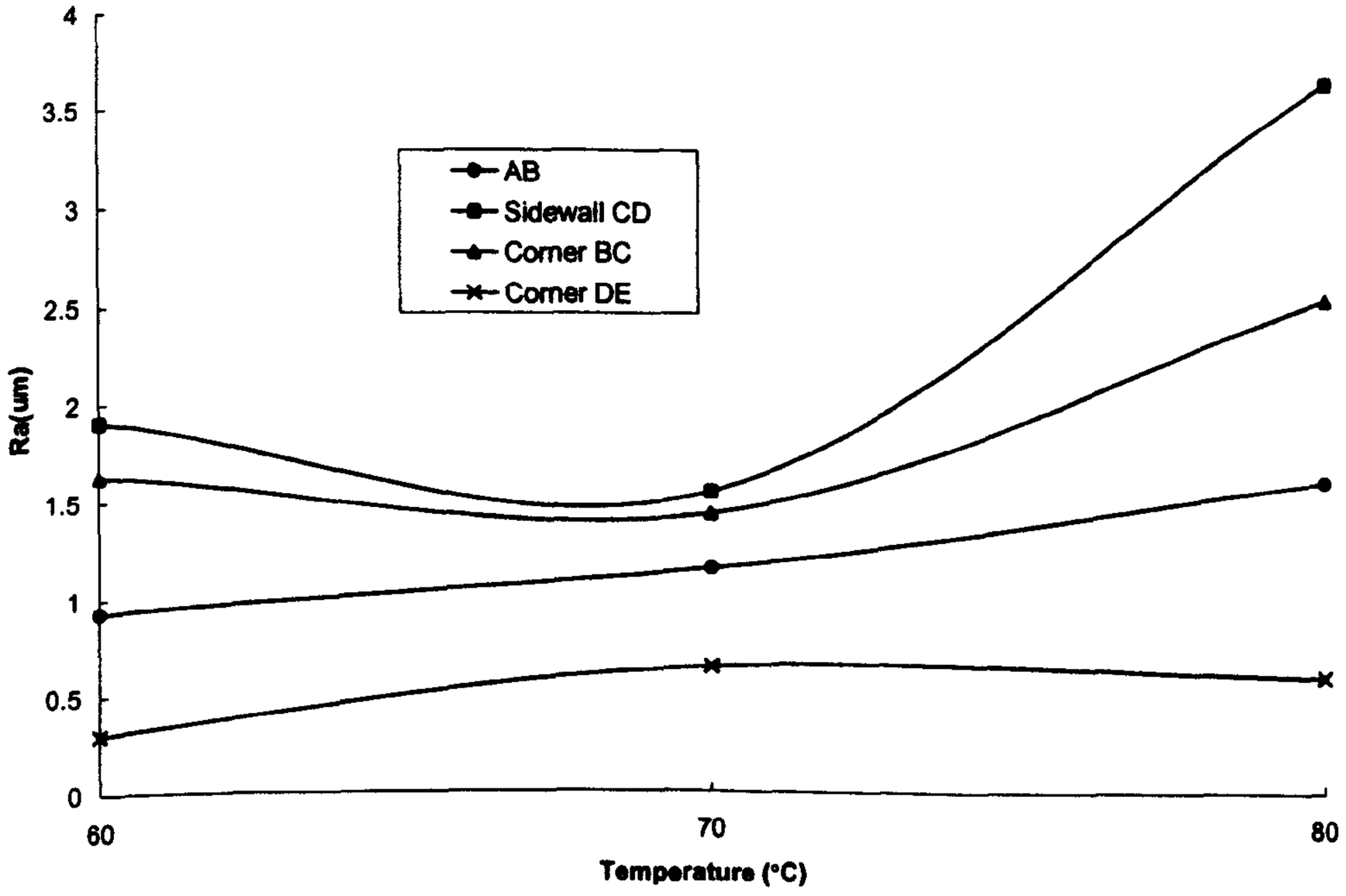

Figure 7.22 Surface roughness under different forming temperature

7.4 Friction Test of the Superplastic Reverse Forming

Numerical analysis of the friction behaviour during a reverse forming process has been previously conducted in Section 5.3. The work carried out in this section is to experimentally investigate the frictional behaviour in a practical reverse forming process using the method described in Section 7.3. As the cost associated with a full scale testing is very high and the die provided by the industry sponsor has a complex configuration, a 1/3 scaled die was studied in the laboratory.

7.4.1 Experimental Device Design

A superplastic forming experimental setup consists of a pressure control unit, a temperature control unit and a set of forming tools as previously described. To carry out a reverse forming experiment and investigate the frictional behaviour, a similar test rig, shown in Figure 7.9, was used. The main difference is that the more complicated forming dies had to be redesigned.

The reverse forming process undergoes two stages, where the material is first inflated into a pre-forming die before it finally reaches into the final die. During the pre-forming process, the sheet undergoes considerable deformation including thinning. Finally, the material flows into the final die cavity and the component is formed. Two dies are therefore necessary for the reverse forming experiment. The shape of a pre-forming die should be designed by the analyst in order to get a good thickness distribution in a pre-forming component and eventually control the thickness distribution of the final formed component. A carefully selected pre-form process can contribute significantly to the reduction of production costs and it is a dominant factor for a successful reverse forming. A detailed schematic illustration of the reverse forming dies is shown in Figure 7.23, which consists of a pre-forming die on the top and a final forming die at the bottom. Between these two forming dies there are four sets of M10 bolts and nuts, which together with two groups of sealing grooves machined on both surfaces are used to seal up the pressure chamber. Both dies have

water inlet and outlet designed as shown in Figure 7.23. During the reverse forming process, one pair of water inlets and outlets is actually connected to the pipework when the sheet is inflated into either dies. This reduces heat loss and water leaking.

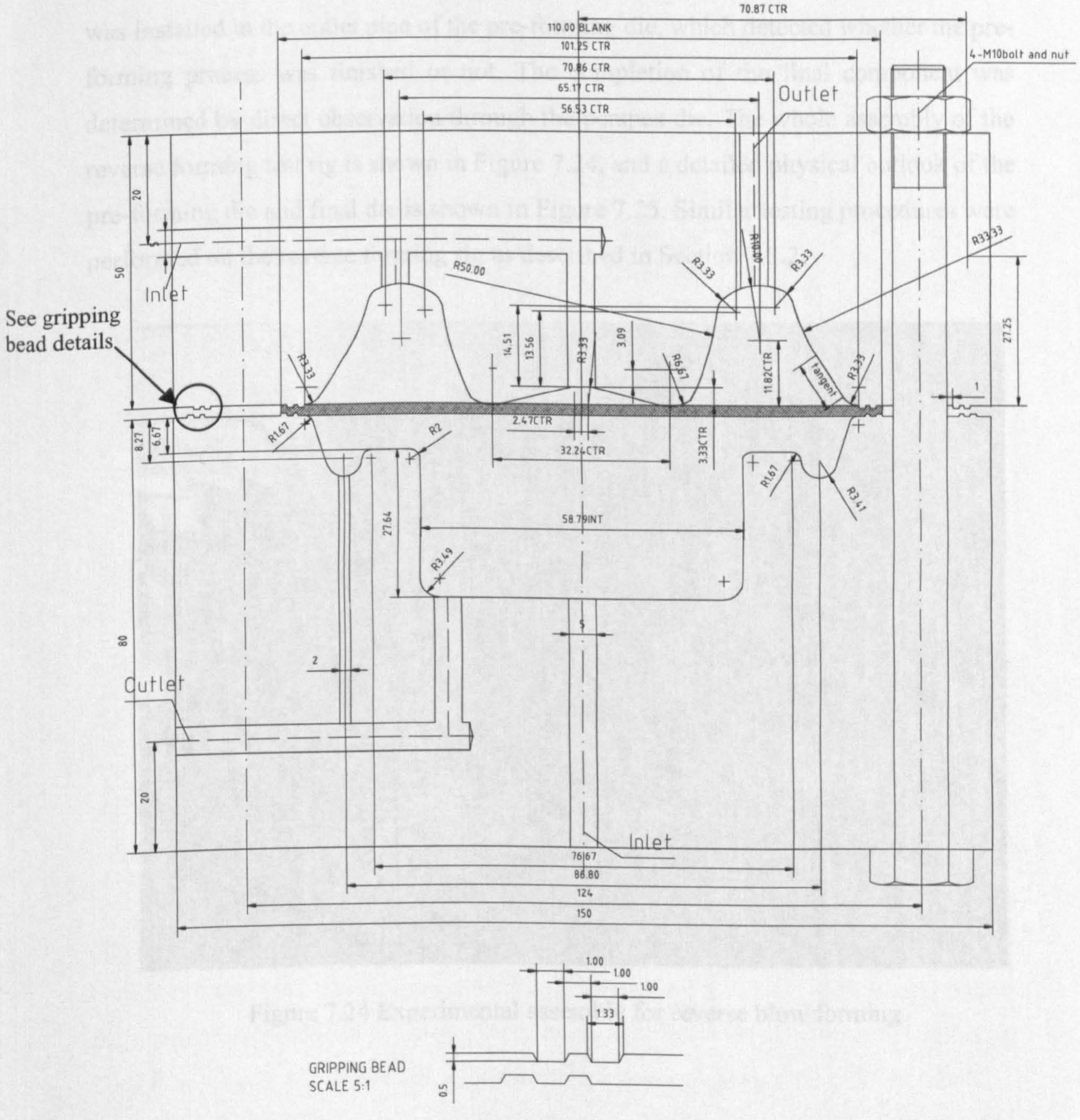

Figure 7.23 Assembly of reverse blow forming dies (unit: mm)

Because of its complex geometry, the pre-forming die was made in a sinterstation rapid prototyping machine. Duraform polyamide - nylon powder is melted, layer by layer, by a computer-directed heat laser. Additional powder is deposited on top of each solidified layer and sintered to produce the pre-forming die. The final die was again made of perspex block for the observation and data acquisition. A depth probe was installed in the outlet pipe of the pre-forming die, which detected whether the pre-forming process was finished or not. The completion of the final component was determined by direct observation through the perspex die. The whole assembly of the reverse forming test rig is shown in Figure 7.24, and a detailed physical outlook of the pre-forming die and final die is shown in Figure 7.25. Similar testing procedures were performed on the reverse forming rig as described in Section 7.3.2.

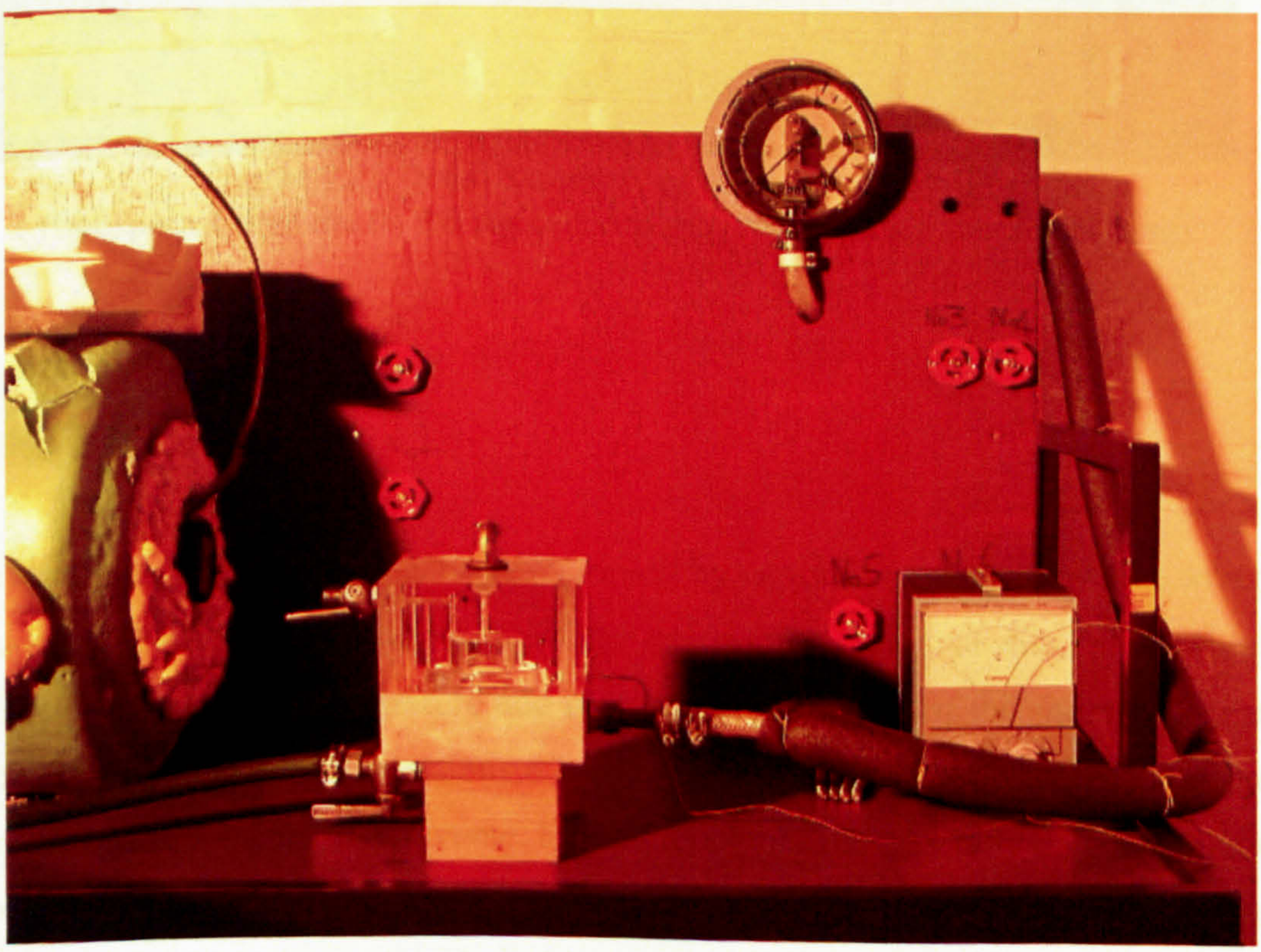

Figure 7.24 Experimental assembly for reverse blow forming

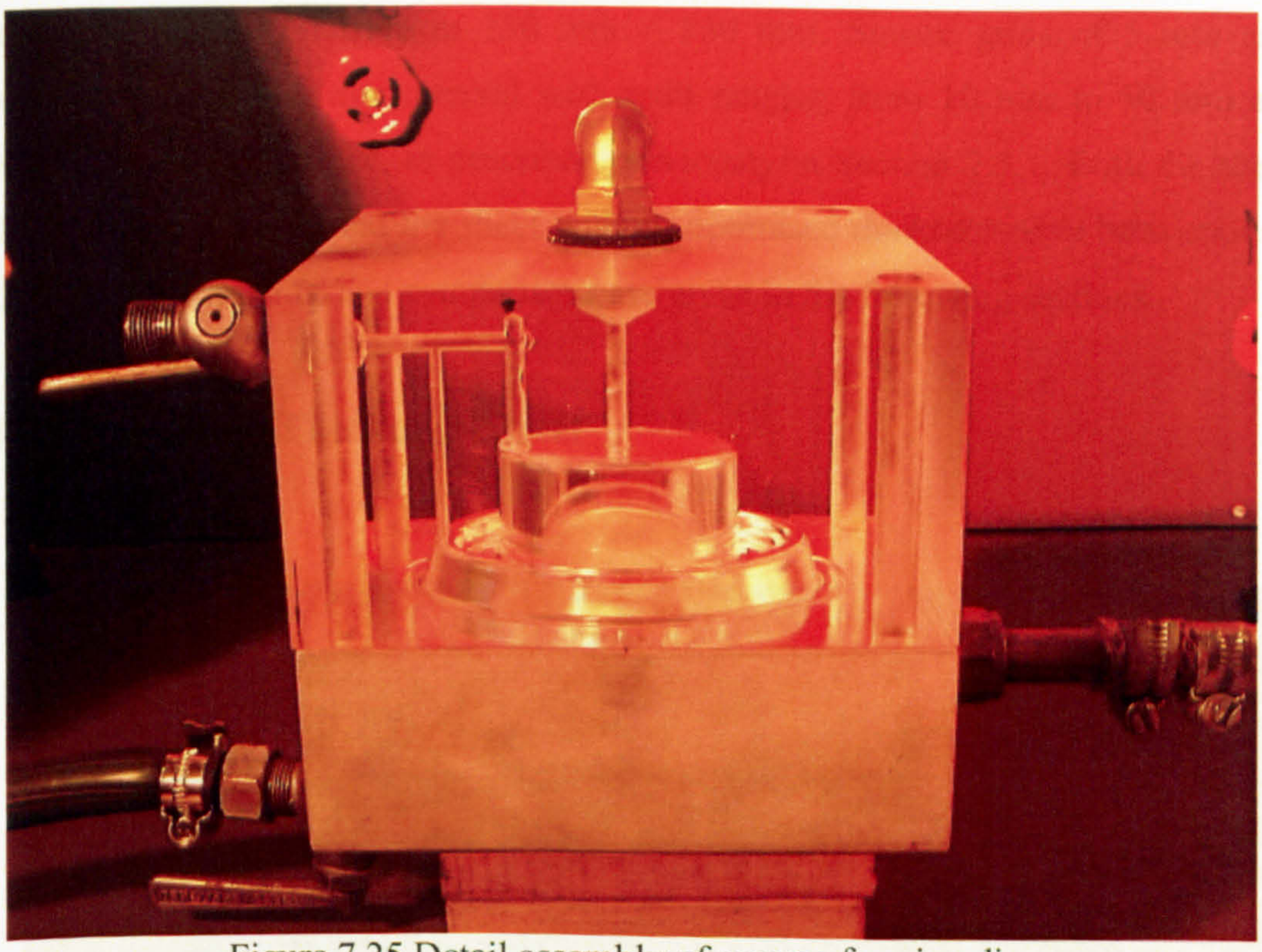

Figure 7.25 Detail assembly of reverse forming dies
(transparent final die on the top and opaque pre-forming die at the bottom)

7.4.2 Pilot Experiments

A reverse blow forming process is characterised by various process parameters, which include the forming sequence, shape of the preforming and final dies, initial sheet profile, friction, initial temperature and mechanical properties of the sheet and those of the dies. Making proper selections regarding controllable process parameters is the main consideration. As the reverse formed components generally have complex shapes, non-uniform final thickness distribution presented in the formed products is a common technical problem. It is desirable to design the process so that more uniform thickness distributions of the final components can be achieved. One of the technical means to control the thickness distribution actively on formed parts is to modify a blank sheet with intended pattern of thickness distribution (Suzuki et al, 2001). Pilot experiments have been carried out in order to ensure a satisfactory formability of the final component from the formal experiments.

The blank sheet is prepared in 130 mm × 130 mm. Square grids of 5 mm and concentric circles in 1 mm interval with radii ranging from 10 mm to 50 mm are drawn on the sheet surface, as described previously in Section 7.3.1. Both the sheet with constant thickness and the sheet with an optimised thickness have been applied in the pilot experiments, and comparisons are given in the following sections.

7.4.2.1 Constant Thickness Sheet

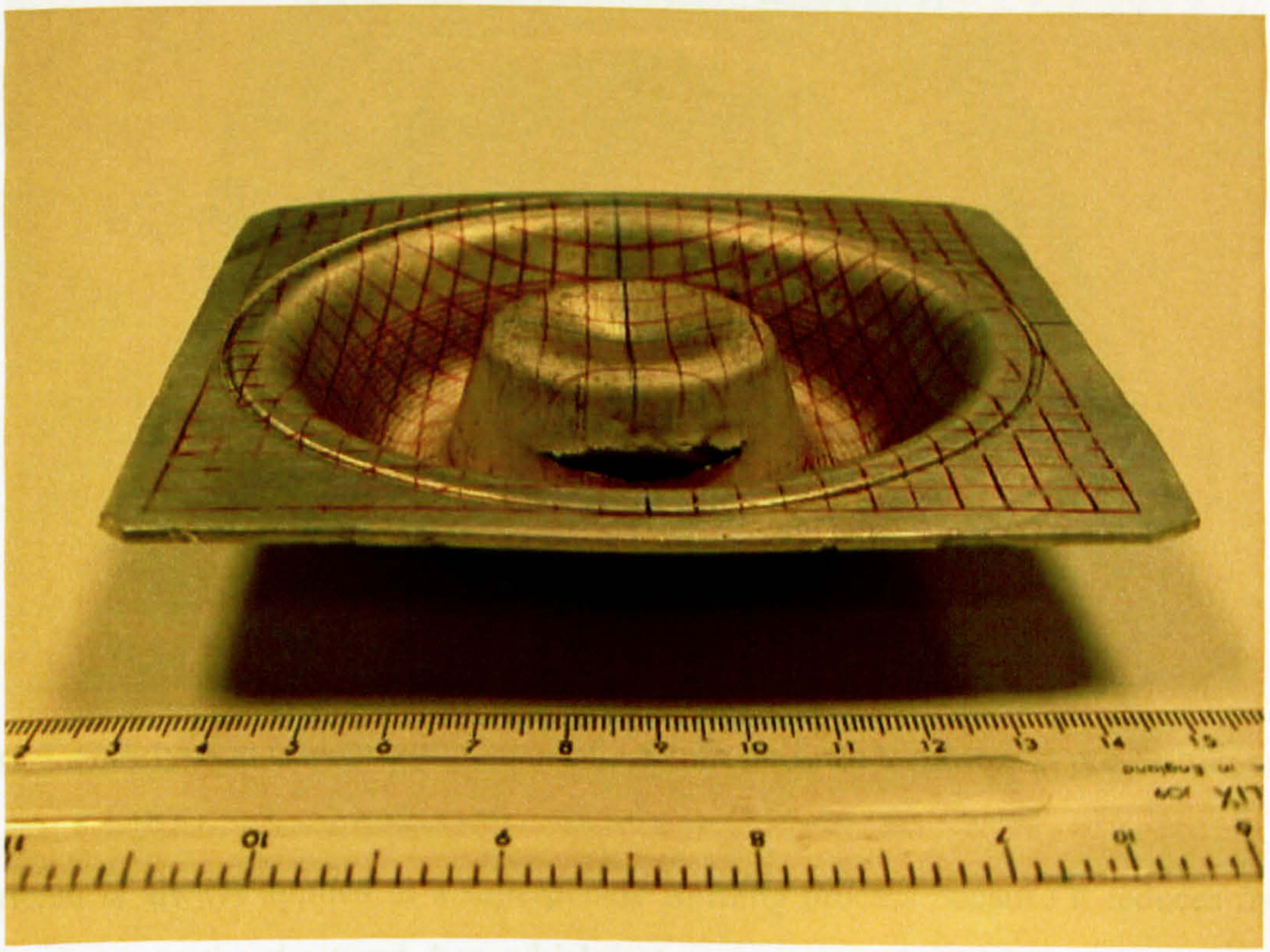

Figure 7.26 A typical broken component of 2mm uniform thickness at pre-forming stage

Constant thickness sheets were chosen because they were easy to prepare in the experiments. Sheets of 2 ± 0.02 mm thickness were first employed in the pilot experiment under a temperature of 80^0C and a forming pressure of 360 kPa. No lubricant was applied between the sheet and the dies in the trial. However, the pre-forming process could not be fulfilled as cracks and rupture always occurred. A typical example is shown in Figure 7.26. It can be seen that around the failure area, i.e., the middle bending area of the contour, the grid was stretched severely, which indicates a large deformation of material at that region. This can be explained by the

fact that a stress state of combined stretching and bending occurred there, making it the prevalent site of failure. A large amount of thinning can be seen at the failure area as there was not enough material flowing into this area. Thus for a given geometry, it is of practical importance to predict thinning (or final thickness) of the component.

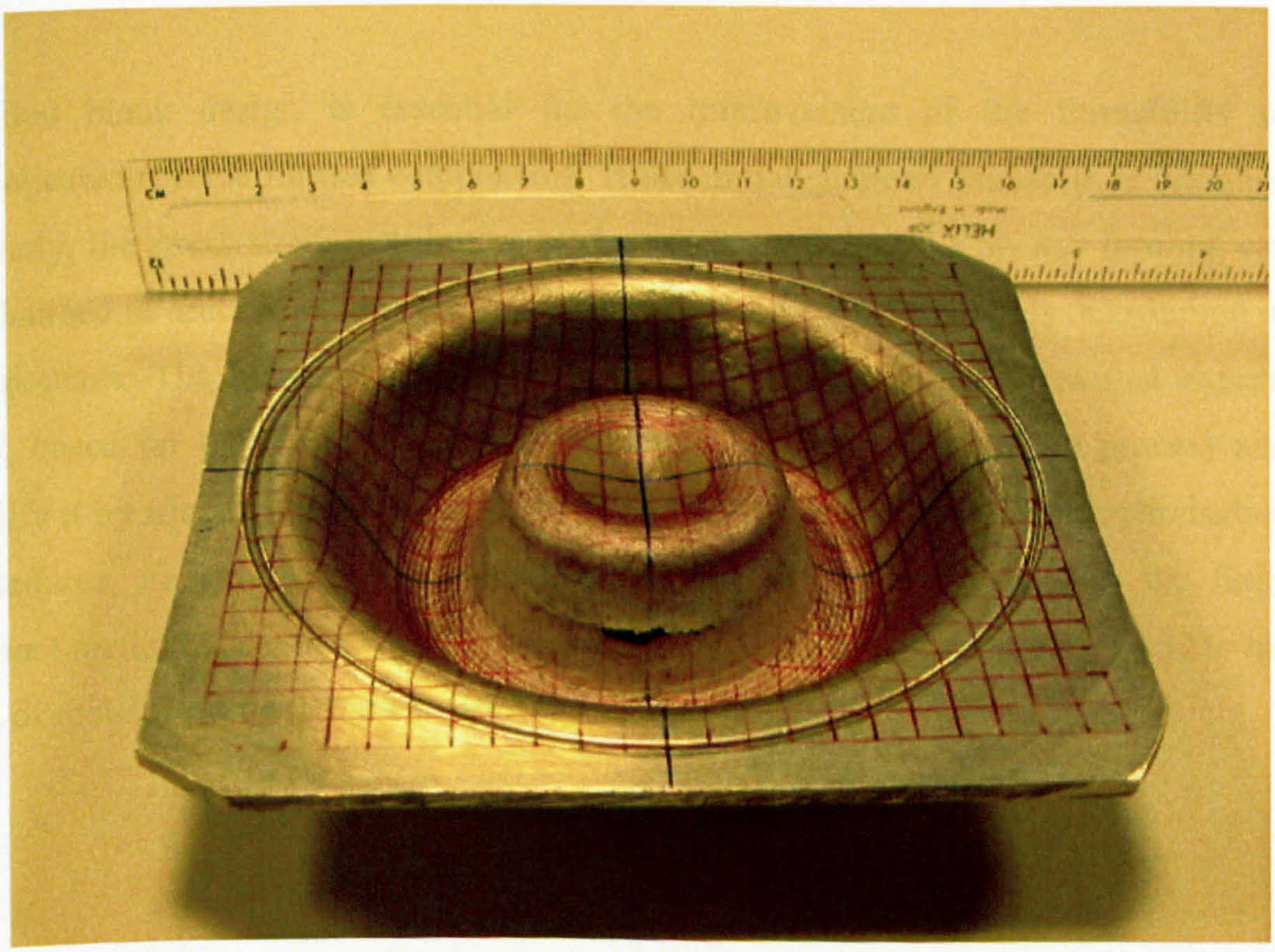

Figure 7.27 A typical broken component of 2.8 mm uniform thickness at pre-forming stage

Lubricant is always applied in a superplastic forming process because it reduces the friction between the sheet and dies, which in turn improves the thickness distribution accordingly. To overcome the aforementioned problem, a liquid lubricant, PTFE, was spread on the surface of the 2 ± 0.02 mm thick blank sheet, which was formed again under the same conditions. This proved to be successful for the pre-forming process. However, when the sheet was reversely formed into the final die, it fractured again. This suggests that the effect of lubrication on the thickness control is limited. Another instinctive consideration was to increase the thickness of the blank sheet. Therefore, a sheet with 2.8 ± 0.02 mm thickness was employed and formed under the same conditions. However, fracture occurred again at the same area as shown in Figure 7.27 during the pre-forming process. It is expected that severe thinning will occur even if a thicker sheet is used. These trials indicated that a sheet with an optimum thickness

pattern was necessary, to carry out the reverse forming experiment and also to control the thickness actively on the formed parts and eliminate severe forming failure.

7.4.2.2 Profiled Thickness Sheet

Profiled blank design is essential for the improvement of the formability of complicated reverse formed components. If the initial shape of the blank is designed properly, the stress-strain distribution of the specimen during the reverse forming can be changed in order to reduce the non-uniformity of the final thickness distribution of components. The blank design has been traditionally conducted by skilled experts who, based on their past experience and intuition, build a prototype process and modify it by trial and error (Sanders, 1999 and 2001). Recently efficient optimisation procedures, integrating the mathematical methods of optimisation with the finite element method, have been developed and applied to structural engineering and to the area of metal forming (Sanders, 1999 and 2001).

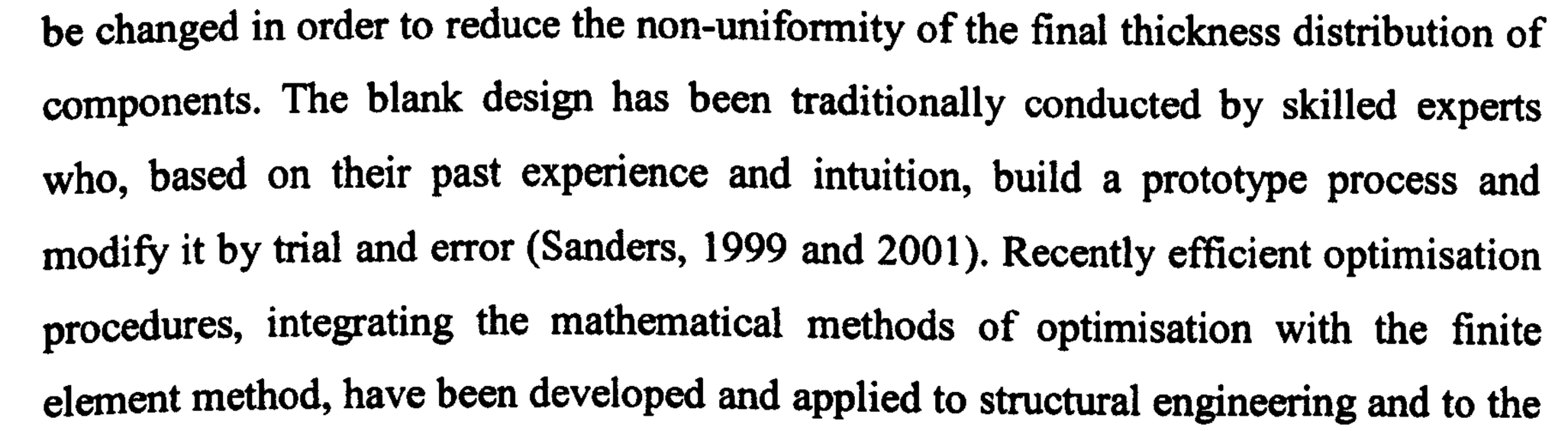

Figure 7.28 Thickness profile of a sheet (unit: mm)

Figure 7.28 shows a blank sheet profile design which was machined locally in order to control the target variation of thickness after forming. After being machined by a lathe to achieve the designed thickness profile, a typical blank sheet is shown in Figure 7.29. The same forming temperature and pressure as in the previous pilot experiments, were applied to these sheets. No lubricant was applied on the blank and the dies. The profiled thickness sheet was successfully inflated into the pre-forming

die and reversely formed to the final die, as shown in Figures 7.30 and 7.31 respectively. The grids on the pre-forming component were stretched much more evenly than those with the constant thickness sheet, especially around the middle bending area where failure previously occurred. This verified that the pre-machined blank, of designed thickness distribution, can be reverse formed successfully without rupture. The resultant cross-section of the final reverse formed component is shown in Figure 7.32. It can be seen from the thickness profile, shown in Figure 7.32, that even though the forming failures have been eliminated using the designed sheets, the non-uniform thickness distribution is obviously presented with maximum thinning occurring at the top corner. This may be explained that during the preforming process, the sheet undergoes considerable deformation. When it flows into the final die cavity, although those areas that are thinned excessively in the pre-forming stage, are compensated by some material flow, they will still stretch to some extent.

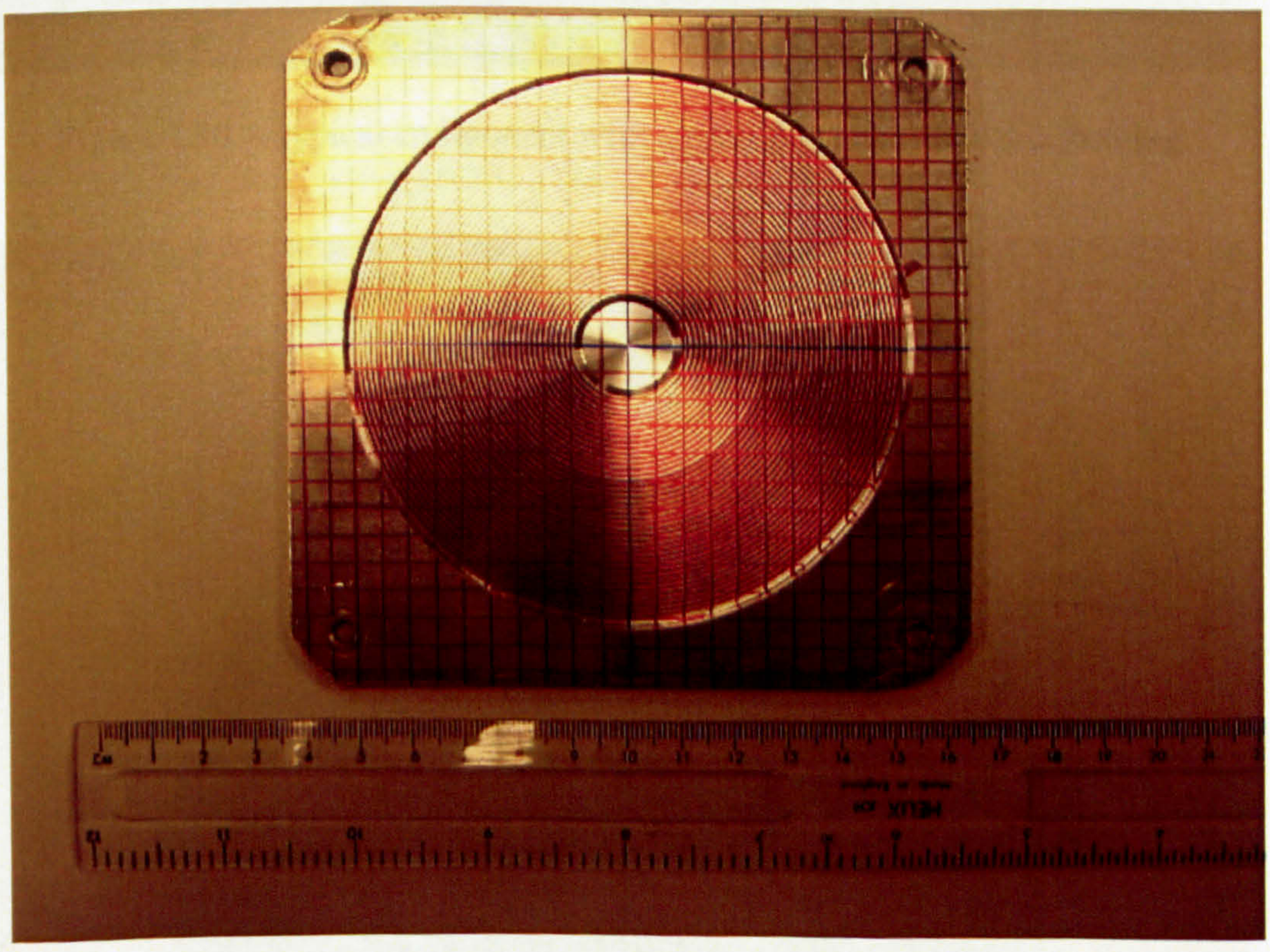

Figure 7.29 A machined blank with profiled shape

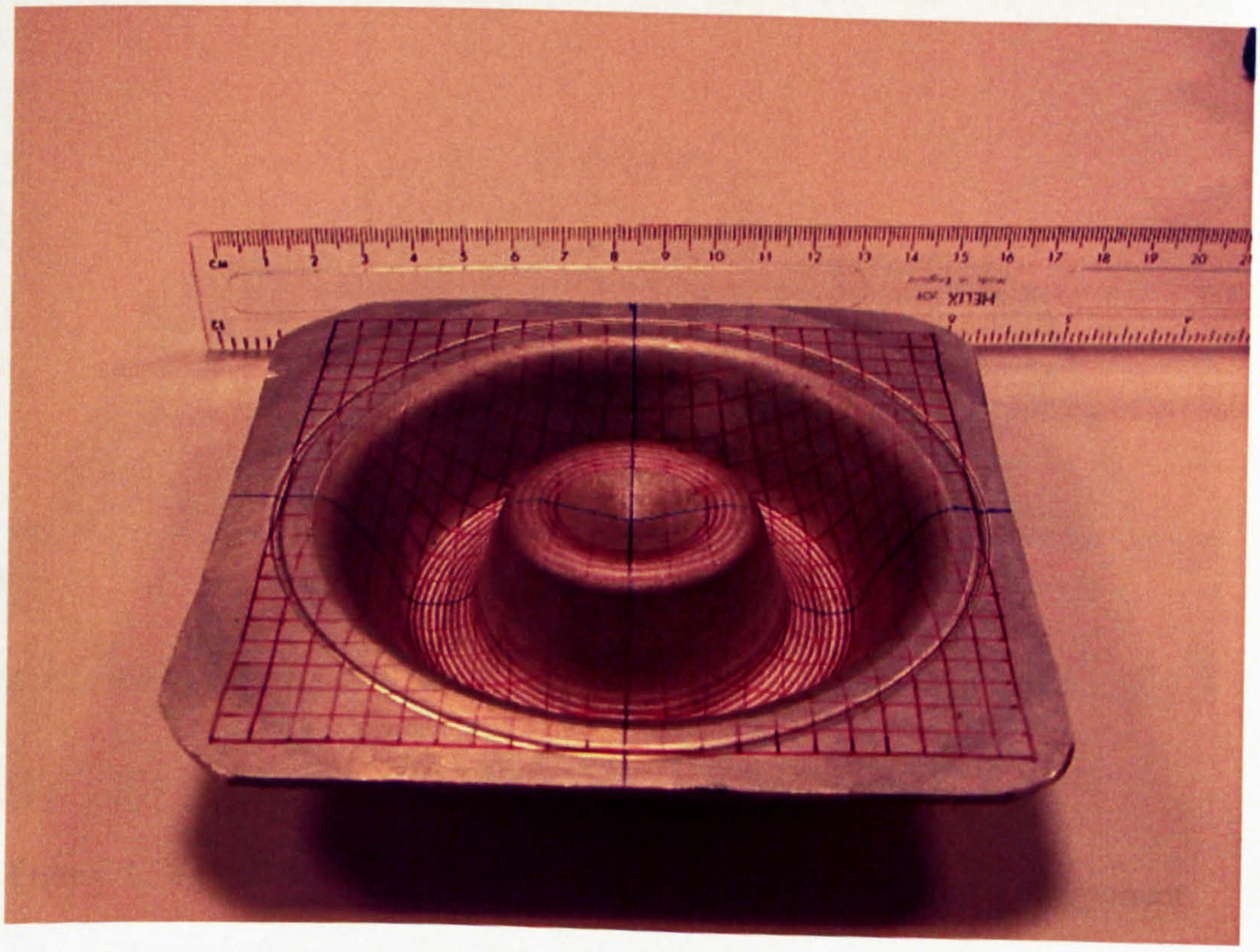

Figure 7.30 A typical component with a profiled shape after pre-forming

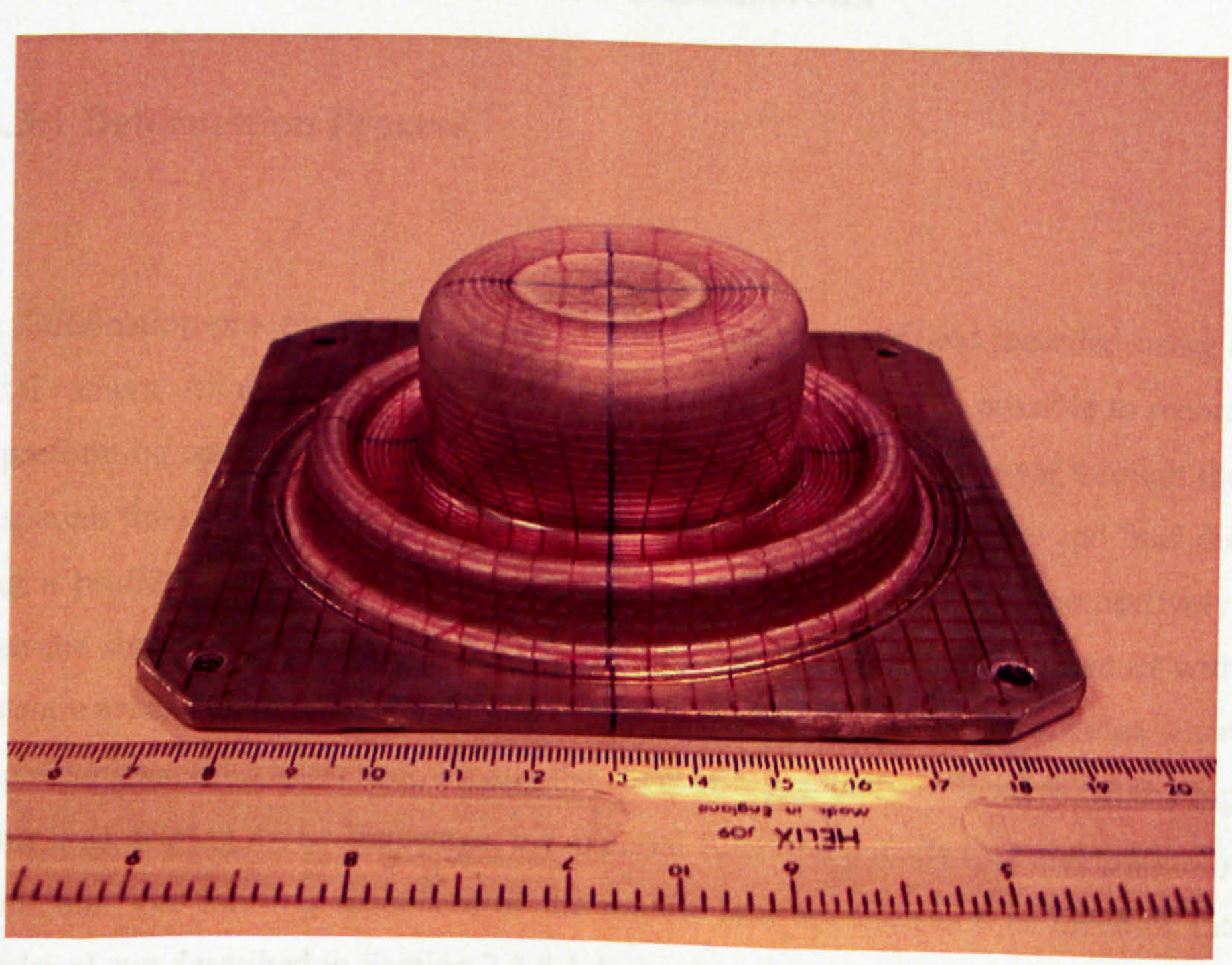

Figure 7.31 A typical component with a profiled shape after final forming

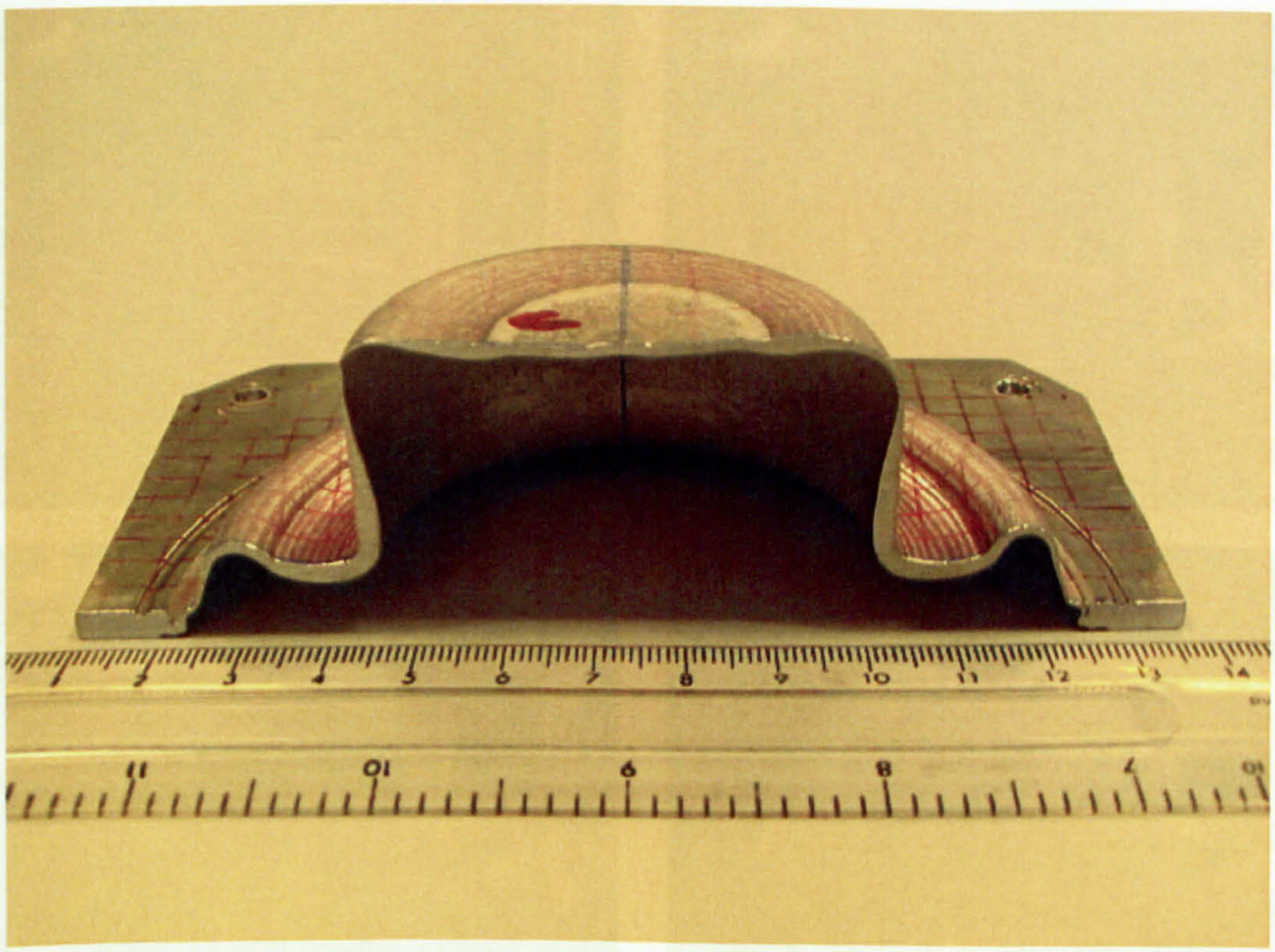

Figure 7.32 Final thickness distribution of a reverse blow formed component

7.4.3 Experimental Results and Discussions

7.4.3.1 Deformation Process

The deformation process of reverse forming has been observed and recorded using a digital camera. Although the preforming die is not transparent, it is possible to record the preforming operation by directing the camera lens to look at an angle through the transparent final die. Typical inflating sequences into the pre-forming die and final die using a profiled thickness sheet are shown in Figures 7.33 and 7.34 respectively. When the sheet was inflated into the pre-forming die, it first came into contact with the centre area, then touched the middle bending area which was the failure area when using a constant thickness sheet. Finally the sheet was gradually inflated to fill the big bubble area. During the second stage, the material filled the outside first and gradually the middle. The forming sequences of the middle part are the same as those of the cylindrical cup described in Section 7.3.4.1.1.

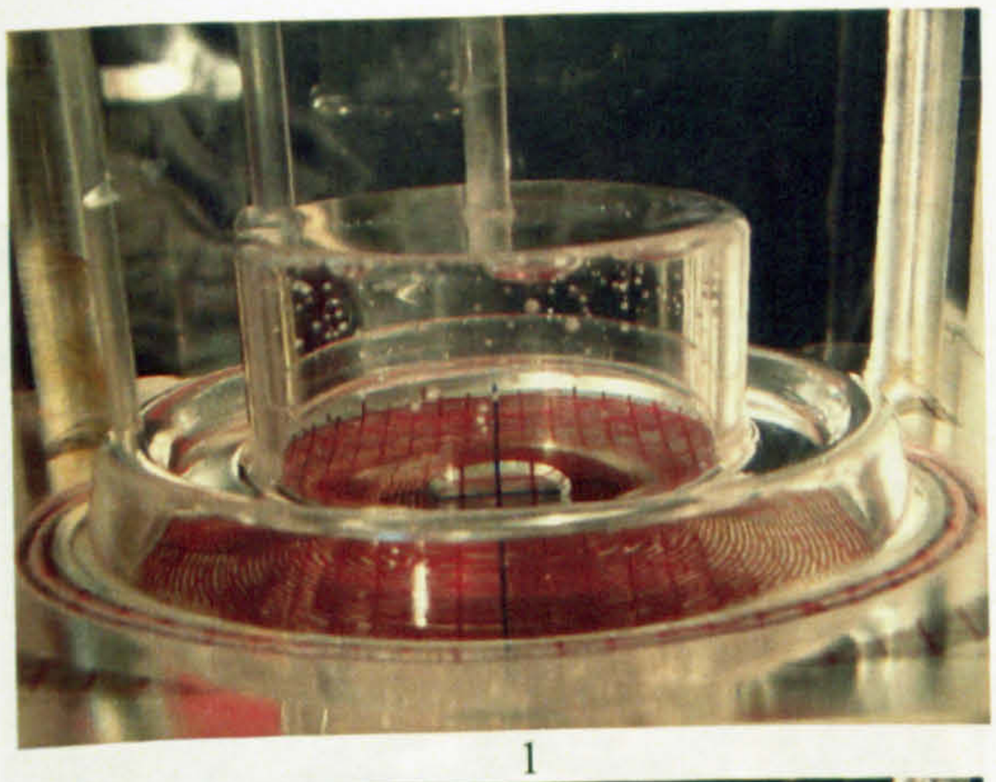

1

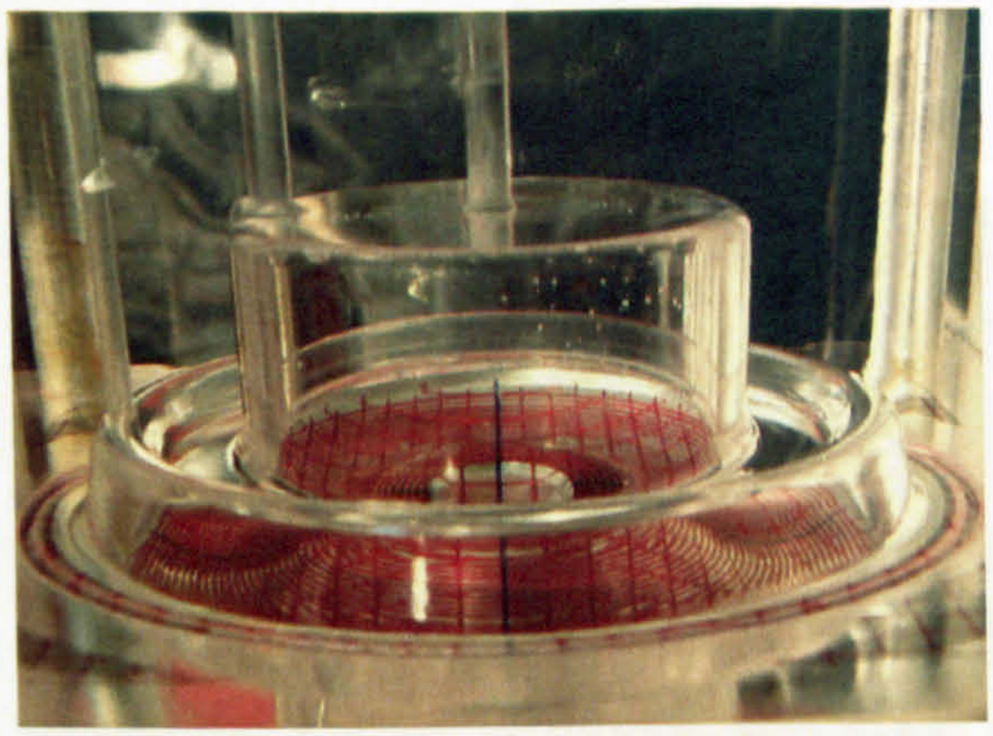

2

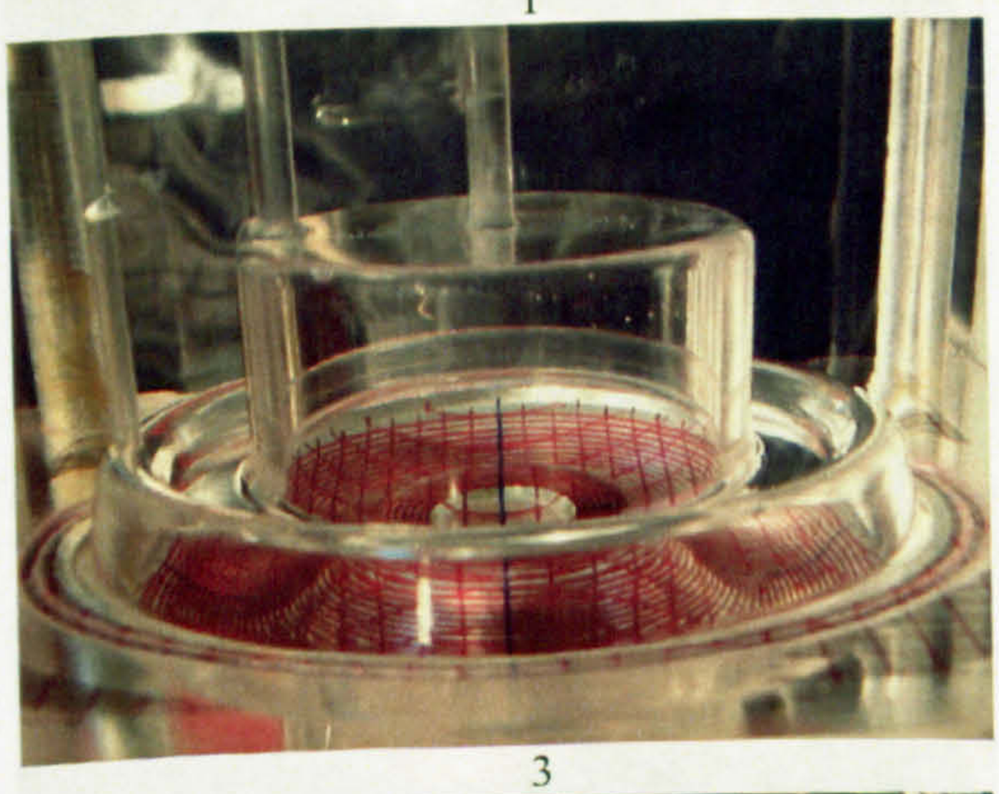

3

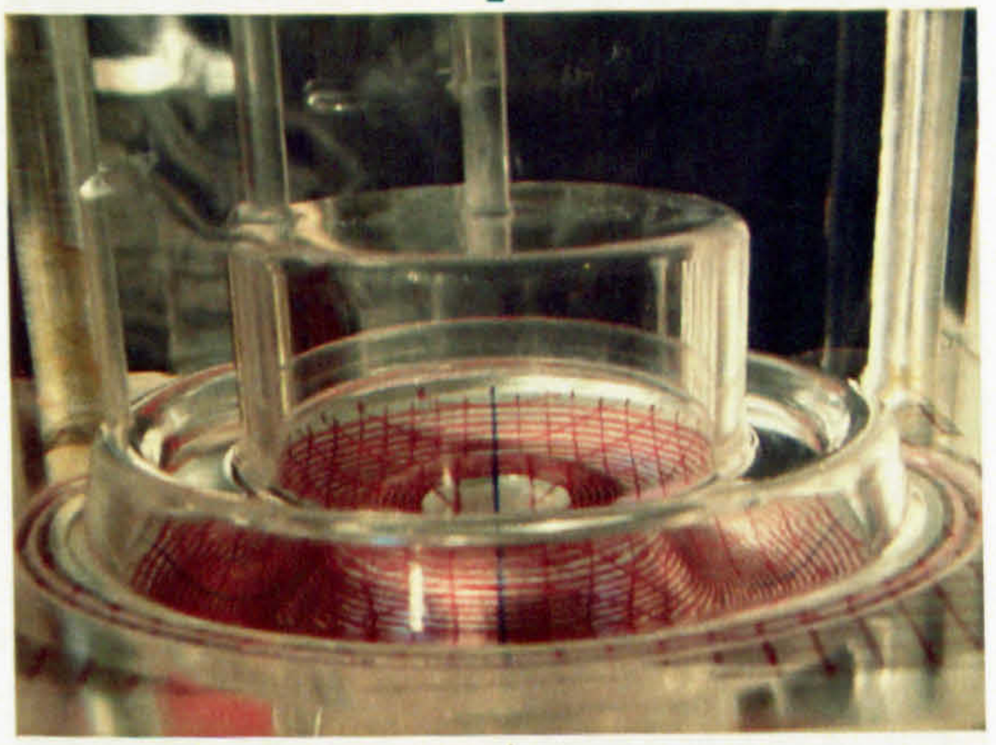

4

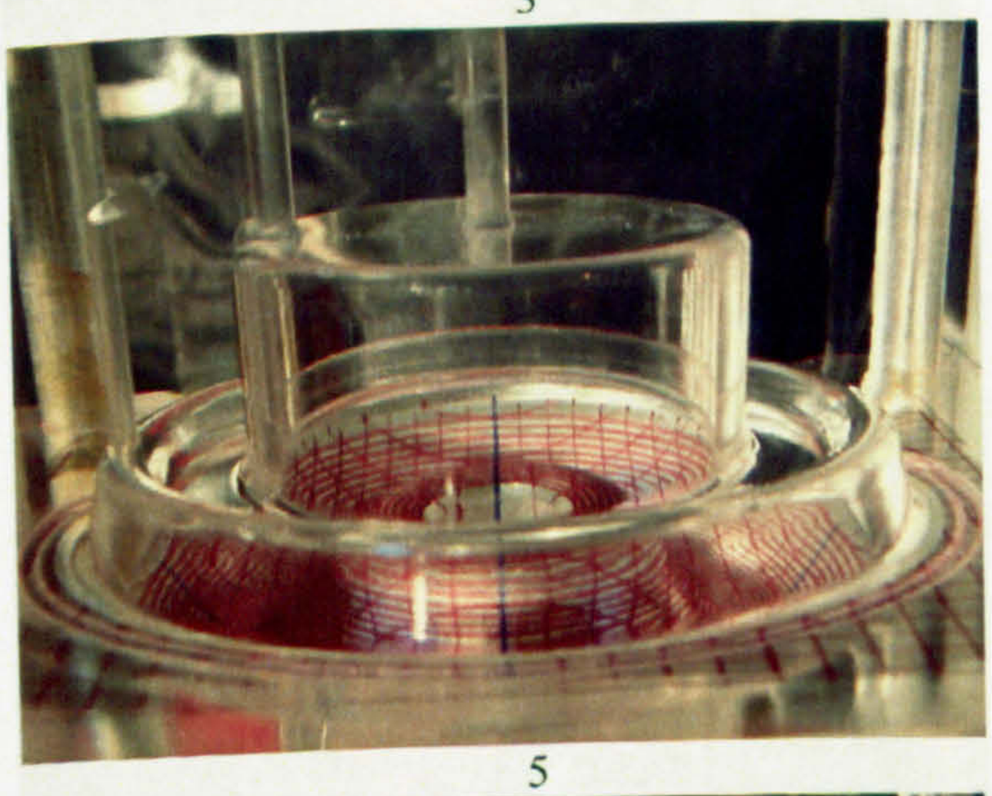

5

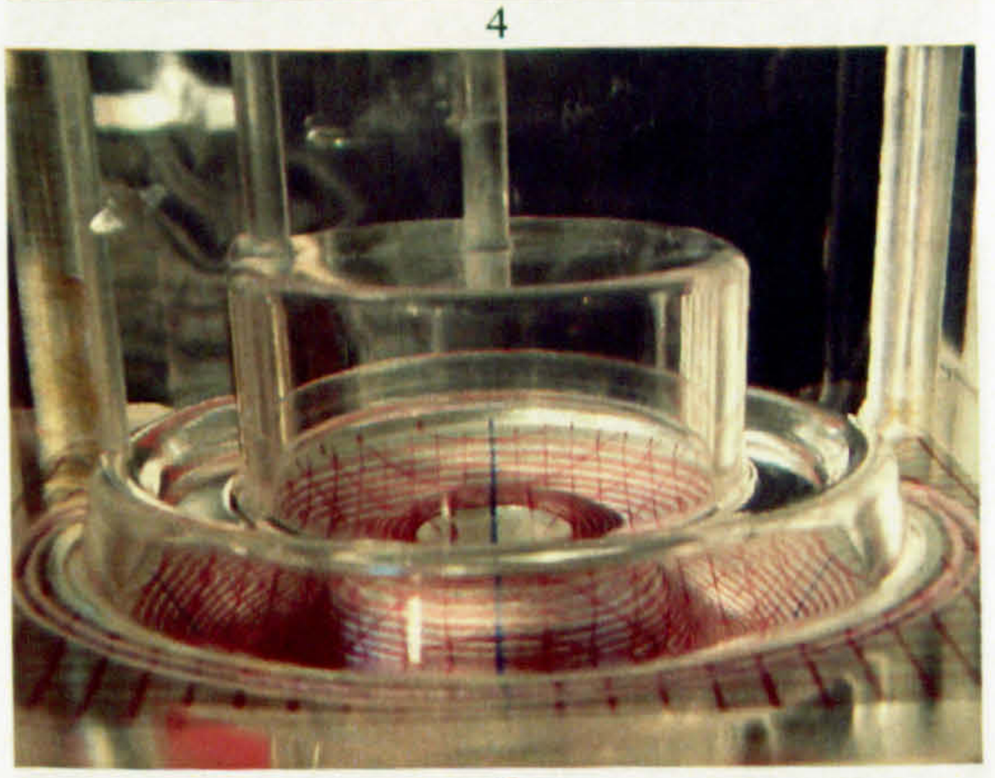

6

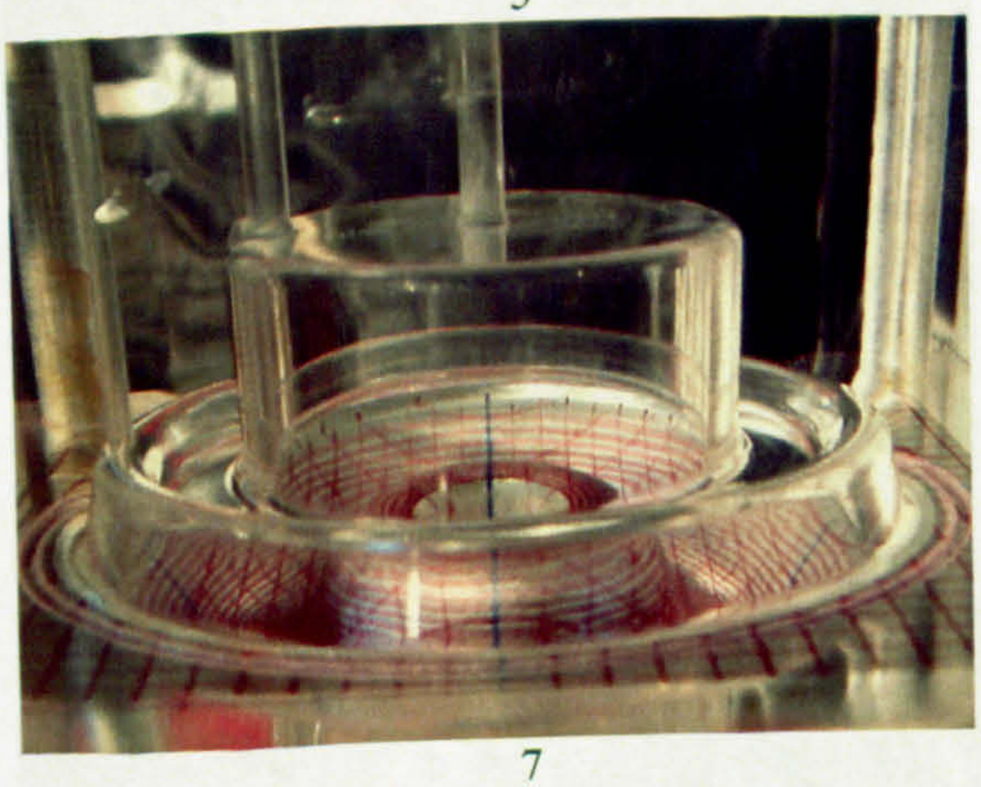

7

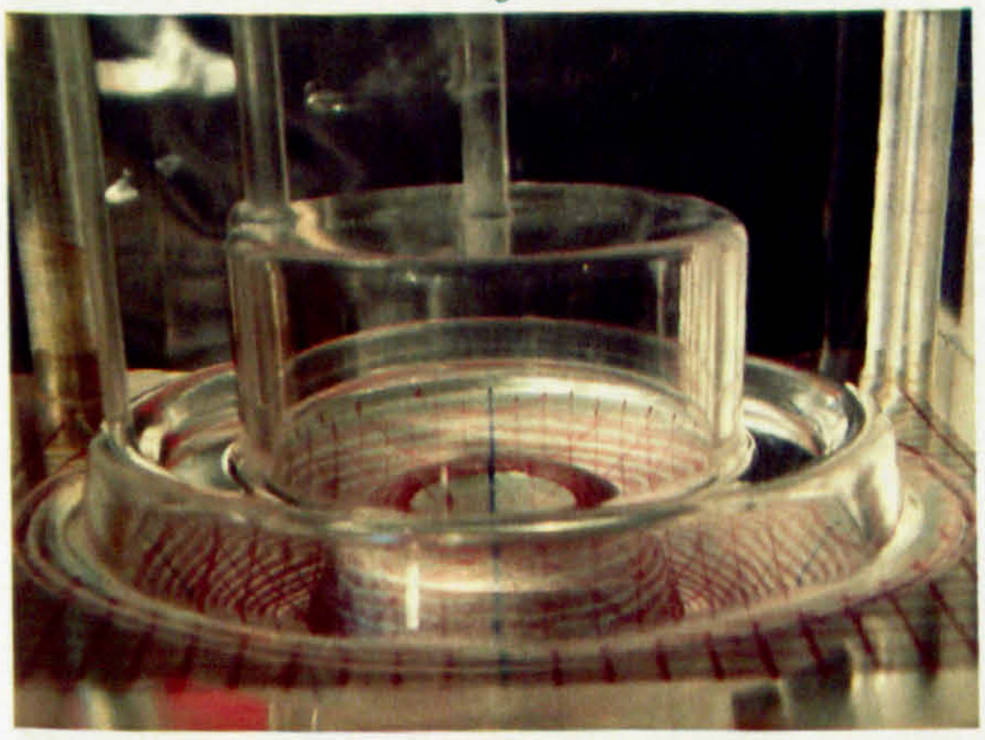

8

Figure 7.33 The forming sequences to the pre-forming die

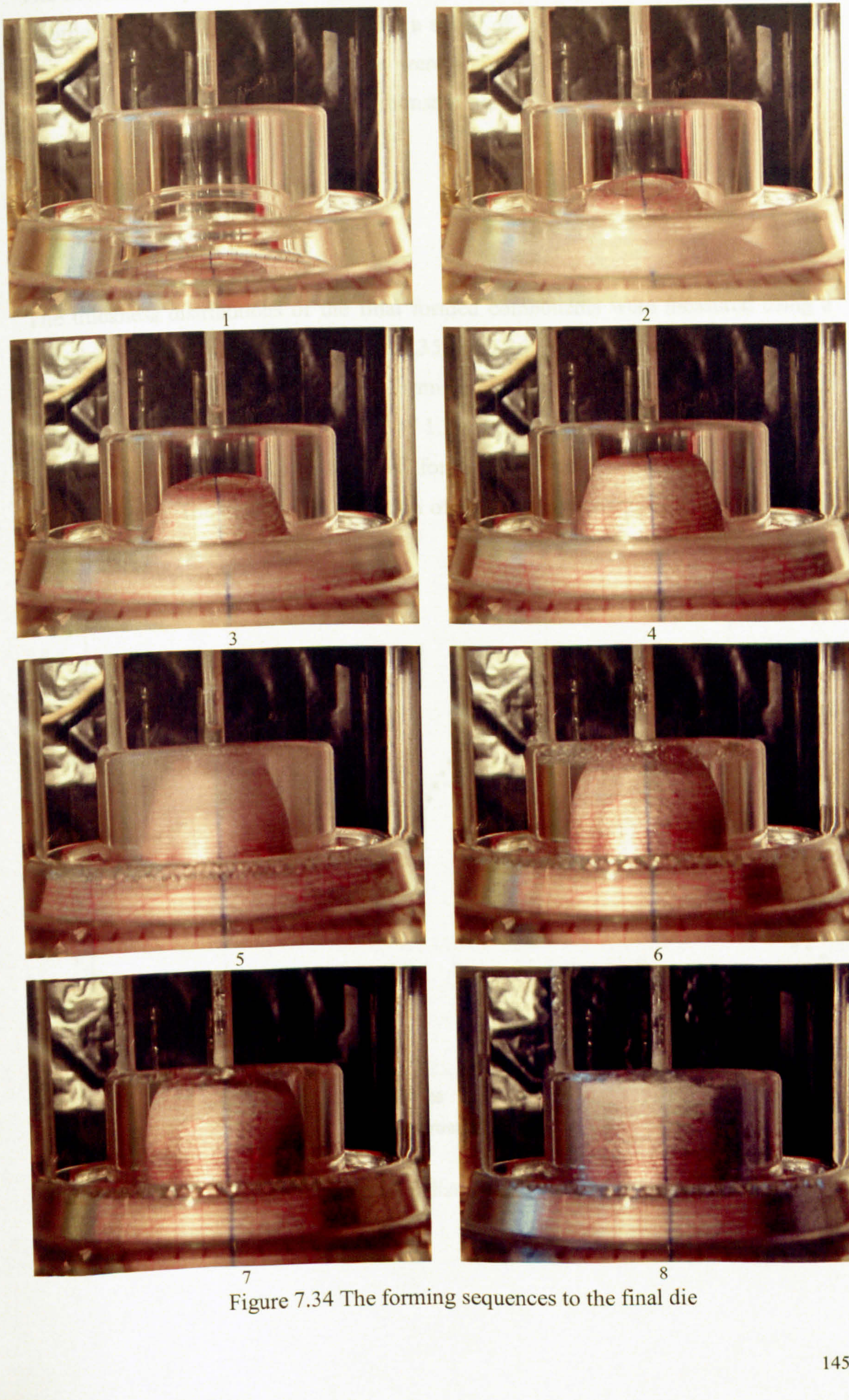

1 2 3 4 5 6 7 8

Figure 7.34 The forming sequences to the final die

The deformation process to the final die has also been recorded by a KODAK motion recorder analyzer (KODAK, 2000) with a speed of 1 frame per 20 seconds through the perspex die. The recorded images were analysed and an animation movie was created as shown in Appendix 4 for demonstration.

7.4.3.2 Thickness Distribution

The thickness distributions of the final formed components were measured using a coordinate measuring machine. Figures 7.35 and 7.36 show the thickness distributions along the axial direction of the pre-forming component and the final component respectively. The minimum thickness of 1.28 mm occurred at the top corner of the pre-forming process, while in the final forming process the minimum thickness is only 0.34 mm. The thickness distribution of the final component is much lower than that of the pre-formed component.

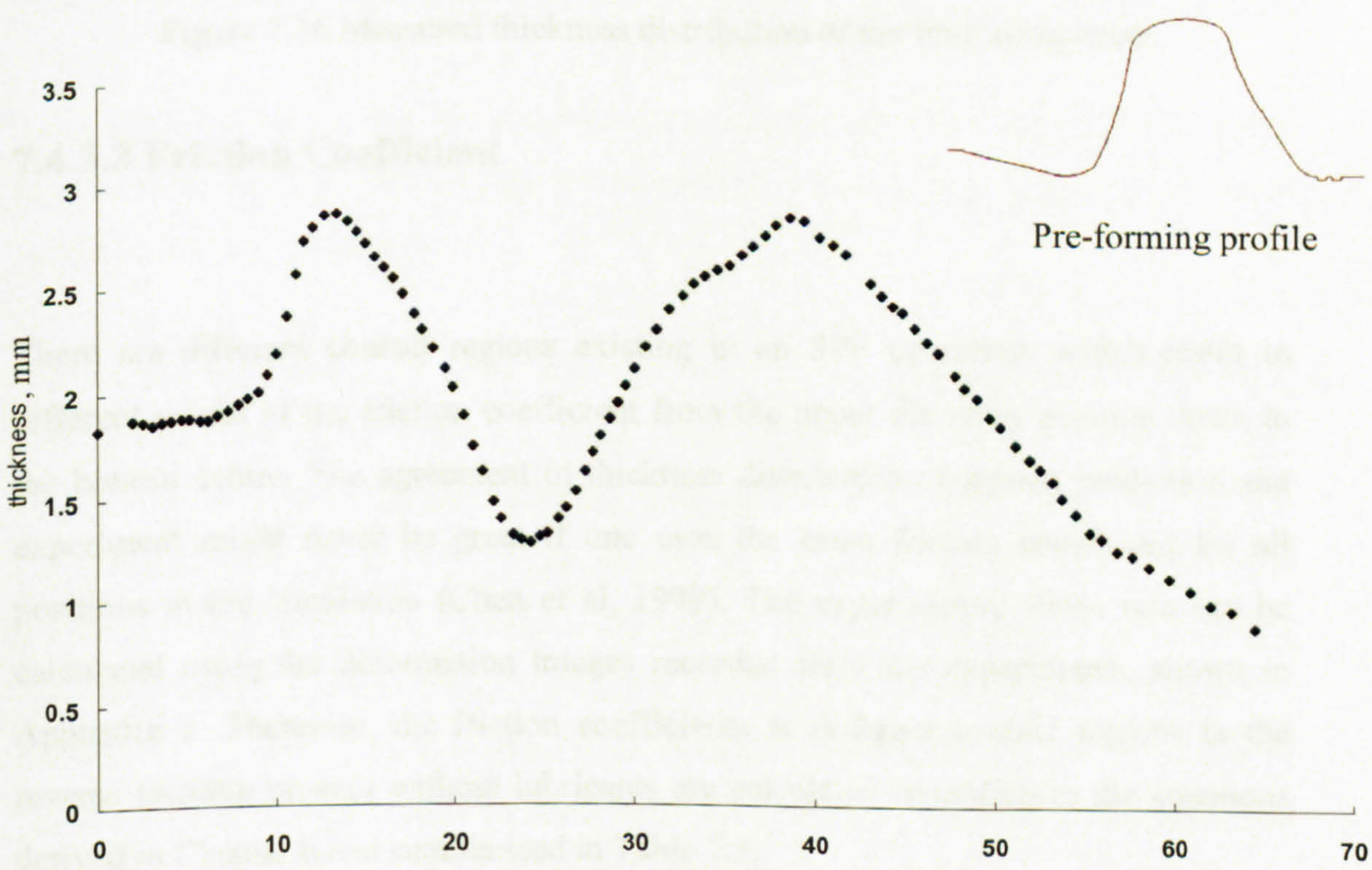

Figure 7.35 Measured thickness distribution of the pre-formed component

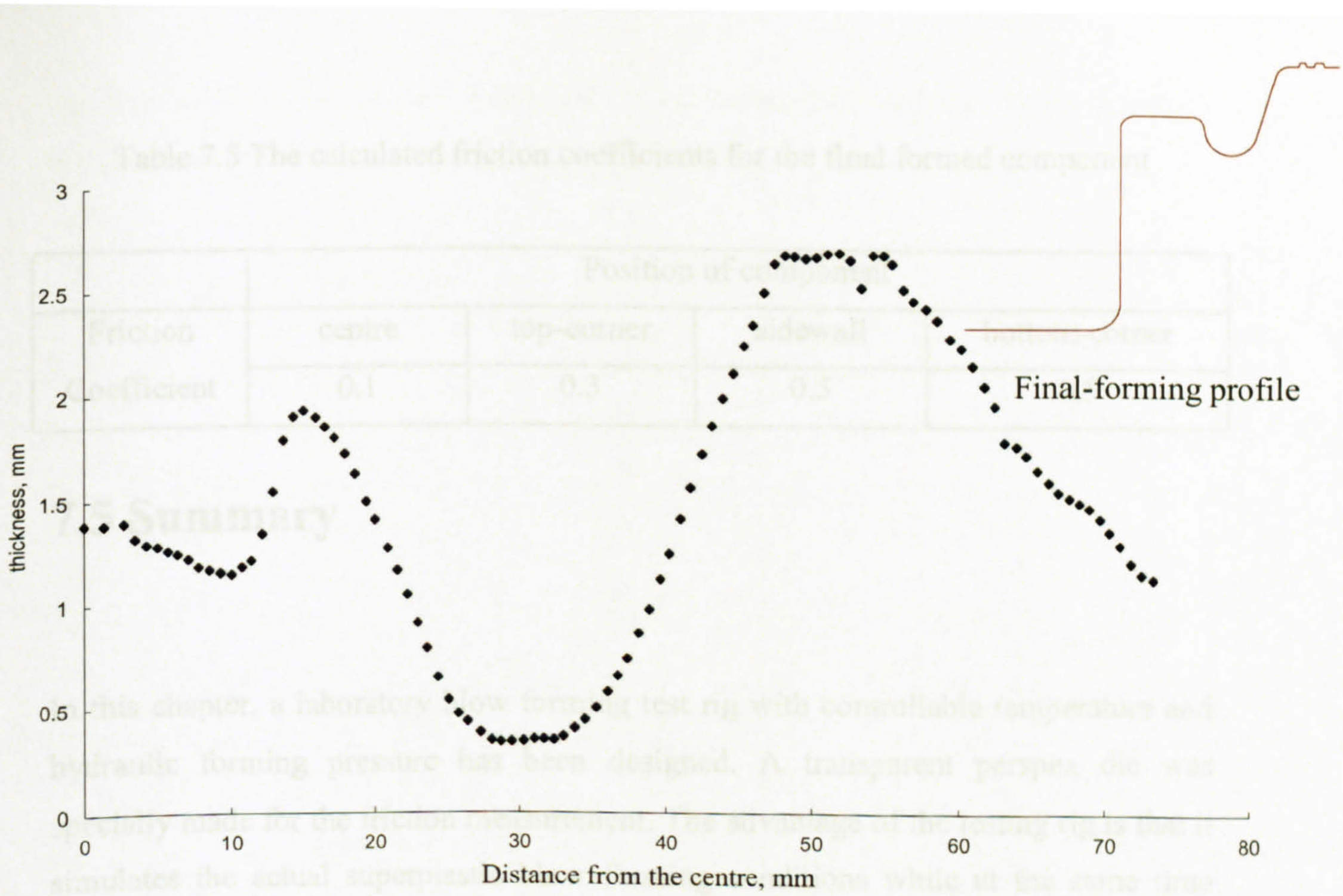

Figure 7.36 Measured thickness distribution of the final component

7.4.3.3 Friction Coefficient

There are different contact regions existing in an SPF operation, which result in different values of the friction coefficient from the upper die entry position down to the bottom centre. The agreement in thickness distributions between prediction and experiment might never be great if one uses the same friction coefficient for all positions in the simulation (Chen et al, 1999). The experimental strain rate can be calculated using the deformation images recorded from the experiments, shown in Appendix 3. Therefore, the friction coefficients at different contact regions in the reverse forming process without lubricants are calculated according to the equations derived in Chapter 6 and summarised in Table 7.5.

Table 7.5 The calculated friction coefficients for the final formed component

	Position of component			
Friction Coefficient	centre	top-corner	sidewall	bottom-corner
	0.1	0.3	0.5	0.5

7.5 Summary

In this chapter, a laboratory blow forming test rig with controllable temperature and hydraulic forming pressure has been designed. A transparent perspex die was specially made for the friction measurement. The advantage of the testing rig is that it simulates the actual superplastic blow forming conditions while at the same time provides a possibility to measure the frictional behaviour at different contact regions.

Tensile testing shows that the superplastic properties of Pb-Sn alloy have a strong relation with the applied strain rate and temperature. Elongations of up to 830% were achieved in the experiments.

Blow forming experiments using uniform Pb-Sn alloys, 2 ± 0.02 mm in thickness, into simple cylindrical cups were first conducted under various pressures and temperatures. Further reverse forming experiments of Pb-Sn alloy sheets into complicated components were carried out. In particular, sheets of uniform thickness and profiled thickness were used. It was found that the proposed reverse forming experiments have to employ sheets with profiled thickness. With the profiled sheet the thickness variation of the component has been largely minimized and successfully reverse formed components were obtained. The deformation process and thickness distributions were investigated in both experiments and the friction coefficients at different contact regions were calculated. The calculated friction coefficients will be input into the validated finite element model as developed in Chapter 5. The reliability and accuracy of the proposed experimental methodology for the calculation of friction

coefficients will be further validated by a comparison of the final thickness distributions both from experiment and simulation.

Chapter 8

Interpretation of Experimental Results

8.1 Introduction

The main objective of this chapter is to verify the proposed experimental methodology and evaluate the reliability and accuracy of the friction coefficient measurements by means of finite element simulation.

The simulation of the SPF steps, utilising the finite element method, has gained increasing importance for component and process design. Simulation serves to examine production feasibility, to analyse and optimise the final component quality and expected process reliability. A finite element model has been developed and validated by experiments (Kim et al, 1996), as described in Chapter 5, for the simulation of the superplastic forming process. Therefore, the whole experimental process of forming Pb-Sn sheets into the cylindrical cup and the complicated component described in Chapter 7 can be simulated by incorporating the experimentally derived friction coefficients, at different contact regions, with the material parameters measured from the tensile tests, into the validated finite element model.

The final components will thin locally as they experience a large amount of deformation during the superplastic forming process. Thinning will be non-uniform throughout the component, and will depend mainly on local friction features as well as on material properties. Thus for a given material, accurate prediction of the final thickness distribution, of a formed component, depends on the accuracy of the input friction coefficients. As a result, a comparison of final thickness distributions from simulation and experiment can be an indicator to verify the reliability and accuracy of

the calculated friction coefficients and the experimental methodology proposed in Chapter 7.

8.2 Comparison between Simulations and Experiments

The blow forming experiments of a cylindrical cup and a reverse formed component, carried out in Chapter 7, have been modelled using the finite element method in order to verify the accuracy of the friction coefficient measurements. All parameters in the simulation including the geometries of the sheet and the dies, the material properties from tensile tests, the calculated friction coefficients, the applied forming pressure and temperature are the same as those in the experiments. Multiple loading steps were employed in the simulation to model the different forming stages in the reverse blow forming process. Comparisons between simulations and experiments have been conducted in terms of the deforming process and the final thickness distributions.

8.2.1 Blow Forming of a Cylindrical Cup

The modelled cylindrical cup is shown in Figure 7.10. An axis symmetric cross section of the dies and the sheet assembly was modelled. The four-node reduced integration axisymmetric quadrilateral continuum element (CAX4R) was employed according to the element study presented in Section 5.2.2. A uniform sheet of 2.0 mm thickness was used in the blow forming experiments of a cylindrical cup and therefore was modelled in the simulation with periphery clamped between the forming dies. The contact and friction algorithms as described in Section 5.2.1.3, were employed using the friction coefficients calculated in Section 7.3.4.2. As constant forming pressures were applied in the experiments, a constant loading scheme was applied in the simulation, with magnitudes taken from experiments. Forming temperatures used in the experiments were also fed into the finite element model for an accurate simulation of the superplastic blow forming process.

8.2.1.1 Deformation Process

A typical predicted sequence of deformation during various stages of forming is shown in Figure 8.1, which is in good agreement with the experimental deformation process as shown in Figure 7.15. In both forming sequences, contact occurs first at the die entry area and the sheet will gradually stretch and slide over the die surface. The following stages of the deformation, corresponding to the inflation of the sheet into the top centre, the side wall and the final die corner are well matched between the simulation and experiment.

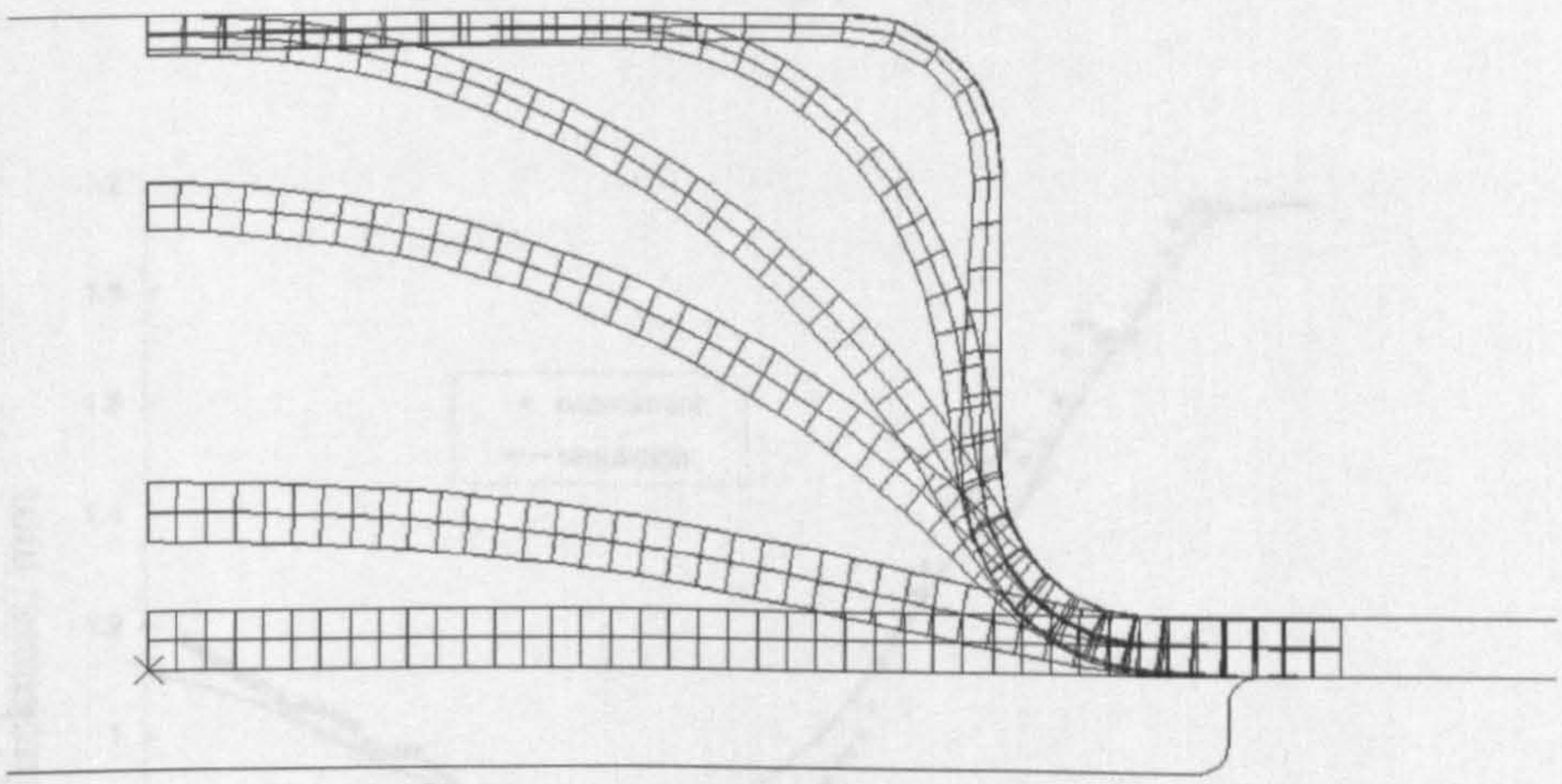

Figure 8.1 Predicted deformation process of a cylindrical cup

8.2.1.2 Thickness Distribution

Figures 8.2 to 8.7 give comparisons of the thickness distributions of the final components obtained from simulations and experiments for the forming of cylindrical cup. The pressure and temperature used in each simulation were taken from the test conditions shown in Table 7.4. At each contact area the values of the friction coefficient were taken from the corresponding experimental results (see Figure 7.19, Figure 7.21). The comparisons demonstrate that the thickness distributions predicted from simulations are in reasonable agreement with the experimental measurements

with the maximum deviation less than 30%. The overall thinning trends of the thickness distribution from both simulation and experiment are very similar. The lowest section thickness is located at the corner of the upper die, while the thicknesses at the edge and at the centre of the upper die are relatively greater than those at other areas. Discrepancies between the experimental and predicted thickness distribution, may be attributed to the idealised assumptions made in the simulation and some experimental errors in the experiments. For example, small but non-negligible errors remained in the preparation of the initial sheet which was not perfectly uniform and was limited by the manufacturing equipment. However, the comparisons in terms of thickness distributions of the final components demonstrated that, the proposed experimental devices and methodology are capable of obtaining an estimate of the friction coefficient in the superplastic forming process.

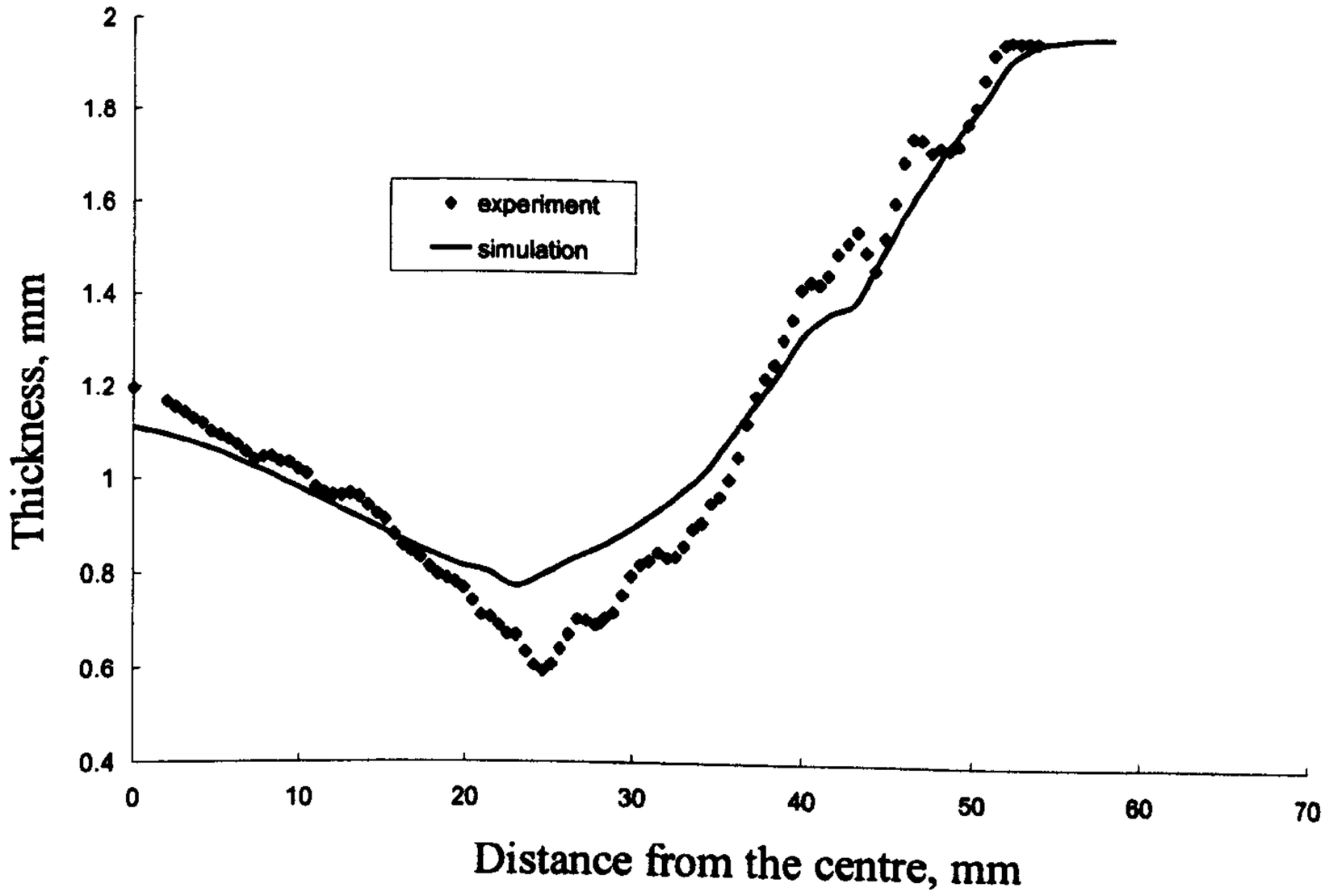

Figure 8.2 Thickness distribution comparisons between experiment and simulation (P=360KPa, T=80°C, Blow forming a cylindrical cup)

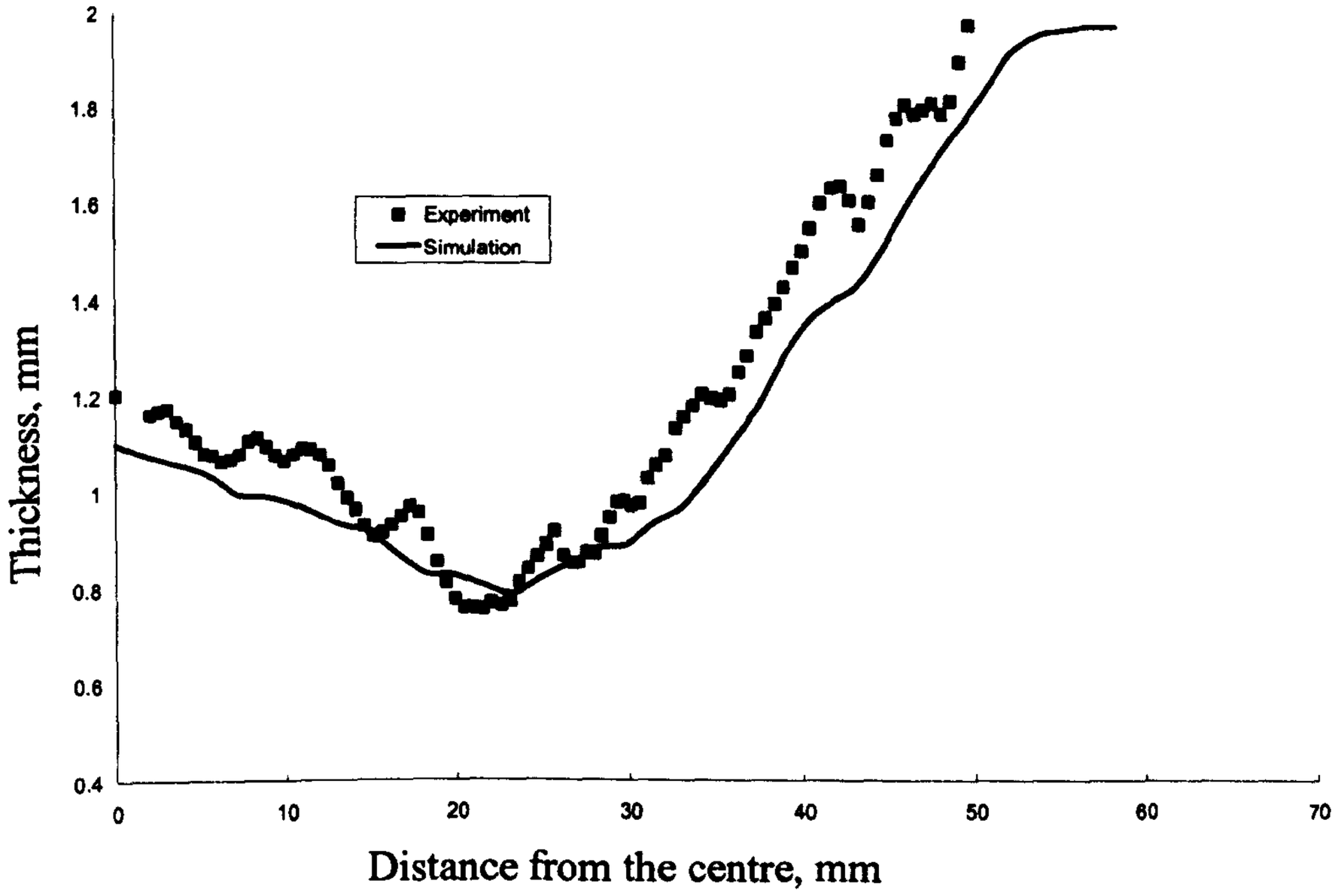

Figure 8.3 Thickness distribution comparison between experiment and simulation (P=300KPa, T=80^{0}C, Blow forming a cylindrical cup)

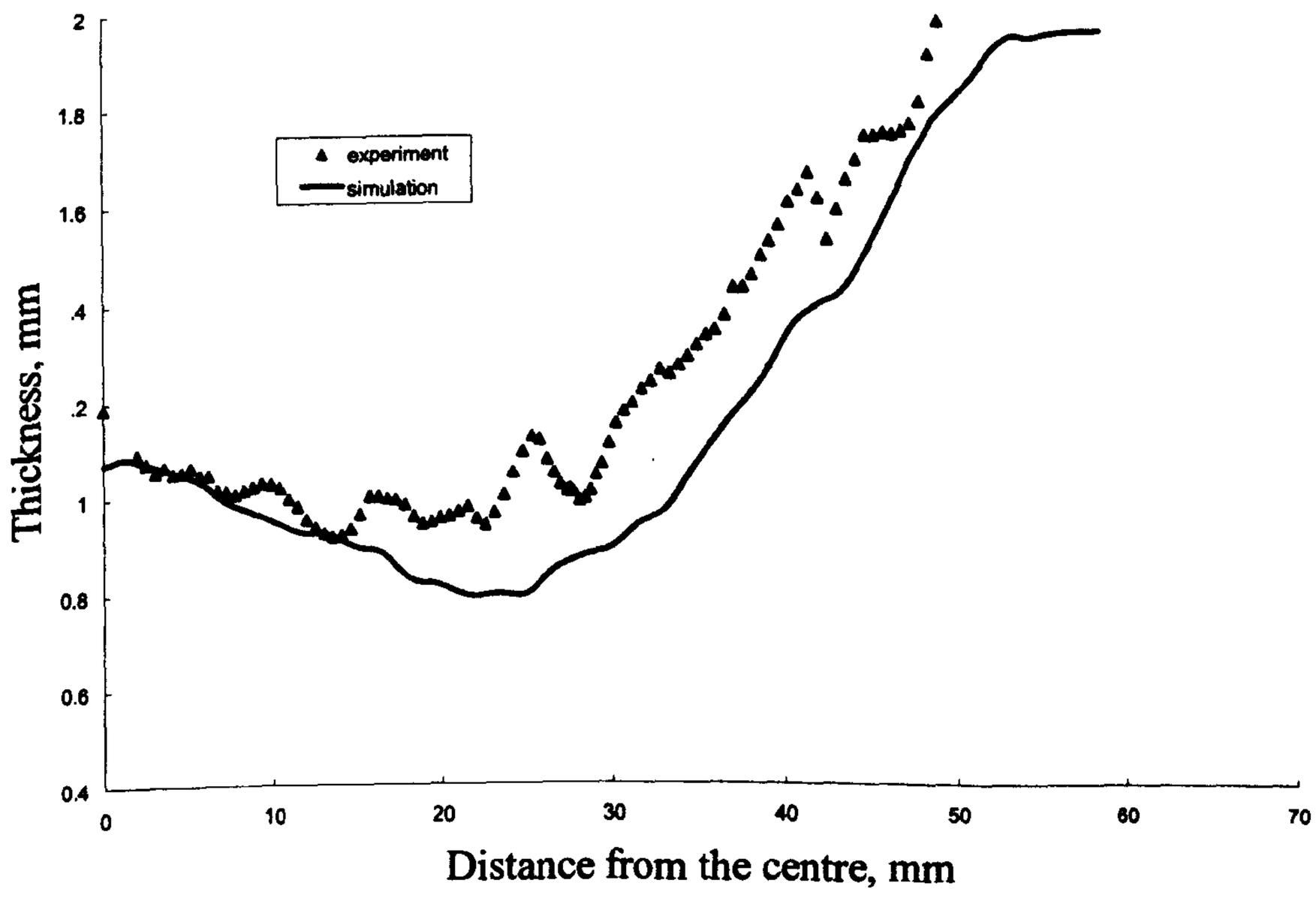

Figure 8.4 Thickness distribution comparison between experiment and simulation (P=250KPa, T=80^{0}C, Blow forming a cylindrical cup)

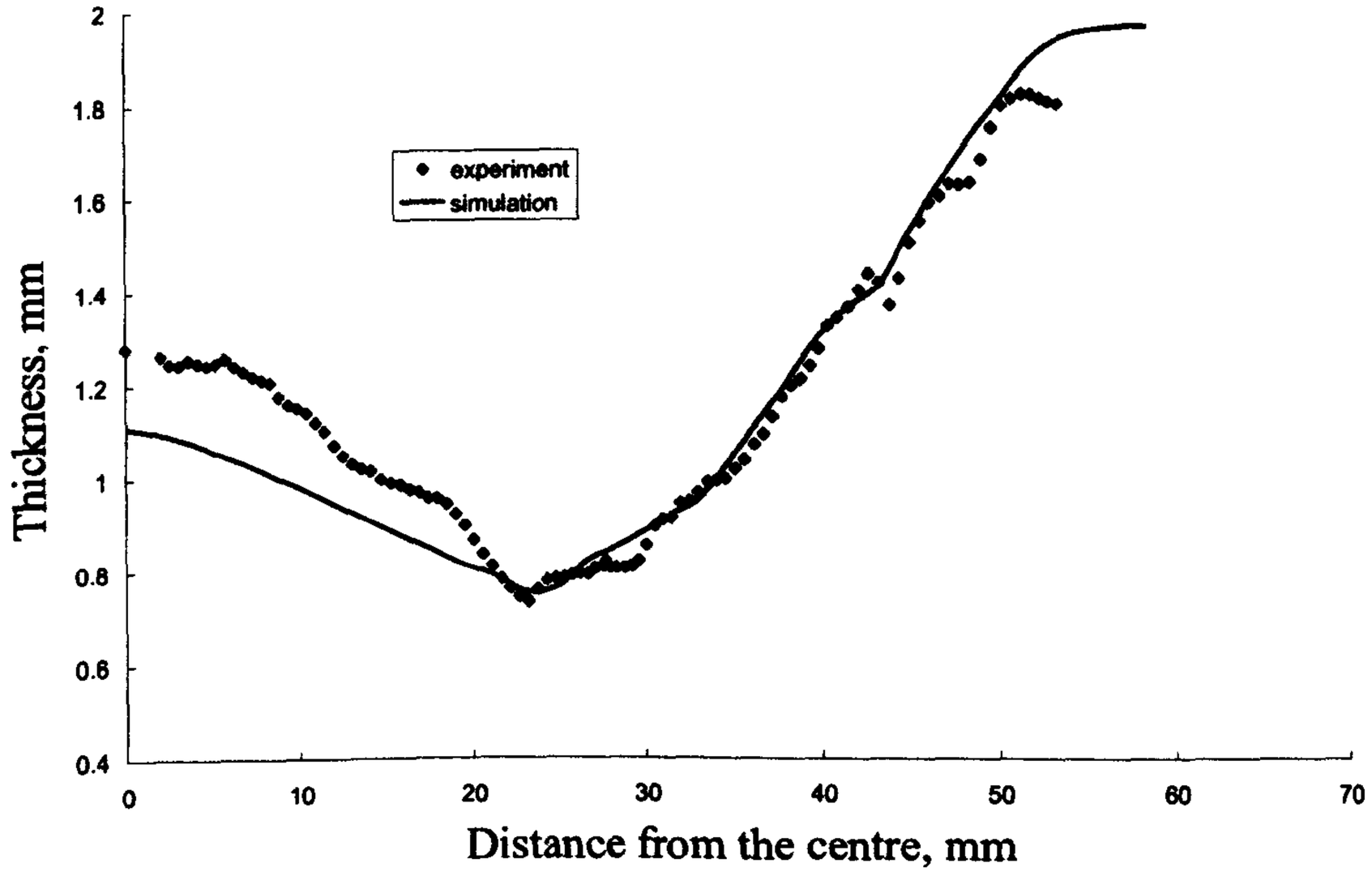

Figure 8.5 Thickness distribution comparison between experiment and simulation (P=200KPa, T=80^{0}C, Blow forming a cylindrical cup)

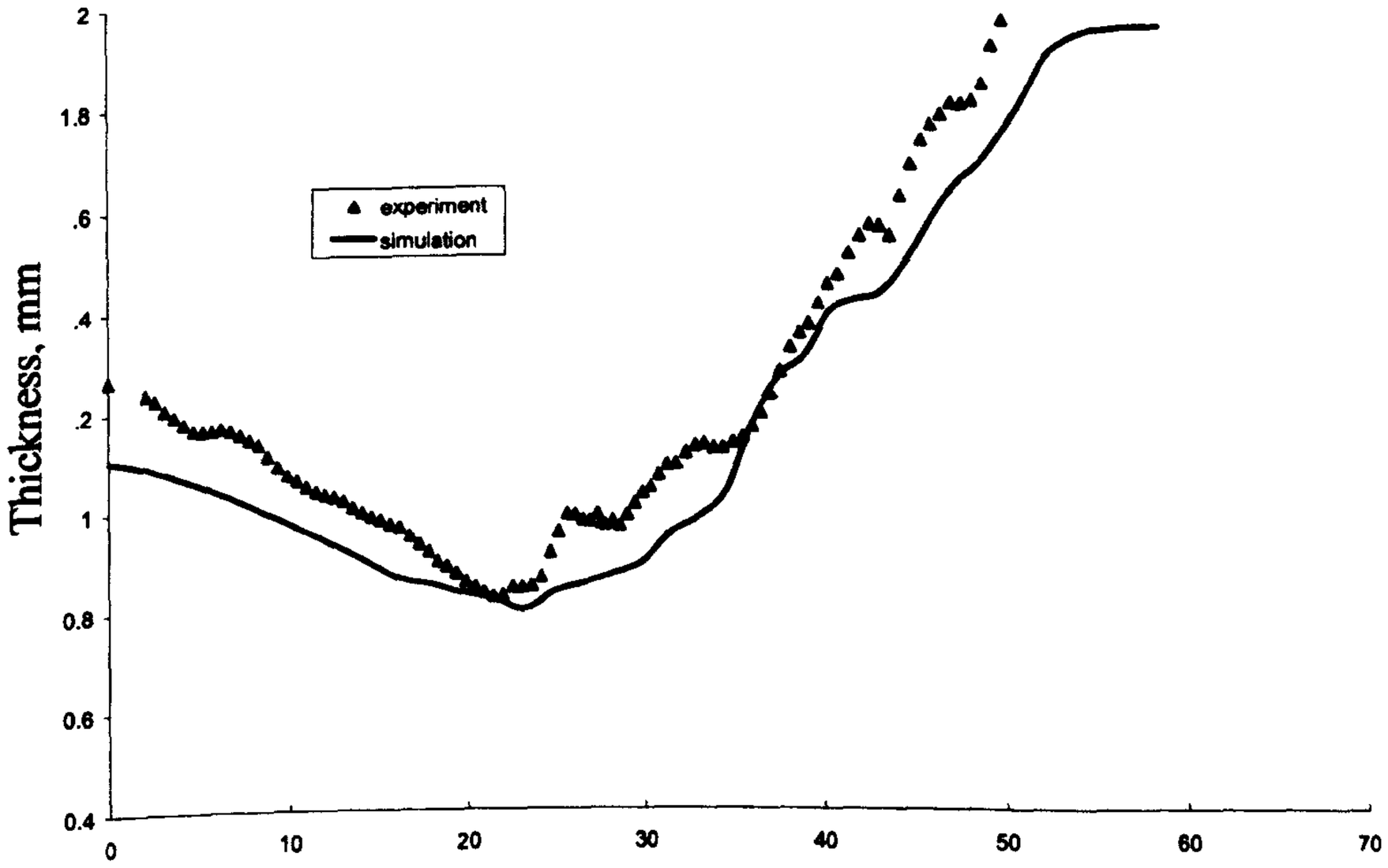

Figure 8.6 Thickness distribution comparison between experiment and simulation (P=360KPa, T=70^{0}C, Blow forming a cylindrical cup)

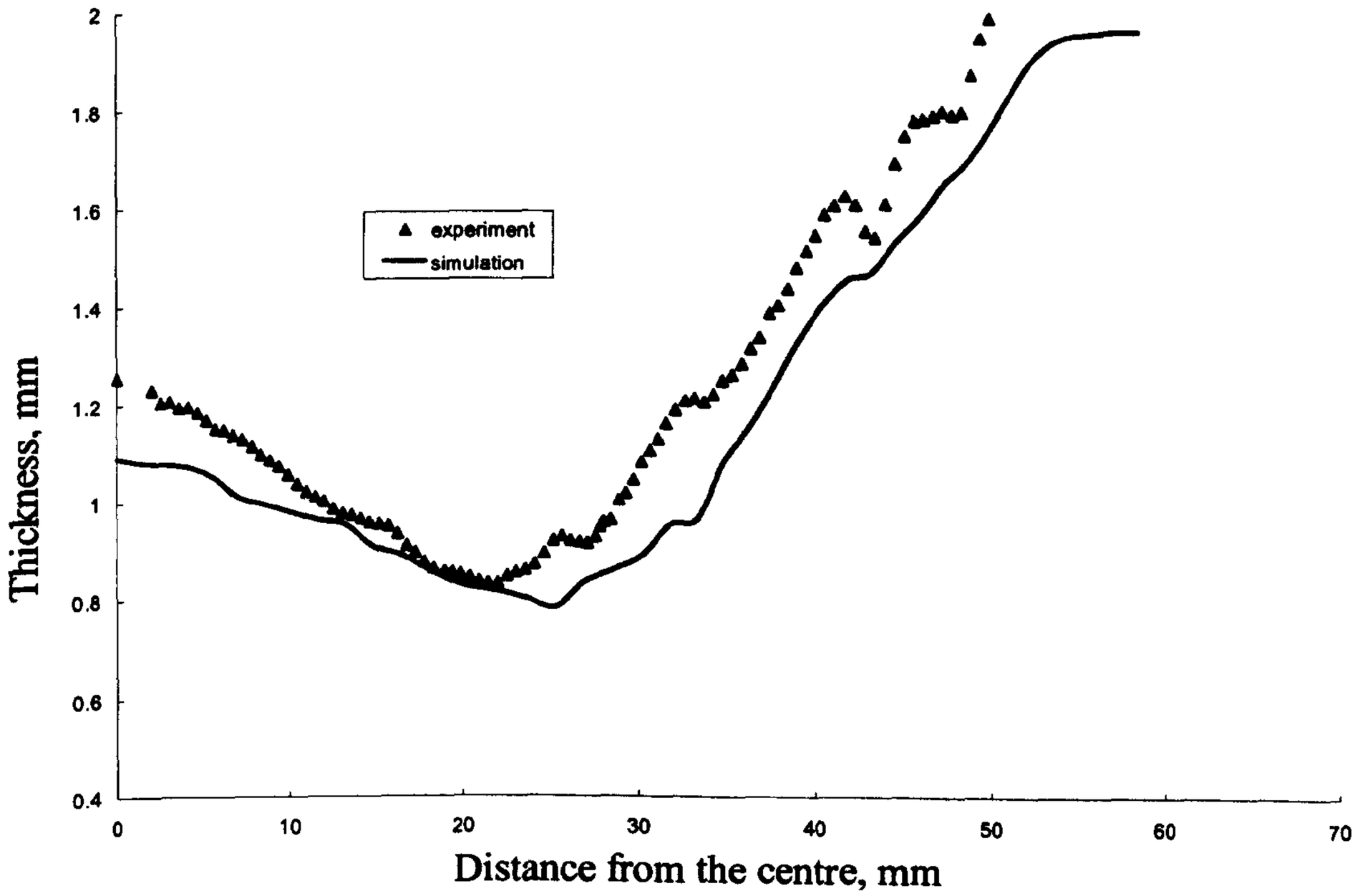

Figure 8.7 Thickness distribution comparison between experiment and simulation (P=360KPa, T=60^{0}C, Blow forming a cylindrical cup)

8.2.2 Reverse Blow Forming of a Complicated Component

The reverse blow forming of a complicated component from a Pb-Sn alloy sheet, as shown in Figure 7.23, was simulated using the calculated friction coefficients (see Table 7.5). A section of the whole assembly of the dies and the sheet was modelled because of symmetry. Modelling techniques as described in Section 8.2.1 were applied. A constant forming pressure of 360 kPa was implemented in all reverse forming simulations in accordance with the experiments. Both uniform and profiled thickness sheets, which were used in the reverse forming experiments, were modelled in the simulation to verify the advantages with a profiled thickness sheet.

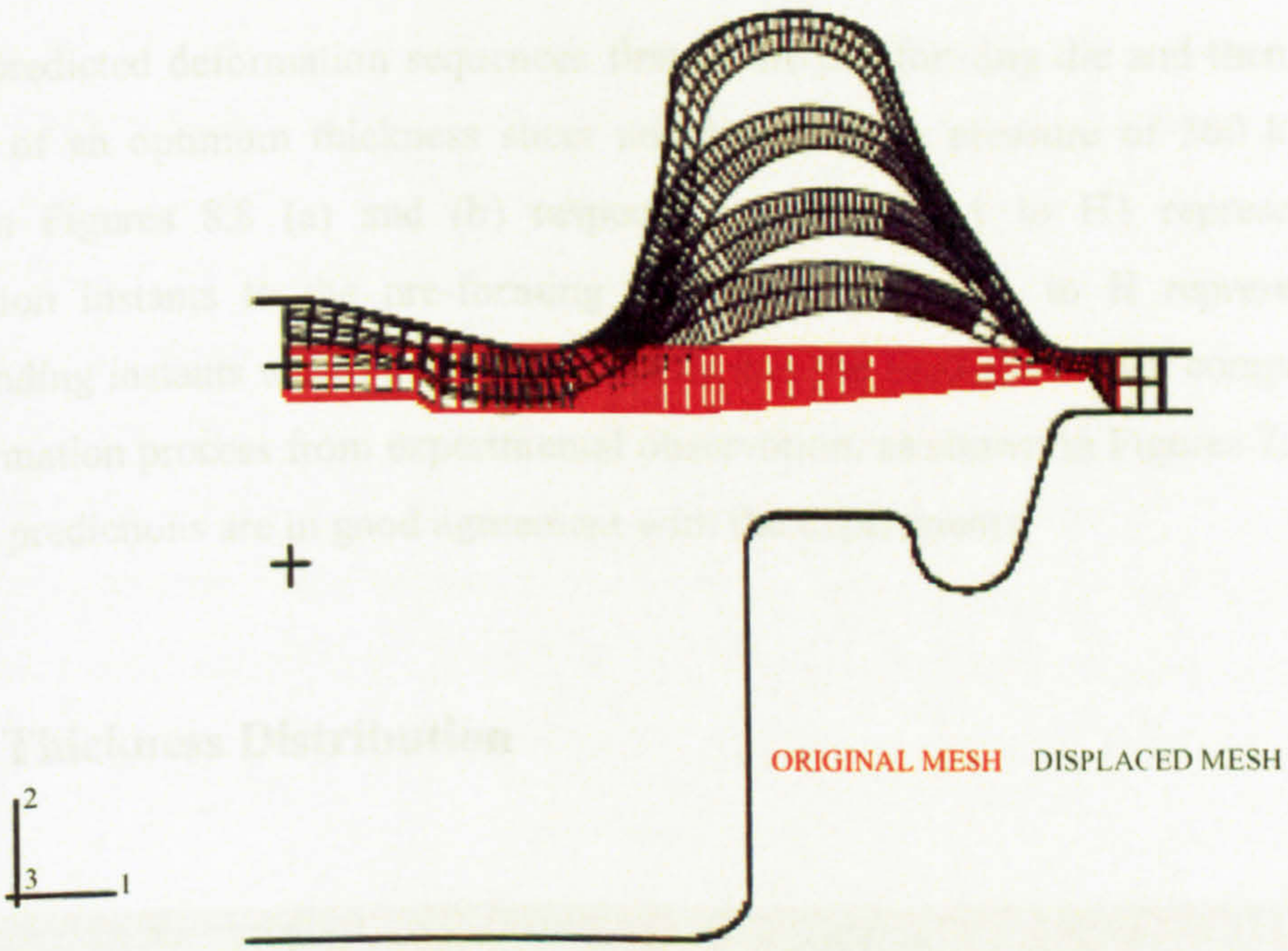

(a) Simulation sequence to the pre-forming die

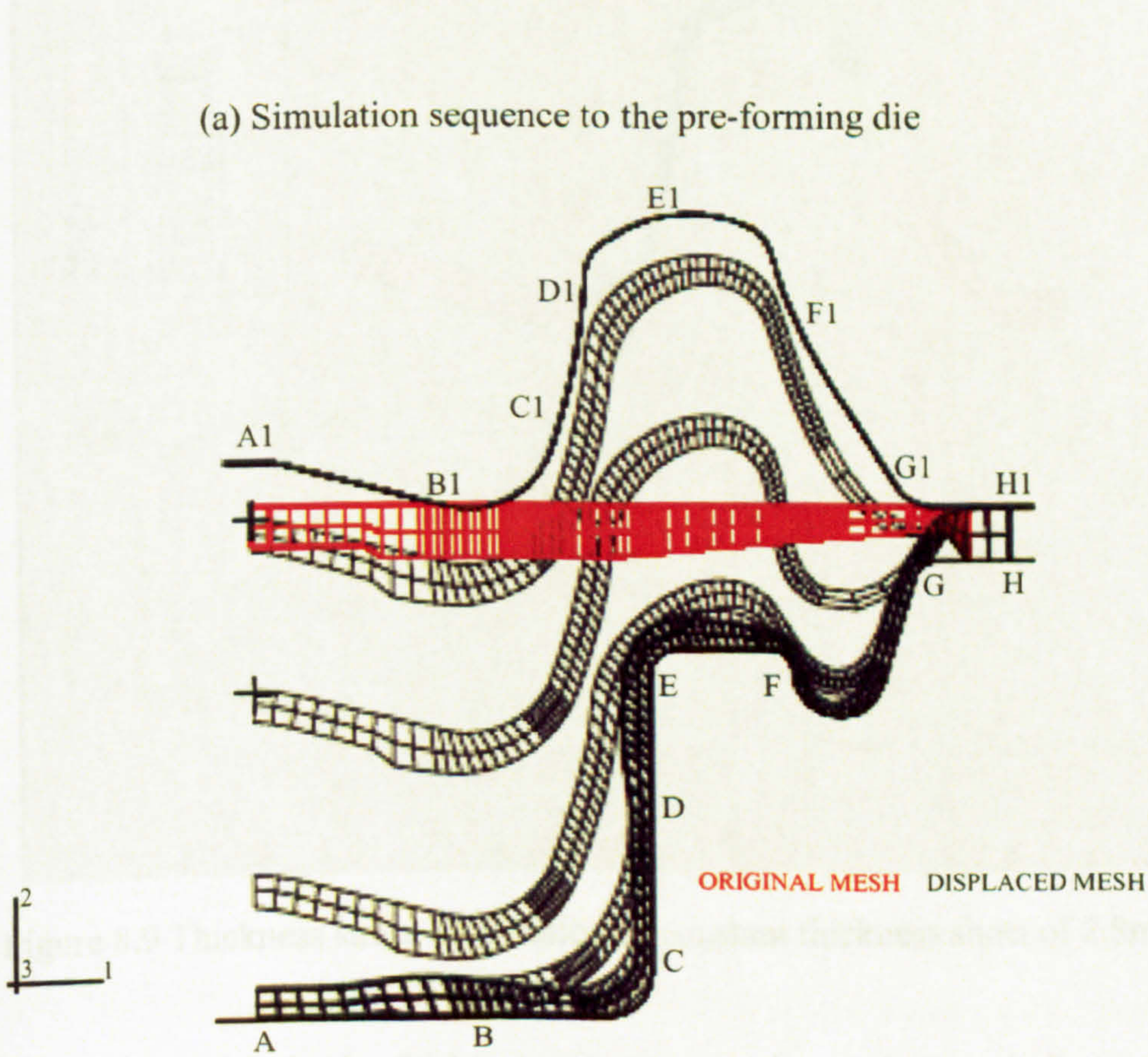

(b) Simulation sequence to the final die

Figure 8.8 Deformation process of reverse forming from simulation

8.2.2.1 Deformation Process

Typical predicted deformation sequences first to the pre-forming die and then to the final die of an optimum thickness sheet under a forming pressure of 360 kPa are shown in Figures 8.8 (a) and (b) respectively. Points A1 to H1 represent the deformation instants to the pre-forming die whilst points A to H represent the corresponding instants where the material flows into the final-die. When compared to the deformation process from experimental observation, as shown in Figures 7.33 and 7.34, the predictions are in good agreement with the experiments.

8.2.2.2 Thickness Distribution

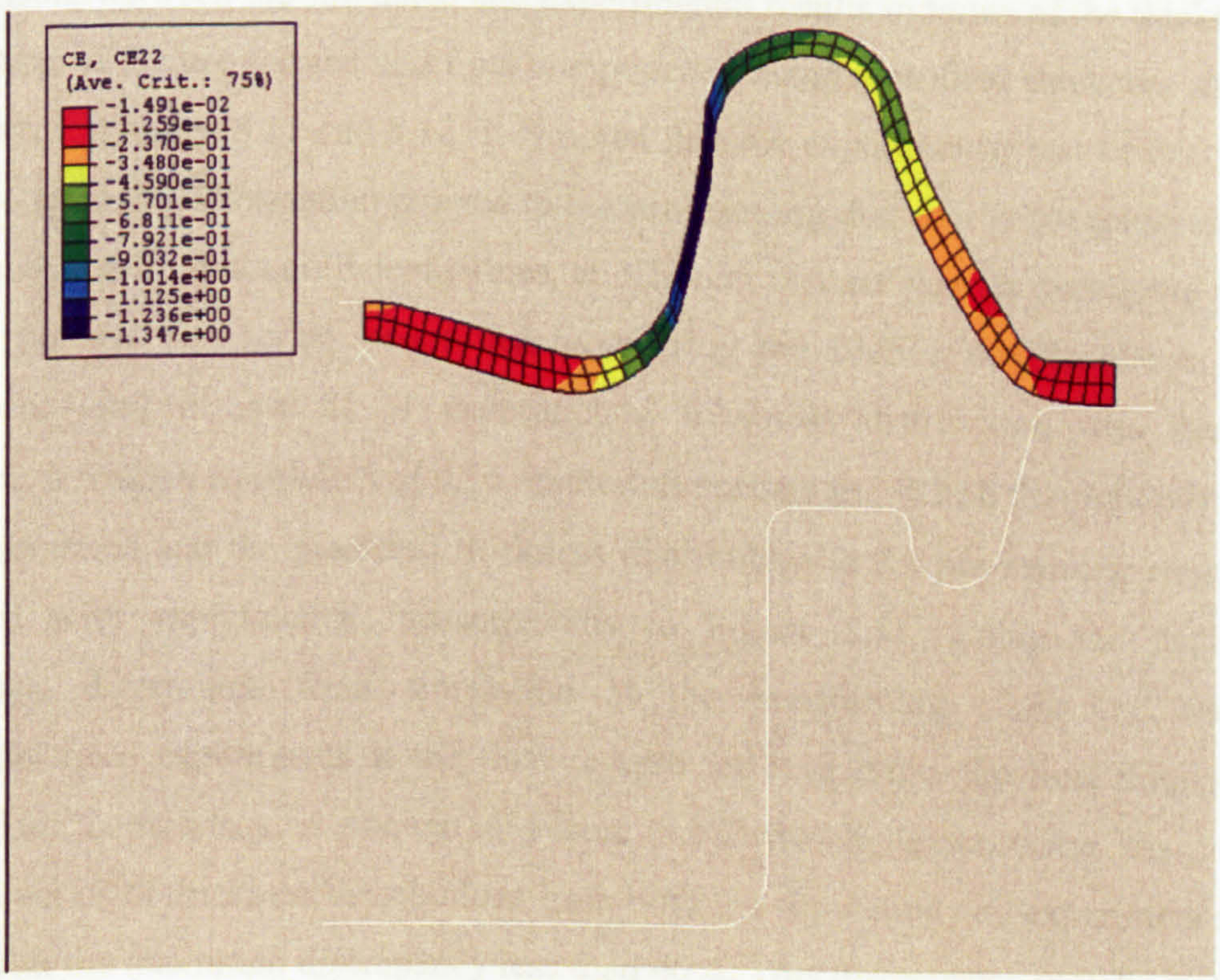

Figure 8.9 Thickness strain distribution of constant thickness sheet of 2.8mm

The strain distribution in the thickness direction can be used as an indicator of the uniformity of complex components. Figure 8.9 shows the predicted strain distribution in the thickness direction of the pre-forming component using a uniform sheet of 2.8

mm thickness. It can be seen that the maximum thickness strain is near the middle bending area where failures were seen in the pilot experiments (see Figure 7.27). This demonstrates that numerical simulation of blow forming can be used for an industrial application to provide an explanation for the experimental phenomenon. The thickness strain distributions of the pre-formed and final components, using a profiled thickness sheet are shown in Figures 8.10 (a) and (b) respectively. Comparison between Figures 8.9 and 8.10 (a) demonstrated, the maximum thickness strain of the pre-formed component using a thickness profiled sheet is about half of that for a uniform thickness sheet. As a result, excessive thinning was prevented using a profiled sheet during the pilot experiments and failure did not occur in the reverse blow forming experiments. The maximum thickness strain occurs around the corner of the middle cup as shown in Figure 8.10 (b), which is in accordance with the fact that this area is the last filled and thinnest in the experiment as shown in Figure 7.34.

Comparisons between the simulated and experimental results in terms of the thickness distribution of the pre-formed and final components, using a profiled thickness sheet, are shown in Figures 8.11 and 8.12. It is noted that the experimental test device was unable to trace the deformation process to the pre-forming die, as it is not transparent. As a result, the friction coefficient values, at different contact regions during the pre-forming process, had to be determined by varying the friction coefficients in the simulation, until a best fit of experimental thickness distribution was found. Therefore, a friction coefficient of 0.15 on the left portion and 0.2 on the right portion were determined and the predicted thickness distribution at the pre-forming stage is compared with experimental measurements in Figure 8.11. Using the friction coefficients determined from simulation at the pre-forming stage and those determined from experiments at the final reverse forming stage, the final thickness distributions comparison is shown in Figure 8.12, which demonstrates that, the variation trends of thickness distributions from both the simulation and experiment are similar with the maximum discrepancy less than 40%. This discrepancy may be traced back to the accumulated error from the pre-forming process, as the friction coefficients during the pre-forming process were fitted to the experimental data by curve-fitting.

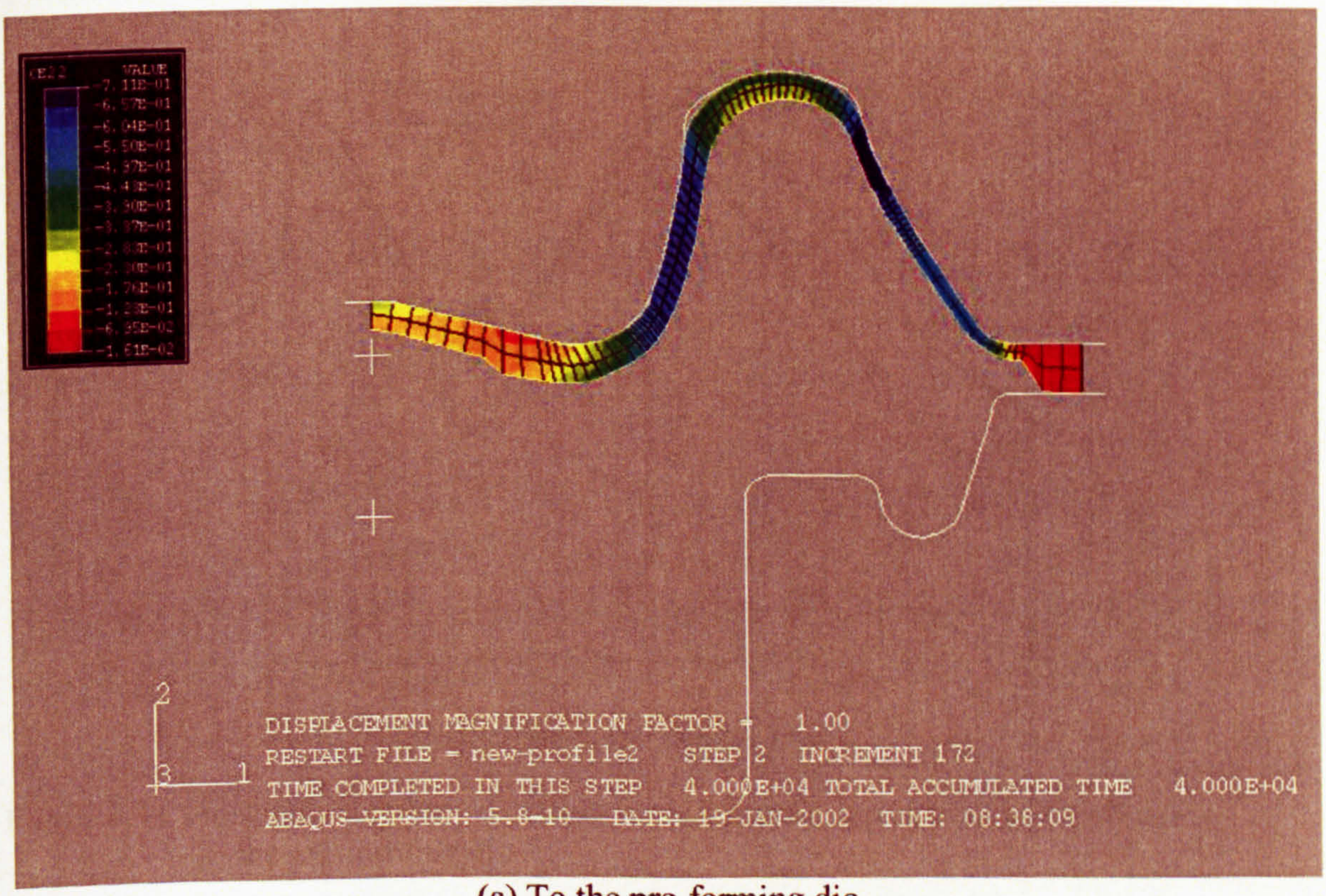

(a) To the pre-forming die

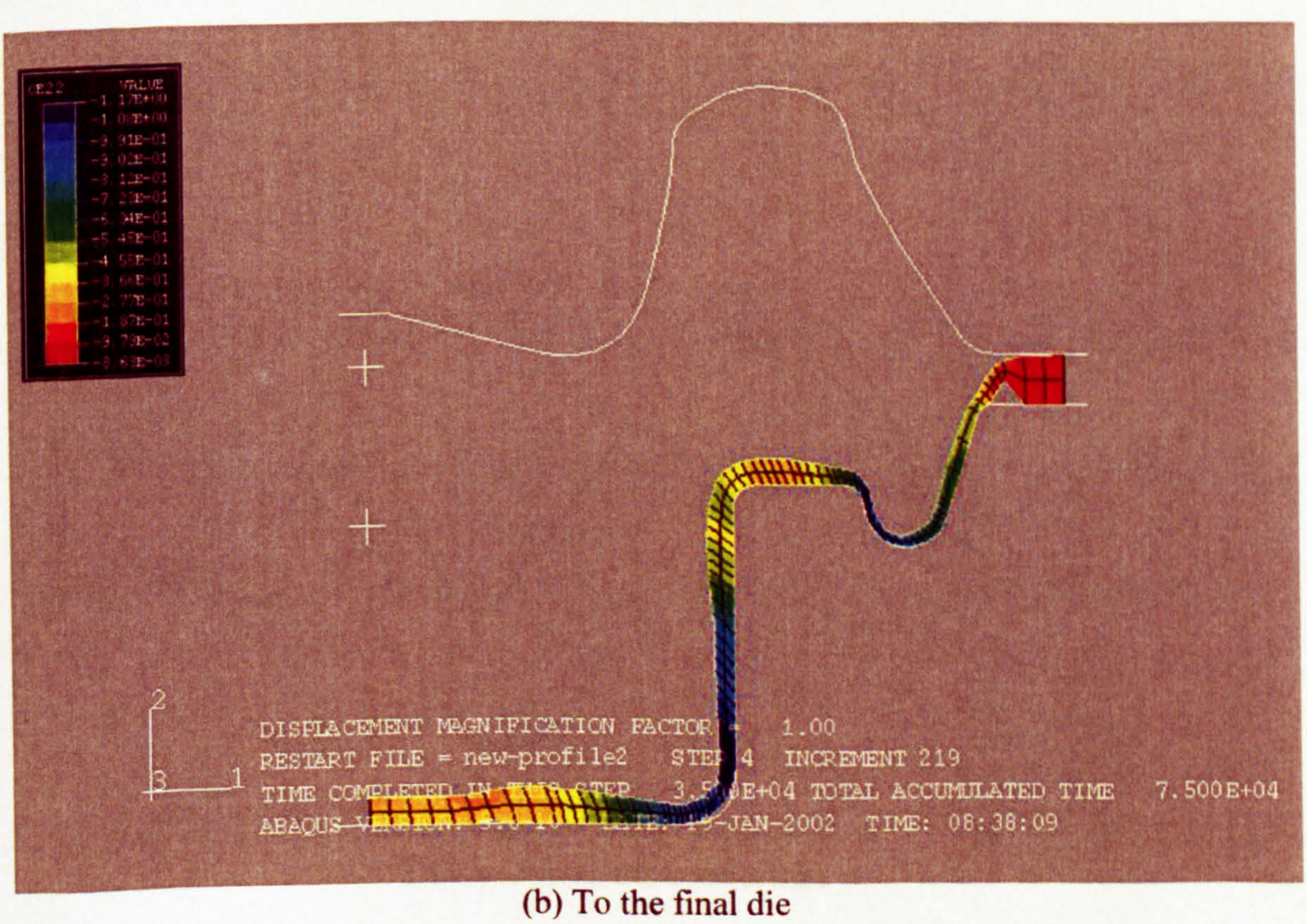

(b) To the final die

Figure 8.10 Thickness strain distribution forming with a profiled thickness sheet

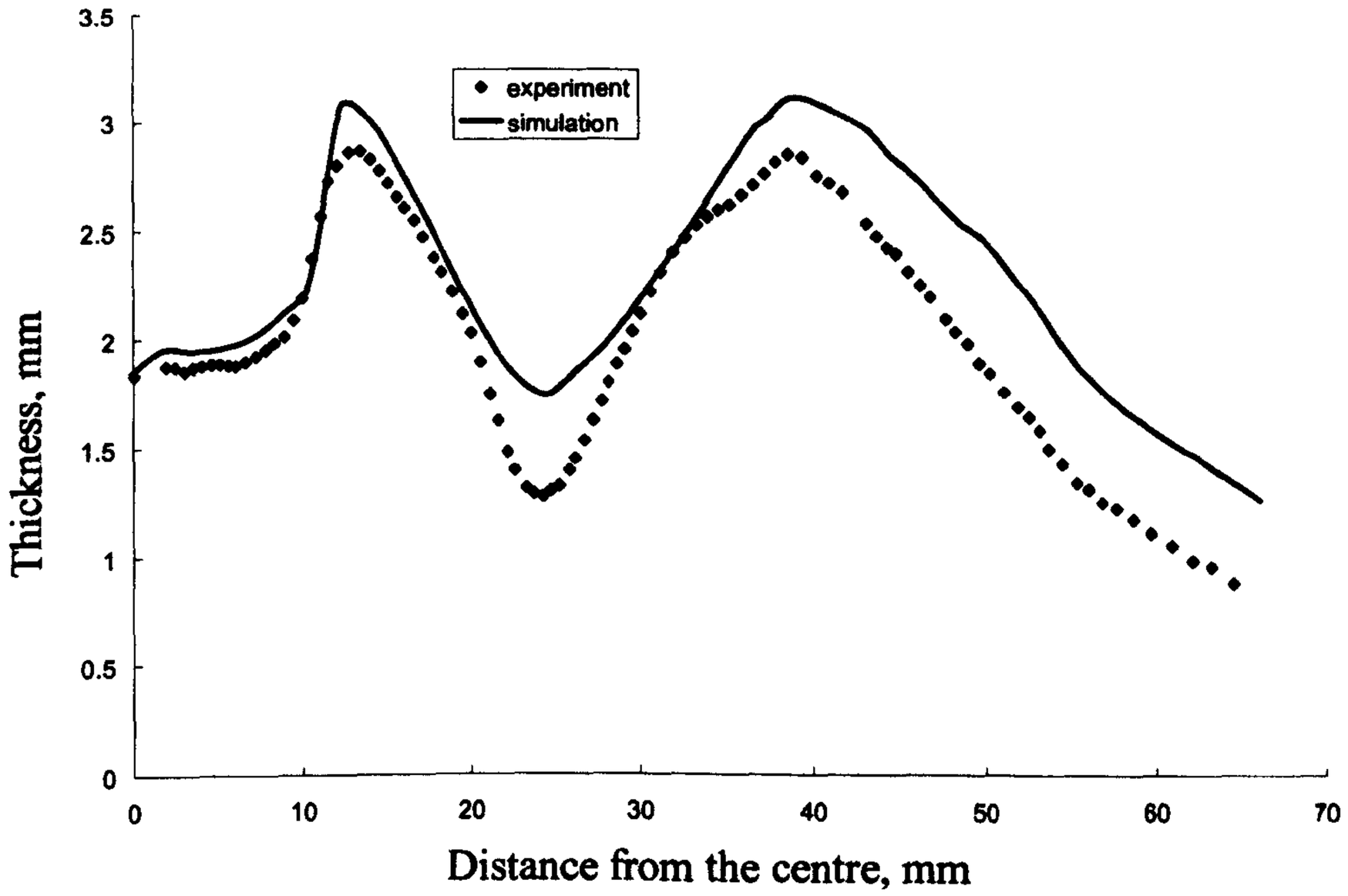

Figure 8.11 Thickness distribution comparisons between experiment and simulation to the pre-forming die

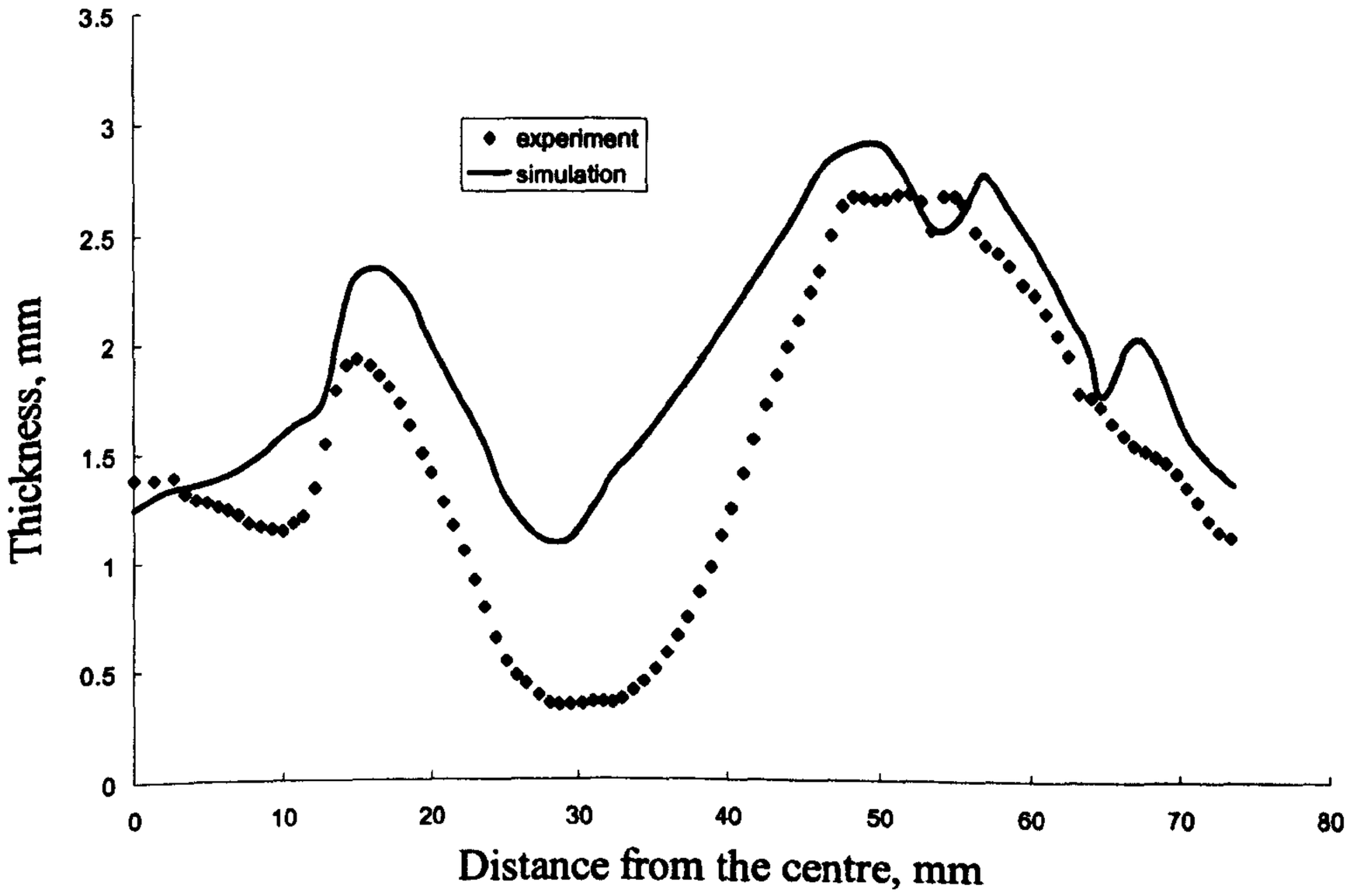

Figure 8.12 Thickness distribution comparisons between experiment and simulation to the final die

8.3 Summary

Simulations of superplastic blow forming of cylindrical cups and reverse blow forming of a complicated component have been achieved. Comparisons in terms of the deformation process and thickness distribution between simulations and experiments have been conducted.

It was found that the predicted deformation processes are in good agreement with experimental observations presented in Chapter 7. For the simple case of a cylindrical cup, the thickness distributions from simulations show a reasonable agreement with the experimental measurements with a deviation less than 30%. For a reverse formed component, deviations between the predictions and measurements are less than 40%. The predicted maximum thickness strain of a uniform thickness sheet is coincident with the failure area observed in the experiments. The discrepancies of thickness distribution of a profiled sheet between the experiments and the simulations may be traced back to the following factors: (a) small but non-negligible error in the preparation of the profiled thickness sheet due to the manufacturing process; (b) the idealisation of a simple friction model in the simulation leading to an error in the calculation of friction coefficient, (c) measurement error in the physical experiments (e) commonly used material constitutive behaviour with no strain hardening effect considered. Although deviations present between the predicted and experimental thickness distributions, the predicted trend of the thinning variation is in a reasonable agreement with the experimental result. In summary, comparisons between the experiments and simulations have demonstrated that the numerical simulation can successfully predict the geometrical deformation and the thinning within a reasonable agreement. In turn, the effectiveness of the simulation proves the effectiveness of the experimental methodology in this research.

Chapter 9

Conclusions and Future Work

9.1 Conclusions

1. An FEM model has been proposed to simulate the superplastic blow forming process of an alloy sheet into a cylindrical cup. The accuracy and reliability of the FE model has been validated by experimental data (Kim et al, 1996). The effects of friction coefficient and the strain rate sensitivity index on the thickness distribution were investigated. The FE model has been extended to investigate the reverse forming process of a complex component design provided by Rolls-Royce Plc using multi-step loading technique with a particular interest on thickness control. Comparisons demonstrate that reverse blow forming results in less thinning in the thickness of the formed component than could be obtained from a non-reverse forming process.

2. A set of friction coefficient equations at four contact regions under superplastic blow forming conditions has been derived. It is found that the friction coefficient is sensitive to material properties, the strain rate and final thickness distribution.

3. A new test rig was designed and built to investigate the frictional behaviour in a blow forming process. The rig was designed to simulate the actual superplastic blow forming conditions as close as practically possible while at the same time to provide a possibility to measure frictional behaviour at different contact regions indirectly. Blow forming experiments of Pb-Sn sheets into cylindrical cups and complicated reverse formed components have been carried out. Based on the recorded deformation process and thickness distribution, the friction coefficient is calculated according to the corresponding equations at different contact regions.

4. Simulations of the blow forming process have been conducted using the friction coefficients obtained from the experiments as an input. Detailed comparisons, including deformation process and thickness distribution, between simulations and experiments demonstrate that, the proposed experimental methodology is able to obtain the friction coefficients in a superplastic blow forming process within a reasonable accuracy.

5. A comprehensive methodology to investigate the friction mechanism in a superplastic blow forming process has been presented. Experiments based on the methodology have been conducted and the experimental thickness distributions are in a reasonable agreement with the predictions from the simulations. A set of equations derived in Chapter 6, together with the experimental setup are able to obtain the friction values in the blow forming process. It is anticipated that the implementation of the methodology will improve understanding of the friction mechanism in the blow forming process and thus better control the thickness distribution of a superplastic formed component.

9.2 Recommendations for Future Work

Two kinds of pressure control are usually adopted in the superplastic blow forming process. The constant forming pressure is easy to achieve and control, while constant strain rate forming, by varying the pressure profile, is more often used in industry. It was reported that a reduced forming time and a satisfactory thickness profile could be achieved when compared with forming under constant pressure (Yang et al, 1996). As a first step in the development of a frictional test rig, constant pressure control was implemented in the current experimental design. Therefore, further work is recommended to design a pressure control system to achieve a constant forming strain rate. The system includes a PC running main control software, digital pressure transducers, a stepper drive system to a control stepper motor and pressure control valves. The pressure control valve can be adjusted according to the difference between the pressure measured by the transducer and the user-specified pressure profile. Furthermore, with the application of constant strain rate control in the

experimental rig, the effects of different strain rates on frictional behaviour can be studied. In addition, it is proposed to machine the pre-forming die using transparent perspex block so that both forming processes can be investigated in the future work. Due to the complexity of the pre-forming die and the limitation of the manufacturing equipment, it was not possible to be manufactured when this research was carried out.

The frictional behaviour of blow forming has been investigated in this thesis, with specific geometry – a cylindrical cup and a specific material – Pb-Sn sheet which exhibits superplasticity at room temperature. However, in many cases, the structures for the aerospace are very complicated and the forming temperature for the superplastic material is normally very high, for example, around 925°C for Ti-6Al-4V alloys. For a complete investigation of the frictional behaviour, superplastic sheets bulged into complex forming dies at high temperature is recommended for further work. A test rig with a high temperature chamber is necessary to perform the experiment at high temperature. With the high temperature test rig, the material used by the industry can be directly studied in the research work, so that no model material has to be used in the laboratory.

In this study, the commonly used power law, shown in Equation (2.1), was employed to describe the superplastic material behaviour (Rebelo et al, 1990; Kim et al, 1996; Cheng, 1996; Hwang et al, 1998; Carrino and Giuliano, 2001). The effects of temperature and grain size were taken into account in the calculation of the material constant K, see Equation (2.2) (Arieli and Mukherjee, 1982; Ashby and Verall, 1973). In this model, superplastic materials are assumed to be ideally strain rate sensitive (e.g., little strain hardening occurs) and have stable grain size, so that K remains relatively constant at a specific temperature (Pilling and Ridley, 1989). There are other constitutive material models published with the temperature dependency represented explicitly. For example, a hyperbolic sine relationship was proposed to represent the superplasticity of Inconel 718 (Zhang et al, 2004) as follows,

$$\dot{\varepsilon} = \exp(-\frac{Q}{RT})\frac{Sinh(\alpha\sigma)^{1/m}}{B} \tag{9.1}$$

Where, $\dot{\varepsilon}$ is the strain rate, Q the activation energy for flow, R Boltzmann's constant, T the absolute temperature, α the constant, B the material parameter, σ

the true stress and m the strain rate sensitivity. It is noted that strain hardening effect is considered in the derivation of Equation (9.1). Considering the importance of the material constitutive behaviour, it is proposed to perform a full evaluation of the available material constitutive models so that the best model can be employed to simulate the superplastic forming process.

Superplastic blow forming experiments were conducted at various temperatures and forming pressures. Due to limited budget for the project, only one experiment was performed at a specific temperature and forming pressure. As a result, it is not possible in this research to give any error bars from statistics point of view as there has no enough samples taken under the same experimental conditions. The final distributions of the formed components were measured once by University technicians and no error bar was reported as well. It is now widely recognised that all experimental measurements should be accompanied by an estimate of the uncertainty of measurement as outlined in the ISO TAG4 (1994). Further information and guidance on estimating measurement uncertainties are available elsewhere including a Guide from Bell (1999) as well as more comprehensive documents (Kandil *et al*, 2000). For a complete investigation to determine the friction coefficients for use as input data for the simulation models, it is necessary to perform a full error analysis in the thesis. The issues concerning the estimation of uncertainty of measurement are addressed for future work.

FE package ABAQUS (2002) was available at the University of Wolverhampton when the research work was carried out. The capability of ABAQUS was validated through projects conducted within the Engineering Simulation Group in the School of Engineering and Built Environment. There are many FE packages commercially available on the market, for example, ANSYS and FEMSYS etc. It is proposed to perform a comparison study to justify the application of ABAQUS in the investigation for future work.

References

ABAQUS/Standard, User's Manual, Vol.1-3, Version 6.1, Hibbitt, Karlsson and Sorensen Inc., USA, 2002.

ABAQUS/Stand, Example Manual, Vol.1-2, Version 6.1, Hibbitt, Karlsson and Sorensen Inc., USA, 2002.

ABAQUS/Stand, Theory Manual, Version 6.1, Hibbitt, Karlsson and Sorensen Inc., USA, 2002.

Agarwal S P, Boyer P R, and Weisert E D, "Titanium Science and Technology", (Edited Kimura H. and Izumi O.), New York, American Institute of Mining and Metallurgical Engineers, pp 1057-1066, 1980.

Ahmed M. I., Mohamed F.A. and Langdon T.G., "Factors Influencing Ductility in the Superplastic Zn-22%Al Eutectoid", Metallurgical Transactions 8A, pp. 933, 1977.

Akkus N, Manabe K, Kawahara M and Nishimura H, "A finite-element model for the superplastic bulging deformation of Ti-alloy pipe", Journal of Materials Processing Technology, Vol. 68, pp. 215-220, 1997.

Akkus N, Suzuki K, Kawahara M and Nishimura H, "Influence of performing on the final thickness distribution of the superplastically deformed domes", Materials Science Forum, Vols. 304-306, pp. 759-764, 1999.

Alden T H, "Observations of strain rate transients in the superplastic lead-tin eutectic alloy", Scripta Metallurgica, Vol. 21, pp 735-738, 1987.

Al-Naib T Y M and Duncan J L, "Superplastic metal forming", International Journal of Mechanical Sciences, Vol. 12, pp 463-477, 1970.

Al-Salehi F A K And Firbank T C and Lancaster P G, " An experimental determination of the roll pressure distribution in cold rolling", International Journal of Mechanical Sciences, Vol. 15, pp 693-710, 1973.

Amonton G, "De la resistance causee des machines simple", Memoires de l'Academic royal A, pp 275-282, 1699.

Arieli A, Mukherjee A K, "The rate-controlling deformation mechanisms in superplasticity-a critical assessment", Metallurgical and Materials Transactions A, Vol. 13A, pp 717-731, 1982.

Ashby M F and Verall R A, "Diffusion-accommodated flow and superplasticity", Acta Metallurgica, Vol. 21, pp 149-163, 1973.

Avitzur B, "Metal Forming: Processes and Analysis", McGraw-Hill, New York, pp. 81-102, 1968.

Avitzur B, "Bulge in hollow disk forging", Report of the inst. For Metal Forming, Air Force Materials Laboratory Technical Report TR-69-261, 1969.

Backofen W A, Turner I R and Avery D H, "Superplasticity in an Al-Zn alloys", Trans ASM, Vol. 57(6), pp 980-990, 1964.

Bandon J F, Lecoanet H and Oytana C, International Journal of Mechanical Sciences, Vol. 21, pp 379-386, 1979.

Barcellona A, Forcellese A, Gabrielli F and Micari F, "Effect of mechanical and geometrical features of workpiece on friction behaviour in double cup extrusion", In Proceedings of the 9th International Cold Forging Congress, Solihull, pp 231-237, 1995.

Barcellona A, Cannizzaro L, Forcellese A and Gabrielli F, "Validation of frictional studies by double-cup extrusion tests in cold-forming", Annals of the CIRP, Vol. 45(1), pp 211-214, 1996.

Barnes A, "Industrial applications of superplastic forming: Trends and prospects", Materials Science Forum, Vols.357-359, pp3-16, 2001.

Baschhausen A, Weinmann K, Lee J Y and Altan T, "Evaluation of lubrication and friction in cold forging using a double backward-extrusion process", Journal of Materials Processing Technology, Vol. 33, pp 95-108, 1992.

Bate P S, Price D C, Barrett D J, Roberts W T, "The simulation, control and optimisation of the gas-pressure forming of aluminium alloy sheet at elevate temperatures", Journal of Materials Processing Technology, Vol. 38, pp 589-612, 1993.

Bay N and Hansen B G, "Simulation of friction and lubrication in cold forging", Proceedings of the 7th International Cold Forging Congress, pp 55-62, 1985.

Beilei T R, Neih T G, Wadsworth J and Muhkerjee A K, "Superplastic-like behaviour at high strain rates in a mechanically alloy aluminium", Scripta Materialia, Vol. 22, pp 81-86, 1998.

Bell, S, "A beginner's guide to uncertainty of measurement", Good Practice Guide No 11, ISSN 1368-6550, Pub: National Physical Laboratory, 1999.

Bengough G D, "Superplasticity in an Al-Zn alloy", Journal of the Institute of Metals, Vol. 7, pp 123-128, 1912.

Beynon J H, Li Y H, Krzyzanowski M, Sellars C M, " Measuring modelling and understanding friction in the hot rolling of steel", Metal Forming 2000, Pietrzyk et al.(eds), Balkema, Rotterdam, pp 3-10, 2000.

Bochmann E and Doege E, " Friction as a critical phenomenon in the simulation of metal forming", Proceeding of Developments in production engineering design and control, editors: El-Ashram A E and Youssef, H A, pp 307-316, 1992.

Bochvar A A, Sviderskaia Z. A., "Superplasticity in Zinc-Aluminium alloy", Izvest.Akad.Nauk SSSR, Otdel. Tekh. Nauk, Vol. 9, pp 821-830, 1945.

Bonet J, Wood R D, "Solution procedures for the finite element analysis of superplastic forming of thin sheet", In: Proceedings of International Conference on computational plasticity models, software and applications, part 2, Pineridge Press, pp 927-939, 1987.

Bonet J, Wood R D and Wargadipura A H S, "Numerical simulation of the superplastic forming of thin sheet components using the finite element methods", International Journal for Numerical Methods in Engineering, Vol. 30, pp 1719-1737, 1990.

Bonet J, Bhargava P and Wood R D, "The incremental flow formulation for the finite element analysis of 3-dimensional superplastic forming processes", Journal of Materials Processing Technology, Vol. 45, pp 243-248, 1994.

Bonet J, Wood R D and Collins R, "Pressure control algorithms for the numerical simulation of superplastic forming", International Journal of Mechanical Sciences, Vol. 36(4), pp 297-309, 1994.

Bowden F P and Tabor D, "The theory of metallic friction and the role of shearing and ploughing", Bull.145, Comm. Of Australia, Council Science and Industry Research, 1942.

Boyer P R and Magnuson J E, "An apparent anomaly in the superplastic behaviour of Ti-6Al-4V", Mettallurgical Transactions A, Physical Metallurgy and Materials Science, Vol. 10A, pp 1191-1193, 1979.

Brooks M. R. and Loveday M S, "Friction and oxide strength data for forging & rolling process modelling", CMMT (MN) 071, Pub: National Physical Laboratory, 2000.

Capu J M and Cockcroft M G, "Coefficients of friction in cold rolling derived from measurements of relative slip", Journal of the Institute of Metals,, pp 31-32, 1963-1964.

Carleer B D, Haar R T, Hurtink H and Schipper D J, "Sheet metal forming simulations with a friction model based on local contact conditions", NUMISHEET'96, pp 40-46, 1996.

Carrino L and Giuliano G, "Modelling of superplastic blow forming", International Journal of Mechanical Sciences, Vol. 39, No.2, pp 193-199, 1997.

Carrino L and Giuliano G, "Analysis of superplastic testing by using constant pressure in prismatic die", Materials Science Forum, Vols. 357-359 ,pp 219-224, 2001.

Chandra N, "Analysis of superplastic metal forming by a finite element method", International Journal for Numerical Methods in Engineering, Vol. 26, pp 1925-1944, 1988.

Chandra N and Chandy K, "Superplastic process modelling of plane strain components with complex shapes", Journal of Material shaping technology, Vol. 9, pp 27-36, 1991.

Chandra N and Kannan D, "Superplastic sheet metal forming of a generalized cup part II: non-uniform thinning", Journal of Material Engineering and Performance, Vol. 1, pp 813-822, 1993.

Chandrasekaran N, Gogorth R E and Haisler W E, "Finite element formulation of superplastic metal forming processes", American Society for Metals, Metals/Materials Technology Series, Materials Week, 1985, paper 8511-004, pp 1-8, 1985.

Chen T R, Huang J C, Hwang Y M and Wang T D, "Different friction coefficient at different positions of superplastically formed parts", Materials Science Forum, Vol. 304-306, p p741-746, 1999.

Chen Z and Thomson P F, "Friction against superplastic aluminium alloys", Wear, Vol. 201, pp 227-232, 1996.

Cheng J H, "A procedure for designing initial thickness variation for superplastic free inflation", International Journal of Mechanical Sciences, Vol. 36(11), pp 981-1000, 1994.

Cheng J H, "The determination of material parameters from superplastic inflation tests", Journal of Materials Processing Technology, Vol. 58, pp 233-246, 1996.

Cheng S C, Wolfenstine J, Sherby O D, "Superplastic behaviour of two-phase titanium aluminides", Metallurgical Transactions A, Physical Metallurgy and Materials Science, Vol. 23A, pp 1509-1513, 1992.

Chenot J L, Bellet M, "The viscoplastic approach for the finite element modelling of metal forming processes", In: P.Hartley et. al. Ed. "Numerical modelling of material deformation processes: research, development and applications", Springer-Verlag, Berlin, pp 179-224, 1992.

Cheung Y, Lo S and Leung A, "Finite Element Implementation", Blackwell Science, 1996.

Cook R, Malkus D and Plesha M, "Concepts and Applications of Finite Element Analysis"" 3rd Edition, John Wiley and Sons, 1989.

Cornfield G C and Johnson R H, "The forming of superplastic sheet metal", International Journal of Mechanical Sciences., Vol. 10, pp 479-490, 1970.

Coulomb C A, "Theories des machines simple", Memoires de mathematique et de physique de l'academie royal, pp 161-342, 1785.

Ding X D, Zbib H M and Hamilton C H, "On the stability of biaxial stretching with application to the optimization of superplastic blow-forming", Transaction Of the ASME, Journal OF Engineering Materials and Technology, Vol. 119, pp 26-31, 1997.

Doege E and Bederna C H, "Indirect analysis of Boundary stresses", Journal of Materials Processing technology, Vol. 45, pp 57-62, 1994.

Duncan J L, Shabel B S and Filho J G, "A tensile strip test for evaluating friction in sheet metal forming", Society of Automotive engineering technical paper, No.780391, 1978.

Dutta A and Mukherjee A K, "Superplastic forming: an analytical approach", Materials Science and Engineering, Vol. A157, pp 9-13, 1992.

Edward J and Kubel J, "Titanium nns technology shaping up", Advanced Materials & Progresses inc. Metal Progress, Vol. 2, pp 46-50, 1987.

Edwards C M and Halling J, "Experimental study of the plastic interaction of model surface asperities during sliding", Journal of Mechanical Engineering, Vol. 10, pp 121-132, 1968.

Enikeev F U and Kruglov A A, "An analysis of the superplastic forming of a thin circular diaphragm", International Journal of Mechanical Sciences, Vol. 37(5), pp 473-483, 1995.

Ezugwu E O, Wang Z M, "Titanium alloys and their machinability - a review", Journal of Materials Processing Technology, Vol. 68, pp 262-274, 1997.

Felder E and Montagut Y L, "Friction and wear during hot forging of steels", Tribology International, Vol. 13, pp 61-68, 1980.

Feng I M, "Metal transfer and wear", Journal of Applied Physics, Vol. 23, pp 1011-1019, 1952.

Fletcher J D, Li Y H, Beynon J H and Sellars C M, "The influence of surface conditions in hot forming determined by ring upsetting: a numerical and experimental investigation", Proceeding – Institution of Mechanical engineers, Vol. 212 (Part J), pp 453-465, 1998.

Foetz R L, Jain V K, Morgan J T and Wierschke M W, "Effect of material and processing conditions upon ring calibration curves", Wear, Vol. 143, pp 71-86, 1991.

Forcellese A, Gabrielli F, Barcellona A, Micari F, "Evaluation of friction in cold metal forming", Journal of Materials Processing Technology, Vol. 45, pp 619-624, 1994.

Geiger R, "Metal flow in combined can extrusion", Berichte aus dem Institut fur Umformtechnik der Universitat Stuttgart 36, 1976.

Ghobrial M I, Lee J Y and Altan T, "Factors affecting the double cup extrusion test for evaluation of friction in cold and warm forging", Annals of the CIRP, Vol.42(1), pp 347-351, 1993.

Ghosh, A K, "Superplasticity in Aluminium Alloys", Superplastic Forming, S.P. Agrawal ed., The American Society of Metals, pp 23-31, 1985.

Ghosh A K and Bieler T R, "Superplasticity and superplastic forming", TMS, 1998.

Ghosh A K and Hamilton C H, "Superplastic Forming of a Long Rectangular Box Section - Analysis and Experiment." In Process Modeling, Fundamentals and Applications to Metals, ASM, Metals Park, Ohio, 1979.

Ghosh A K and Hamilton C H, Proceeding of "Process modelling: fundamentals and applications to metals", edited by Altan T et al., ASM, Metals park, OH, pp 303-331, 1980.

Ghosh A K and Hamilton C H, "Influences of material parameters and microstructure on superplastic forming", Metallurgical and Materials Transactions, Vol. 13A, pp 733-743, 1982.

Green A P, "Friction between unlubricated metals, a theoretical analysis of the junction model", Proceedings of Royal Society, 228A, pp 181-204, 1955.

Grimes R, Stowell M J and Watts B W, "Superplasticity aluminium-based alloys", Metals Technology, pp 154-160, 1976.

Grivas D, Murty K L and Morris J W, "Deformation of Pb-Sn eutectic alloys at relatively high strain rates", Acta Metallurgica, Vol. 27(5), pp 731-741, 1979.

Guo Z X and Ridley N, "Modelling of superplastic bulge forming of domes", Materials Science and Engineering, Vol. 114A, pp 97-104, 1989.

Guo Z X, Piling J and Ridley N, "Superplasticity and Superplastic forming", C.H.Hamilton and N.E.Paton, Eds., TMS, Warrendale, PA, pp 303-311, 1988.

Hamilton C H, "Superplasticity in titanium alloys", Superplastic Forming, S.P.Agrawal ed., The American Society of Metals, pp 12-22, 1985.

Hamilton C H and Paton N E, "Superplasticity and superplastic forming", TMS-AIME, Warrendale, Pa. 1989.

Hansen B G and Bay N, "Two methods for testing lubricants for cold forging", Journal of Mechanical Work Technology., Vol. 13, pp 189-204, 1986.

Hardy Sir W B, "Collected Works", Cambridge University Press, 1936.

Hartley P, Pillinger I, Hall R and Sturgess C E N, "Contact and friction in non-linear modelling of forming processes", NAFEMS seminar on Finite-Elements, Contact and Friction, Warrington, 1992.

Hartley P, Sturgess C E N and Rowe G W, "Friction in finite element analyses of metalforming processes", International Journal of Mechanical Sciences, Vol. 21, pp 301-311, 1979.

Holt D L and Backofen W A, "Superplasticity in the Al-Cu eutectic alloy", Transaction of ASM, Vol. 59, pp 755-768, 1966.

Holt D L, "An analysis of the bulging of a superplastic sheet by lateral pressure", International Journal of Mechanical Sciences., Vol. 10, pp 491-497, 1970.

Huang A, Cardew-Hall M J, Lowe A, "Sheet thickness optimization for superplastic forming of Engineering structures", Journal of Manufacturing Science and Engineering, Vol. 122, pp 117-123, 2000.

Huh H, Han S S, Lee J S, Hong S S, "Experimental verification of superplastic sheet-metal forming analysis by the finite-element method", Journal of Materials Processing Technology, Vol. 49, pp 355-369, 1995.

Hwang Y M, Liew J M, Chen T R and Huang J C, "Analysis of superplastic blow-forming in a circular close-die", Journal of Materials Processing Technology, Vol. 57, pp 360-372, 1996.

Hwang Y M, Yang J S, Chen T R and Huang J C, "Analysis of superplastic sheet-metal forming in a circular close-die considering non-uniform thinning", Journal of Materials Processing Technology, Vol. 65, pp 215-227, 1997.

Hwang Y M, Yang J S, Chen T R et al, "Analysis of superplastic blow-forming in a conical closed die", International Journal of Mechanical Sciences.,Vol. 40(9), pp 867-885, 1998.

Imayev R M, Kaibyshev O A and Salishev G A, "Mechanical behaviour of fine grained TiAl intermetallic compounds", Acta Metallurgica et Materialia, Vol. 40, pp 581-587, 1992.

ISO TAG4, "Guide to the expression of uncertainty in measurement", International Standard Organisation, 1994.

Johnson R H, "superplasticity", Metallurgical Reviews, Vol. 15(146), pp 154-160, 1970.

Johnson W, Al-Naib T Y M and Duncan J L, "Superplastic forming techniques and strain distributions in a Zn-Al alloy", Journal of the Institute of Metals, Vol. 100, pp 45-50, 1972.

Johnson W and Meller P B, Engineering Plasticity, Ellis Horwood Limited, UK, 1983

Jovane F, "An approximate analysis of the superplastic forming of a thin circular diaphragm: theory and experiments", International Journal of Mechanical Sciences, Vol.10, pp 403-427, 1968.

Kandil F et al, "UNCERT- Manual of codes of practice for the determination of uncertainties in mechanical tests on metallic material", Section 1: Introduction to the evaluation of uncertainty. UKAS, M3003, 2000.

Khaleel M A, Johnson K I, Hamilton C H and Smith M T, "Deformation modelling of superplastic AA-5083", International Journal of Plasticity, Vol. 14, pp 1133-1154, 1998.

Kim Y H, Hong S S, Lee J S and Wagoner R H, "Analysis of superplastic forming processes using a finite-element method", Journal of Materials Processing Technology, Vol. 62, pp 90-99, 1996.

Kim Y H, Lee Jung-Min, Hong S S, "Optimal design of superplastic forming processes", Journal of Materials Processing Technology, Vol. 112, pp 166-173, 2001.

KODAK motion recorder analyzer, KODAK, 2000.

Kudo H, "An analysis of plastic compressive deformation of lamella between rough plates by energy method", Proceedings of 5th National Congress of Applied Mechanics, Vol. 5, pp 75-85, 1955.

Kunogi M, "On the plastic deformation of the hollow cylinder under axial load", J.Sci.Res.Inst., Japan, Vol. 30(2), pp 63-92, 1954.

Langdon T G, "The mechanical properties of superplastic materials", Metallurgical and Materials Transactions, Vol. 13A, pp 689-701, 1982.

Laylock D B, "In Superplastic forming of structural alloys", Edited.by Paton N E and Hamilton C H, New York, The Metallurgical Society of AIME, pp 257-271, 1982.

Lee C H and Altan T, "Influence of flow stress and friction upon metal flow in upset forging of rings and cylinders", ASME Journal of Engineering for Industry, Vol. 94, pp 775-782, 1972.

Lee D and Backofen W A, "Superplasticity in some titanium and zirconium alloys", Trans. AIME, Vol. 239, pp 1034-1040, 1967.

Lee J H, Song Y J, Shin D H and Lee C S, "Microstructural evolution during superplastic bulge forming of Ti-6Al-4V alloys", Materials Science and engineering, Vol. 243A, pp 129-125, 1998.

Lee K S, Huh H, "Numerical simulation of the superplastic moving die forming process with a modified membrane finite element method", Journal of Materials Processing Technology, Vol. 113, pp 754-760, 2001.

Lee S, "Thickness distribution in a superplastically formed rectangular pan under plane-strain conditions", Journal of Materials Processing Technology, Vol. 65, pp 59-64, 1997.

Lenard J G, "The effect of temperature on the coefficient of friction in flat rolling", Annals of the CRIP, Vol. 40, pp 223-234, 1991.

Lenard, J. G. and Kalpakjian, S., "An experimental study of boundary conditions in hot and cold flat rolling," Annals of CIRP, Vol. 39, 279-282, 1990,.

Li Y, Hu P and Cao Y, "Numerical simulation of the superplastic constrained bulging of sheet metals in cylindrical dies", Journal of Materials Processing Technology, Vol. 59, p243-249, 1996.

Lim L S and Lenard J G, "Study of friction in cold strip rolling", ASME Journal of Engineering Materials and Technology, Vol. 106, pp 139-146, 1984.

Lunt R W and Maclellan G D S, "An extension of wire drawing theory with special reference to contributions of K.B.Lewis", Journal of the Institute of Metals, pp 67-96, 1946.

Ma Y and Langdon T C, "Communication: Factors Influencing the Exceptional Ductility of a Superplastic Pb-62 pct Sn Alloy", Metallurgical and Materials Transactions, Vol. 25A, pp 2309-2311, 1994.

Male A T and Cockcroft M G, "A method for the determination of the coefficient of friction of metals under conditions of bulk plastic deformation", Journal of the Institute of Metals, Vol. 93, pp 38-45, 1964-1965.

Male A T and Depierre V, "The validity of mathematical solutions for determining friction from the ring compression test", ASME Journal of Lubrication technology, Vol. 92, pp 389-397, 1970.

Matsuki K, Minami K, Tokizawa M and MurKmi Y, "Superplastic behaviour in normally single-phased and two-phased Al-Cu alloys", Metal Science, Vol. 11, pp 619-625, 1979.

Mayo M J and Nix W D, "Micro-indentation study of superplasticity in Pb-Sn and Sn-38wt% Pb", Acta Metallurgica, Vol. 36, pp 2183-2192, 1988.

Mcfarlane J and Tabor D, "Relation between friction and adhesion", Proceedings of Royal Society, Vol. 202A, pp 244-253, 1950.

Nagpal V, Lahoti G D and Altan T, "A Numerical Method for simultaneous prediction of metal flow and temperatures in upset forging of rings", ASME Journal of Engineering for Industry, Vol. 100, pp 413-420, 1978.

Nieh T G, Wadsworth J and Sherby O D, "Superplasticity in metals and ceramics", Cambridge University Press, Cambridge, England, 1997.

Nobuki M, Vanderschueren D, Nakamura M, "High temperature mechanical properties of vanadium alloyed gamma base titanium-aluminides", Acta Metallurgica et Materialia, Vol. 42, pp 2623-2632, 1994.

Orowan E, "The calculation of roll pressure in hot and cold flat rolling", Proceedings of the Institution of Mechanical engineers, Vol. 150 (4), pp 140-167, 1943.

Osada K, Shirakawa K, "Influence of lubrication on aluminium superplastic forming", Materials Science Forum, Vol. 304-306, pp 813-818, 1999.

Owen D and Hinton E, "Finite Elements in Plasticity: Theory and Practice", Pineridge Press Limited, Swansea, UK.

Paton N E and Hamilton C H, "Micro-structural influences on superplasticity in Ti-6Al-4V", Metallurgical and Materials Transactions, Vol. 10A, pp 241-250, 1979.

Pawelski O, Rasp W and Hoerster C, "The ring compression test as simulation test for the investigation of friction in hot metal forming", Steel Research, Vol. 60, pp 395-402, 1989.

Pawelski O, Rasp W and Wolff C, "Analysis of the asymmetric upsetting test with extremely high strain rate as tool for friction measurement", Journal of Materials Processing Technology, Vol. 80-81, pp 287-291, 1998.

Pearce R, "Sheet Metal Forming", IOP publishing ltd., 1991.

Pearsall G W and Backofen W A, "Frictional boundary conditions in plastic compression", ASME Journal of Engineering Industry, Vol. 85, pp 68-75, 1963.

Pearson C E, "Viscous properties of extruded eutectic alloys of Pb-Sn and Bi-Sn", Journal of Industry Metals, Vol. 54, pp 111-123, 1934.

Peterson M B and Ling F F, "Friction and lubrication at extreme pressures", Proceedings of friction and lubrication in metal forming processing, pp 39-68, 1966.

Petersen S B, Martins P A F and Bay N, "Friction in bulk metal forming: a general friction model vs. the law of constant friction", Journal of Materials Processing Technology, Vol. 66, pp 186-194, 1997.

Petty D M, "Fiction models for Finite element modelling", Journal of Materials Processing Technology, Vol. 45, pp 7-12, 1994.

Phaipu S, "The effect of microstructural gradient on superplastic forming of Ti-6Al-4V", Journal of Materials Processing Technology, Vol. 80-81, pp 90-95, 1998.

Picksley J, Hall R and Pillinger I, "Metalforming of Titanium: Experimentation, microstructure and computer simulation", Journal of Material Processing Technology, Vol. 45, pp491-496, 1994.

Pilling J and Ridley N, "Superplasticity", London, Institute of Metals, 1989.

Ragab A R, "Thermoforming of superplastic sheet in shaped dies", Journal of Metal Technology, Vol. 10, pp 340-348, 1983.

Rama S C and Chandra N, "Development of a pressure prediction method for superplastic forming processes", International Journal of Non-Linear Mechanics, Vol. 26, pp 711-725, 1991.

Rao S, "The Finite Element Method in Engineering", 2nd Edition, Pergammon Press, 1989.

Rebelo N, Nagtegaal J C and Hibbitt H D, "Finite element analysis of sheet forming processes", International Journal for Numerical Methods in Engineering, Vol. 30, pp 1739-1758, 1990.

Rudkins N T, Hartley P, Pillinger I and Petty D, "Friction modelling and experimental observations in hot compression tests", Journal of Materials Processing Technology, Vol. 60, pp 349-353, 1996.

Sahi M, Rahouadj R, Herbach R and Choulier D, "The influence of viscoplasticity in the interpretation of the ring test", Journal of Materials Processing Technology, Vol. 58, pp 286-292, 1996.

Sanchez L R, Weinmann K J and Story J M, "A friction test for extrusion using combined flow with emphasis on backward extrusion", Proceedings of.NAMRC XIII, 1985.

Sanders D G, "Superlastic forming manufacturing technology moves towards the twenty-first century", Materials Science Forum, Towards innovation in superplasticity II, Vol. 304-306, pp 805-812, 1999.

Sanders D G, "The current state-of-the art and the future in airframe manufacturing using superplastic forming technologies", Materials Science Forum, Vol. 357, pp 17-22, 2001.

Sastry S M L, Lederich R J, Mackay T L, Kerr W R, " Superplastic forming characterization of titanium alloys", Journal of Metals, Vol. 35, pp 48-53, 1983.

Schey J A, "Metal deformation processes – friction and lubrication ", Marcel Dekker Inc., 1970.

Schey J A, "The validity of simulating tests in evaluating lubricants for deformation processes", In A.L.hoffmanner (ed.), Metal forming: Interrelation between theory and practice, New York, plenum Press, pp 275-292, 1971.

Schey J A, "Tribology in metalworking – friction, lubrication and wear", American society for metals, ASME, 1983.

Schipper D J, "Transitions in the lubrication of concentrated contacts", PhD dissertation, University of Twente, The Netherlands, 1988.

Semiatin S L, Seetharaman V, Weiss I, "Hot workability of titanium and titanium aluminide alloys – an overview", Materials Science and Engineering, Vol. A243, pp 1-24, 1998.

Shaw M C, Ber A and Mamin P A, "Friction characteristics of sliding surfaces undergoing subsurface plastic flow", Transactions of the ASME, serial D, Journal of Basic Engineering, Vol. 82, pp 342-362, 1960.

Shaw M C, "The role of friction in deformation processing", Wear, Vol. 6, pp 140-158, 1963.

Siegert K, Haussermann M, Losch B, Rieger R, "Recent developments in hydroforming technology", Journal of Materials Processing Technology, Vol. 98, pp 251-258, 2000.

Stephen D, "Superplastic forming and diffusion bonding of titanium", in 'Designing with titanium', The Institute of Metals, pp 108-124, 1986.

Story J M, "Superplasticity and superplastic forming", Ed. C.H.Hamilton and N.E.Paton, TMS, Warrendale, PA, USA, pp 297-302, 1988.

Suzuki N, Kohzu M, Tanabe S and Higashi K, "Control of thickness distribution in a Al7475 axisymmetric cup", Materials Science Forum, Vols. 357-359, pp 565-570, 2001.

Tabor D, "Friction - the present states of our understanding", ASME Journal of Lubrication Technology, Vol. 103, pp 169-179, 1981.

Tabor D, "Friction and wear - developments over the last fifty years", in "Tribology – Friction, Lubrication and Wear Fifty Years on", IMECHE, pp 157-172, 1987.

Takahashi A, Shimizu Sand Tsuzuku T, Japan Soc.for Tech.of Plasticity, Vol. 31(336), pp 1128-1134, 1990.

Tan X, "Friction-reducing contact area expansion in upsetting", Proceedings of Institution of Mechanical engineers, Part J, Journal of Engineering Tribology, Vol. 215, pp 189-200, 2001.

Tan X, Martins P A F, Bay N and Zhang W, "Friction studies at different normal pressures with alternative ring-compression tests", Journal of Materials Processing Technology, Vol. 80, pp 292-297, 1998.

Tan X, Bay N and Zhang W, "On parameters affecting metal flow and friction in the double cup extrusion test", Scandinavian Journal of Metallurgy, Vol. 27(6), pp 246-252, 1998.

Tang S and Robbins T L, "Bulging rupture of a superplastic sheet", Transactions of ASME, Vol. 96(1), p77-89, 1974.

Thiruvarudchelvan S, Lewis W, "A note on hydroforming with constant fluid pressure", Journal of Materials Processing Technology, Vol. 88, pp 51-56, 1999.

Tiesler N and Engel U, "Microforming - effects of miniaturization", Metal forming 2000, Pietrzyk et al.(eds), Balkema, Rotterdam, pp 355-360, 2000.

Underwood E E, "A review of superplasticity and related phenomenon", Journal of Metal Technology, Vol. 14, pp 914-919, 1962.

Valiev R Z, Korznikov A V, and Mulyukov R R, Material Science and Engineering, Vol. A168, pp 141-148, 1993.

Van Rooyen G T and Backofen W A, "A study of interface friction in plastic compression", International Journal of Mechanical Sciences, Vol. 1, pp 1-27, 1960.

Vetrano J S, "Superplasticity: mechanisms and applications", JOM, Vol. 53(3), pp 22-24, 2001

Vieillendent D and Fourment L, "Metallurgical qualities improvement by automatic preform design of forging processes", Metal Forming 2000, pp 157-162, 2000.

Wagoner R H, Wang W and Sriram S, "Development of OSU formability test and OSU friction test", Journal of Materials Processing Technology. Vol. 45, pp 13-18, 1994.

Wang F and Lenard J G, "An experimental study of interfacial friction-hot ring compression", ASME Journal of Engineering Materials and Technology, Vol. 114, pp 13-18, 1992.

Wang N M, "A mathematical model of drawbead forces in sheet metal forming", Journal of applied metalworking, Vol. 2, pp 193-205, 1982.

Wanheim T, "Friction at high normal pressures", Wear, Vol. 25, pp 225-244, 1973.

Wanheim T and Bay N, "A model for friction in metal forming processes", Annals of CIRP, Vol. 27(1), pp 189-194, 1978.

Wanheim T, Bay N and Peterson A S, "A theoretically determined model for friction in metal working processes", Wear, Vol. 29, pp 251-258, 1974.

Weisert E D, "A structural basis for superplasticity", Titanium Science and Technology, Vol. 2, pp 1221-1225, 1984.

Wert J A, Paton N E, Hamilton C H and Mahoney M W, "Grain refinement in 7075 aluminium by thermomechanical processing", Metallurgical Transactions A, Physical Metallurgical and Material Science, Vol. 12A, pp 1267-1276, 1981.

Williams J A, "Engineering Tribology", Oxford Science Publications, 1994.

WinDIG 2.5 Data Digitzer, Dominique Lovy, 1994-2002.

Wolff C, Pawelski O and Pasp W, "A newly developed test method for characterization of frictional conditions in metal forming", Metal Forming 2000, pp 91-97, 2000.

Wood R D, Bonet J, "A review of the numerical analysis of superplastic forming", Journal of Materials Processing Technology, Vol. 60, pp 45-53, 1996.

Xing H L and Wang Z R, "Finite-element analysis and design of thin sheet superplastic forming", Journal of Materials Processing Technology, Vol. 68, pp 1-7, 1997

Yang C F, Chiu L H M and Lee S C, "Superplastic forming of 7475 Al alloy by variable-pressure blowing", Scripta Materialia, Vol. 34(10), pp 1555-1560, 1996,

Yang H S and Mukherjee A K, "An analysis of the superplastic forming of a circular sheet diaphragm", International Journal of Mechanical Sciences, Vol. 34(4), pp 283-297, 1992.

Zienkiewicz O, "The Finite Element method", McGraw-Hill, 1977

Zienkiewicz O C, Onate E and Cheinrich J, "Plastic flow in metal forming, 1. Coupled thermal, 2. Thin sheet forming, Applications of numerical methods to forming processes", Proceedings of Winter Annual Meeting ASME New York, Vol. 28, pp 107-120, 1978.

Zienkiewicz O and Taylor R, "The Finite Element Method", Vols. 1-2, 4th Edition, McGraw Hill, Nov. 1989.

Zhang B, Mynors D J, Mugarra, A and Ostolaza K, "Representing the superplasticity of Inconel 718", Journal of Materials and Processing Technology, 2004.

Zhang S H, "Developments in hydroforming", Journal of Materials Processing **Technology**, Vol. 91, pp 236-244, 1999.

Zhang W C, Wood R D and Zienkiewicz O C, "Superplastic forming analysis using a **finite** element viscous flow formulation", Proceedings of Aluminium Technology'86, **London**, pp1111-1116, 1986.

Zhou D J, Lian J and Suery M, "Numerical study of superplastic deformation with **superimposed** pressure for cavity sensitive materials", Materials Science and **Technology**, Vol. 4, pp 348-353, 1988.

Appendix 1 Typical ABAQUS Input Files for Simulation

1.1 Two Dimensional Cylindrical Cup Case

```
*HEADING
 SUPERPLASTIC BLOW FORMING OF CYLINDRICAL CUP WITH Ti-6Al-4V
 WITH FOUR-NODED AXISYMMETRIC ELEMENT CAX4R,
**Note: This input file is used in Chapter 5 for preliminary studies.
** The simulations carried out in Chapter 8, geometry definition, material property
**(Pb-Sn alloy) and friction coefficient should be changed respectively.
**----------------------------------------------------------------------
*RESTART, WRITE, FREQUENCY=5
**----------------------------------------------------------------------
**GEOMETRY DEFINITION (INCLUDING NODES AND ELEMENT
**DEFINITION)
**----------------------------------------------------------------------
*NODE
 1,0,0
 45,0.045,0
 75,0.051,0
 113,0.089,0
 158,0.098,0
 171,0.11,0
 4001,0,0.00125
 4045,0.045,0.00125
 4075,0.051,0.00125
 4113,0.089,0.00125
 4158,0.098,0.00125
 4171,0.11,0.00125
*NGEN, NSET=BOT
 1,45,1
 45,75,1
 75,113,1
 113,158,1
 158,171,1
*NGEN, NSET=TOP
 4001,4045,1
 4045,4075,1
 4075,4113,1
 4113,4158,1
 4158,4171,1
*NSET, NSET=AXIS, GENERATE
 1,4001,1000
*NSET, NSET=RIGHT, GENERATE
 171,4171,1000
*NFILL, NSET=PLATE
 BOT, TOP, 4, 1000
*NSET, NSET=MIDLEFT, GENERATE
 2001,2125,1
*NSET, NSET=MIDRIGHT, GENERATE
 2150,2171,1
*ELEMENT, TYPE=CAX4R, ELSET=PLAIN1
```

```
 1,1,2,1002,1001
*ELGEN, ELSET=PLAIN
 1,170,1,1,4,1000,1000
*ELSET, ELSET=SHEET-BOTTOM, GENERATE
 1,170,1
*ELSET, ELSET=SHEET-TOP, GENERATE
 3001,3170,1
*ELSET, ELSET=SHEET-BOT1, GENERATE
 1,152,1
*ELSET, ELSET=SHEET-BOT2, GENERATE
 143,170,1
**-----------------------------------------------------------------------
**UPPER-DIE DEFINITION
**-----------------------------------------------------------------------
*RIGID SURFACE, TYPE=SEGMENTS, NAME=DIE, FILLET RADIUS=0.005,
    REF NODE=10000
 START, 0.125, 0.00125
 LINE, 0.095, 0.00125
 CIRCL, 0.09, 0.00625, 0.095, 0.00625
 LINE, 0.09, 0.07625
 CIRCL, 0.085, 0.08125, 0.085, 0.076253115
 LINE, -0.01,0.08125
*NODE, NSET=REFDIE
 10000,0,0.00125
**-----------------------------------------------------------------------
**CONTACT SURFACE DEFINITION-SHEET & UPPER DIE
**-----------------------------------------------------------------------
*SURFACE DEFINITION, NAME=PLAIN-TOP
 SHEET-TOP, S3
*CONTACT PAIR, INTERACTION=FRIC2, HCRIT=0.01
 PLAIN-TOP, DIE
*SURFACE INTERACTION, NAME=FRIC2
*FRICTION
 0.4
**-----------------------------------------------------------------------
**LOWER-DIE DEFINITION
**-----------------------------------------------------------------------
*RIGID SURFACE, TYPE=SEGMENTS, NAME=DIE-DOWN, FILLET
RADIUS=0.005,
    REF NODE=30000
 START, 0.09, -0.01
 LINE, 0.09, 0.
 LINE, 0.125,0
*NODE, NSET=REFDIE-DOWN
 30000,0.125, -0.01
**-----------------------------------------------------------------------
**CONTACT SURFACE DEFINITION-SHEET & LOWER DIE
**-----------------------------------------------------------------------
*SURFACE DEFINITION, NAME=PLAIN-BOT
 SHEET-BOT2, S1
```

```
*CONTACT PAIR, INTERACTION=FRIC3, HCRIT=0.01
 PLAIN-BOT, DIE-DOWN
*SURFACE INTERACTION, NAME=FRIC3
*FRICTION
 0.4
**------------------------------------------------------------------------
**MATERIAL PROPERTIES DEFINITION
**------------------------------------------------------------------------
*SOLID SECTION, ELSET=PLAIN, MATERIAL= Ti-6Al-4V
*ORIENTATION, NAME=LOCAL
 1.,0.,0.,0.,1.,0.,
*MATERIAL, NAME= Ti-6Al-4V
*ELASTIC
 2.0e10, 0.3
**------------------------------------------------------------------------
** CREEP DEFINITION
**------------------------------------------------------------------------
*CREEP, LAW=TIME
 1.9853e-15, 1.63,0
**------------------------------------------------------------------------
**MINIMUM AND MAXIMUM LIMITS OF LOADING
**------------------------------------------------------------------------
*AMPLITUDE, DEFINITION=SOLUTION DEPENDENT, NAME=AUTO
 1., 0.0001, 1.e6
**========================================================================
**STEP 1 PUSH THE UPPER-DIE AND BLANK TOGETHER
**========================================================================
*STEP, INC=50, NLGEOM
*STATIC
 1., 1.
*CONTACT INTERFERENCE, SHRINK
 PLAIN-TOP, DIE
 PLAIN-BOT, DIE-DOWN
*BOUNDARY
 MIDRIGHT, 2
 MIDLEFT, 2
 AXIS, XSYMM
 10000,1,1
 10000,2, ,-1.e-8
 10000,6
 30000,1,2
 30000,6
 RIGHT, 1, 1
*END STEP
**========================================================================
**STEP 2 REMOVE THE MIDDLE CONSTRAINT
**========================================================================
*STEP, INC=50,NLGEOM
*STATIC
 1.0,1.0
```

```
*BOUNDARY, OP=NEW
 MIDLEFT, 2
 AXIS, XSYMM
 10000,1
 10000,6
 10000,2,,-1.e-8
 30000,1,2
 30000,6
 RIGHT, 1, 1
*END STEP
**=============================================================
**STEP 3 APPLY PRESCRIBED FORCE ON THE UPPER-DIE
**=============================================================
*STEP, INC=100,NLGEOM
*STATIC
 0.1,1.0
*BOUNDARY, OP=NEW
 MIDLEFT,2
 AXIS, XSYMM
 10000,1,1
 10000,6
 30000,1,2
 30000,6
 RIGHT, 1, 1
*CLOAD
 10000,2, -1e5
*END STEP
**=============================================================
**STEP 4 ADD PRESSURE ON THE BOTTOM OF THE BLANK
**=============================================================
*STEP, INC=30,NLGEOM
*STATIC
 0.1,1.0
*BOUNDARY, OP=NEW
 AXIS, XSYMM
 10000,1,1
 10000,6
 30000,1,2
 30000,6
 RIGHT, 1, 1
*DLOAD
 SHEET-BOT1, P1, 500
*CONTACT PRINT, FREQUENCY=10
*CONTACT FILE, FREQUENCY=10
*END STEP
**=============================================================
**STEP 5 CREEP FORMING PROCESS
**=============================================================
*STEP, INC=1000,NLGEOM, UNSYMM=YES
*VISCO, CETOL=5.e-3
```

```
 1e-6, 2100
*BOUNDARY, OP=NEW
 AXIS, XSYMM
 10000,1,1
 10000,6
 30000,1,2
 30000,6
 RIGHT, 1, 1
 10000,2
*DLOAD, AMPLITUDE=AUTO
 SHEET-BOT1, P1, 500
*CREEP STRAIN RATE CONTROL, ELSET=PLAIN, AMPLITUDE=AUTO
 0.001
*NODE FILE, NSET=PLATE, FREQUENCY=5
 U
 COORD
*NODE PRINT, NSET=PLATE, FREQUENCY=5
 COORD
*EL FILE, ELSET=PLAIN, FREQUENCY=5
 LOADS
 S
 E
 CE
 SINV
*END STEP
```

1.2 Reverse Forming Simulation Case

```
*HEADING
REVERSE SUPERPLASTIC BLOW FORMING OF COMPLEX TOOLS WITH
TI-6AL-4V ALLOYS
**Note: This input file is used in Chapter 5 for preliminary studies.
** The simulations carried out in Chapter 8, geometry definition, material property
**(Pb-Sn alloy) and friction coefficient should be changed respectively.
**----------------------------------------------------------------------
*RESTART, WRITE, FREQUENCY=15
**----------------------------------------------------------------------
**GEOMETRY DEFINITION (INCLUDING NODES AND ELEMENTS
**DEFINITION)
**----------------------------------------------------------------------
*NODE
1,0,0
37,0.037,0
533,0.16,0
4001,0,0.003
4037,0.037,0.003
4533,0.16,0.003
*NGEN,NSET=BOT
1,37,1
37,533,1
*NGEN,NSET=TOP
4001,4037,1
4037,4533,1
*NSET,NSET=AXIS,GENERATE
1,4001,1000
*NSET, NSET=RIGHT, GENERATE
533,4533,1000
*NFILL,NSET=PLATE
BOT,TOP,4,1000
*ELEMENT,TYPE=CAX4R,ELSET=PLAIN1
1,1,2,1002,1001
*ELGEN,ELSET=PLAIN
1,532,1,1,4,1000,1000
*ELSET, ELSET=SHEETTOP, GENERATE
3001,3532,1
*ELSET, ELSET=SHEETBOT, GENERATE
1,532,1
**----------------------------------------------------------------------
**UPPER-DIE DEFINITION
**----------------------------------------------------------------------
*RIGID SURFACE, TYPE=SEGMENTS, NAME=UPPERDIE, FILLET
RADIUS=0.0001, REF NODE=10000
START,0.18,0.003
LINE,0.15187,0.003
CIRCL,0.1434806,0.0075577,0.15187,0.013
```

```
LINE,0.1287163,0.0303171
CIRCL,0.1159435,0.0591354,0.21261,0.08174
CIRCL,0.1106241,0.0655496,0.106285,0.05654
CIRCL,0.0799134,0.0624075,0.097755,0.03845
CIRCL,0.0746402,0.0533264,0.084795,0.05368
CIRCL,0.0663806,0.0135948,-0.075,0.06371
CIRCL,0.0432701,0.0029285,0.04836,0.02227
LINE,0.00625,0.0126707
CIRCL,0.003705,0.013,0.003705,0.003
LINE,-0.003,0.013
*NODE, NSET=REFUPPERDIE
10000,0,0.003
**----------------------------------------------------------------
**CONTACT SURFACE DEFINITION –SHEET & UPPER DIE
**----------------------------------------------------------------
*SURFACE DEFINITION, NAME=PLAINTOP
SHEETTOP,S3
*CONTACT PAIR, INTERACTION=FRIC1, HCRIT=0.01
PLAINTOP, UPPERDIE
*SURFACE INTERACTION, NAME=FRIC1
*FRICTION
0.4
**----------------------------------------------------------------
**LOWER-DIE DEFINITION
**----------------------------------------------------------------
*RIGID SURFACE, TYPE=SEGMENTS, NAME=LOWERDIE, FILLET
RADIUS=0.0001, REF NODE=20000
START,-0.01,-0.10293
LINE,0.070965,-0.10293
CIRCL,0.080965,-0.09293,0.070965,-0.09293
LINE,0.08818,-0.02596
CIRCL,0.09414,-0.02,0.09414,-0.02596
LINE,0.115,-0.02
CIRCL,0.1202016,-0.024978,0.115,-0.025
CIRCL,0.1397706,-0.0276988,0.1302,-0.0248
LINE,0.1470847,-0.0035506
CIRCL,0.15187,0,0.15187,-0.005
LINE,0.18,0
*NODE, NSET=REFLOWERDIE
20000,0, -0.01
**----------------------------------------------------------------
**CONTACT SURFACE DEFINITION –SHEET & LOWER DIE
**----------------------------------------------------------------
*SURFACE DEFINITION, NAME=PLAINBOT
SHEETBOT, S1
**
*CONTACT PAIR, INTERACTION=FRIC2, HCRIT=0.02
PLAINBOT, LOWERDIE
*SURFACE INTERACTION, NAME=FRIC2
*FRICTION
```

```
0.4
*SOLID SECTION, ELSET=PLAIN, MATERIAL=TI6/4, ORIENTATION=LOCAL
*ORIENTATION,NAME=LOCAL
1.,0.,0.,0.,1.,0.,
0,0.,
*MATERIAL,NAME=TI6/4
*ELASTIC
2.3e10,0.3
**----------------------------------------------------------------------
** CREEP DEFINITION
**----------------------------------------------------------------------
*CREEP,LAW=TIME
2.673e-14,1.43,0
**----------------------------------------------------------------------
**MINIMUM AND MAXIMUM LIMITS OF LOADING
**----------------------------------------------------------------------
*AMPLITUDE, DEFINITION=SOLUTION DEPENDENT, NAME=AUTO
1.,0.0001,1.e6
**----------------------------------------------------------------------
**BOUNDARY CONDITIONS
**----------------------------------------------------------------------
*BOUNDARY
AXIS,xsymm
10000,1,2
10000,6
20000,1,2
20000,6
right,1,1
1533,2
2533,2
3533,2
**======================================================================
**STEP 1 ADD PRESSURE ON THE BOTTOM OF THE BLANK
**======================================================================
*STEP,INC=25,NLGEOM
*STATIC
0.001,1.0
*DLOAD
SHEETBOT,P1,500.
*END STEP
**======================================================================
**STEP 2 CREEP TO THE UPPERDIE
**======================================================================
*STEP,INC=250,NLGEOM,UNSYMM=YES
*VISCO,CETOL=0.05
1.e-6,1900
*DLOAD,AMPLITUDE=AUTO
SHEETBOT,p1,500.
*CREEP STRAIN RATE CONTROL, ELSET=PLAIN, AMPLITUDE=AUTO
0.001
```

```
*NODE FILE, NSET=PLATE,FREQUENCY=15
U
COORD
*NODE PRINT,NSET=PLATE,FREQUENCY=15
COORD
U
*EL FILE,ELSET=PLAIN,FREQUENCY=15
LOADS
S
E
CE
SINV
*EL PRINT, ELSET=PLAIN, FREQUENCY=15
LOADS
S
E
CE
CEEQ
*PRINT, CONTACT=YES
*CONTACT INTERFERENCE, TYPE=CONTACT PAIR
PLAINBOT,LOWERDIE,0.000001
PLAINTOP, UPPERDIE,0.000001
*END STEP
**==========================================================
**STEP 3 REMOVE THE CONTACT SURFACE OF THE UPPERDIE AND
**SHEET
**==========================================================
*STEP, INC50, NLGEOM, UNSYMM=YES
*VISCO, CETOL=0.05
1.e-5,1.
*BOUNDARY, FIXED
PLATE, 1,2
*MODEL CHANGE, TYPE=CONTACT PAIR, REMOVE
PLAINTOP, UPPERDIE
*DLOAD, OP=NEW
*CREEP STRAIN RATE CONTROL, AMPLITUDE=AUTO, OP=NEW
*PRINT,MODEL CHANGE=YES
*END STEP
**==========================================================
**STEP 4 CREEP TO THE LOWERDIE
**==========================================================

*STEP,INC=600,NLGEOM,unsymm=yes
*VISCO,CETOL=0.05
1e-6,3200
*DLOAD,AMPLITUDE=AUTO, OP=NEW
SHEETTOP,p3,5000
*CREEP STRAIN RATE CONTROL, ELSET=PLAIN, AMPLITUDE=AUTO,
OP=NEW
0.001
```

```
*BOUNDARY, OP=NEW
AXIS,XSYMM
10000,1,2
10000,6
20000,1,2
20000,6
right,1,1
1533,2
2533,2
3533,2
*NODE FILE,NSET=PLATE,FREQUENCY=20
U
COORD
*NODE PRINT,NSET=PLATE,FREQUENCY=20
COORD
U
*EL FILE,ELSET=PLAIN,FREQUENCY=20
LOADS
S
E
CE
SINV
*EL PRINT, ELSET=PLAIN, FREQUENCY=20
LOADS
S
E
CE
CEEQ
*CONTACT INTERFERENCE, TYPE=CONTACT PAIR
PLAINTOP, LOWERDIE, 0.00003
*END STEP
```

Appendix 2 Fortran Codes for Thickness and Strain Distribution

2.1 Thickness distribution

```
      PROGRAM MAIN
C     THIS PROGRAM READS ABAQUS OUTPUT DATA, CALCULATE THE
C     ARC DISTANCE FROM THE CENTRE AND THICKNESS
C     ------------------------------------------------------------------
C     PARAMETER AND ARRAY DEFINITION
C     ------------------------------------------------------------------
      parameter(Mesh=318)
      double precision distance,thick,u1(5*mesh,3),arc_dis_cen(mesh,3)
      open(1,file='coords-geom6.txt',status='old')
      open(2,file='Th_arcdis_geom6.dat',status='unknown')
C     ------------------------------------------------------------------
C     READ ABAQUS OUTPUT COORDINATES INTO THE PROGRAM
C     ------------------------------------------------------------------
      read(1,*) ((u1(i,j),j=1,3),i=1,5*Mesh)
C     ------------------------------------------------------------------
      arc_dis_cen(1,2)=0.0
      arc_dis_cen(1,1)=2001.
C     ------------------------------------------------------------------
C     CALCULATION OF THE ARITHMETIC ARC LENGTH ALONG THE
C     COMPONENT
C     ------------------------------------------------------------------
      do i=2*mesh+1,3*mesh-1
         distance=dsqrt((u1(i,2)-u1(i+1,2))**2+(u1(i,3)-u1(i+1,3))**2)
         arc_dis_cen(i+1-2*mesh,2)=distance+arc_dis_cen(i-2*mesh,2)
         arc_dis_cen(i+1-2*mesh,1)=i+1-2*mesh+2000
      end do
C     ------------------------------------------------------------------
C     CALCULATION OF THE THICKNESS OF THE SHEET
C     ------------------------------------------------------------------
      do i=1,mesh
         Thick=dsqrt((u1(i,2)-u1(4*mesh+i,2))**2+
     &      (u1(i,3)-u1(4*mesh+i,3))**2)
```

```
            arc_dis_cen(i,3)=Thick
        end do
C       ------------------------------------------------------------------
C       OUTPUT
C       ------------------------------------------------------------------
        do i=1,mesh
            write(2,22) arc_dis_cen(i,1),arc_dis_cen(i,2)*1.e3,
     &                  arc_dis_cen(i,3)*1.e3               !mm
22          format(1x, f6.1,4x,d18.8,4x,d18.8)
        end do
C       ------------------------------------------------------------------
C       CLOSE FILES
C       ------------------------------------------------------------------
        close(1)
        close(2)


        end
```

2.2 Strain Distribution

```
      PROGRAM MAIN
C     THIS PROGRAM READS ABAQUS OUTPUT DATA, CALCULATE THE
C     ARC DISTANCE FROM THE CENTRE AND STRAIN DISTRIBUTION----
C     ------------------------------------------------------------------
C     PARAMETER AND ARRAY DEFINITION
C     ------------------------------------------------------------------

      parameter(Mesh=533, MM=532)
      real distance,thick,u1(5*mesh,3), arc_dis_cen(mesh,3)
      real ce(4*MM,9),strain(MM,6)
C     ------------------------------------------------------------------
C     READ COORDINATES INTO THE PROGRAM
C     ------------------------------------------------------------------

      open(1,file='coords-jij07-add.txt',status='old')
      open(2,file='Th_arcdis_jij07-add.dat',status='unknown')
      open(3,file='Th_strain_jij07-add.dat',status='unknown')
      open(4,file='ce-jij07-add-a.txt',status='old')
C     ------------------------------------------------------------------
C     READ ABAQUS OUTPUT COORDINATES INTO THE PROGRAM
C     ------------------------------------------------------------------

       read(1,*) ((u1(i,j), j=1,3),i=1,5*Mesh)
       read(4,*) ((ce(i,j), j=1,9),i=1,4*MM)
C     ------------------------------------------------------------------

      arc_dis_cen(1,2)=0.0
      arc_dis_cen(1,1)=2001.
C     ------------------------------------------------------------------
C     CALCULATION OF THE ARITHMETIC ARC LENGTH OF THE SHEET
C     ------------------------------------------------------------------

      do i=2*mesh+1,3*mesh-1
         distance=sqrt((u1(i,2)-u1(i+1,2))**2+(u1(i,3)-u1(i+1,3))**2)
         arc_dis_cen(i+1-2*mesh,2)=distance+arc_dis_cen(i-2*mesh,2)
         arc_dis_cen(i+1-2*mesh,1)=i+1-2*mesh+2000
      end do
C     ------------------------------------------------------------------
C     CALCULATION OF THE STRAIN THICKNESS OF THE SHEET
C     ------------------------------------------------------------------

      do i=1,mesh
         Thick=sqrt((u1(i,2)-u1(4*mesh+i,2))**2+
     &              (u1(i,3)-u1(4*mesh+i,3))**2)
         arc_dis_cen(i,3)=Thick
```

```
      end do

      do i=1,mesh-1
         strain(i,1)=(arc_dis_cen(i,2)+arc_dis_cen(i+1,2))/2.
         strain(i,2)=ce(i,4)
         strain(i,3)=ce(i+MM,4)
         strain(i,4)=ce(i+2*MM,4)
         strain(i,5)=ce(i+3*MM,4)
         strain(i,6)=(strain(i,2)+strain(i,3)+strain(i,4)+strain(i,5))/4.
      end do
C     ------------------------------------------------------------------
C     OUTPUT
C     ------------------------------------------------------------------

      do i=1,mesh
         write(2,22) arc_dis_cen(i,1),arc_dis_cen(i,2)*1.e3,
     &                  arc_dis_cen(i,3)*1.e3          !mm
22       format(1x, f6.1,4x,f18.8,4x,f18.8)
      end do

      do i=1,MM
         write(3,23) strain(i,1)*1.e3, strain(i,2), strain(i,3),
     &               strain(i,4), strain(i,5), strain(i,6)
23       format(1x, d18.8,4x,f18.8,4x,f18.8,4x,f18.8,4x,f18.8,4x,f18.8)
       end do
C     ------------------------------------------------------------------
C     CLOSE FILES
C     ------------------------------------------------------------------

      close(1)
      close(2)
      close(3)
      close(4)

       end
```

Appendix 3 An Illustration of Image Processing for the Calculation of Strain Rate

Calculation of the Strain Rate

It is very difficult to directly measure the strain rate using a strain gauge during superplastic forming. Not only does a large amount of deformation occur, which is far in excess of the measuring capacity of an ordinary strain gauge, but also because the introduction of a strain gauge within the sealed pressure container inevitably changes the friction behaviour. Indirect method is employed in this research by using a digital camera in the experiments to record the deformation process then calculate the strain rate. For this purpose, a transparent die made from Perspex is designed and built to enable the whole deformation process to be recorded. As the strain rate is proportional to the deforming length the acquisition of the deformed length is the main consideration.

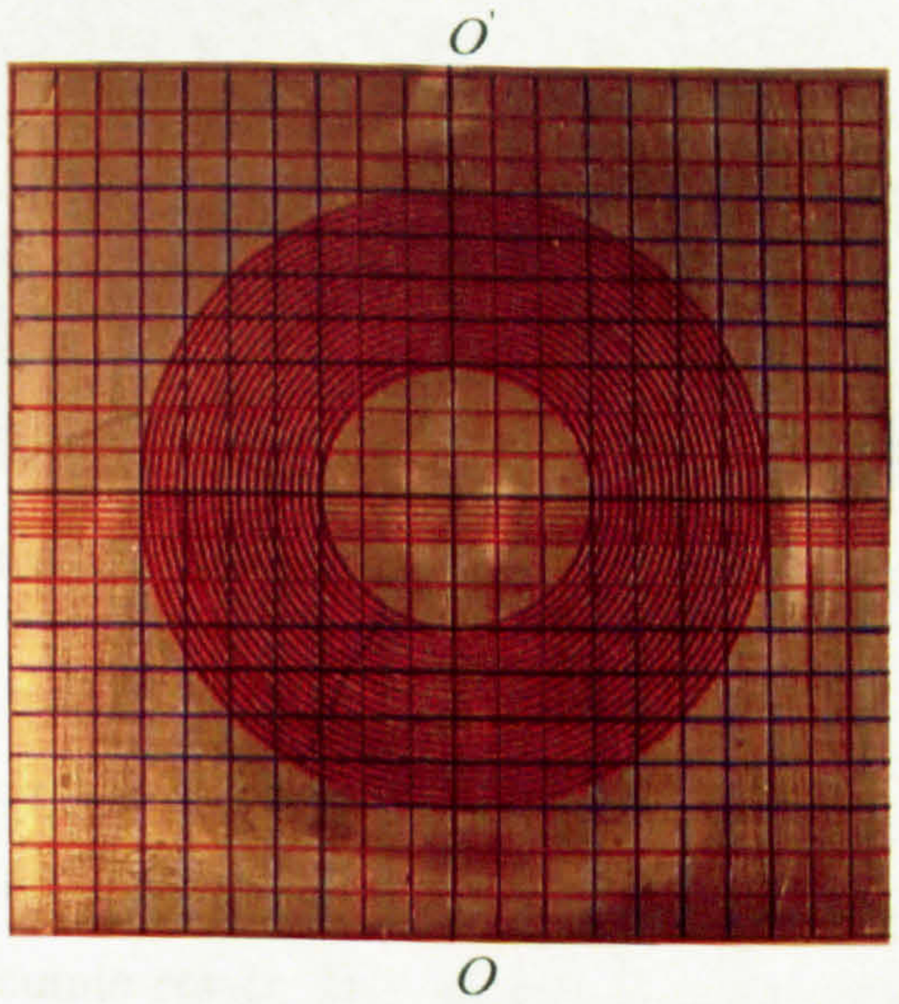

Figure A1 Undeformed sheet

In order to obtain the deformed length, two points in contact between the sheet and the die in a time interval Δt must be obtained. For this purpose, the surface of a blank sheet is drawn with grids and concentric circles with 1 mm intervals as shown in Figure A1. When the sheet is gradually inflated into contact with the forming die, these concentric circles remain circular with their centres in the symmetric axis of the deformed component. The marked grid, OO' shown in Figure A1, is also shown in Figure A2. Because of symmetry, every point in the same concentric circle is in

contact with the die at the same time instant. Therefore, at a given time instant t_1 when point A is in contact with the die, point B is also in contact with the die. At the next time instant t_2, points C and D will be in contact with the die during the blow forming process. The length of AC, l_{AC}, is equal to l_{BD} at each time instant because of symmetry, but in the calculation, the length of BD, l_{BD}, was used because it is relatively easier to acquire with a higher accuracy in practice. Therefore, the strain rate $\dot{\varepsilon}$ is calculated by,

$$\dot{\varepsilon}_{t_2} = \left[\frac{(l_{BD})_{t_2} - (l_{BD})_{t_1}}{(l_{BD})_{t_2}} \right] \Big/ (t_2 - t_1) \tag{A1}$$

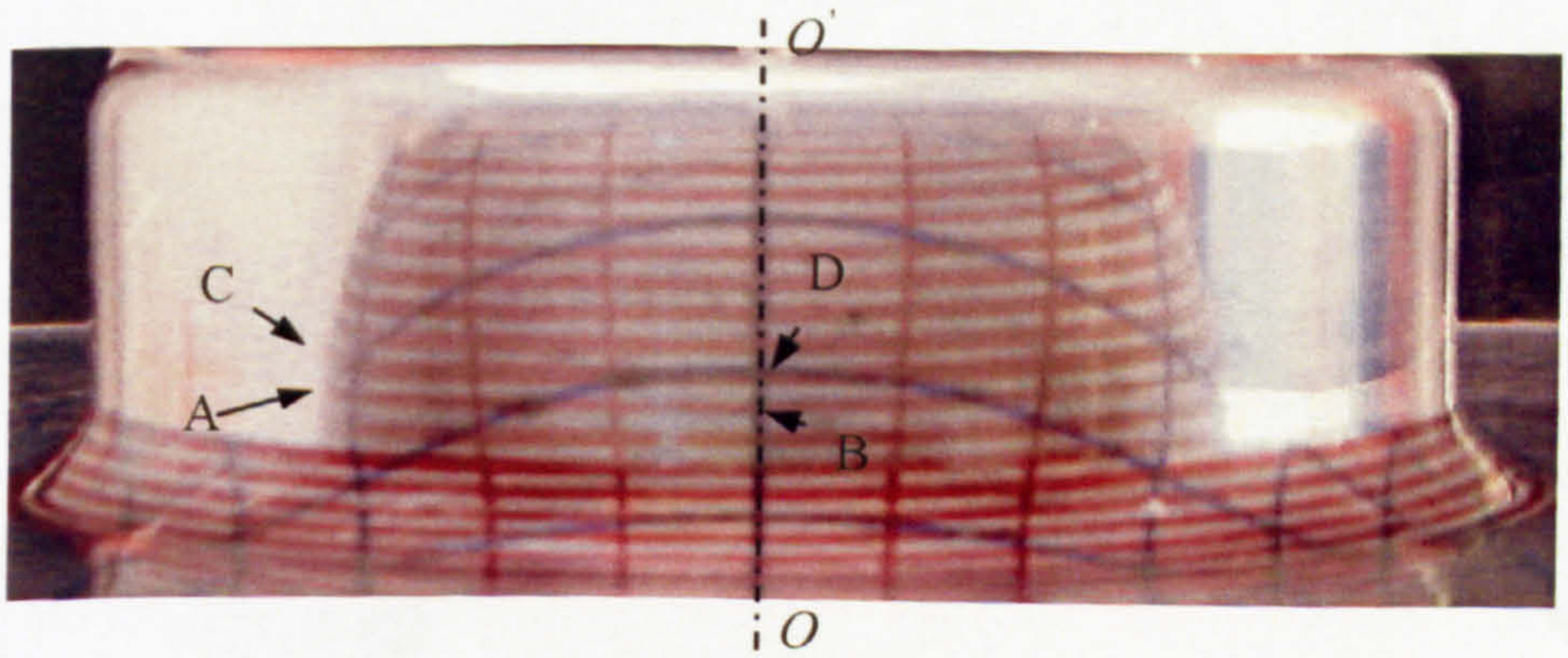

Figure A2 Deforming instant taking by a camera

With each instant of deformation recorded by a digital camera, the strain rate $\dot{\varepsilon}$ can be calculated. In practice, the values of strain rate at different contact regions are averaged for a more accurate result. The calculated strain rates are then input to the derived equations from Chapter 6 to calculate the friction coefficients at each contact region.

Appendix 4 Animation CD of Blow Forming Processes

Appendix 5 Author's Publications

ELSEVIER

Materials and Design 22 (2001) 679–685

Materials & Design

Numerical analysis of superplastic blow forming of Ti–6Al–4V alloys

Y. Chen*, K. Kibble, R. Hall, X. Huang

Engineering Division, School of Engineering and Built Environment, University of Wolverhampton, Wolverhampton, UK

Received 12 October 2000; accepted 3 January 2001

Abstract

The superplastic blow forming of a Ti–6Al–4V sheet into a cylindrical cup has been numerically analysed based on the actual forming process using ABAQUS. A detailed element type study has been performed to eliminate the element dependency in the finite element analysis. The accuracy and reliability of the proposed finite element model has been validated in comparison with experimental data. The validation proves that, there is a good agreement between the simulation and the experiment. In addition, the best prediction of the thickness distribution can be obtained using the continuum element. Furthermore, the effects of major factors such as friction coefficient and the strain rate sensitivity index upon the optimum forming pressure-time and thickness distribution of the component have been studied systematically using the proposed finite element model.

Keywords: Superplastic blow forming; Numerical analysis; Friction

1. Introduction

Superplastic forming (SPF) is a major production method for the manufacture of aircraft parts that have complex shapes and require lightweight design [1]. In general, superplastic materials are polycrystalline solids which have the ability to undergo large uniform strain prior to failure. Among superplastic materials, titanium alloys such as Ti–6Al–4V have found wide applications in the aerospace industry because of their superior properties such as a high strength-to-weight ratio, high temperature tolerance and excellent corrosion resistance. Blow forming process is one of the most important and widely used SPF methods in recent years. During the blow forming process, gas pressure is imposed over a sheet to make it flow into a die of the desired shape. To produce maximum ductility in the SPF process, it is desirable to adjust the forming pressure to keep the strain rate within an optimum range throughout the whole forming process. Friction between the die and the sheet is found to significantly affect thinning of the component during the blow forming process [2]. Severe thinning will lead to failure of the component. Therefore, to obtain successful manufacture of SPF products, it is essential to have a better understanding of the forming process.

Compared to costly experiments, the finite element method (FEM) has evoked considerable interest in superplastic blow forming because it can provide direct information and guidance in reducing the number of tests, or even eliminating the need for expensive trial-and-error testing. Chandra [3] investigated an isoparametric continuum element formulation which can model the effects of bending and shear stress. Bonet et al [4] developed a general 3D finite element formulation by using a three-node triangular membrane ele-

* Corresponding author. Tel.: +44-1902-322273; fax: +44-1902-322680.

E-mail address: y.y.chen@wlv.ac.uk (Y. Chen).

ment. A strain rate constraint equation was also introduced to control the gas pressure to maintain an optimum strain rate during the superplastic forming process. Chenot et. al. [5] developed an isoparametric membrane element approach for the 3D simulation and a plane-strain element formulation for 2D circumstance. However, all of these simulations ignored the fact that the circumference of the sheet is clamped during the actual process. As a result, contact interaction between the clamped part of the sheet and the dies is not considered in the previous literature. In addition, several types of elements have been proposed for the simulation of SPF, but it is still unclear as to which element is the most suitable one in terms of its ability to give the most accurate thickness distribution of the component.

In this paper, the full superplastic blow forming of a Ti–6Al–4V sheet into a cylindrical cup is carefully simulated using ABAQUS [6]. It is noted that not only is the clamped rim of the sheet considered, but also it follows the actual experimental process. Different element types and mesh densities have been studied to eliminate the element and mesh dependencies of the proposed analysis. The prediction of thickness distribution with different elements has been carefully compared with the experimental data. Furthermore, the effects of friction coefficient, the strain rate and the strain rate sensitivity index have been fully investigated.

2. FEM analysis

Superplastic blow forming is a complicated process involving large strain, large deformation, material non-linearity and usually deformation dependent boundary conditions. Consequently, the numerical analysis of such a highly non-linear system presents formidable computational problems. Fortunately, the superplastic behaviour of materials is characterised by the dependency of the flow stress upon the strain rate, which allows the material to be described as rigid viscoplastic. Therefore, the simulation of superplastic blow forming can be performed using the creep strain rate control scheme within ABAQUS.

A schematic diagram of a Ti–6Al–4V cylindrical cup is shown in Fig. 1. The diameter of the circular sheet is 200 mm, of which the 10-mm outer rim is clamped between the upper die and the lower die. The initial thickness of the sheet is 1.25 mm. Because of its symmetry, only half of the sheet was modelled.

Normally the following procedures are carried out during the real blow forming operations [7]. The furnace and forming apparatus are first heated to the required temperature range. The sheet is then clamped around its periphery and a gas pressure is applied to inflate the sheet against the die configuration. Therefore, several load steps corresponding to each operational procedure are carefully modelled to obtain an accurate simulation of a superplastic blow forming process in ABAQUS. A further description is provided as follows: to avoid rigid body motion and contact status oscillation, the first load step is to establish firm contact between the sheet and the two dies by means of a slight displacement of the upper die. Following that, a prescribed force is applied to the upper die to clamp the rim of the sheet as in the actual SPF process. Then the gas pressure is imposed from the bottom of the sheet, causing it to flow into the upper die geometry gradually. It should be noted that the sheet is fixed at the outside edge to avoid it slipping into the dies throughout the process. The iterative Newton–Raphson solution is chosen to solve the non-linear equations. In this way, the process of superplastic blow forming can be accurately simulated.

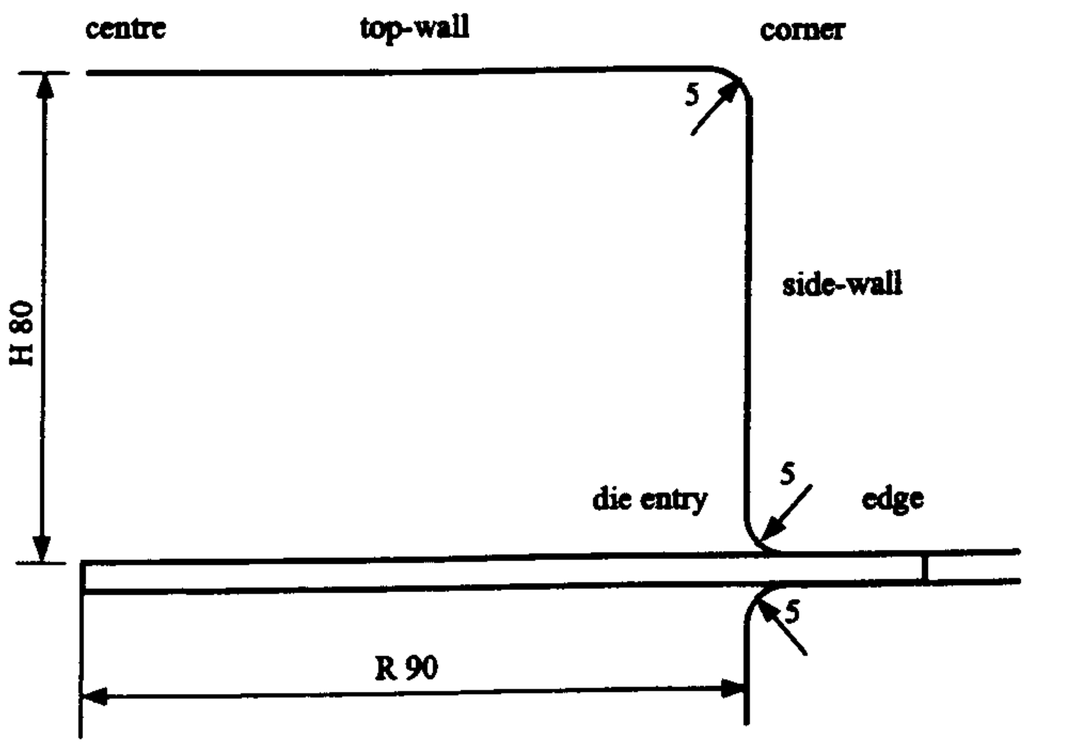

Fig. 1. Geometry of the dies and the sheet.

2.1. Material constitutive behaviour

The material constitutive behaviour of the component is very crucial for an accurate prediction of the thickness distribution during a SPF process. In this paper, the material flow behaviour is described by the empirical equation [8]:

$$\sigma = K\dot{\varepsilon}^m \tag{1}$$

Where σ is the flow stress, $\dot{\varepsilon}$ is the strain rate, K is a material constant and m is the strain rate sensitivity index, respectively. This equation defines that the flow stress is governed by the strain rate sensitivity m, which is a function of the material properties. In the simulation, this constitutive equation has been implemented using the isotropic creep material model within ABAQUS. Moreover, a special solution dependent magnitude scheme is employed to control the imposed gas pressure and maintain an approximate constant strain rate in the simulation.

2.2. Element and mesh studies

Numerical analysis of the superplastic blow forming process is generally carried out with membrane element [4,5], shell element [9] and continuum element [3,10]. Naturally, the question of which element will be the most suitable one arises. Simulations of sheet forming are performed dominantly using a membrane element because of the reduced computational cost. However, a membrane element is a surface element that only transmits the in-plane force without considering moments and bending stiffness. While in some superplastic forming processes, the sheet thickness is not small enough in comparison with the other dimensions, so that the bending effect can not be neglected. As a result, a shell element is proposed as a substitution for the membrane element. However, both membrane and shell element methods are assumed that, the thickness strain can be computed as a function of the in-surface deformation due to material incompressibility [10]. This simplified assumption does not allow for the development of stress in the thickness direction of the sheet. In fact, both sides of the sheet will be in contact with the rigid dies during a SPF process. It is difficult for either a membrane or a shell element to model this contact because they can not accommodate the thickness stresses. Therefore, a continuum element is necessary for its capability in modelling complicated non-linear analysis involving contact and large deformation [3,10].

In order to obtain a further comparison among these different elements during a superplastic blow forming process, a detail element type study has been performed. Elements studied include the four-node reduced integration axisymmetric quadrilateral continuum element (CAX4R), the first-order axisymmetric shell element (SAX1) and the first order axisymmetric membrane element (MAX1). In addition, to accurately model the SPF process, the mesh is refined accordingly in the sheet due to severe distortion and excessive thinning.

2.3. Contact algorithm

During a superplastic blow forming process, contact between the sheet and the die results in friction there. An important consideration in modelling the process is how to simulate this friction effect. In this paper, the contact algorithm between the die and the sheet was simulated by means of a rigid surface and a deformable surface. In addition, a contact pressure–clearance relationship was assigned to the surfaces to monitor the contact interaction. Associated with the contact pairs, the penalty Coulomb friction formulation [6] was employed to model the resultant friction effect characterised by a friction coefficient. The automatic 'shrink' fit option in the ABAQUS input file was used to solve the common problem of 'overclosure' during the contact. While for membrane and shell elements, the contact problems were resolved using the 'softened' contact model [6] to impose the proper clamping pressure in the thickness direction.

Table 1
Element type used in this paper

No.	Label	Element type	CPU time (s)
1	CAX4R	Continuum	794
2	SAX1	Shell	788
3	MAX1	Membrane	268

3. Validation with experimental data

The proposed FEM analysis has been validated through a careful comparison with experimental data [11]. The comparison was made possible by the fact that the simulation modelled the same geometry of configuration, the same material characteristic and the same friction contact as those in the experiment. In addition, a detail element in terms of its ability to accurately predict the thickness distribution of the component was performed and evaluated in comparison with the experimental data.

An initial comparison in terms of the computational time with different elements is summarised in Table 1. It is clearly shown that the membrane formulation is the most economical approach, as only 268 s are needed. While for the continuum and shell elements, approximately three times more will be necessary for this particular study.

The predicted distributions of sheet thickness from different elements in comparison with the experiment are shown in Fig. 2. A fairly good agreement between the prediction and experiment can be found. In addition, the experiment indicated a greater thinning existed at the corner of the upper die, which was proved in accordance with the predicted thickness variation trend from all simulations. Although the least computational time is needed, the maximum discrepancy compared to the experiment in Fig. 2 is found to be that with membrane element. Furthermore, It is clearly shown that the prediction from continuum element is the most accurate in comparison with those from shell and membrane elements, possibly because the membrane and shell elements are constructed with simple assumptions which are not valid during the superplastic blow forming process. Moreover, mesh study proves that there is no difference between the predictions from a four-layer and a two-layer continuum elements. It can be therefore concluded that the simulation using continuum element gives the most accurate prediction,

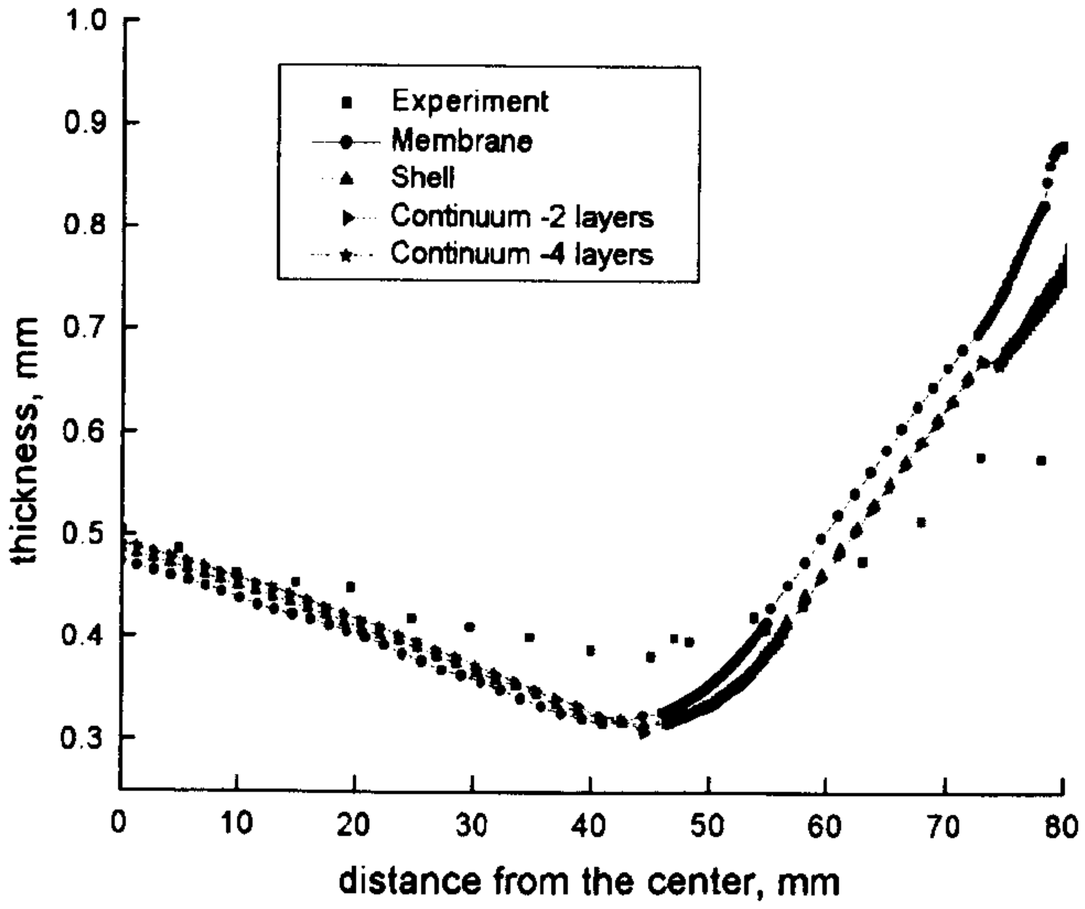

Fig. 2. Comparison of thickness distributions of different element types with experiment type.

though more computational time may be required. On the basis of the above comparison, the continuum element with two layers was chosen to carry out the following parametric studies.

4. Results and discussion

It has been demonstrated that the proposed FEM model can be used to predict accurately the thickness distribution along the component. In addition, the process of the deformed configurations of the sheet can be obtained as shown in Fig. 3. With the increase of the forming time, the sheet inflated gradually to come into contact with the upper die entry, the top wall and the side-wall of the upper die, respectively. As can be seen clearly from Fig. 3, the corner of the upper-die is the last deformed area. Furthermore, a parametric study of the effects of main factors on the thickness distribution in the superplastic forming has been fully investigated as follows.

4.1. The effect of friction coefficient

Friction is widely recognised as an important factor affecting the thinning of SPF components. The material parameters of Ti–6Al–4V alloy are taken from Cheng [12]. For an initial study, the friction coefficient is assumed uniformly along the contact surface. In addition, it is reasonable to assume that the friction coefficient ranges from 0.1 to 0.9 according to experimental measurements. Therefore, the effects of friction upon the forming pressure and the quantitative thickness distribution of the component are shown in Fig. 4a and b. The predicted optimum pressure–time curves illustrated in Fig. 4a typically show that the pressure initially rises rapidly, followed by a comparably stable region, then increasing again sharply. With the increase of friction coefficient, the forming time is increased, while the corresponding forming pressure is decreased. From Fig. 4b, it is found that the thickness at the edge and at the centre of the upper die is relatively greater than that elsewhere, while the minimum part is located at the corner of the upper die regardless of what value the friction coefficient is. In addition, the thickness of the clamped circumference of the sheet keeps stable. 'Kink' thinning is found near to the junction of the die entry and the side-wall. From Fig. 4b, it is easily seen that a lower friction coefficient results in a more uniform thickness distribution along the component.

The above observations can be explained by the following. With the outer edge being fixed in the deformation process, the material can only slide from the outer edge to the die entry. Due to the symmetry

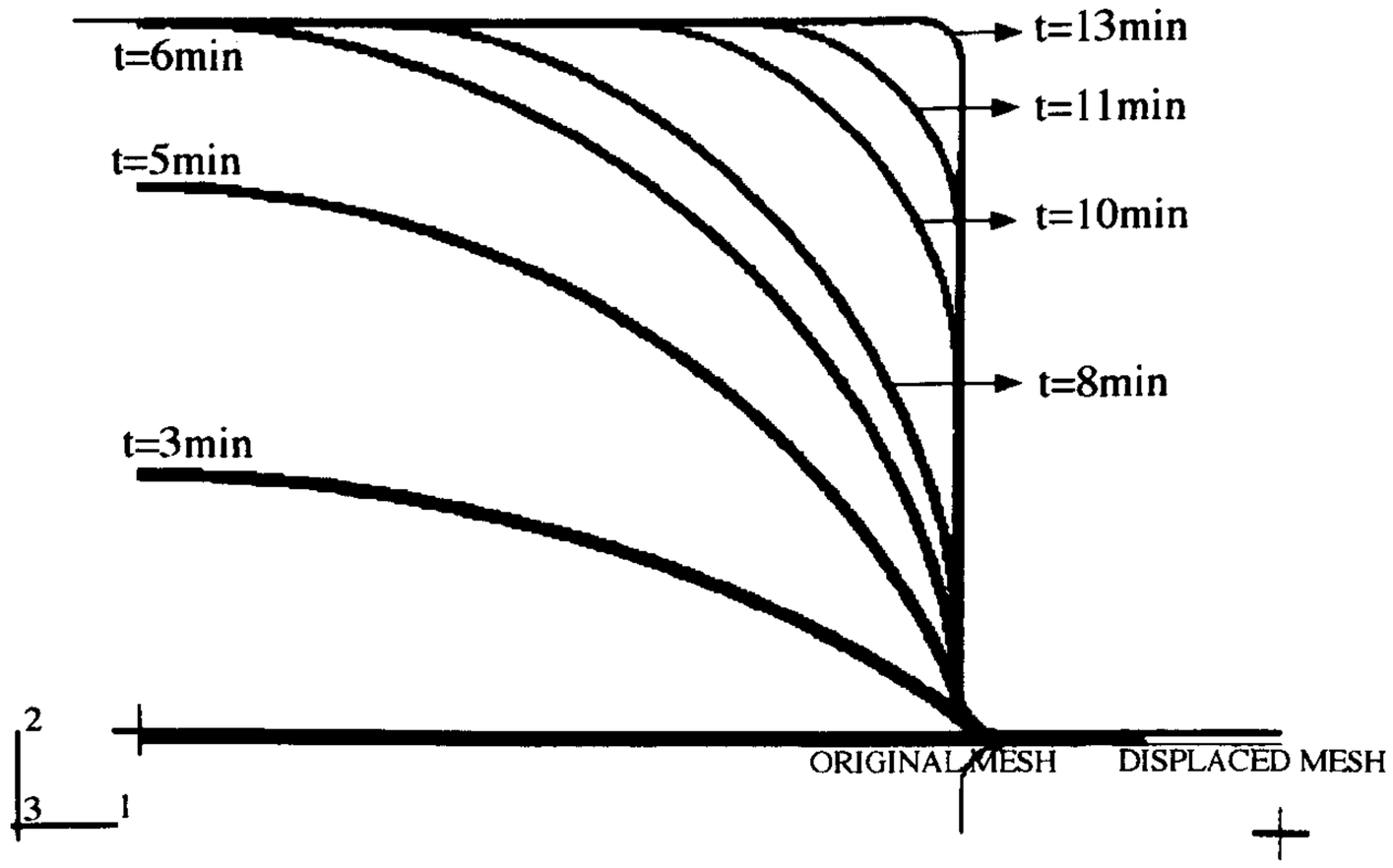

Fig. 3. Different deformation processes with time from FEM.

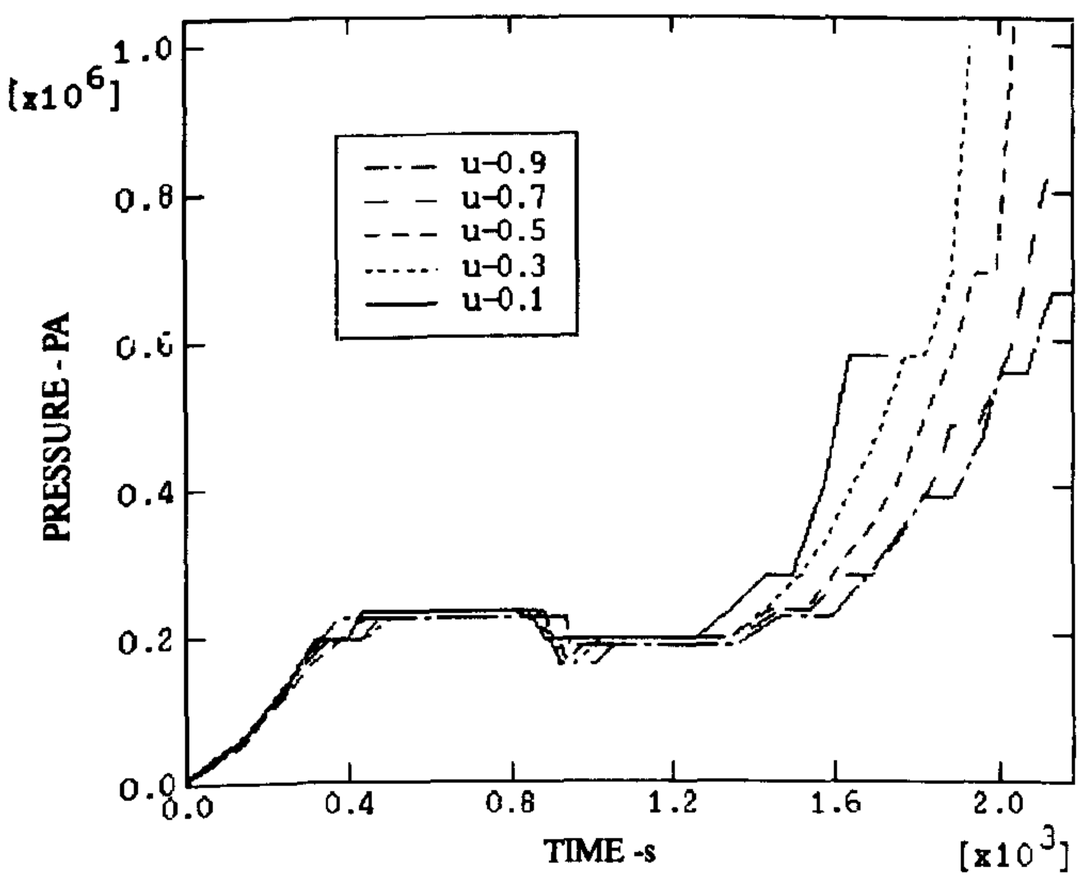

(a) pressure-time curve

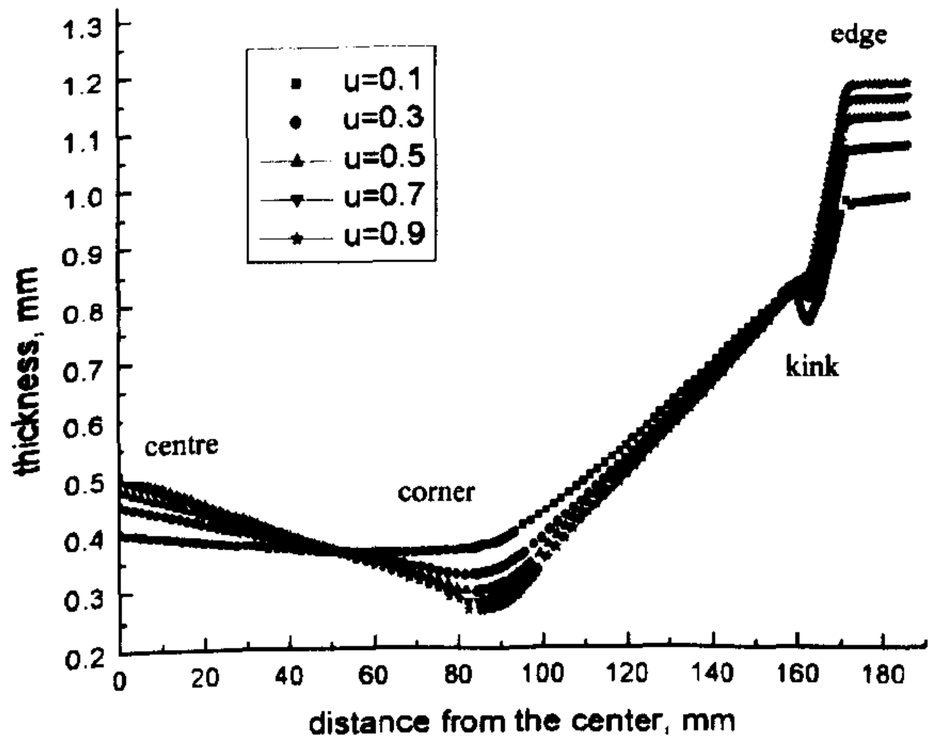

(b) thickness distribution

Fig. 4. Effects of friction of coefficient. (a) The pressure–time curve, (b) thickness distribution.

constraint, the material can only flow from the centre to the corner of the upper die. The lower the coefficient of friction is, the more volume flows into the corner, which reduces severe thinning around the corner and more forming pressure is needed to fill the corner.

4.2. *The effect of the strain rate and the strain rate sensitivity index*

The determination of material parameters such as material constant K and the strain rate sensitivity index m are normally based on experiments. The strain rate sensitivity index m is sensitive to the strain rate, which has a maximum value at an optimum strain rate. In this analysis, the relationship between m and the strain rate $\dot{\varepsilon}$ of Ti–6Al–4V alloys at $T = 900°C$ is provided by experiments [13]. While for material constant K, it is suggested to be a function of structure, temperature T and strain rate $\dot{\varepsilon}$ [8]. However, since this relationship is currently not available from experiments, K is assumed to be a constant in accordance with Cheng [12].

The effects of the strain rate and the strain rate sensitivity index upon the pressure profile and thickness variation are shown in Fig. 5a,b. From Fig. 5a, it is clearly seen that a low value of m leads to a dramatic increase of forming pressure. With a decrease in the strain rate, the necessary forming time increases greatly. The thickness distribution in Fig. 5b shows that a better, homogeneous thickness distribution can be obtained with a relatively higher value of m. When the strain rate sensitivity is close to the maximum m value, it is expected that there is no significant influence on the thickness variation. This is because a high m value confers a high resistance to neck development and, thus results in good material flow.

5. Conclusions

An FEM model has been proposed to simulate the actual superplastic blow forming process of Ti–6Al–4V sheet into a cylindrical cup. To verify the accuracy and reliability of the proposed FE model, the numerical prediction has been validated by experiment. Furthermore, a detail element type study in terms of the ability to predict the thickness distributions of the component has been performed and evaluated in comparison with the experimental data. It is found that the best prediction can be achieved using a continuum element. Major factors such as friction coefficient and the strain rate sensitivity index have been fully investigated using the proposed FEM model. The following conclusions can be drawn:

1. The superplastic forming is sensitive to the coefficient of friction. A low friction coefficient normally leads to a better homogenisation of the thickness distribution along the component.
2. It is found that the value of strain rate sensitivity index m plays an important role in the thickness variation. A relatively higher value of m improves the homogeneity of the thickness distribution.

Acknowledgements

The authors would like to thank Rolls-Royce Plc., Derby, for support in this research work.

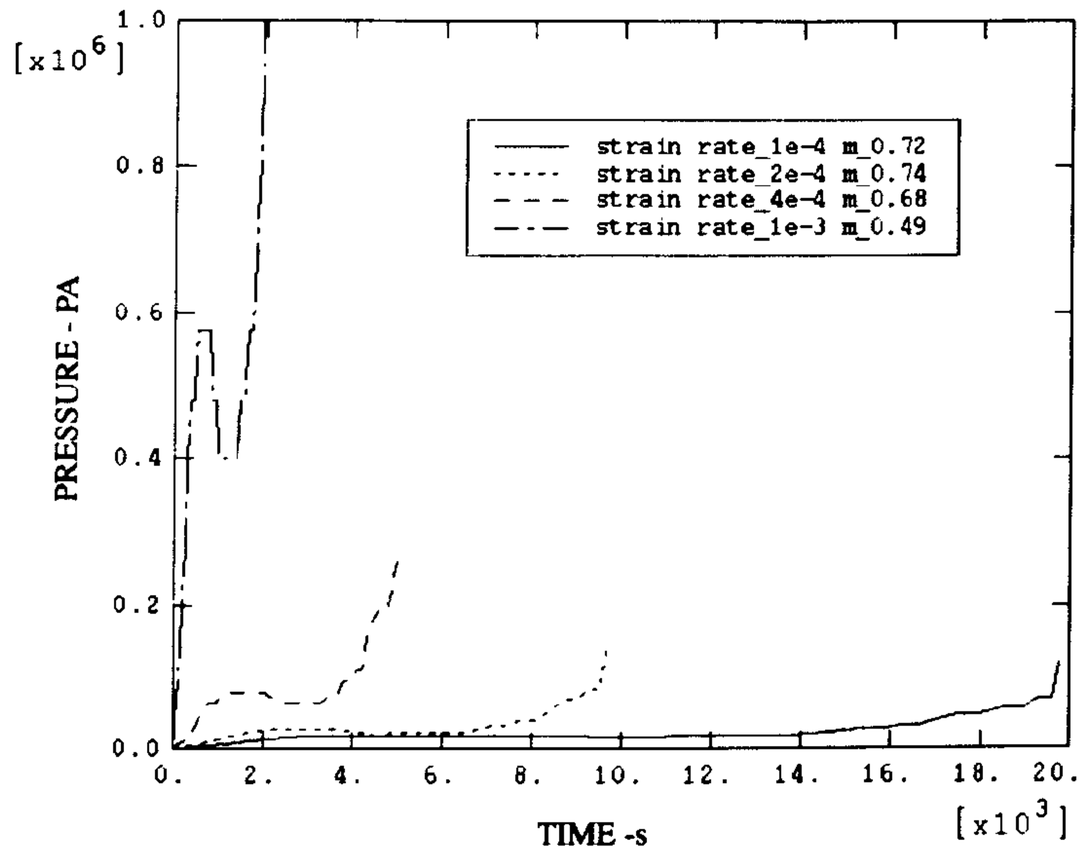

(a) pressure-time curve

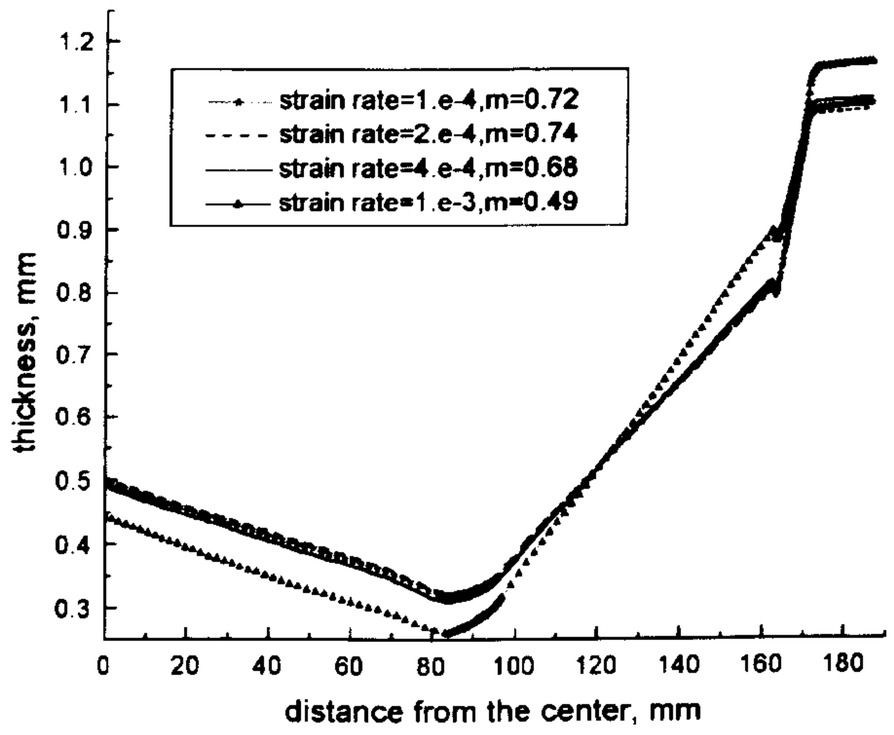

(b) thickness distribution

Fig. 5. Effects of the strain rate and the strain rate sensitivity index. (a) The pressure–time curve, (b) thickness distribution.

References

[1] Hamilton HC, Paton NE. Superplasticity and superplastic forming. Warrendale: TMS-AIME, 1989.

[2] Lee S. Thickness distribution in a superplastically formed rectangular pan under plane-strain conditions. J Mater Process Technol 1997;65:59–64.

[3] Chandra N. Analysis of superplastic metal forming by a finite element methods. Int J Numer Methods Eng 1988; 26:1925–1944.

[4] Bonet J, Wood RD, Wargadipura AHS. Numerical simulation of the superplastic forming of thin sheet components using the finite element method. Int J Numer Methods Eng 1990;30:1719–1737.

[5] Chenot JL, Bellet M. The viscoplastic approach for the finite element modelling of metal forming processes. In: Hartley P et al., editor. Numerical Modelling of Material Deformation Processes: Research, Development and Applications. Springer-Verlag, Berlin, 1992:179–224.

[6] Hibbit HD, Karlsson GI, Sorensen EP. ABAQUS user's manual, Version 5.8, Hibbit, Karlsson and Sorensen Co., USA.

[7] Hwang YM, Liew JM, Chen TR et al. Analysis of superplastic blow-forming in a circular closed-die. J Mater Process Technol 1996;57:360–372.

[8] Arieli A, Mukherjee AK. The rate-controlling deformation mechanisms in superplasticity — a critical assessment. Metall Trans 1982;13A:717–731.

[9] Bonet J, Wood RD. Solution procedures for the finite element analysis of superplastic forming of thin sheet. Proc Int Conf on

Computational Plasticity Models, Software and Applications, part 2. Pineridge Press, 1987:927–939.

[10] Rebelo N, Nagtegaal JC, Hibbitt HD. Finite element analysis of sheet forming processes. Int J Numer Methods Eng 1990;30:1739–1758.

[11] Kim YH, Hong SS, Lee JS et al. Analysis of superplastic forming processes using a finite-element method. J Mater Process Technol 1996;62:90–99.

[12] Cheng JH. The determination of material parameters from superplastic inflation tests. J Mater Process Technol 1996;58:233–246.

[13] Stephen D. Superplastic forming and diffusion bonding of titanium. Designing with Titanium. Institute of Metals, 1986:108–124.

NUMERICAL ANALYSIS OF REVERSE BLOW FORMING

Y. Chen, K. A. Kibble, R. Hall

Engineering Division, School of Engineering and Built Environment, University of Wolverhampton, UK

ABSTRACT

It is important that thinning of components be accurately predicted and controlled in the superplastic forming manufacturing process. Reverse superplastic blow forming of a Ti-6Al-4V sheet into a complex shape component has been simulated in this paper using finite element method in ABAQUS, to achieve a better understanding of the optimized control of thickness variations. The deformation process, pressure versus time curve, variation of thickness strain and the effect of a change in friction coefficient have been carefully investigated. In addition, simulation of the same structure with non-reverse forming has also been carried out and a detailed comparison has been made between results from different forming processes.

1. INTRODUCTION

Superplastic forming (SPF) has been widely accepted as an economical method to produce highly complex, lightweight and integral parts with a single forming operation in modern industry, especially in the aerospace industry. Generally, superplastically formed parts experience a great amount of elongation, thus leading to potentially large thickness variations. As the shape of a component becomes more complicated, thinning will become severe which is normally undesirable. Therefore it is important to investigate the thickness variation to improve the uniformity of thickness distribution of the component [1].

During a superplastic forming process, thinning of components depends on several parameters including the shape of the die, the material properties, and the forming conditions such as pressure and temperature [2]. Reverse blow forming is widely recognized as an effective technique to obtain good thickness distribution control in complex components [3]. Generally a reverse forming process consists of two operations starting from an initial sheet as shown in Fig. 1. In the first operation, gas pressure is imposed on top of the heated sheet. After producing the preforming shape, the forming pressure is reversed forcing the material to flow into the final tool [4]. An optimal shape of the preforming tool should be initially designed in order to obtain a prescribed thickness distribution in the final component.

A number of simulations have been performed on the simple shape of a superplastic blow forming component such as a cylindrical cup and a rectangular box [5-7]. However, the main concerns of those studies are to predict the pressure loading cycles and the final thickness distributions, which have led to a basic understanding of the superplastic blow forming process. There is little on the available publications for a reasonable interpretation of the good thickness control in the reverse

blow forming process. This study has been initiated and guided by the need to establish a clear understanding of the thickness control mechanism in the reverse forming process.

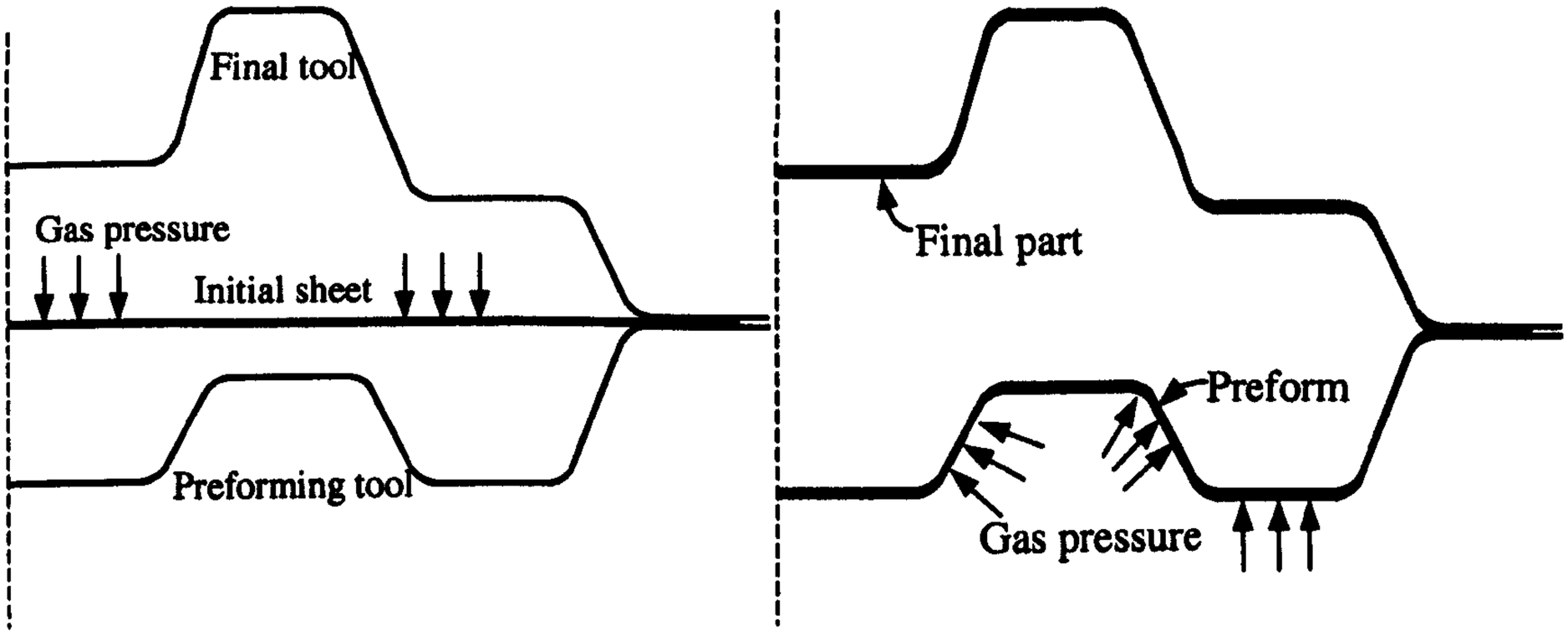

1. Schematic diagram of reverse blow forming

Finite element analysis offers an efficient method to visualize and model the thinning process in a more intuitive way in the analysis of complicated superplastic blow forming components. It provides valuable guidelines on how the parameters in a current process should be modified to meet the requirements of the process and components. In this study, the multi-step reverse forming of a Ti-6Al-4V sheet into a complicated component has been carefully simulated within ABAQUS [8]. The deformed processes at different loading stages and the strain and the stress distribution in the final stage have been fully investigated. For the purpose of comparison, simulation of the same structure under non-reverse forming has been carried out and a detailed comparison has been made between the reverse forming and non-reverse forming. Furthermore, the effect of friction coefficients has been studied.

2. FINITE ELEMENT ANALYSIS OF REVERSE BLOW FORMING

Simulation of a reverse blow forming process is characterized by large deformation and material non-linearity involved. The complicated contacts between the sheet and the dies are generally presented in the forming process, thus adding difficulty for the simulations. The reverse forming tools simulated in the current study include a pre-forming upper-die and a final forming lower-die. A circular sheet of 3 mm in thickness and 330 mm in diameter, of which the periphery is clamped between the two dies, is subjected to gas pressure. The simulation of reverse blow forming of the sheet studied in this paper can be simplified as a case of 2-D axisymmetric plain strain problem. Because of symmetry, only half of the whole structure is modelled as shown in Fig. 2.

The Ti-6Al-4V sheet is assumed to have an empirical constitutive behaviour of $\sigma = k\dot{\varepsilon}^m$, where $K = 1030.78\,MPa$ and $m = 0.61305$ [9]. The constitutive equation is implemented into an isotropic creep model within ABAQUS. After a detailed element study [10], a continuum element is selected to achieve an accurate modelling of the blow forming process. In addition, the regions

where stress concentrations are significant are constructed with fine meshes. To obtain an accurate modelling of the superplastic deformation, an iterative Newton-Raphson solution technique is employed to solve the governing nonlinear equations. The imposed gas pressure is controlled by a special solution dependent magnitude scheme [8] to maintain an approximately constant strain rate (the target value) in the simulation.

The problem of friction associated with the contacts between the sheet and the dies is very important for a superplastic reverse blow forming process. An important factor in accurate modelling of the process is how to simulate the friction effect due to contact. In this paper, the two dies are treated as rigid and the contact interactions between the dies and the sheet are modelled as rigid surfaces and a deformable surface. The penalty Coulomb friction formulation [8] is used to model the friction effect associated with the contact pairs by specifying a friction coefficient. A reasonable penetration of the deformable surface into the rigid surfaces has been assigned to monitor the contact interaction.

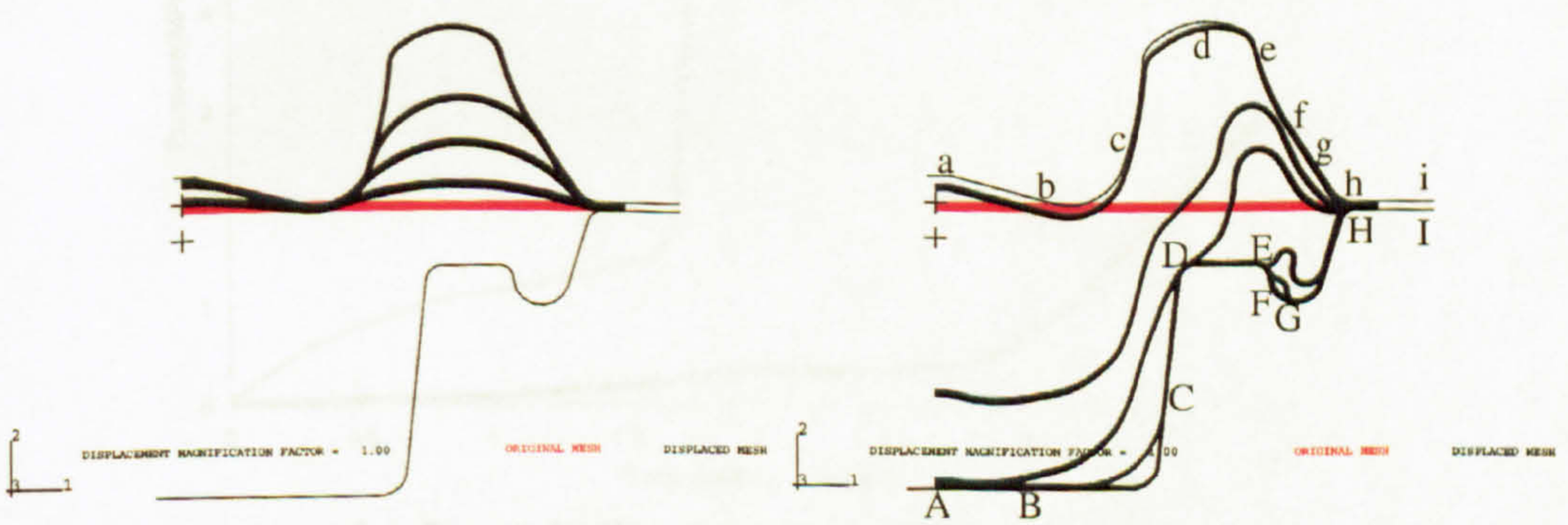

(a) blow forming to the upper-die (b) reverse forming to the lower-die

2. Finite element simulation of reverse blow forming process

A reverse forming process is different from customary blow forming methods in that a preforming process is necessary before the final shape is produced. The whole process can be accurately modelled using multiple loading steps. Pressure has to be applied underneath the sheet to make it inflate into the upper-die first. As the initial application of the pressure is assumed to occur so quickly, a purely elastic response is performed in the first step. The inflation process of the sheet into the upper-die is then carried out in the second step. The third step is to remove all contact pairs of the upper-die and the sheet, and the target creep stain rate defined in the second step. Finally the reversed pressure is imposed on the top of the sheet to force the sheet to flow into the lower-die. The above procedures enable the FEM program to accurately model the reverse forming process.

3. RESULTS AND DISCUSSION

It is important that a good FEM model is capable of predicting the reverse forming behaviour. Typical deformation configurations in the reverse forming process have been predicted and shown in Fig. 2. In particular, Fig. 2 (a) shows the processes of the sheet bulged into the upper-die whilst Fig. 2 (b) is the reverse process into the final tool. For the convenience of description, points a to i

represent the deformation instants to the upper-die whilst points A to I represent the corresponding instants where the material flow into the lower-die. It can be clearly seen that the large deformation is concentrated around the bubble area (region c to h) in the preforming process, resulting in a thickness profile in which the centre and the clamped area is thicker than the bubble area. After filling the upper-die, the sheet flows downward gradually to the bottom AB, region DE and the bottom corner BC respectively. The outside small corner FG is the last filled area.

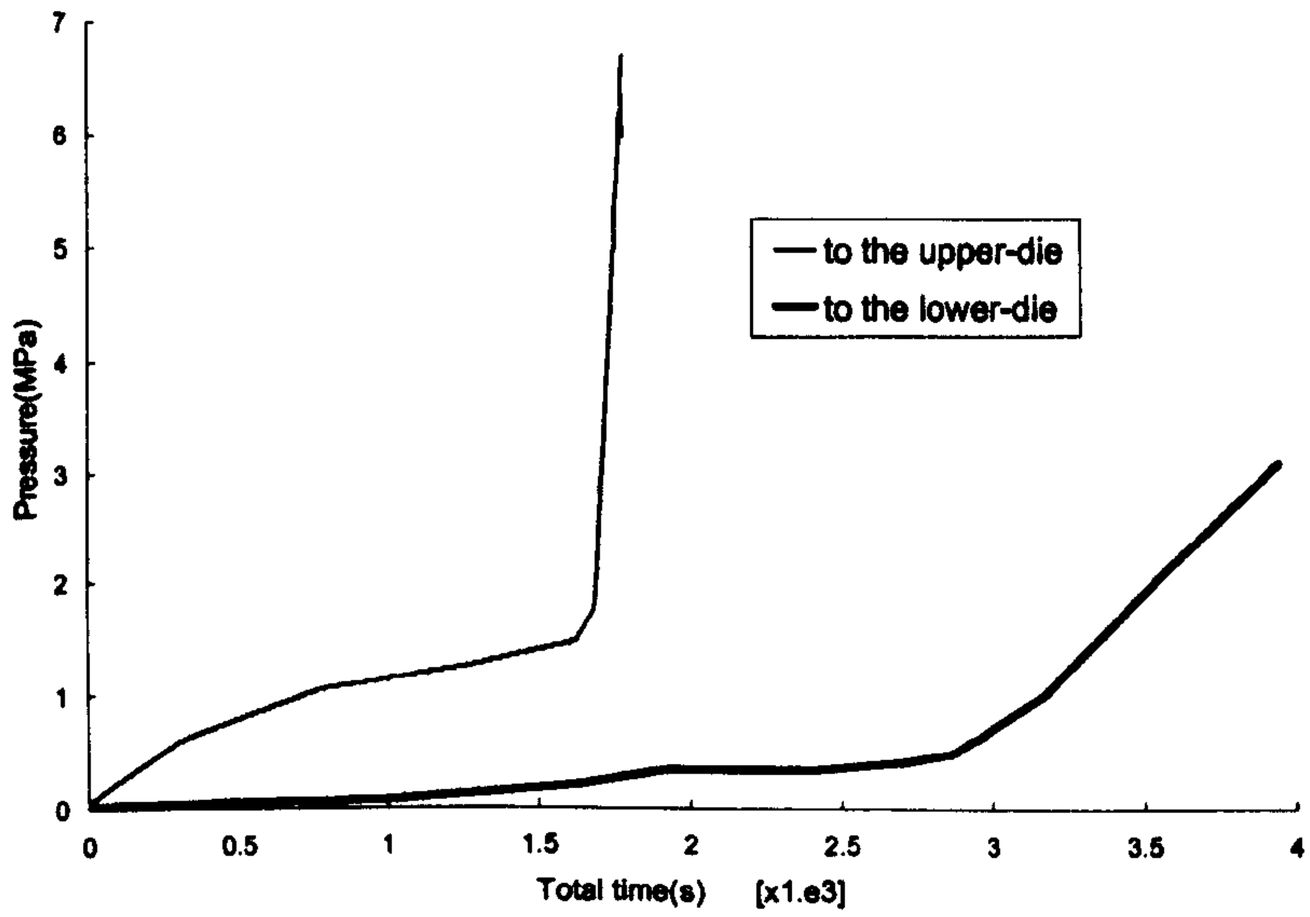

3. Pressurization curves in the reverse forming process

The predicted pressure versus time curves of the sheet inflated into the upper-die and the lower-die in the reverse forming process are shown in Fig. 3, in which both initially rise rapidly, followed by a comparable stable region, then increasing again sharply. It is easily seen that a higher pressure is needed in the preforming stage to the upper-die. The distribution of equivalent Mises stress on the deformed component is illustrated in Fig. 4. It is noted that "true" stress is used in the simulation within ABAQUS. It can be clearly observed that the maximum stress occurs at the small corner, which is the last formed area in the reverse forming process.

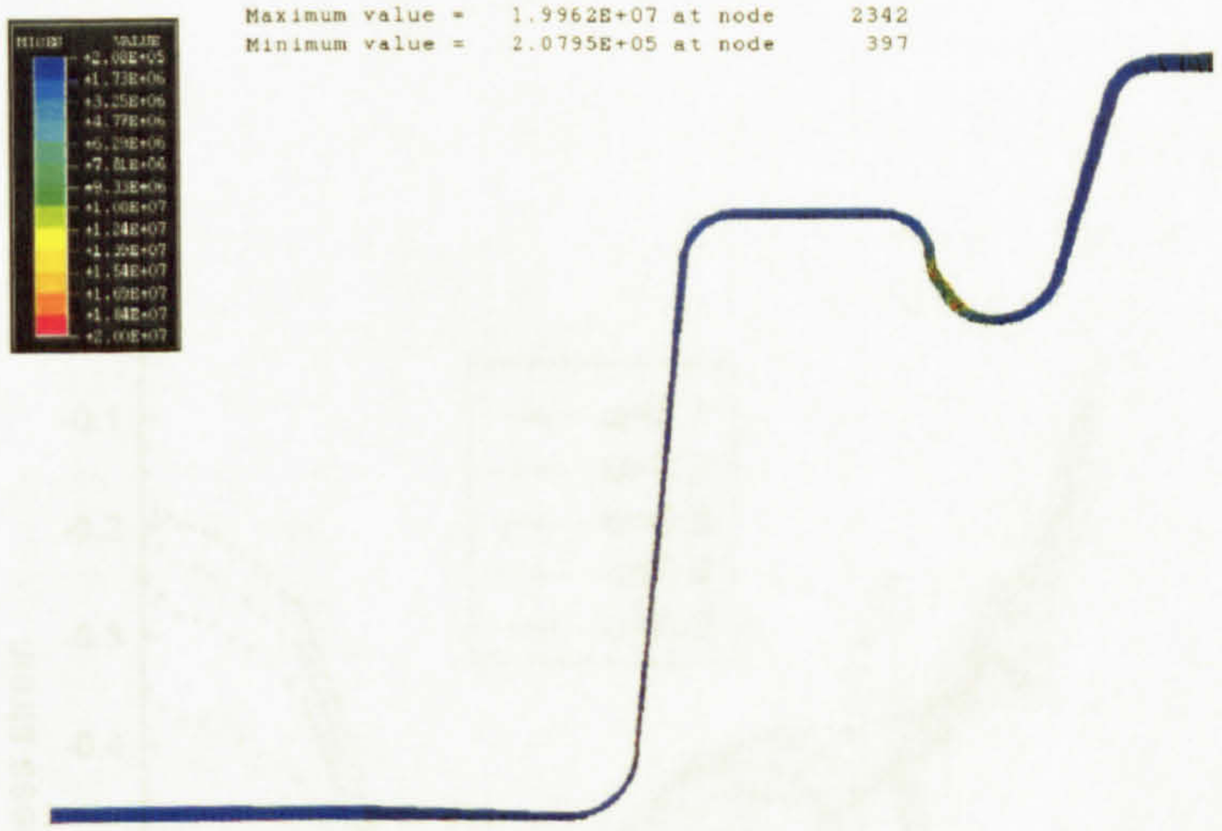

4. Equivalent Mises stress distribution in reverse forming

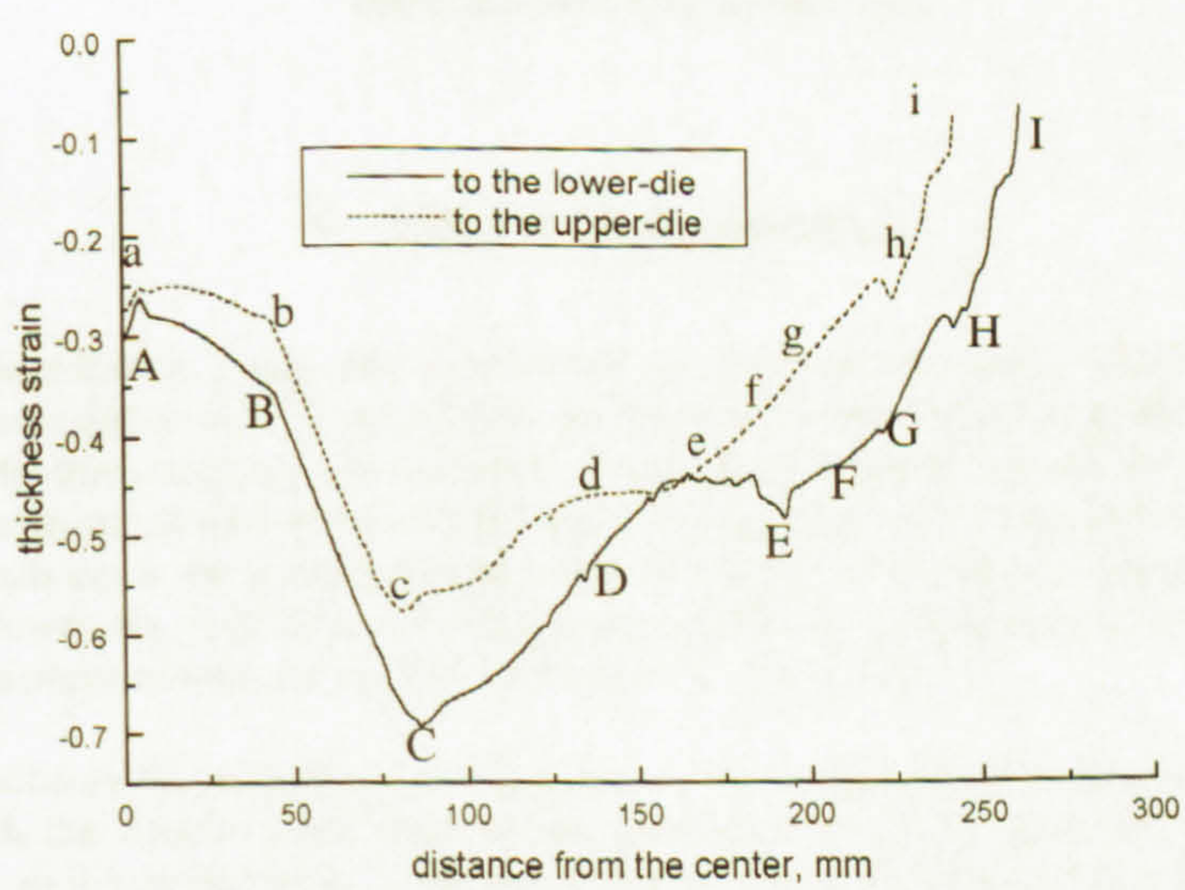

5. Thickness strain of the sheet into the upper-die in comparison with that of into the lower-die

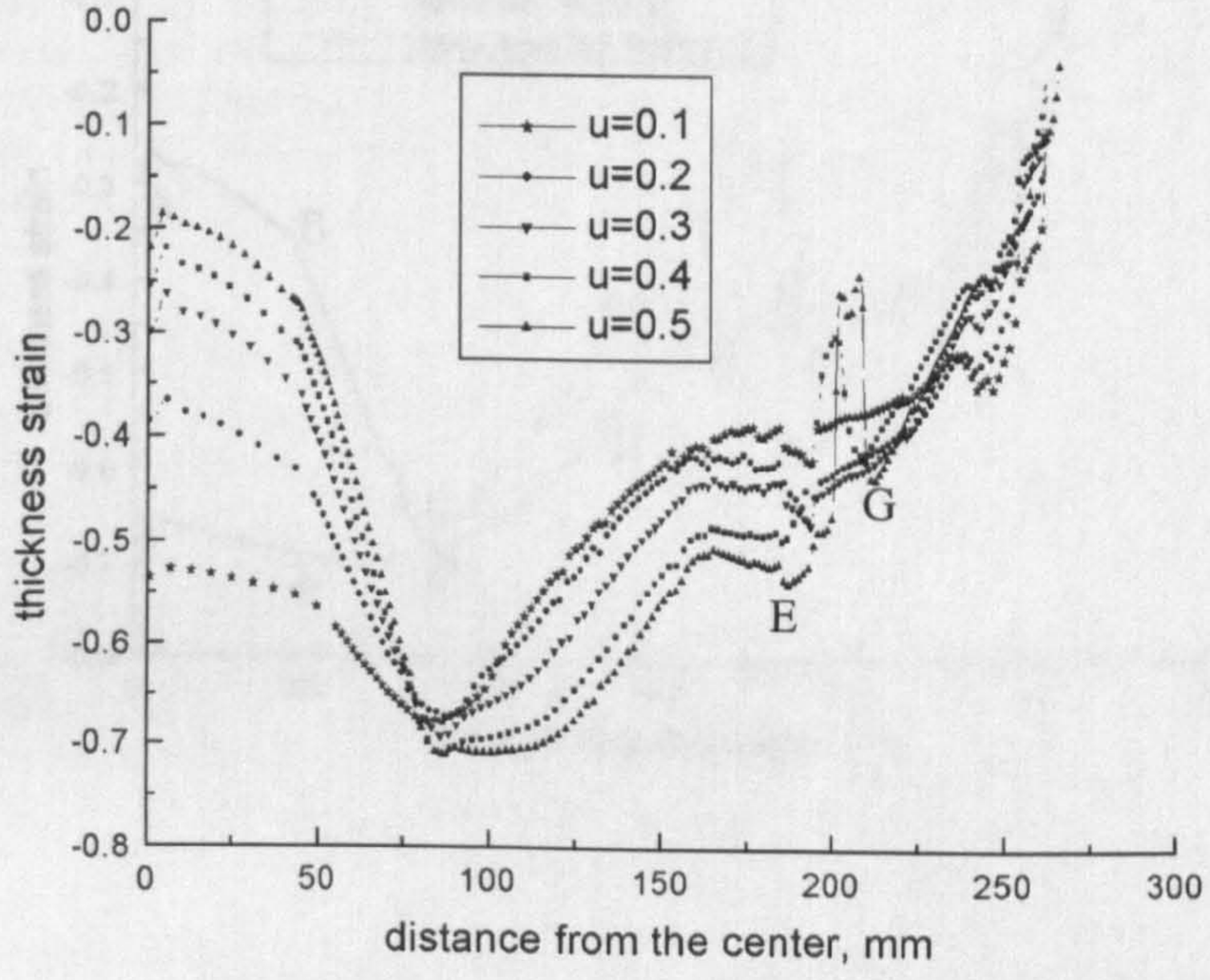

6. Effect of friction coefficient

The thickness distribution along the component is essential to assess whether the formed component is successful or not. To investigate the thickness variation in the preforming and final forming stages, the thickness strain is evaluated in this study. Figure 5 shows the thickness strain distribution of the sheet inflated into the upper-die in comparison with that into the lower-die. It is evident that in both cases the sheet is thinned, but the degree of thinning is greater for the sheet bulged into the lower-die. It is noted that the greatest thinning strains bulged into the upper-die and the lower-die occur around the region c and region C separately.

The effect of friction on the thinning of a component in the reverse blow forming process has been studied, in which the friction coefficient is assumed to be uniform along the contact surface, varying from 0.1 to 0.5 in this paper. The distributions of thickness strain under different friction coefficients are illustrated in Fig. 6. Again, greater thinning occurs around the region C of the lower-die for all values of the friction coefficient studied. The lower the friction coefficient, the more uniform thickness distribution along the component. It should be noted that when the friction coefficient is greater than 0.4, the thickness strain sharply changes around the outside corner (region EG) as illustrated in Fig. 6. This is mainly because a higher friction coefficient tends to resist further deformation of the sheet on contact and thus results in sharp thickness variations in the simulation and an unsuccessful formed component in practice.

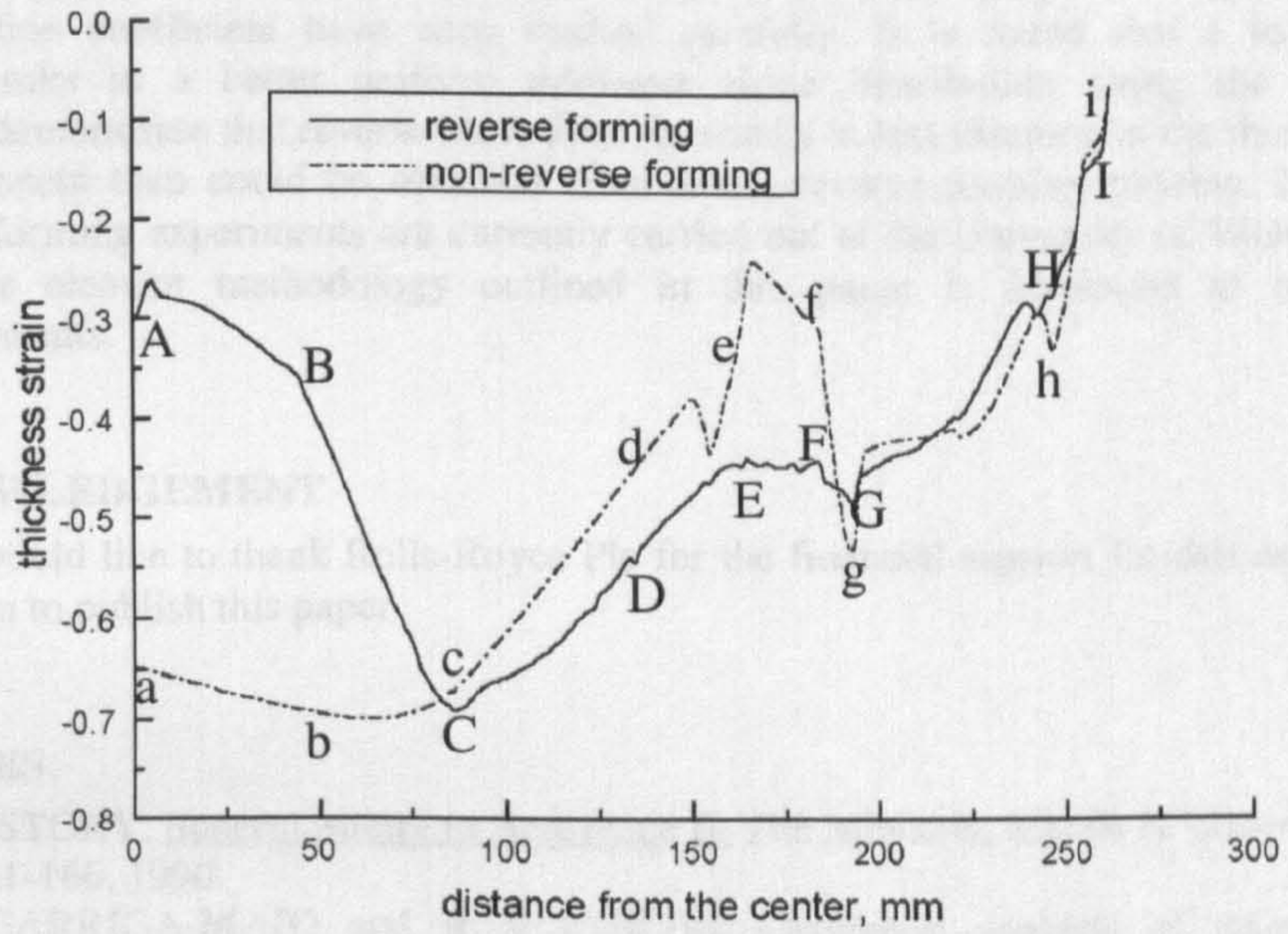

7. Thickness strain distribution comparison between reverse and non-reverse forming

To further understand the effect of reverse blow forming, simulation of a non-reverse forming process for the same sheet has also been conducted for a comparison with that of reverse forming. Similar deformation configurations, as shown in Fig. 2(b), are obtained for a non-reverse forming process. Furthermore, thickness strain distributions along the final component for a reverse forming and non-reverse forming process are compared in Fig. 7. For the convenience of description, reverse blow forming is denoted as case I and non-reverse blow forming as case II. It is evident from Fig. 7 that in both cases the sheet has thinned, but the degree of thinning is less for case I in the bulge area (region AC). However, this trend is different in the middle portion of the lower die (region CG). Although reverse forming causes slightly larger thinning at region CG, it greatly improves the thinning at bottom region AC, which is important in practice. During the initial bulging into the upper-die, deformation is concentrated primarily in the large bubble area (region c to h), i.e. the thickness around the bubble is thinning greatly thus causing more volume flow into the adjacent areas (region ac). When the material is reverse flowed into the lower-die, little additional deformation occurs within the bubble area. Instead, plastic flow is concentrated within zone AC. There is more volume in this area after an initial bulging in case I than that in case II, which results in less thinning in the thickness of the formed component from case I than could be obtained from case II as clearly demonstrated in Fig. 7.

4. CONCLUSIONS

A methodology using finite element analysis has been developed to investigate the superplastic reverse forming process of a Ti-6Al-4V sheet into a complex component. The deformed

configurations, pressure-time curve, thickness strain distribution along the component and the effect of friction coefficient have been studied carefully. It is found that a lower friction coefficient results in a better uniform thickness strain distribution along the component. Comparisons demonstrate that reverse blow forming results in less thinning in the thickness of the formed component than could be obtained from a non-reverse forming process. Furthermore, reverse blow forming experiments are currently carried out at the University of Wolverhampton, and the finite element methodology outlined in this paper is employed to interpret the experimental results.

5. ACKNOWLEDGEMENT

The authors would like to thank Rolls-Royce Plc for the financial support for this research work and permission to publish this paper.

REFERENCES

1. J M STORY, Superplasticity in Aerospace II, The Minerals, Metals & Materials Society, Pp151-166, 1990.
2. D GARRIGA-MAJO and R V CURTIS, Geometric analysis of thinning during superplastic forming, Materials Science Forum, Vol.357-359, Pp213-218, 2001.
3. J PILLING and N RIDLEY, Superplasticity in Crystalline Solids, The Institute of Metals, 1989.
4. D VIEILLEDENT and L FOURMENT, Metallurgical qualities improvement by automatic preform design of forging processes, Metal Forming 2000, Pietrzyk et al. eds., 2000 Balkema, Rotterdam, Pp157-162, 2000.
5. Y H KIM, S S HONG, J S LEE and R H WANGONER, Analysis of superplastic forming processes using a finite-element method, J.Mater.Processing Technol., Vol.62, Pp90-99, 1996.
6. S LEE, Thickness distribution in a superplastically formed rectangular pan under plane-strain conditions", J.Mater.Processing Technol., Vol.65, Pp59-64, 1997.
7. Y M HWANG, J S YANG, T R CHEN and J C HUANG, Analysis of superplastic sheet-metal forming in a circular close-die considering non-uniform thinning, J.Mater.Processing Technol., Vol.65, Pp215-227, 1997.
8. HIBBIT, KARLSSON and SORENSEN, ABAQUS/Standard User's Manual, Version 5.8, Hibbit, Karlsson and Sorensen Co., USA, 2000.
9. J H CHENG, The determination of material parameters from superplastic inflation tests. J.Mater.Processing Technol., Vol.58, Pp233-246, 1996.
10. Y CHEN, K KIBBLE, R HALL and X HUANG, Numerical analysis of superplastic blow forming of Ti-6Al-4V alloys, Materials and Design, Vol.22, Pp679-685, 2001.